University of Alberta

Structure-function study of the human mitotic checkpoint protein Zeste White 10

By

Jakub Konrad Famulski

A thesis submitted to the Faculty of Graduate Studies and Research in partial fulfillment of the requirements for the degree of *Doctor of Philosophy*

Department of Oncology

Edmonton, Alberta
Spring, 2009

Your file Votre référence
ISBN: 978-0-494-55343-5
Our file Notre référence
ISBN: 978-0-494-55343-5

Dedication

To the two loves of my life, Kathy and Bailee

Abstract

The ultimate goal of the cell cycle is to replicate and subsequently segregate the genome into two identical daughter cells. While the replication of our genome occurs during S-phase, the physical segregation of our genetic material occurs during mitosis. Although it is the shortest stage of the cell cycle, mitosis is a highly coordinated and mechanistically sophisticated cellular event. Failure or improper execution of mitosis is catastrophic for individual cells as well as a potential precursor to malignancy. The mis-segregation of even one chromosome can negatively impact cell survival or conversely lead to mis-regulation of cell growth. In fact, many human cancers are associated with elevated levels of aneuploidy that are thought to result from chromosome mis-segregation. Understanding the mechanisms that govern as well as power the mitotic machinery has thus been the focus of research for almost an entire century.

My PhD research project has focused on the mitotic function of the human RZZ-dynein/dynactin kinetochore complex through a direct molecular structure-function study of one of its components, *Zeste White 10*. Using fluorescence as well as live cell microscopy, I have deciphered the mechanism regulating kinetochore residency of the RZZ complex, as well as its role in mitotic checkpoint response to inter-kinetochore tension. My work has reinforced the importance of studying the regulation of mitotic checkpoint component kinetochore dynamics as well as the importance of dynein/dynactin-mediated transport of checkpoint proteins off kinetochores.

Acknowledgements

Firstly I acknowledge my supervisor and mentor, Dr. Gordon Chan. He has been a wealth of knowledge and expertise throughout my graduate training. I feel lucky to consider Gordon a colleague and friend.

Secondly, I acknowledge all of the support and encouragement of my peers, fellow lab members as well as other faculty at the Cross Cancer Institute. The environment, people as well as facilities at the Cross Cancer Institute are unsurpassed and without them I could not have been nearly as successful during my graduate training. There are numerous other people that have had a significant influence on my graduate training. As such, I would like to personally acknowledge several of them. Ray, Larissa, Raja, Sashin, Dr. Godbout, Mesfin, Alan, Dr. Murray, Dr. Winefeld, Dr. Hendzel, Karen, Vanessa, Anthony and Anne. Furthermore, I would also like to acknowledge my supervisory committee, Dr. Joan Turner, Dr. Neil Adames and Dr. Shelagh Campbell, for all their help and support.

Thirdly, I am especially indebted to Dr. X. Sun, the Cross Cancer Institute Cell Imaging Facility manager. Dr. Sun has taught me all that I know about microscopy and I credit his dedication and expertise to fostering my newly acquired passion for live cell imaging. I know that the skills I have gained from Dr. Sun will ensure my continued success during my postdoctoral training.

Table of Contents

List of Figures

List of Tables

List of Figures

List of Symbols, Abbreviations and Nomenclature Epigraph

~.....approximately
+/-.....plus or minus
%.....percentage
3D.....three dimensional
aa.....amino acid
ACA.....anti centromere antigen
APC/C.....Anaphase Promoting Complex/Cyclosome
APC/C^{cdh1}.....Cdh1 activated Anaphase Promoting Complex/Cyclosome
APC/C^{cdc20}.....Cdc20 activated Anaphase Promoting Complex/Cyclosome
ATP.....adenosine triphosphate
bp.....base pair
BUB.....budding uninhibited by benzimidazole
CCD.....charge coupled device
CIN.....Chromosomal Instability
cDNA.....copy DNA
C-terminus.....carboxy terminus
ch.....chicken
ce.....*C.elegans*
CENP.....centromere protein
CATD.....CENP-A targeting domain
Cdk.....Cyclin dependent kinase
CREST..... calcinosis, Raynaud's phenomenon, esophageal dysmotility, sclerodactyly and telangiectasia
CCAN.....constitutive centromere associated network
CPC.....chromosome passenger complex
^{o}C.....degrees Celsius
DMEM.....dulbecco's modified eagle's media
DNA.....deoxyribonucleic acid
dm.....*D.melanogaster*
DAPI.....4',6-diamidino-2-phenylindole
dIC.....dynein intermediate chain
(E)GFP.....(enhanced) green fluorescent protein
EMCCD.....electron multiplying charge coupled device
EM.....electron microscopy
FCS.....fetal calf serum
FRAP.....fluorescence recovery after photobleaching
Fig.....figure
g.....gravitational force
g.....grams
GTP.....guanosine triphosphate
GST.....glutathione-S-transferase
GDP.....guanosine diphosphate
GEF.....guanosyl exchange factor

GTPase.....guanosyl triphosphatase
gal.....galactose
HIS.....histidine
HEK.....human epithelial kindey
H2B.....histone H2B
h.....hours
HeLa.....cervical canver epithelilal cells derived from Henrietta Lacks
HCl.....hydrochloric acid
k-MT.....kinetochore-microtubule
k-fiber.....full assortment of k-MT attachments
KMN.....KNL-1, Ndc80, Mis12 network
kDa.....kilo Dalton
L.....liter
LSM.....laser scanning microscope
MGS.....mutation generation system
(m).....mouse
m.....meter
mL.....milli liter
µL.....micro liter
MAD.....mitosis arrest deficient
MCAK.....mitotic centromere-associated kinesin
MT(s).....microtubule(s)
µM.....micro molar
mM.....milli molar
µm.....micro meter
min.....minute
MAPs.....microtubule associated proteins
MDa.....mega Dalton
Mad2-O.....open conformation of Mad2
Mad2-C.....closed conformation of Mad2
MCC.....mitotic checkpoint complex
MCF2.....mitotic checkpoint factor 2
NDGA.....nordihydroguaiaretic acid
NA.....numerical aperture
n-terminus.....amino terminus
NuMa.....Nuclear mitotic apparatus protein
n.....number of samples
OD.....optical density
pH.....-log[H^+]
PCR.....polymerase chain reaction
PAGE.....polyacrylamide gel electrophoresis
PBS.....phosphate buffered saline
PTK.....*Potorous tridactylis*
PEI.....polyethyleneamine
p50.....dynamitin
ROD.....roughdeal

RZZ.....complex of ZW10, ROD and Zwilch
raff.....raffinose
STLC.....S-*trytil*-L-*cystine*
SDS.....sodium dodecyl sulfate
siRNA.....small interfering ribonucleic acid
SD.....standard deviation
sec.....second
SD.....synthetic yeast media
s.....second
$t_{1/2}$.....time to achieve one half
TRP.....tryptophan
UBC.....ubuquitin conjugating enzyme
UV.....ultra violet
URA.....uracil
X.....fold
xl.....*X.laevis*
YFP.....yellow fluorescent protein
ZW10.....*zeste white 10*

Chapter I: *Introduction*

1.1 Mitosis

Cell division is traditionally divided into six specific stages of mitosis: prophase, prometaphase, metaphase, anaphase, telophase and finally cytokinesis (Figure 1.1). Mitosis begins during prophase, when the chromatin begins to condense and the replicated centrosomes segregate to the opposite poles of the cell. Biochemically, cells enter mitosis upon the association and subsequent activation of the Cdk1 kinase with its cyclin activating subunit cyclin B [reviewed in (Morgan, 1997)]. The Cdk1 kinase initiates all of the subsequent biochemical pathways that are required to complete mitosis.

As the cell continues into prometaphase the nuclear envelope begins to disassemble and the two centrosomes begin to nucleate microtubules (MTs) in order to establish the mitotic spindle. MTs emanating from the two spindle poles attach to chromosomes at mitotic specific structures called kinetochores. Each chromosome contains two sister kinetochores that assemble at the centromere, also known as the primary constriction. The establishment of kinetochore-MT (k-MT) attachments enables the MTs to exert pulling forces on the chromosomes and therefore drive chromosome movement toward the spindle poles. Attachment of both sister kinetochores to MTs emanating from opposite spindle poles, or bi-polar k-MT attachment, results in the equalization of pulling forces and subsequently the alignment of the chromosome at the metaphase plate.

Metaphase occurs once all of the chromosomes have achieved bi-polar k-MT attachments as well as chromosome alignment at the metaphase plate. Chromosome alignment during metaphase is followed by the physical separation of sister chromatids and their subsequent segregation to the opposite poles of the cell during anaphase. During telophase, sister chromatids continue to move to the opposite spindle poles while a cleavage furrow forms at the site of the metaphase plate also known as the spindle midzone. Furthermore, nuclear envelopes begin to reassemble around the two newly segregated genomes.

Finally, during cytokinesis, the two daughter cells are physically separated as the cells are pinched off from each other, nuclear envelopes complete reformation, chromosomes decondense and as such, the two new cells re-enter the G1 phase of the cell cycle. Although mitosis is the shortest stage of the cell cycle, it is a complex and highly regulated process. In the following sections I will describe in detail the machinery that drives mitosis and the molecular pathways that regulate its progression and ensure accurate chromosome segregation.

Figure 1.1

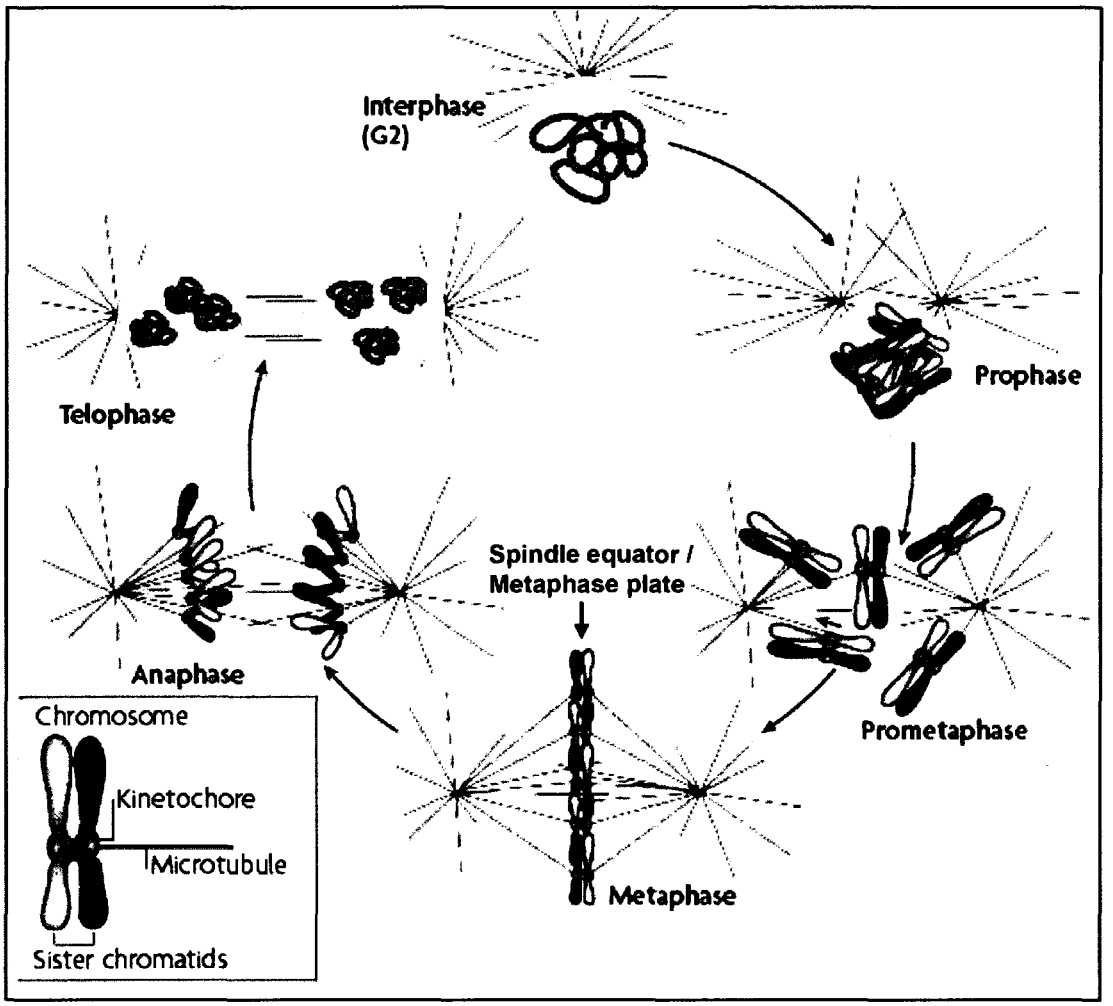

Figure 1.1: **Mitosis.**
The ultimate goal of mitosis is the equal segregation of chromosomes into each daughter cell. Equal chromosome segregation is a complex and highly regulated cellular event. It depends on the physical attachment of spindle microtubules (MTs) to chromosomes at kinetochores. Kinetochores are mitosis-specific proteinaceous tri-laminar disk structures that assemble on centromeres, the primary constrictions of chromosomes, and physically capture spindle MTs. Each kinetochore attaches to MTs emanating from a single spindle pole, thus resulting in bi-polar attachment of the sister chromatid pair. Bi-polar kinetochore-MT attachment drives the alignment of chromosomes at the spindle equator. Once all of the chromosomes become aligned at the spindle equator, sister chromatids physically dissociate and begin to segregate into the two daughter cells. Following cytokinesis, the two daughter cells decondense their chromosomes and re-enter the cell cycle. (Figure adapted from Cheeseman and Desai, 2007)

1.2 The Mitotic Spindle

Mechanistically, chromosome segregation ultimately depends on the dynamic tubular protofilaments known as MTs. During mitosis, MTs assemble into anti-parallel arrays, known as the mitotic spindle. The mitotic spindle is the machine that aligns chromosomes at the metaphase plate and subsequently segregates them into the two daughter cells. High fidelity chromosome segregation is essential for the continuation of proper cell function, and as such, the assembly and function of the mitotic spindle is a highly complex and tightly regulated process.

1.2.1 Microtubules

MTs are highly dynamic fibers of polarized parallel protofilaments of α-/β-tubulin heterodimers arranged head to tail forming a tubular structure consisting of 13 protofilaments (Desai and Mitchison, 1997). The minus ends of MTs are embedded at the sites of MT nucleation while the plus ends reside at the growing tips of MTs. Assembly of MTs initiates at MT nucleation sites, or MT-organizing centers, which in most spindles are associated with centrosomes [reviewed in (Bornens, 2002)]. Upon nucleation, MTs continue to grow through the addition of GTP-β-tubulin subunits to their plus ends. Once incorporated into the protofilament, the GTP molecule is hydrolyzed to GDP. GDP-bound-tubulin forms the basis of the MT polymer lattice, however, as a polymer the GDP bound form of tubulin is also unstable. Growing MTs remain stable through the constant addition of GTP-β-tubulin to their plus ends. This terminal GTP-β-tubulin acts as a "cap" and prevents dissociation of the polymer (Caplow and Shanks, 1996). However, if the GTP-β-tubulin cap is lost, the GDP-bound β-tubulin subunits found within the lattice dissociate, causing MTs to rapidly disassemble and depolymerize. MT polymers are therefore highly dynamic and stochastically switch between polymerization and depolymerization, a process also known as dynamic instability (Desai and Mitchison, 1997). In other words, MTs are constantly growing and shrinking. To facilitate the regulation of this process, there are numerous MT associated proteins (MAPs) which either stabilize or enhance MT depolymerization [reviewed in (Cassimeris and Spittle, 2001)]. MT end binding proteins such as CLIP-170, CLASP1 and EB1 are thought to copolymerize with new tubulin and therefore aid in MT growth (Schuyler and Pellman, 2001). On the other hand, depolymerizing kinesins of the KinI family disrupt the MT lattice and therefore promote MT de-polymerization (Walczak, 2003). The regulation of MT polymerization by the plus end MT binding proteins as well as the induction of MT de-polymerization by the KinI kinesins has been shown to be essential for proper mitotic spindle formation as well as function (Walczak, 2003).

1.2.2 Mitotic Spindle Structure

The mitotic spindle is composed of three functional components: centrosomes (spindle poles), chromosomes and most importantly microtubules arrays (O'Connell and Khodjakov, 2007) (Figure 1.2). In human somatic cells all three components are essential for the establishment of a mitotic spindle. Mitotic spindle assembly ultimately requires the attachment of chromosomes to MTs and MTs to spindle poles. MTs are tethered with their minus ends at the poles and their plus ends extending toward the chromosomes. Centrosome tethering and focusing of MTs is known to involve MT cross-linking proteins as well as MT motors. Dynein/dynactin and NuMa are the best studied components of this pathway and function by cross-linking spindle pole associated MTs and generating sliding forces between them (Compton, 1998). Additionally, the mitotic

spindle also consists of interpolar MTs which extend and overlap at the spindle midzone. These interpolar MTs help stabilize the spindle during prometaphase and metaphase, in addition to enabling spindle pole separation during late mitosis (Scholey et al., 2003).

1.2.3 Chromosome-MT Attachments

The function of the mitotic spindle is to segregate the replicated genome. In order to do so, the mitotic spindle is responsible for the attachment and subsequent alignment of all chromosomes at the metaphase plate. The physical attachment between chromosomes and spindle MTs occurs when the rapidly growing MT plus ends interact with and attach to mitosis-specific macromolecular structures called kinetochores (discussed in detail below in section 1.4). The resulting interaction is thought to involve lateral as well as end-on binding of the MT plus end to the kinetochore complex (discussed in detail in section 1.5). Kinetochore attached MTs are called kinetochore-fibers (k-fiber) because kinetochore attachment stabilizes MTs (Inoue and Salmon, 1995). In vertebrates, k-fibers consist of 20-40 MTs attached to a single kinetochore (McEwen et al., 1997). During mitosis, k-fiber maturation is thought to depend on cooperative mechanisms of MT growth and MT attachment as well as MT motor-mediated transport [reviewed in (O'Connell and Khodjakov, 2007)]. The molecular pathways of k-MT attachment will be discussed in detail later on in section 1.5.

1.2.4 The "Search and Capture" Hypothesis

During vertebrate mitosis, the majority of spindle MTs are nucleated at centrosomes, or spindle poles, by the γ-tubulin ring complex, γ-TuRC. γ-TuRC caps the minus ends of MTs and therefore inhibits MT depolymerization (Gunawardane et al., 2000; Job et al., 2003). Additionally, spindle poles also contain several MT stabilizing MAPs, such as the XMAP215/ch-TOG/Msps family, which in turn aid in the initial MT outgrowth (Lee et al., 2001). MTs growing out of spindle poles are thought to randomly probe the cytoplasm in order to encounter and establish end-on attachments with kinetochores. This phenomenon has been termed the "search and capture" model (Kirschner and Mitchison, 1986). The model stated that centrosomal-based dynamic MT outgrowth would lead to random capture of kinetochores and therefore establishment of k-fibers. Monopolar attachments would occur initially, when chromosomes are closest to on spindle pole, while the continuous probing of longer MTs would eventually establish of bi-polar attachments. Bi-polar attachment would subsequently lead to chromosome alignment at the metaphase plate and signal the cell to complete mitosis.

Although this model was widely accepted, it could not explain several key observations of mitotic spindle assembly. First, according to the model k-MT attachments occur randomly, but computer modeling studies showed that simply random k-MT attachments alone cannot account for the rapid k-MT attachment observed in live cells (Wollman et al., 2005). Second, upon entry into prometaphase most chromosomes initially mono-orient close to a single pole, which according to the model would actually delay the chance of bi-polar k-MT attachment and therefore chromosome alignment (Hayden et al., 1990; Skibbens et al., 1993). Last, it has been shown that mitotic spindle assembly and subsequent chromosome segregation can occur without spindle poles, which according to the search and capture model are required as the source of MTs (Basto et al., 2006; Heald et al., 1996; Hinchcliffe et al., 2001; Khodjakov et al., 2000). In the following, I will detail recent refinements of the search and capture model.

Figure 1.2

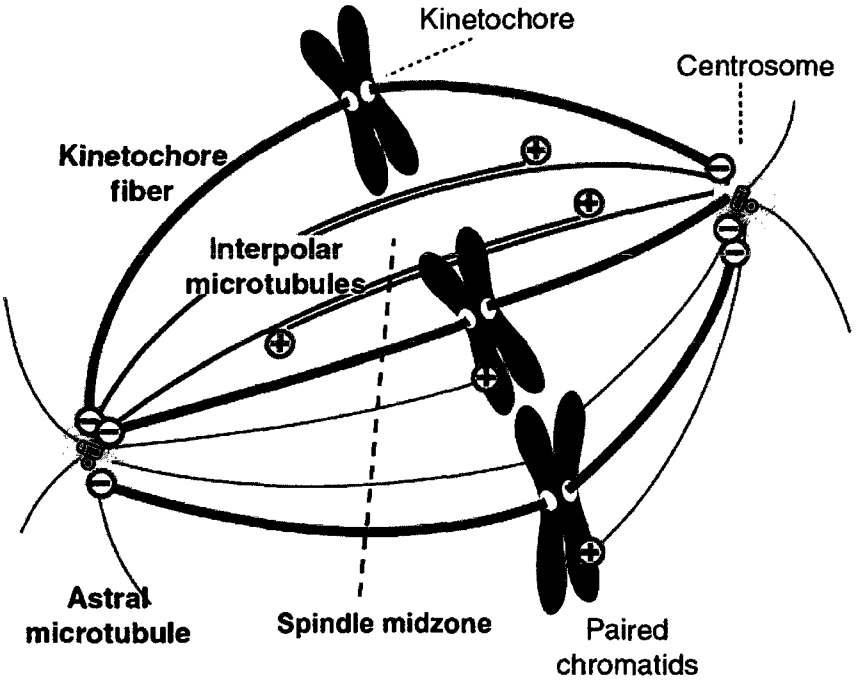

Figure 1.2: **The mitotic spindle.**
The spindle is composed of microtubules (red) anchored by their minus ends at centrosomes (green oval) and attached to kinetochores (yellow oval) at their plus ends. The attachment of 20-40 microtubules to one kinetochore results in a kinetochore-fiber (thick red line). Unattached microtubules consist of those probing for kinetochores, those interacting at the spindle midzone and forming an antiparallel array of interpolar and astral microtubules. (Figure adapted from Gadde and Heald 2004).

1.2.5 A Refined "Search and Capture" Model.

In addition to spindle poles, MT nucleation has also been observed to occur in regions proximal to kinetochores (Khodjakov et al., 2003; Maiato et al., 2004b). This kinetochore-mediated MT nucleation has been shown to depend on a gradient of a small GTPase called Ran (Carazo-Salas et al., 2001; Wilde et al., 2001). The RanGTP gradient, which in mitosis has it highest concentration near mitotic chromosomes, is established by the chromatin associated RanGEF (Guanine exchange factor) RCC1 (Carazo-Salas et al., 1999; Kalab et al., 2006; Kalab et al., 2002). Functionally, the RanGTP gradient ensures chromatin specific release of TXP2, an MT stabilizing MAP, as well as other spindle assembly factors from α-importin (Ems-McClung et al., 2004; Gruss et al., 2001; Nachury et al., 2001; Wiese et al., 2001). Interestingly, MTs nucleated in the vicinity of kinetochores orient themselves similarly to MTs nucleated by the spindle poles (minus end pointed toward the spindle pole and plus end toward the kinetochore) and subsequently become attached to kinetochores (Khodjakov et al., 2003).

In order to incorporate into the spindle, kinetochore nucleated MTs interact with MT motor proteins, such as cytoplasmic dynein and the MT cross-linker NuMa which cross-link kinetochore MTs with centrosomal MTs (Khodjakov et al., 2003; Maiato et al., 2004b). This ultimately results in transport of the kinetochore nucleated MTs along centrosomal MTs toward spindle poles where kinetochore nucleated MTs become attached to the centrosome and subsequently stabilize as k-fibers. Kinetochore nucleated MTs therefore increase the rate of k-fiber maturation and aid in mitotic spindle assembly [reviewed in (Wadsworth and Khodjakov, 2004)]. K-fiber maturation also involves alignment of mono-oriented chromosomes at the metaphase plate without the establishment of bi-polar k-MT attachment. Unattached vertebrate kinetochores have established a mechanism where they can achieve lateral attachments with mature k-fibers of other chromosomes and in doing so congress along those k-fibers toward the metaphase plate (Kapoor et al., 2006). The presence of unattached kinetochores at the metaphase plate increases their chance of establishing bi-polar k-fibers and therefore maintaining their alignment at the metaphase plate.

Taken together, the "search and capture" hypothesis has now been modified to incorporate the cooperative nature of MT nucleation, both centrosomal and acentrosomal, as well as MT-kinetochore capture, both stochastic and kinetochore driven (O'Connell and Khodjakov, 2007).

1.3 The centromere

The centromere is located at the primary constriction of mitotic chromosomes and acts as a scaffold for the assembly of kinetochores during entry into mitosis as well as a site for the cohesion of sister chromatids. Because the centromere acts as a building site for kinetochores, it is essential that only one centromere exists on each chromosome. The exception occurs on *C. elegans* chromosomes which assemble holocentric centromere/kinetochores. In human cells, multiple centromeres result in multiple kinetochore-MT attachments leading to chromosome breakage during cell division (Voullaire et al., 1999). Specification of centromere localization and number is therefore essential for proper execution of human mitosis.

1.3.1 Specification of centromere localization

The centromere is composed of heterochromatic DNA and the protein scaffold that assembles upon it. The DNA sequence that defines the centromere ranges from a specific stretch of 125 bp of the budding yeast "point" centromere to the highly complex mega-base centromeres found in mammals (Keith and Fitzgerald-Hayes, 2000; Tyler-Smith and Floridia, 2000). Apart from the point centromere of budding yeast, all other eukaryotic centromeres are defined by highly repetitive tandem sequences that associated with highly condensed heterochromatin (Henikoff et al., 2001). Interestingly, no consensus sequence has thus far been identified when comparing centromeres between species or even between chromosomes in the same cell. Instead, centromere demarcation is thought to involve epigenetic regulation [for review see (Heit et al., 2006; Vos et al., 2006)].

Epigenetics refers to the modification of chromatin structure, more specifically post translational modification of histone tails or DNA methylation (Bradbury, 1992). In terms of centromere specification, it is thought that epigenetic modifications play the central role. The biochemistry of chromatin found within centromeres has been shown to be distinctively different from the remainder of the chromosome. First, the centromere is found within regions of highly condensed heterochromatin. Second, the centromere is bordered by pericentromeric heterochromatin and constitutive heterochromatin (Sullivan, 2001). It has been shown that these regions are defined by specific epigenetic marks, such as di-methylation of histone 3 lysine-4 at the centromere, di-methylation of histone 3 lysine-9 found within the pericentromeric heterochromatin and tri-methylation of the same residue within constitutive heterochromatin (Lam et al., 2006; Sullivan and Karpen, 2004). The balance of heterochromatin and pericentromeric heterochromatin is essential for proper function of centromeres and therefore accurate chromosome segregation (Nakano et al., 2008). Last and most importantly, centromeric chromatin is defined by the presence of CENP-A, a centromere-specific histone H3 variant. Along centromere chromatin fibers, CENP-A assembles fully functional nucleosomes and is found interspersed with canonical histone 3 lysine-4 di-methylated nucleosomes (Sullivan and Karpen, 2004). CENP-A-containing nucleosomes are structurally divergent by having increased structural rigidity conferred by the CENP-A targeting domain (CATD) (Black et al., 2007a; Black et al., 2007b). This increased rigidity may be required to accommodate the extraordinary constraints placed on centromeres during mitosis, such as specialized higher order chromatin folding, kinetochore assembly, and the tension generated by mitotic spindle forces. While CENP-A is essential for determining the location of functional centromeres, and is known to be deposited at the centromere during early G1 phase (Jansen et al., 2007), the mechanism regulating its specific deposition at only one site along the chromosome, the centromere, is not known [reviewed in (Black and Bassett, 2008; Cheeseman and Desai, 2008).

1.3.2 The centromere complex

Ultimately the centromere is a complex of proteins that assembles at this specific chromosomal site in order to facilitate the subsequent assembly of the kinetochores during mitosis. Most of centromere proteins are constitutively present at these sites throughout the cell cycle and act as scaffolds for kinetochore assembly (Hemmerich et al., 2008). Centromere components in humans were first observed as the antigens of sera from patients suffering from the autoimmune disease CREST (calcinosis, Raynaud's

phenomenon, esophageal dysmotility, sclerodactyly and telangiectasia) (Earnshaw and Migeon, 1985). Interestingly, CREST sera antigens were eventually shown to include CENP-A as well as two other non-histone proteins, CENP-B and CENP-C. Since their discovery, CENP-A, B and C have been joined by 13 other characterized centromere (CENP) components (H, I, K-U) (Foltz et al., 2006; Izuta et al., 2006; Okada et al., 2006). Little is known about the individual function of each and every centromere component, however, it is apparent that each one is essential for proper assembly and function of kinetochores.

Much effort has recently been employed in understanding centromere assembly pathways, the culmination of which suggests that there are two interconnected assembly pathways [reviewed in (Vos et al., 2006)]. One is dependent on CENP-A and its interactions with a multitude of proteins contained within the constitutive centromere associated network (CCAN) (Cheeseman and Desai, 2008). The other pathway is dependent on the recruitment of the Mis12 complex through an interaction with heterochromatin associated protein 1 (HP1) that is bound to trimethylated lysine 9 on histone 3 found within the pericentromeric heterochromatin (Lachner et al., 2001; Obuse et al., 2004). The Mis12 arm of the centromere assembly pathway therefore appears to require a specific epigenetic modification of pericentromeric heterochromatin, while the CENP-A pathway relies on the specific deposition of CENP-A at centromeres (Figure 1.3). Interestingly, I have found that hMis12 centromere turnover is inhibited upon entry into mitosis (Famulski and Chan unpublished). Whether this phenomenon plays a role in hMis12-directed centromere assembly remains to be investigated. Additionally, other factors such as the siRNA machinery (specifically Dicer) and chromatin remodeling enzymes have also been shown to play a role in centromere assembly (Fukagawa et al., 2004; Peters et al., 2001). The entire process of centromere specification including the assembly of centromere components is not entirely understood and is a hot topic of investigation. The next frontier of centromere biology will likely involve high resolution structural analysis of centromeres in hopes of further understanding the function and assembly of this complex molecular scaffold.

Figure 1.3

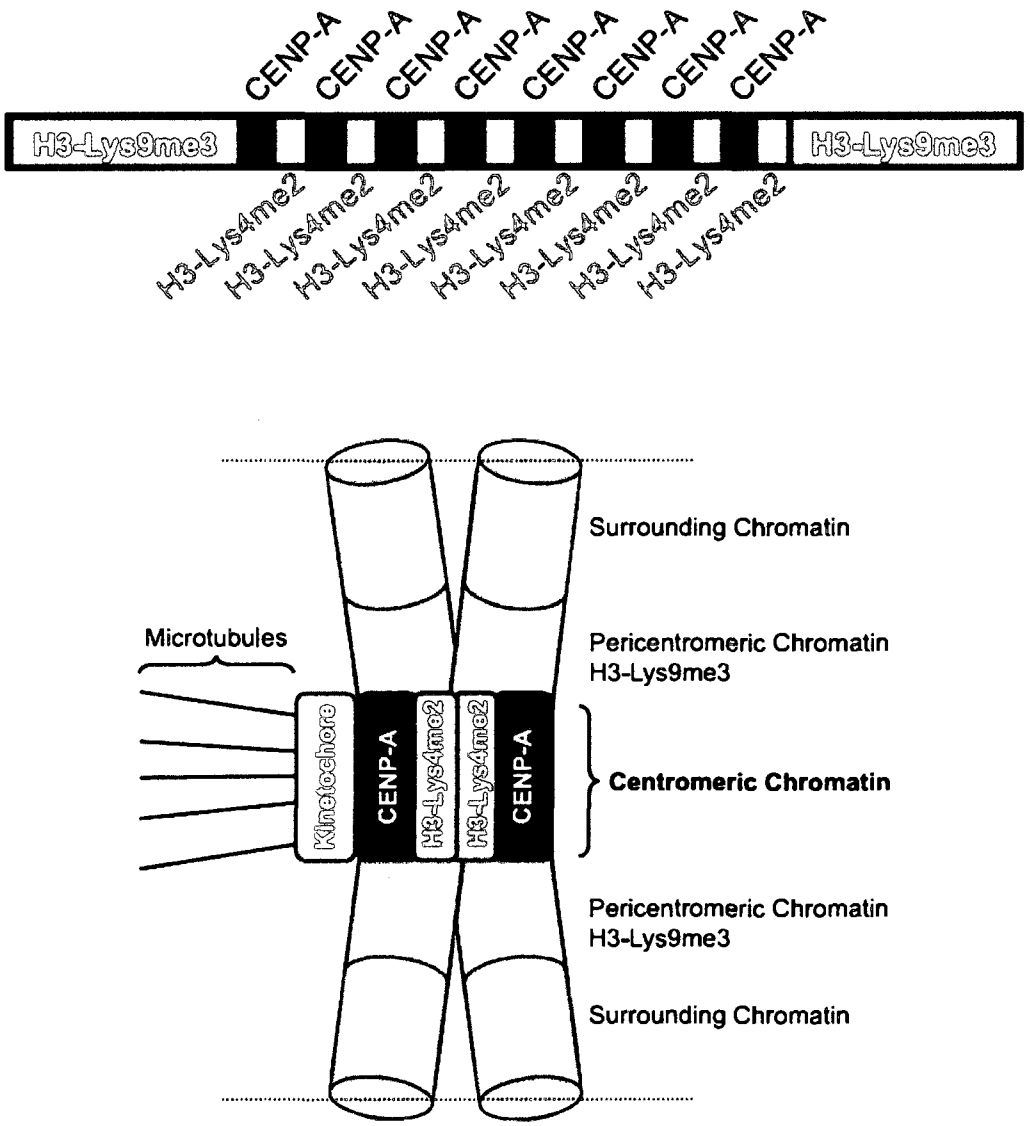

Figure 1.3: **Centromere structure.**
Top: A schematic representation of the linear distribution of CENP-A (blue) and canonical H3 nucleosomes (pink) found flanked by pericentromeric heterochromatin (green). **Bottom**: A 3D model of CENP-A and H3 nucleosome organization at centromeres. CENP-A centrosomes are predicted to face toward the spindle poles and thus specify kinetochore assembly, while the canonical H3 nucleosomes face inward. This organization is hypothesized to result from coiling of centromere nucleosomes. (Figure adapted from Vos 2006.)

1.4 The kinetochore

Kinetochores are mitosis-specific macromolecular protein complexes that assemble on centromeres during the late G2 phase of the cell cycle and that function to facilitate MT attachments to chromosomes. Kinetochores were first observed in the 1960s by the use of electron microscopy (Brinkley and Stubblefield, 1966). Structurally, vertebrate kinetochores appear as tri-laminar, disk-like structures localized to centromeric heterochromatin (Figure 1.4). The innermost layer of the kinetochore, the inner plate, interacts with the chromatin upon which the centromere is assembled. Inbetween the outer and inner layers resides the midzone, a less electron dense layer whose composition and/or function remains unknown. The remainder of the kinetochore, the outer layer, is primarily made up of protein complexes that assemble during late G2 phase, about the time of nuclear envelope breakdown (Brinkley and Stubblefield, 1966; Cooke et al., 1993; McEwen et al., 1993). Outer kinetochore protein constituents carry out the molecular functions of kinetochores, including; MT capture, sensing of k-MT attachment and correction of unproductive kinetochore-MT attachments. Extending out of the outer kinetochore layer is another functional component of kinetochores called the fibrous corona. Interestingly, under the electron microscope, the fibrous corona is only observed in the absence of MTs (Ris and Witt, 1981).

To date, over 80 human kinetochore proteins have been identified [reviewed in (Cheeseman and Desai, 2008)]. Many kinetochore components were originally identified in model organisms such as budding yeast and *D.melanogaster*, and a majority of them have been shown to be conserved amongst higher eukaryotes. Upon the completion of mitosis, kinetochores are disassembled through a yet-to-be identified mechanism that may involve components of nuclear pore complexes (Franz et al., 2007).

Assembly of the outer kinetochore and the fibrous corona depends on a temporally regulated, highly complex and poorly understood interconnected network of protein-protein interactions [reviewed in (Chan et al., 2005; Cheeseman and Desai, 2008; Maiato et al., 2004a; Vos et al., 2006)]. Metazoan kinetochores are hypothesized to assemble as repeated subunits on the interspersed CENP-A containing centromere nucleosomes (Sullivan and Karpen, 2004; Zinkowski et al., 1991). Mis12 has also been shown to be essential for proper kinetochore assembly and is hypothesized to act as a 'keystone' that is required to specify kinetochore assembly to centromeric heterochromatin (Cheeseman and Desai, 2008; Kline et al., 2006). Downstream of CENP-A and Mis12, kinetochore assembly involves the CCAN and the KNL-1-Mis12-Ndc80 (KMN) network (Cheeseman and Desai, 2008). KNL-1 and the Ndc80 complex (Ndc80/Hec1, Nuf2, Spc24, Spc25) are both highly conserved and essential kinetochore components [reviewed in (Kline-Smith et al., 2005)]. CENP-C, H, I and K, components of the CCAN, are all known to be required for proper assembly of the outer kinetochore (Liu et al., 2003b; Liu et al., 2006), while the KMN network is known to interact with outer kinetochore as well as fibrous corona proteins (Cheeseman et al., 2004; Desai et al., 2003). The KNL-1, Mis12 and the Ndc80 complexes therefore bridge the centromere, with the outer kinetochore and fibrous corona during kinetochore assembly (Cheeseman et al., 2008; Cheeseman et al., 2004). Although our knowledge of the composition of kinetochores has greatly increased in the last decade, we still can only speculate as to the order and interactions involved when kinetochores assemble *in vivo*.

Figure 1.4

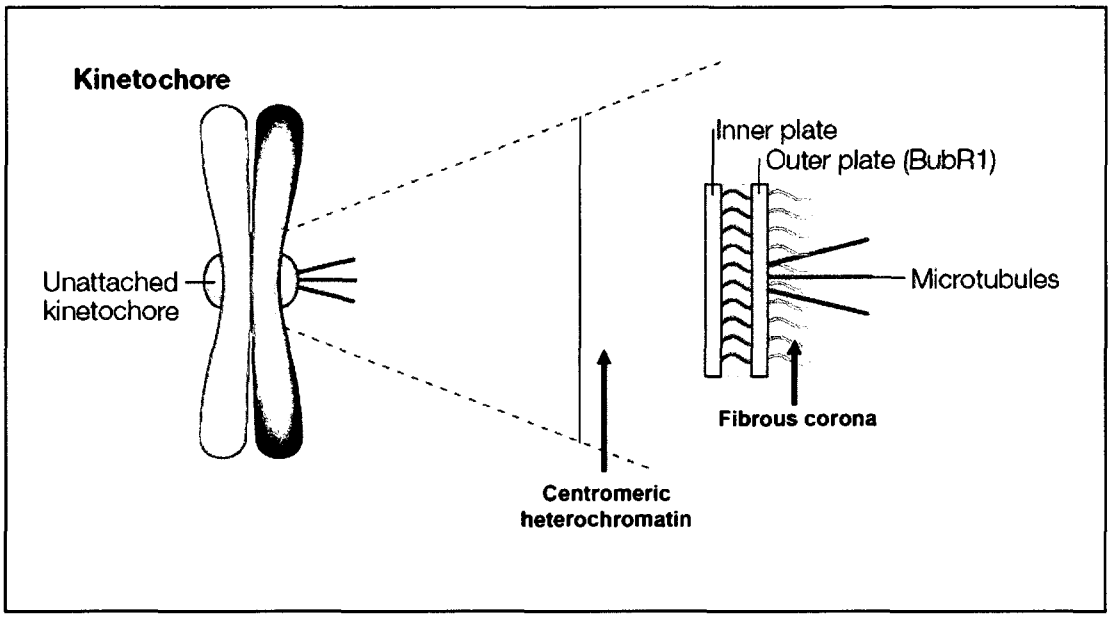

Figure 1.4: **Geography of the mammalian kinetochore.**
Using electron microscopy, the mammalian kinetochore has been observed as a proteinaceous tri-laminar disk structure that assembles on centromeric heterochromatin. Kinetochores are composed of three distinct plates, the inner, the outer, a middle translucent layer as well as the fibrous corona. The centromeric heterochromatin contains constitutive components of centromeres. The inner plate contains many kinetochore proteins that in turn recruit mitotic checkpoint regulators as well as MT motor proteins to kinetochores. The outer plate contains the regulators and effectors of the mitotic checkpoint. The fibrous corona is the site of kinetochore MT capture. The kinetochore as a whole functions to capture MTs as well as regulate mitotic checkpoint signaling. (Figure adapted from Musacchio and Hardwick 2002.)

1.5 Kinetochore-MT attachment

The ultimate function of kinetochores is to capture and attach to spindle MTs. In doing so, kinetochores ensure that upon the completion of mitosis, chromosomes can be equally segregated into two daughter cells. MT capture and attachment are known to involve MT binding proteins and complexes found at the fibrous corona. Kinetochore-MT attachments can occur as either end-on or lateral attachments; however, only end-on attachments mature into k-fibers.

1.5.1 Lateral attachments

Lateral k-MT attachments occur soon after nuclear envelope breakdown, when chromosomes are observed to initiate movements toward the spindle poles (Rieder and Alexander, 1990). The dynein/dynactin MT motor complex has been hypothesized to generate lateral kinetochore-MT attachments and drive subsequent chromosome movement toward the spindle poles (Sharp et al., 2000; Yang et al., 2007b). Dynein/dynactin is a minus-end-directed MT motor, and as such, it can drive the transport of the kinetochores toward the minus ends of MTs anchored at the spindle poles. Once near the spindle pole, kinetochores are more likely to encounter spindle MTs and establish the end-on attachments that lead to k-fiber maturation (Hayden et al., 1990). However, after initially being positioned close to only one spindle pole, chromosomes can be delayed in achieving bi-polar k-MT attachment. In order to overcome this problem, mono-polar attached chromosomes can actually congress to the metaphase plate without bi-polar k-MT attachment (Kapoor et al., 2006). Interestingly, this again requires lateral kinetochore-MT attachments of the kinetochore associated MT plus end directed kinesin CENP-E. Kinetochore bound CENP-E laterally attaches to k-fibers of already aligned chromosomes and uses those k-fibers to drive kinetochores toward the metaphase plate (Kapoor et al., 2006). Once at the metaphase plate, monopolar attached kinetochores are more likely to encounter MTs and establish end-on bi-polar k-MT attachments and therefore complete chromosome alignment.

1.5.2 End-on attachments

Only end-on k-MT attachments will mature into k-fibers with the necessary strength to align and segregate chromosomes. End on attachment is therefore essential for proper mitotic spindle function and chromosome segregation. There are several kinetochore bound MT binding proteins that are known to be involved in end-on attachment.

Kinetochore bound CENP-E and dynein/dynactin are throught to be involved in end-on attachments. Cells depleted of CENP-E are known to suffer defects in chromosome alignment as well as k-MT attachment (McEwen et al., 2001). Furthermore, the CENP-E binding partner hBubR1 (discussed in detail in section 1.7.3) has also been shown to play a role in k-MT attachment (Lampson and Kapoor, 2005). Kinetochore dynein/dynactin on the other hand, appears to not to be required for k-MT capture but more likely stabilzes end-on k-MT attachments (Yang et al., 2007b). Apart from dynein/dynactin and CENP-E, there are several other kinetochore associated MT binding proteins, including; CLIP170, CLASP, EB1, Sgo1 and APC (adenomatous polyposis coil). Although they all bind MTs, they are mostly involved in the regulation of polymerization and depolymerization of already attached kinetochore-MTs and not generation of end-on attachments [reviewed in (Galjart, 2005; Maiato et al., 2004a)].

Any single MT binding protein found at kinetochores cannot account for stable end-on k-MT attachment. Instead, recent evidence has pointed to a 'core' kinetochore-MT attachment site, known as the KMN network, which involves the cooperation of the KNL-1, Mis12 and the Ndc80 complexes. Both KNL-1 and Ndc80 are known to be required for k-MT attachment (Desai et al., 2003; McCleland et al., 2003; Wigge and Kilmartin, 2001). In fact, Ndc80 loss of function is known to elicit one of the most severe loss of k-MT attachment phenotypes (DeLuca et al., 2005). Individually, the components of the KMN network have weak MT binding activities, however; as a complex, their ability to bind MTs is synergistically increased (Cheeseman et al., 2006). Structurally, the Ndc80 complex forms a globular head (composed of Ndc80 and Nuf2) that localizes to the outer kinetochore and directly binds MTs while a rod domain (Spc24 and Spc25) resides closer to the inner kinetochore (Wei et al., 2007). Although the interaction of Ndc80/Nuf2 with MTs is direct, their binding is relatively weak. At the inner kinetochore, the Ndc80 complex is known to interact with the CCAN, KNL-1 and Mis12 complex. KNL-1, which is also highly conserved, can directly bind to MTs, but just like the Ndc80 complex its MT binding is also relatively weak (Cheeseman et al., 2006). The Mis12 complex on the other hand does not bind MTs but is essential for 'core' MT binding. In fact, cooperativity of the weakly binding KNL-1 and Ndc80 complex in conjunction with the Mis12 complex is what generates the 'core' kinetochore MT binding site.

It is predicted that numerous kinetochore associated KMN complexes bind to a single MT and therefore further increase the cooperativity and synergism leading to a stable k-MT attachment (Cheeseman and Desai, 2008). Interestingly, the mechanism of 'core' k-MT attachment is conserved between single k-MT binding kinetochores and those that bind multiple MTs, suggesting that the more complex kinetochores of vertebrates are simply repeat subunits of single MT binding site (Joglekar et al., 2008). Based on current knowledge, the KMN network may in fact represent the 'core' MT binding site, however, the other kinetochore associated MT binding proteins surely also contribute to k-MT attachment. Future research into the regulation of k-MT attachments is therefore still required in order to understand the interplay of all of the kinetochore bound MT binding proteins.

1.6 The Mitotic Checkpoint

Mechanistically, the key event during chromosome segregation is the alignment of all chromosomes at the spindle equator. As outlined previously, chromosome alignment requires bi-polar k-MT attachment and k-fiber maturation. However, kinetochore-MT capture is a stochastic process that often leads to non-productive connections which delay chromosome alignment. The premature onset of anaphase in the presence of unaligned chromosomes leads to aneuploidy and/or cell death. Chromosome instability (CIN) is a hallmark of many human cancers and is often the result of errors occurring during chromosome segregation [reviewed in (Kops et al., 2005b)]. In order to avoid CIN, eukaryotic cells have evolved a surveillance mechanism that prevents the onset of anaphase until all chromosomes are properly aligned at the metaphase plate (Figure 1.5). This surveillance mechanism is called the mitotic or spindle assembly checkpoint (Musacchio and Salmon, 2007; Nicklas, 1997; Rieder et al., 1994).

Figure 1.5

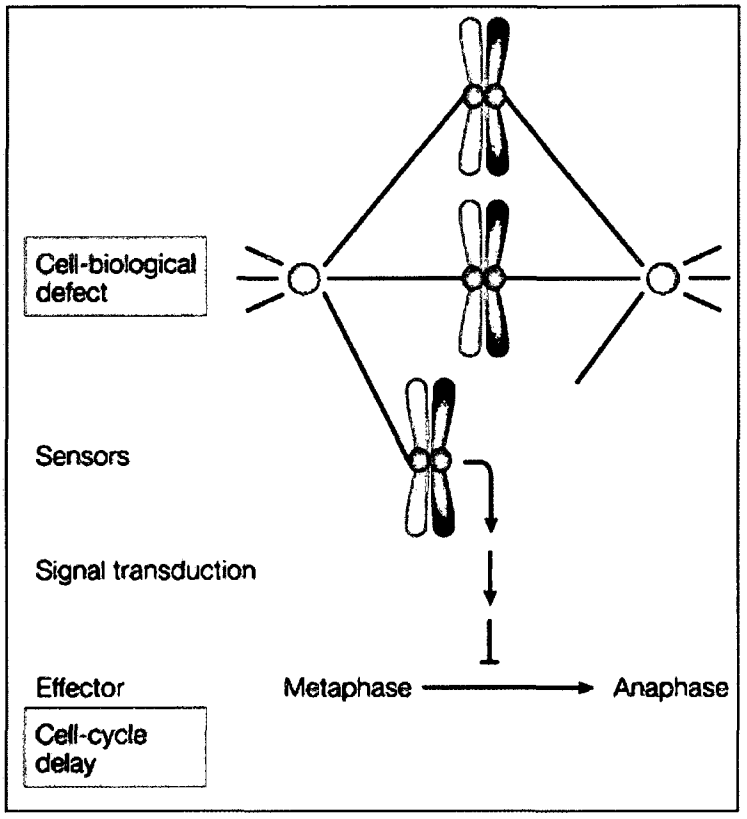

Figure 1.5: **Mitotic checkpoint signaling.**
The mitotic checkpoint monitors defects during chromosome alignment in order to prevent anaphase onset in the presence of unaligned chromosomes. Different sensors found at kinetochores monitor for kinetochore-MT attachments as well as chromosome alignment. In the absence of either, the sensors activate a signal transduction pathway that leads to the activation of the effector. Activity of the effector results in cell cycle arrest. (Figure adapted from Musacchio and Hardwick 2002.)

Early live cell imaging studies indicated that mitotic cells containing chromosomes that are monooriented or unattached to MTs do not proceed into anaphase and do not segregate their chromosomes (Rieder et al., 1994). Furthermore, inhibition of mitotic spindle assembly, mutation of centromeric DNA, or modification of MT dynamics were all known to inhibit the progression of mitotic cells into anaphase (Jordan et al., 1992; Sluder, 1979; Sluder and Begg, 1983; Spencer and Hieter, 1992). Based on such studies, it was hypothesized that a negative feed-back checkpoint mechanism regulates the timing of anaphase entry by monitoring the bi-orientation of all chromosomes (McIntosh, 1991). However, it wasn't until the discovery of the first mitotic checkpoint components that the notion of mitotic checkpoint function during mitosis was finaly accepted. Two independent pioneering genetic screens of the budding yeast *S. cerevisiae* identified the **m**itotic **a**rrest **d**eficient, MAD1, MAD2 and MAD3 (BubR1 in higher eukaryotes), and **b**udding **u**ninhibited by **b**enzimidazole, BUB1 and BUB3 mitotic checkpoint genes (Hoyt et al., 1991; Li and Murray, 1991). Both screens were designed to isolate mutations conferring escape from mitotic arrest induced by disrupted MT function. Exit from mitosis in the presence of MT inhibitors indicates a failure of the mitotic checkpoint and is the classic mutant phenotype of mitotic checkpoint genes. Since their discovery, MAD and BUB homologues have been characterized in frogs, flies, worms, mice as well as humans (Basu et al., 1998; Chen et al., 1996; Kitagawa and Rose, 1999; Li and Benezra, 1996; Taylor and McKeon, 1997). The mitotic checkpoint is therefore evolutionarily conserved. In addition to the MADs and BUBs, several other highly conserved mitotic checkpoint proteins have been identified. In general, mutations of mitotic checkpoint proteins result in premature segregation and consequently missegregation of chromosomes, also known as aneuploidy. Due to the catastrophic consequences of aneuploidy, vertebrate mitotic checkpoint components are essential for life (Baker et al., 2004; Dobles et al., 2000; Iwanaga et al., 2007; Kalitsis et al., 2000). Interestingly, in budding yeast and in the fruit fly *D. melanogaster*, the mitotic checkpoint is only necessary for viability when mitotic spindle damage is present (Buffin et al., 2007).

1.6.1 Mandate of the Mitotic Checkpoint

In order to ensure accurate chromosome segregation, the mitotic checkpoint monitors kinetochore-MT attachments as well as chromosome alignment. The checkpoint activates upon nuclear envelope breakdown and mediates a metaphase arrest in order to allow the cell time to establish bi-polar kinetochore-MT attachment and to complete chromosome alignment. Once both k-MT attachment as well as alignment of all the chromosomes is achieved, the checkpoint is silenced and the cell can proceed into anaphase (Figure 1.5).

Since k-MT attachments are central to ensuring accurate chromosome segregation, kinetochores were predicted as sites of mitotic checkpoint function. Any doubts of this prediction were erased by elegant laser microsurgery experiments showing that even a single unattached kinetochore can signal mitotic checkpoint arrest in living cells (Rieder et al., 1995). Furthermore, bona fide mitotic checkpoint components, such as the MADs and BUBs were shown to localize to and function at unattached vertebrate kinetochores (Chen et al., 1998; Chen et al., 1996; Li and Benezra, 1996; Taylor et al., 1998; Taylor and McKeon, 1997). In fact, all known essential mitotic checkpoint proteins, except for yeast Mad3, are known to localize to and function at kinetochores.

Kinetochore-MT attachments are directly monitored by MT binding kinetochore components such as CENP-E/BubR1 and dynein/dynactin (discussed in detail later). In addition, unattached kinetochores exhibit higher amounts of mitotic checkpoint proteins than those that are attached (Hoffman et al., 2001). For example, the mitotic checkpoint proteins Mad1 and Mad2 are known to localize to unattached kinetochores while they rapidly dissociate from kinetochores upon the establishment of k-MT attachments (Chen et al., 1996; Howell et al., 2000; Li and Benezra, 1996). The presence of high levels of mitotic checkpoint proteins at kinetochores therefore corresponds with checkpoint activity. The binding of MTs to kinetochores is in turn hypothesized to reduce the number of binding sites for checkpoint proteins and thus decrease checkpoint signaling (Burke and Stukenberg, 2008).

In addition to k-MT attachment, the mitotic checkpoint also monitors for chromosome alignment. This relies on the phenomenon of inter-kinetochore tension. Sister kinetochores that have achieved bi-polar k-MT attachments are physically under tension generated by the MTs attached to opposing spindle poles. Sister kinetochores of aligned chromosomes are therefore actually further apart, up to two times further, than those at monopolar or unattached chromosomes (Goshima and Yanagida, 2000; He et al., 2000; Tanaka et al., 2000; Waters et al., 1996). This change in the inter-kinetochore distance is referred to as inter-kinetochore tension. Inter-kinetochore tension is the mechanical readout of chromosome alignment and is therefore an essential component of the mitotic checkpoint [reviewed in (Pinsky and Biggins, 2005; Zhou et al., 2002)]. Inter-kinetochore tension has also been shown to enhance k-MT stability and overall MT occupancy at kinetochores (King and Nicklas, 2000).

Mitotic checkpoint response to kinetochore tension was first discovered in budding yeast. The loss of cohesin function resulted in chromosomes that could attach MTs, but could not establish tension during mitosis (Stern and Murray, 2001). In these cells the mitotic checkpoint was activated and the cells remained arrested in mitosis. The presence of a tension-sensitive checkpoint response in metozoans was elegantly proven through micro-needle manipulations of sex chromosomes in living cells (Nicklas et al., 1995). When kinetochores were placed under tension, the cells were able to exit mitosis. However, in the absence of tension the cells remained arrested until the tension was restored. Furthermore, the authors also showed that the presence of tension directly resulted in biochemical signaling through the de-phosphorylation of the kinetochore bound mitotic checkpoint protein hBubR1 (Nicklas et al., 1995; Wong and Fang, 2007). Furthermore, it has been shown that mitotic checkpoint proteins such as hBubR1 and hBub1 respond to the loss of inter-kinetochore tension by accumulating at tension-less kinetochores (Skoufias et al., 2001). Lack of inter-kinetochore tension often results from improper k-MT attachments. These types of attachments include syntelic attachments, where both sister kinetochores attach to MTs emanating from a single spindle pole, and merotelic attachments, where one kinetochore is bound to MTs emanating from both spindle poles while the other kinetochore is bound to MTs from only one spindle pole. It has been shown that the mitotic kinase Aurora B (discussed in detail later) is responsible for the correction of these improper attachments during mitosis [reviewed in (Salmon et al., 2005)].

1.6.2 Mitotic Checkpoint Proteins

Mitotic checkpoint proteins are believed to function within three major components of the checkpoint (Chan and Yen, 2003). The first is a kinetochore bound mechanosensor that directly monitors for kinetochore-MT attachment as well as chromosome alignment. This mechanosensor generates a "wait anaphase" signal in the absence of kinetochore-MTs and/or chromosome alignment at the spindle equator. The second is a signal amplification cascade that globally amplifies the wait anaphase signal. And the third is the actual biochemical activity that is activated by the amplification cascade and that directly mediates checkpoint induced metaphase arrest.

Not surprisingly, mitotic checkpoint proteins assemble and function at kinetochores. Furthermore, activity of the checkpoint has been correlated with the levels of checkpoint proteins found on kinetochores. Kinetochores are the sites of MT attachment and as such are the optimum site for the localization of the molecular sensors that monitor k-MT attachments. Up to 80 proteins have thus far been classified as components of the human kinetochore (Cheeseman and Desai, 2008). These can be further subcalsified as structural components, typically found on the centromere or the inner plate of the kinetochore; regulatory proteins, typically found on the outer plate and the fibrous corona; and finally MT motor proteins which are also found in the fibrous corona. Structural components of kinetochores, such as the Ndc80 complex, are known to be stable residents of kinetochores (Hori et al., 2003). On the other hand, many of the regulatory components of the mitotic checkpoint, such as hMad2 and hBubR1 are known to be dynamic residents of kinetochores, implying that kinetochore turnover plays a role in mitotic checkpoint signaling (Howell et al., 2004; Shah et al., 2004). Interestingly, only a small subset of kinetochore proteins are actually mitotic checkpoint proteins. In human cells these include: hMad1, hMad2, hBub3, Blinkin, the Ndc80 complex, and the RZZ complex (discussed in detail later); the mitotic kinases: hAurora B, Cdk1, hMps1, hPlk1, hNEK2, hBubR1 (MAD3 human homologue), and hBub1; and finally the kinetochore associated MT motor proteins hCENP-E and dynein/dynactin [reviewed in (Chan et al., 2005; Maiato et al., 2004a; Musacchio and Salmon, 2007)]. All of the remaining kinetochore components are thought to ensure the proper assembly of the outer kinetochore as well as the 'core' MT binding site.

1.6.3 Target of the Mitotic Checkpoint

In order to prevent premature sister chromatid segregation, the mitotic checkpoint directly regulates the degradation of both cyclin B and the anaphase inhibitor securin. When polyubiquitinated, cyclin B and securin are degraded by the 26S proteosome. Polyubiquititaion of cyclin B and securin is mediated by the Anaphase Promoting Complex/Cyclosome (APC/C), an E3 ubiquitin ligase complex that specifically targets cyclin B as well as securin for polyubiquitination. In order to control the timing of cyclin B and securin degradation and therefore anaphase onset, APC/C activity is negatively regulated by the mitotic checkpoint.

Cdk1 kinase activity is required for many events during mitosis. However, in order to initiate anaphase and exit mitosis, Cdk1 kinase activity must first be inactivated. Cyclin B is required for the activity of the Cdk1 kinase, and consequently cyclin B levels are known to rise upon entry into mitosis and decrease sharply upon anaphase onset (Murray and Kirschner, 1989; Murray et al., 1989). The decline of cyclin B levels at anaphase onset results from ubiquitin-mediated proteosome degradation (Glotzer et al.,

1991). The presence of non-degradable cyclin B mutants results in permanent mitotic arrest and therefore signifies the importance of Cdk1 inactivation for exit from mitosis (Chang et al., 2003).

Securin, on the other hand, plays a direct role in the physical segregation of chromosomes by regulating the cleavage of cohesin (Figure 1.6). Cohesin is a protein complex required for the physical attachment between sister chromatids [reviewed in (Nasmyth, 2002)]. After DNA replication, the entire lengths of chromosomes are joined by cohesin complexes. However, by the time cells enter mitosis, cohesin complexes dissociate from chromosome arms and are found exclusively at the centromeres (Sumara et al., 2000; Waizenegger et al., 2000). The persistence of cohesin at centromeres is believed to be required during chromosome alignment in order to prevent the opposing MT generated forces from tearing apart the two sister chromatids (Tanaka et al., 2000). In order to initiate anaphase, the cohesin complex is cleaved by the enzyme separase, allowing MT-generated forces to segregate sister chromatids to the opposite spindle poles (Hauf et al., 2001; Uhlmann et al., 2000). To ensure timely cleavage of cohesin, separase remains inhibited by a chaperone protein called securin (Jallepalli et al., 2001). Securin, also known as Pds1 and Sic1, was identified as an inhibitor of anaphase in yeast and is highly conserved in eukaryotes (Cohen-Fix et al., 1996; Funabiki et al., 1996a; Funabiki et al., 1996b). Similar to cyclin B, securin was also shown to be degraded through the ubiquitin-mediated proteosome degradation pathway (Holloway et al., 1993). The function of separase therefore remains in check until securin is degraded in order to prevent premature segregation of sister chromatids.

Both securin and cyclin B contain a stretch of amino acids termed the destruction box (D-box), which targets proteins for ubiquitin mediated proteosome degradation (Glotzer et al., 1991). Ubiquitin-mediated proteosome degradation is an enzymatic pathway in which the assembly of ubiquitin polypeptide chains on target substrates leads to degradation by the 26S proteosome [reviewed in (Hershko, 1991)]. Polyubiquitination typically requires three enzymes called E1, E2 and E3. The E1 enzyme interacts with ubiquitin and transfers it onto the E2 or ubiquitin conjugating enzyme (UBC). The E2 enzyme transfers the ubiquitin onto a target substrate forming a peptide bond, however, the E2 must first complex with the E3 enzyme, also known as the ubiquitin ligase. The E3 ligase enzyme is the rate limiting step as is responsible for target substrate recognition. Once the target is mono-ubiquinated, polyubiquitination results from subsequent cycles of ubiquitination of the ubiquitin residue it self. Since substrate specificity and regulation of the ubiquitin-mediated proteosome degradation pathway rests upon the E3 enzymes, inhibition of APC/C E3 ligase activity is a perfect target for the mitotic checkpoint. By inhibiting the APC/C, the checkpoint can prevent securin and cyclin B and degradation and thus delay sister chromatid separation and exit from mitosis.

Figure 1.6

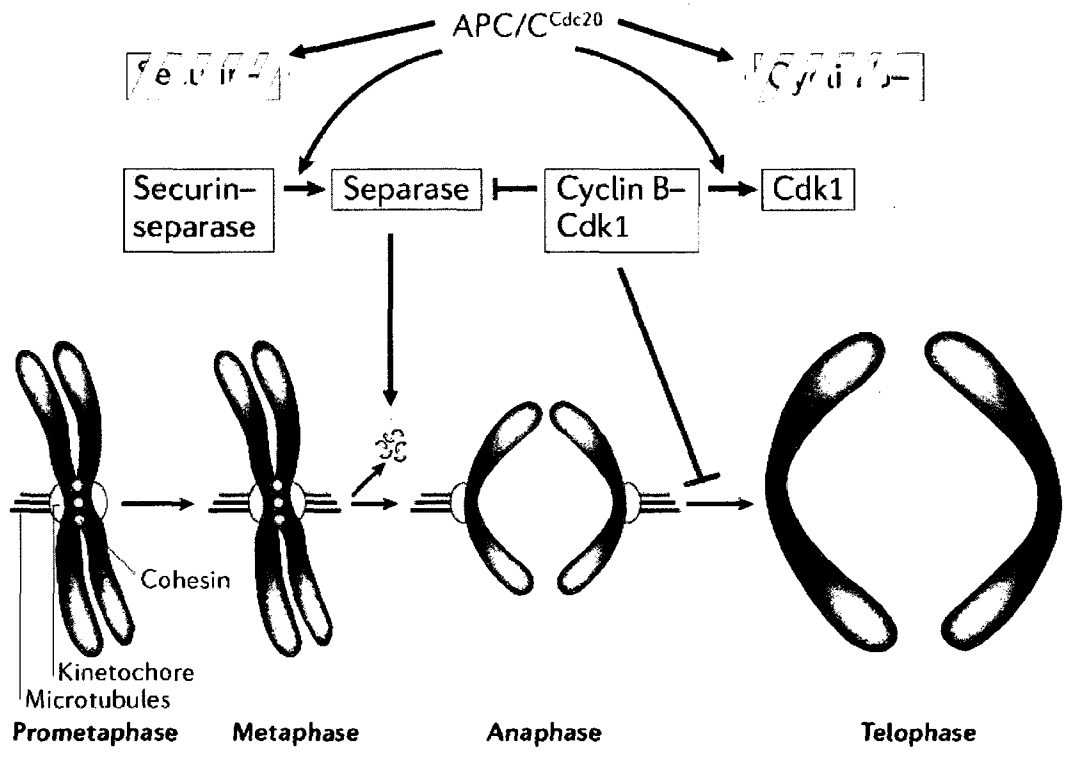

Figure 1.6: **APC/C regulation of chromosome segregation and mitotic exit.**
Upon entry into mitosis cohesin complexes (red circles) are exclusively found at centromeres. During prometaphase and metaphase centromere associated cohesin ensures integrity of the chromosome by preventing microtubule (green lines) induced separation of the two sister chromatids. At the same time, separase is inactivated by securin (blue securin-separase) and Cdk1 is activated by Cyclin-B (red Cyclin-B-Cdk1) which maintains the cell in mitosis. Once the APC/C^{Cdc20} is active, securin and cyclin B are ubiquitinated and subsequently degraded (dashed boxes), thus activating separase (red colored separase) and deactivating Cdk1 (blue colored Cdk1). Active separase cleaves the cohesin complex and thus releases the two sister chromatids which can now be segregated toward the opposite spindle poles. The inactivation of Cdk1 activity allows the cell to exit mitosis. (Figure adapted from Peters 2006.)

The APC/C was discovered as the E3 component required for the ubiquitin-mediated proteosome degradation of cyclin B (King et al., 1995; Sudakin et al., 1995). It is a 12 subunit, 1.5 MDa enzyme complex that assembles throughout the cell cycle and is conserved from yeast to human [reviewed in (Peters, 2006)]. The APC/C associates with two E2 enzymes, UBCH5 and UBCH10, of which UBCH10 is essential for APC/C function in mitosis (Townsley et al., 1997). In addition to the 12 core subunits, the APC/C also associates with cell cycle-specific regulators of its ligase activity called Cdc20 and Cdh1 (these complexes are referred to as APC/C^{cdc20} or APC/C^{cdh1}) (Fang et al., 1998b; Schwab et al., 1997; Visintin et al., 1997). It has been shown that Cdc20 and Cdh1 can directly bind to the APC/C and activate its ubiquitin ligase activity. While Cdh1 is required for APC/C function in the G1 phase of the cell cycle, it is Cdc20 that is required for the APC/C to target cyclin B and securin during mitosis (Fang et al., 1998b; Pfleger and Kirschner, 2000).

1.6.4 Cdc20, the Key to the Checkpoint

Cdc20 was originally isolated as a yeast mutant that failed to initiate anaphase and thus arrested in mitosis (Hartwell et al., 1973). The protein encodes a WD40 motif similar to the β subunit of trimeric G proteins containing seven-bladed β propeller structures that are known to mediate protein-protein interaction [reviewed in (Yu, 2007)]. Cdc20 is highly conserved among eukaryotes both structurally and functionally. Cdh1 (Cdc20 homolog 1) shares the same functional properties as Cdc20, but is known to mediate APC/C targeted degradation of substrates distinctively different from those targeted by APC/C^{cdc20} (Fang et al., 1998b; Pfleger and Kirschner, 2000). Moreover, APC/C^{cdc20} and APC/C^{cdh1} substrates have been shown *in vitro* to have different targeting sequence motifs (Fang et al., 1998b). As such, the Cdc20 family of proteins serve as substrate-specific activators of the APC/C during the cell cycle. The association of Cdh1 and Cdc20 with the APC/C is tightly regulated throughout the cell cycle by both phosphorylation and protein degradation [reviewed in (Yu, 2007)] (Figure 1.7). First, upon mitotic entry, when Cdk1 activity is high, Cdk1 phosphorylates certain APC/C subunits, and this enables more efficient binding of Cdc20 to the APC/C (Kraft et al., 2003). Furthermore, Cdk1 also phosphorylates Cdh1 and in doing so prevents activation of APC/C^{cdh1} (Zachariae et al., 1998). These phosphorylation events ensure that APC/C^{cdc20} is the prevalent form of active APC/C during mitosis. Upon entry into anaphase, APC/C^{cdc20} selectively targets securin and cyclin B for degradation, leading to sister chromatid segregation and inactivation of the Cdk1 kinase. At this point, APC/C^{cdh1} is no longer inhibited and now functions to target Cdc20 for degradation (Prinz et al., 1998; Reis et al., 2006). In doing so, APC/C^{cdh1} now becomes the prominent functional APC/C. By the time the cell re-enters G1 phase of the cell cycle, only APC/C^{cdh1} activity remains.

Several biochemical assays have shown that the quintessential mitotic checkpoint proteins Mad2 (Fang et al., 1998a) and BubR1 (Mad3) (Fang, 2002; Tang et al., 2001) can directly bind Cdc20 and in doing so inhibit the ligase activity of the APC/C^{cdc20}. These assays have therefore branded Cdc20 as the key molecular target of the mitotic checkpoint. In the absence of k-MT attachment or chromosome alignment, the checkpoint inhibits the function of the APC/C by directly inhibiting its activator, Cdc20. Currently there are several proposed molecular pathways for how the mitotic checkpoint signals direct inhibition of Cdc20; these will be discussed in sections 1.6.5 and 1.6.6..

Figure 1.7

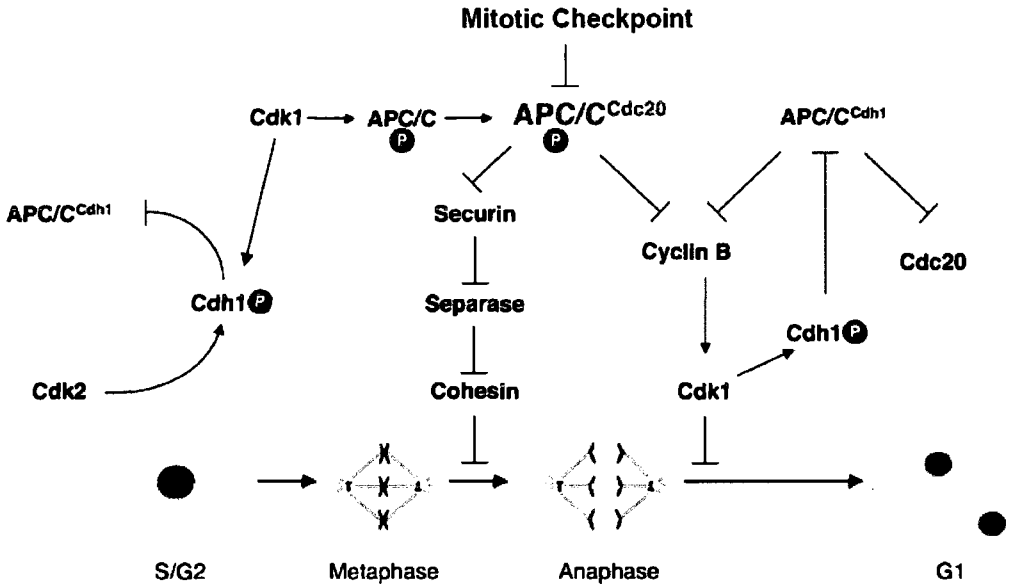

Figure 1.7: **Regulation of APC/C^{Cdc20} activity throughout mitosis.**
Upon entry into mitosis, Cdk2 phosphorylates (purple oval) Cdh1 and inhibits APC/C^{Cdh1}. In early mitosis, Cdk1 and other mitotic kinases phosphorylate the APC/C, promoting its binding to Cdc20. Furthermore, Cdk1 phosphorylates Cdh1 to further prevent the activation of APC/C^{Cdh1}. Inactivation of the spindle checkpoint allows activation of APC/C^{Cdc20}, which promotes the degradation of securin and cyclin B. This in turn leads to the activation of separase, cleavage of cohesin, and anaphase onset. APC/C^{Cdc20}-dependent degradation of cyclin B reduces Cdk1 activity, resulting in the dephosphorylation of Cdh1 and activation of APC/C^{Cdh1} in late anaphase. APC/C^{Cdh1} then orchestrates the degradation of a wide spectrum of substrates, facilitating mitotic exit and cytokinesis. (Figure adapted from Yu 2007.)

1.6.5 The Mad2 Template Model

In vitro, Mad2 can directly bind to Cdc20 and prevent APC/C activation. The inhibition of APC/C activity by Mad2 has been hypothesized to occur either directly while in complex with Cdc20, or through the sequerastation of Cdc20 away from the APC/C.

Mad2 is recruited to unattached kinetochore through its direct association with Mad1 (Chen et al., 1999; Chen et al., 1998). Calculations of Mad2 kinetochore dynamics revealed that 50% of Mad2 is stably bound to kinetochores, while the other 50% actively exchanges with the cytoplasmic pool (Shah et al., 2004). Kinetochore Mad1 on the other hand is totally stable (Howell et al., 2004). Mad2 is known to inhabit two conformation states, Mad2-O (open) or Mad2-C (closed) (Luo et al., 2004). These conformation states refer to the position of flexible domain within Mad2 that regulates its interaction with Mad1 and Cdc20. During mitosis most Mad2-C is bound to either Mad1 or Cdc20, thus making Mad2-O the most prevalent form of free Mad2 (Chung and Chen, 2002). *In vitro*, Mad2-C has a higher affinity to Cdc20, and is a more potent inhibitor of Cdc20 than Mad2-O (Luo et al., 2002). Mad2-O is converted into Mad2-C upon interaction with Mad1 (Luo et al., 2002), Interestingly, it has been shown that Mad2-C in complex with Mad1 can dimerize with Mad2-O and this dimerization can induce the conversion of Mad2-O to Mad2-C (De Antoni et al., 2005; Nezi et al., 2006). This conversion of Mad2-O to Mad2-C now enables the interaction of Mad2-C with Cdc20.

By taking together the observed kinetochore dynamics and the biochemical interactions of Mad2, the 'template model' for Mad2-mediated mitotic checkpoint inhibition of Cdc20 has been proposed (Figure 1.8). It predicts that the stably bound kinetochore pool of Mad2 in fact represents the Mad1-Mad2-C kinetochore complex, while the dynamic pool of kinetochore Mad2 represents the Mad2-C molecule that is generated from the dimerization of Mad1-Mad2-C with Mad2-O (Vink et al., 2006). The dynamic pool of Mad2-C is predicted to interact with Cdc20, dissociate from the Mad1-Mad2-C kinetochore complex and inhibit APC/C activity (Mapelli et al., 2006; Musacchio and Salmon, 2007). In support of this model both hCdc20 and hMad2 actively exchange at kinetochores, and with similar dynamics (Howell et al., 2004). Lastly, the dimerization between Mad2-C and Mad2-O also occurs when Mad2-C is complexed with Cdc20. The template model therefore also predicts that the interaction between Mad2-C with Cdc20 further amplifies the level of Mad2-C that is available to bind and inhibit Cdc20 (De Antoni et al., 2005). This then leads to exponential amplification of Mad2-C, a prion-like property of Mad2, and may explain the rapid and global inhibition of APC/C during mitosis (Chan et al., 2005). Ultimately, the template model provides a molecular framework for how unattached kinetochores can convert cytosolic Mad2 into an active form that can interact with Cdc20 and globally inhibit the APC/C. Silencing of the mitotic checkpoint may also hinge on the principles of the "template" model and will be discussed in section 1.9.2.

Figure 1.8

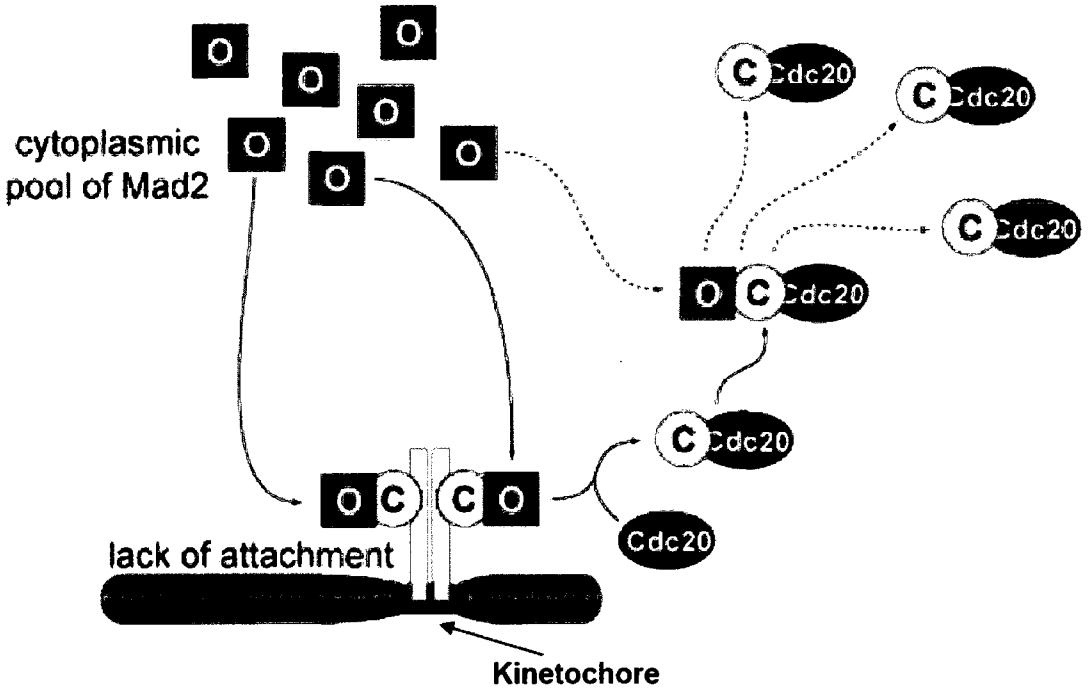

Figure 1.8: **The Mad2 template model.**
Kinetochore bound Mad1 (grey bar)-Mad2-C (yellow oval) complex is able to recruit a cytoplasmic Mad2-O (red square) molecule through the direct dimerization of Mad2-C and Mad2-O. Upon dimerization, Mad2-O is converted into Mad2-C, the form of Mad2 that is able to efficiently interact with Cdc20 (black oval) and inhibit APC/C activity. Upon formation of Cdc20-Mad2-C the complex dissociates from kinetochores to allow another Mad2-O to dimerize with the 'core' Mad1-Mad2-C kinetochore complex. In the cytoplasm, Mad2-C bound to Cdc20 can also dimerize with Mad2-O and convert it into Mad2-C. Mad2-C is therefore exponentially amplified leading to robust and global inhibition of the APC/C (Figure adapted from DeAntoni *et al.* 2005.)

1.6.6 The Mitotic Checkpoint Complex

Although recombinant Mad2 can inhibit Cdc20-mediated activation of APC/C activity *in vitro*, it has been shown that this inhibition is very inefficient. Furthermore, another mitotic checkpoint protein hBubR1 has also been shown to directly bind Cdc20 and inhibit APC/C activity. These findings have suggested that APC/C inhibition may require more checkpoint proteins than just Mad2.

Biochemical purification of an APC/C inhibitor from mitotic HeLa cells led to the discovery of the Mitotic Checkpoint Complex (MCC). This complex consists of hMad2, hBubR1, hBub3 and hCdc20 and has been shown to inhibit APC/C activity *in vitro* up to 3000-fold more effectively than recombinant Mad2 alone (Sudakin et al., 2001). Furthermore, the MCC is conserved in yeast and frogs (Chung and Chen, 2003; Hardwick et al., 2000). The interaction between the MCC and Cdc20 is catalyzed through Mad2 and BubR1. Cdc20 contains separate binding sites for both Mad2 and BubR1 (Tang et al., 2001; Wu et al., 2000); however, binding of BubR1 to Cdc20 requires Cdc20 to first interact with Mad2 (Chen, 2002; Davenport et al., 2006). Moreover, Mad2 and BubR1 act synergistically to inhibit APC/C function (Fang, 2002). Functionally, the MCC binds to Cdc20 in complex with the APC/C, and directly inhibits APC/C ligase function (Chan et al., 1999; Sudakin et al., 2001). Direct inhibition of the APC/C by the MCC may explain why the MCC is a much more potent inhibitor of the APC/C than Mad2 or BubR1 alone. Since its discovery, the MCC has become accepted as the mitotic checkpoint molecular inhibitor of APC/C function and therefore the "wait anaphase signal" (Chan et al., 2005).

Surprisingly, the MCC is found to remain assembled throughout the cell cycle. However, the MCC is only able to inhibit the mitotic form of APC/C (Sudakin et al., 2001). This finding has led to a hypothesis where a preassembled MCC would instantly activate the mitotic checkpoint upon entry into mitosis. It also suggests that MCC formation may not require kinetochores. Conversely, it has been shown and hypothesized that kinetochores may 'sensitize' the MCC to further enhance APC/C inhibition (Sudakin et al., 2001). The MCC would be recruited to unattached, or tension-less, kinetochores where it could be modified by phosphorylation or other post-translational modifications, thus making it a more potent APC/C inhibitor (Acquaviva et al., 2004; Sudakin et al., 2001; Topper et al., 2002). Lastly, the loss of Mad2 or BubR1 function can accelerate time spent in mitosis, while loss of Mad1, Bub3 or Bub1 function does not (Meraldi et al., 2004). This acceleration suggests that Mad2 and BubR1, working within the MCC, may function in controlling the timing of mitosis in a kinetochore-independent manner, while kinetochore Mad1, Bub3 and Bub1 function to sensitize and prolong the MCC, or Mad2-C mediated APC/C inhibition. In other words, the pre-assembled, kinetochore-independent MCC may function to ensure that the mitotic cell remains arrested upon entry into mitosis. In the absence of either Mad2 or BubR1, the MCC is no longer functional and upon entry into mitosis the cell is therefore never under mitotic checkpoint arrest. However, in the absence of Mad1 or Bub1 function, the pre-assembled MCC still activates the checkpoint upon initial entry into mitosis. Without the kinetochore based sensitization machinery, the MCC cannot indefinitely sustain APC/C inhibition and these cells do eventually escape checkpoint arrest [reviewed in (Chan et al., 2005; Musacchio and Salmon, 2007)]. The only outstanding issue regarding the sensitization hypothesis stems from the fact that an interphase MCC has not been isolated in other systems.

Although it has not been shown, the MCC and the template model must somehow converge. Perhaps MCC sensitization actually represents the formation of new MCC complexes at unattached or unaligned kinetochores. In support of this hypothesis, all of the MCC components have been shown to exhibit kinetochore dynamics similar to that of Mad2. Furthermore, assembly of the MCC requires the pre-association of Mad2 and Cdc20, and the molecular mechanism of this interaction has been elegantly outlined by the template model. Perhaps an extension of the model should involve determining whether the Mad2-Cdc20 complex is in fact the seed for MCC formation and whether this leads to continued inhibition of the APC/C.

Interestingly, in addition to the MCC there appears to be another inhibitor of the APC/C called mitotic checkpoint factor-2 (MCF2) (Eytan et al., 2008). Very recently an MCC independent APC/C inhibitory activity was purified from HeLa extracts. Although the identity of this new inhibitor remains unknown, the inhibition of the APC/C by MCF2 also involved antagonizing Cdc20-mediated activation of the APC/C. Future studies will need to determine the functional interplay and regulation of the MCC and MCF2 during mitotic checkpoint activation and silencing.

1.7 Molecular Pathways of Mitotic Checkpoint Signaling

As outlined previously, the mitotic checkpoint consists of three major functional components. The first is the mechanosensor, the second a signaling cascade and finally the third is the biochemical inhibitor of the APC/C. It is well established that Mad2 and the MCC function as the biochemical inhibitor of the APC/C. At the same time, components and functions of the mechanosensor and the amplification cascade are less understood and involve many other mitotic checkpoint proteins and kinases.

1.7.1 Mitotic kinases

Phosphorylation provides an effective, robust and reversible means to regulate biochemical pathways. Not surprisingly, phosphorylation plays a major role in regulating the mitotic checkpoint. In fact, there are close to 600 phosphorylation sites that map to 72 known human mitotic spindle proteins (Nousiainen et al., 2006). Mitotic kinases are therefore obviously playing key roles during kinetochore assembly, regulation of chromosome segregation as well as during mitotic checkpoint signaling. Outlined below are the functions of several mitotic kinases known to influence the mitotic checkpoint.

The Bub1 serine/threonine kinase localizes to both unattached and attached kinetochores; however, the level of kinetochore Bub1 is greatly decreased upon chromosome alignment (Taylor et al., 2001). Functionally, Bub1 is required for kinetochore recruitment of several mitotic checkpoint proteins [reviewed in (Musacchio and Salmon, 2007)]. Additionally, Bub1 is involved in the formation and interaction of the MCC with the APC/C (Morrow et al., 2005). It remains unclear whether the kinase activity of Bub1 is required for its mitotic checkpoint function, but, Bub1 does phosphorylate Cdc20 resulting in APC/C inhibition (Chen, 2004; Tang et al., 2004a). Bub1 also plays a role in the recruitment and function of Sgo1 and the PP2A phosphatase to centromeres (Kitajima et al., 2005; Tang et al., 2004b). Sgo1 is required for proper cohesion between sister chromatids and is therefore essential for proper chromosome alignment and segregation. Finally, as mentioned earlier Bub1 responds to the lack of inter-kinetochore tension by accumulating at tension-less kinetochores (Famulski and Chan, 2007; Skoufias et al., 2001).

Plk1 (polo like kinase 1) is a threonine/serine kinase originally identified as a classic cell division mutant in yeast and flies (Hartwell et al., 1973; Sunkel and Glover, 1988). It is highly conserved and is considered a key regulator of mitosis [reviewed in (Petronczki et al., 2008)]. During mitosis Plk1 translocates from centrosomes in prophase to kinetochores in prometaphase, followed by central spindle localization during anaphase; and finally, it resides at the spindle mid body during telophase. This pattern of localization is typical of chromosome passenger complex proteins (discussed in section 1.7.2). The mechanism behind this temporally regulated spatial distribution of Plk1 depends on a phosphoepitope binding domain of Plk1 called the Polo Box Domain (PBD) (Elia et al., 2003). The PBD specifically binds 'primed' pre-phosphorylated peptide motifs found in proteins located at centromeres, kinetochores or the spindle mid body (Lowery et al., 2004). Priming phosphorylations of Plk1 interacting partners therefore function to spatially regulate Plk1 localization during mitosis. Interestingly, many of these Plk1 interaction partners are also substrates for subsequent Plk1 phosphorylation.

During mitosis Plk1 is involved in almost all aspects of chromosome segregation including mitotic spindle assembly, k-MT attachments and cytokinesis [reviewed in (Petronczki et al., 2008)]. In terms of mitotic checkpoint signaling, Plk1 is known to phosphorylate Bub1, PBIP1 (Polo Box Interacting Protein-1), MCAK (Mitotic Centromere Associated Kinesin), INCENP (Inner Centromere Protein), PICH (Plk1 Interacting Checkpoint Helicase), NudC and BubR1 as well as several subunits of the APC/C (Petronczki et al., 2008; van Vugt and Medema, 2005). Moreover, many of these interactions depend on prior phosphorylation of the PBD recognition motif by Cdk1. Cdk1 may therefore function as a key priming kinase for Plk1 substrates. Although Plk1 can phosphorylate APC/C subunits, the relevance of these modification on mitotic checkpoint signaling remains unclear [reviewed in (van Vugt and Medema, 2005)]. On the other hand, phosphorylation of BubR1 by Plk1 and Cdk1 has been show to represent the well known tension-sensitive phosphorylation target recognized by the 3F3/2 monoclonal antibody (Wong and Fang, 2007). Plk1 may therefore play a role in mitotic checkpoint response to kinetochore tension. Like other checkpoint proteins, Plk1 levels increase at unattached kinetochores and decrease upon chromosome alignment. However, loss of Plk1 function does not inhibit mitotic checkpoint signaling, but rather activates it [reviewed in (Petronczki et al., 2008)]. Lastly Plk1 also appears to play a role in the activation and function of another key mitotic kinase Aurora B (discussed later) (Rosasco-Nitcher et al., 2008). In summary, the role of Plk1 during mitotic checkpoint signaling likely involves requlation of mitotic spindle assembly, tension response as well as regulation of APC/C subunits.

Mps1 (monopolar spindle 1), a dual specificity kinase, was identified in a yeast genetic screen and is highly conserved (Lauze et al., 1995; Winey et al., 1991; Winey and Huneycutt, 2002). Although originally thought to only play a role in spindle pole duplication, Mps1 is also clearly an essential mitotic kinase that is essential for mitotic checkpoint function. Like many other mitotic checkpoint signaling proteins, Mps1 accumulates at unattached kinetochores, and similar to Mad2 and Cdc20, has high kinetochore turnover rate (Howell et al., 2004). Loss of Mps1 function overrides the checkpoint while its over-expression activates it (Abrieu et al., 2001; Hardwick et al., 1996; Winey et al., 1991). Mps1 phosphorylates Mad1 and is also required for kinetochore localization of Mad1, Mad2, CENP-E and Plk1. Furthermore, the kinase

activity of Mps1 is specifically required for Mad2 kinetochore recruitment (Tighe et al., 2008). Aditionally, Mps1 functions in the correction of improper k-MT attachments and in the sensing of inter-kinetochore tension (Jelluma et al., 2008a; Jelluma et al., 2008b; Maure et al., 2007).

1.7.2 Aurora B and the Chromosomal Passenger Complex

The Chromosomal Passenger Complex (CPC) obtained its name from the highly dynamic mitotic localization pattern of its components [reviewed in (Ruchaud et al., 2007)]. The CPC localizes to chromosome arms in early mitosis but becomes restricted to centromeres by prometaphase. Furthermore, the CPC relocates to the spindle midzone during anaphase and to the spindle body during cytokinesis (Cooke et al., 1987). The CPC is directly involved in k-MT attachment, regulation of mitotic checkpoint signaling as well as cytokinesis. Similar to the Plk1 kinase, the CPC has been hypothesized to function as another master regulator of mitotic events (Ruchaud et al., 2007).

The CPC is composed of the Aurora B kinase, INCENP, Survivin and Borealin (Gassmann et al., 2004; Honda et al., 2003; Terada et al., 1998). All components of the complex are interdependent for both localization and function (Lens et al., 2006). Ultimately, the CPC functions through the kinase activity of Aurora B, while the other subunits function in CPC targeting as well as activation of Aurora B kinase activity (Lens et al., 2006; Vader et al., 2006).

Aurora B is a serine/threonine kinase that was identified in the budding yeast as a mutant with increased polyploidy (Ipl1) (Chan and Botstein, 1993). Homologues of Aurora B are conserved amongst eukaryotes and play essential roles during mitosis (Terada et al., 1998). The initial mitotic function of Aurora B is the phosphorylation of histone H3 on serine 10 and 28 (Hsu et al., 2000; Murnion et al., 2001). Although these modifications correlate with condensation of mitotic chromosomes, the functional consequence of this event remains unclear (Goto et al., 2002). Upon entry into mitosis, Aurora B is required for both the assembly and stability of the mitotic spindle through phosphorylation of stathmin and MCAK (Andersen et al., 1997; Gadea and Ruderman, 2006; Ohi et al., 2004). Stathmin is a MT destabilizing protein involved in spindle assembly, whose function is inhibited by Aurora B phosphorylation. MCAK, a kinesin-13 MT depolymerase is also essential for mitotic spindle assembly, and like stathmin, its function is inhibited by Aurora B phosphorylation (Andrews et al., 2004; Hunter et al., 2003; Lan et al., 2004; Zhang et al., 2007). By inhibiting the chromatin-associated MT destabilizing activities of MCAK and stathmin, Aurora B may contribute to kinetochore-initiated spindle assembly and stability.

In addition to spindle assembly, Aurora B kinase activity is essential for the correction of improper kinetochore-MT attachments [reviewed in (Cimini, 2007)]. Early studies in budding yeast showed that Aurora B is required for the release of k-MT attachments in the absence of kinetochore tension (Biggins and Murray, 2001; Biggins et al., 1999). In vertebrate cells Aurora B is enriched at tension-less as well as kinetochores that exhibit merotelic k-MT attachments (Knowlton et al., 2006). Furthermore, the kinase activity of Aurora B is also required for the elimination of improper merotelic k-MT attachments (Cimini, 2007). Molecularly, Aurora B has been shown to disrupt 'core' k-MT attachments (the KMN) by phosphorylating the Ndc80 component Hec1 (Cheeseman et al., 2006; Cimini, 2007). This phosphorylation subsequently leads to the release of improper k-MT attachments and therefore prevents chromosome missegregation. Aurora

B-mediated regulation of MCAK MT depolymerase activity has also been postulated to be involved in correction of improper k-MT attachments, although the mechanism is not yet clear (Andrews et al., 2004; Knowlton et al., 2006; Lan et al., 2004).

Centromere/kinetochore activation of Aurora B kinase activity is regulated by the presence of MTs, TD-60 (Telophase disc 60), as well as Mps1, Cdk1 and Plk1 kinase phosphorylation of Aurora B substrates (Jelluma et al., 2008b; Rosasco-Nitcher et al., 2008). Importantly, the kinase activity of Aurora B is also required for proper kinetochore assembly, as Aurora B loss of function disrupts chromosome alignment as well as diminishes k-MT attachments (Ditchfield et al., 2003; Hauf et al., 2003).

Interestingly, Aurora B function is required for mitotic checkpoint activation specifically in response to the loss of kinetochore tension (Biggins and Murray, 2001; Ditchfield et al., 2003; Famulski and Chan, 2007; Hauf et al., 2003). Furthermore, the mitotic checkpoint function of the CPC is independent from its k-MT attachment regulation (Vader et al., 2007). Cells arrested with unattached kinetochores do not escape mitotic arrest in the presence of Aurora B kinase inhibitors or in the absence of any CPC subunits. However, in the presence of k-MT attachments but lack of tension, as can be achieved using a low dose of taxol, the inhibition of Aurora B kinase function, or the loss of any of the other CPC components, results in escape from mitotic checkpoint arrest (Carvalho et al., 2003; Ditchfield et al., 2003; Hauf et al., 2003; Lens and Medema, 2003; Lens et al., 2003). Aurora B and the CPC have therefore been suggested to function as kinetochore tension sensors for the mitotic checkpoint. In fact, it has been shown in yeast that INCENP/survivin and Aurora B establish a physical link with the centromere CBF3-DNA complex and physically sense the presence of tension (Sandall et al., 2006).

How Aurora B kinase activity induces mitotic checkpoint activation in response to the lack of kinetochore tension is an ongoing debate. In yeast, Aurora B responds to the absence of tension by generating unattached kinetochores, through phosphorylation of Ndc10p, and therefore activating the mitotic checkpoint (Biggins and Murray, 2001). However, it remains unclear whether the checkpoint in higher eukaryotes is also activated indirectly by generating unattached kinetochores or whether tension-less kinetochores can directly signal the checkpoint. One hypothesis suggests that in the absence of kinetochore tension, mitotic checkpoint proteins such as Bub1 or BubR1 may be in closer proximity to the centromere associated CPC and therefore become viable substrates for Aurora B phosphorylation (Lens and Medema, 2003). Phosphorylation of BubR1 and Bub1, as well as other possible targets, may result in amplification, or sensitization, of the APC/C inhibitor and therefore checkpoint arrest. In support of this idea, Aurora B kinase activity plays a role in promoting MCC mediated APC/C inhibition (Morrow et al., 2005). Upon the re-establishment of tension, the phosphorylated kinetochore checkpoint proteins would be removed from the site of Aurora B kinase activity and subsequently de-phosphorylated by the kinetochore associated PP1 phosphatase (Emanuele et al., 2008). Future studies to identify kinetochore substrates of Aurora B may shed more light onto the mechanism of tension sensing.

1.7.1 The BubR1/CENP-E Mechanosensor

The BubR1 mitotic kinase is known to interact with CENP-E at kinetochores (Chan et al., 1998; Cooke et al., 1997; Jablonski et al., 1998; Yao et al., 2000). As previously outlined, CENP-E is required for chromosome congression as well as k-MT attachment. Interestingly, hBubR1 is also involved in maintaining stable k-MT

attachment (Lampson and Kapoor, 2005). Taken together, the interaction of a kinase and a MT binding protein has driven the hypothesis that hBubR1/CENP-E functions as a mechanosensor for kinetochore-MT attachments (Chan et al., 1998). In support of this hypothesis, hBubR1 kinase activity is activated by CENP-E in the absence of MTs and this leads to mitotic checkpoint arrest (Chan et al., 1999; Mao et al., 2003). However, when CENP-E binds MTs, the hBubR1 kinase activity is now inhibited and this leads to silencing of hBubR1-induced mitotic arrest (Mao et al., 2005). The only disputed component of the mechanosensor model is the direct consequence of BubR1 kinase activation and deactivation on mitotic checkpoint signaling. Certain studies have found that the kinase activity of BubR1 is not required for mitotic checkpoint function (Chen, 2002). In addition, the yeast homolog of BubR1, Mad3, completely lacks the kinase domain of BubR1. Although it still remains to be determined what effect the regulation of BubR1 kinase activity by CENP-E has on mitotic checkpoint signaling, the BubR1/CENP-E complex is the first example of a mechanosensor directly regulated by k-MT binding.

1.8 The RZZ Complex

The majority of essential mitotic checkpoint components are highly conserved. However, the mitotic checkpoint of multi-cellular eukaryotes also contains components that are not conserved in yeast. These include Zeste White10, Roughdeal and Zwilch, which assemble into the RZZ complex during mitosis and function during mitotic checkpoint signaling [reviewed in (Karess, 2005)].

1.8.1 Zeste White 10 and Roughdeal

Zeste White 10 (ZW10) and *Roughdeal* (ROD) were both isolated as *Drosophila* mutants conferring phenotypes associated with chromosome segregation defects (Karess and Glover, 1989; Williams et al., 1992). *ZW10* and *ROD* mutant embryos exhibited high levels of aneuploidy as well as nondisjunction and lagging chromatids during anaphase. Additionally, *ZW10* and *ROD* mutant cells do not arrest in mitosis in the presence of pharmacologically induced spindle damage (Basto et al., 2000). These findings indicate that ZW10 and ROD are *bona fide* mitotic checkpoint proteins. ZW10 and ROD are conserved in higher eukaryotes, but interestingly lack homologues in yeast (Starr et al., 1997). Similar to *Drosophila*, inhibition of human, frog or worm ZW10 and ROD function by either antibody injection or siRNA mediated depletion results in override of the mitotic checkpoint and chromosome missegregation (Chan et al., 2000; Kops et al., 2005a; Scaerou et al., 2001). The absence of yeast homologues suggests that ZW10 and ROD may function in a mitotic checkpoint pathway that has evolved to ensure accurate chromosome segregation of the larger and more complex multi cellular eukaryotic genomes.

1.8.2 Mitotic Checkpoint Function of the RZZ Complex

Phenotypes of *ZW10* and *ROD* mutants are almost identical, and the combination of both does not increase the severity, thus indicating they function in the same pathway (Scaerou et al., 2001). In mitosis, ZW10 and ROD are known to interact and assemble into a conserved complex that also includes the Zwilch protein (Scaerou et al., 2001). Zwilch was identified through immunoaffinity purification as a ZW10 interacting partner and has identical mutant phenotypes to that of ZW10 and ROD (Williams et al., 2003). Furthermore, Zwilch is also not conserved in yeast. Together, **Z**W10, **R**OD and **Z**wilch

comprise the mitotic RZZ complex (Figure 1.9). This complex is evolutionarily and functionally conserved in all metozoans studied to date. Gel exclusion chromatography has predicted an ~800 kDa size for the complex, which based on the predicted molecular weights of ZW10, ROD and Zwilch suggests that the complex may dimerize (Scaerou et al., 2001). Functionally, all components of the complex are interdependent. Immunofluorescence and live cell imaging of the RZZ complex indicates that it localizes to kinetochores from early prometaphase up until late metaphase (Basto et al., 2000; Chan et al., 2000; Williams et al., 1996). Like other mitotic checkpoint components, the RZZ complex accumulates on unattached kinetochores (Williams and Goldberg, 1994). Furthermore, dmROD has also been observed to localize along k-MT of chromosomes undergoing chromosome alignment and stream toward the spindle poles (Basto et al., 2004). This behavior is known to be dependent on dynein/dynactin 'stripping' (discussed later) and transport of the RZZ complex off kinetochores and onto spindle poles. Aligned chromosomes exhibit very little kinetochore RZZ. As such, kinetochore accumulation of RZZ complexes may be sensitive to kinetochore tension. Aditionally, ZW10 and ROD localize to spindle poles during prometaphase and metaphase. Although it has not been directly investigated, this localization likely stems from the transport of the RZZ complex off kinetochores and onto spindle poles by dynein/dynactin (discussed in detail in section 1.9.1)

Kinetochore recruitment of the RZZ complex is known to depend on the direct interaction between ZW10 and Zwint-1 (ZW10 interacting protein-1) (Wang et al., 2004a). hZwint-1, although not conserved in files, interacts with ZW10 in the yeast two-hybrid assay and localizes to kinetochores prior to hZW10 (Starr et al., 2000). hZwint-1 is therefore thought to function as a scaffold for RZZ kinetochore binding. siRNA mediated depletion of hZwint-1 results in the loss of kinetochore hZW10 and hROD (Wang et al., 2004a). Moreover, hZwint-1 interacts with the Mis12 and Ndc80 complexes, thus linking the KMN to RZZ kinetochore recruitment (Cheeseman et al., 2004).

The RZZ complex is required for kinetochore recruitment of cytoplasmic dynein/dynactin. Dynein/dynactin recruitment to kinetochores hinges on the direct interaction between ZW10 and the dynactin component dynamitin (also known as p50). ZW10 and p50 interact directly in the yeast two-hybrid assay and the loss of ZW10 function results in the loss of kinetochore dynein/dynactin (Starr et al., 1998). In fact, disruption of any of the RZZ components leads to the loss of dynein/dynactin specifically from kinetochores but not other mitotic sites such as the spindle. Interestingly, while the loss of RZZ components leads to the loss of mitotic checkpoint function, the loss of dynein/dynactin function actually activates the mitotic checkpoint (Wojcik et al., 2001). Loss of kinetochore dynein/dynactin is therefore not the essential mitotic checkpoint function of the RZZ complex.

Figure 1.9

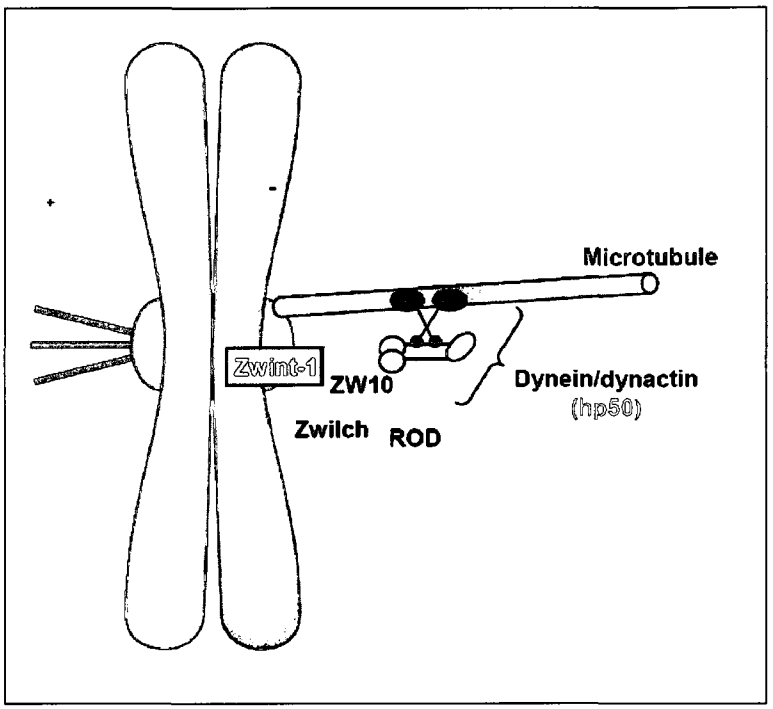

Figure 1.9: **The RZZ complex.**
ZW10, ROD and Zwilch assemble into a kinetochore associated complex (RZZ) during mitosis. The RZZ complex is recruited to kinetochores (purple half oval) during prophase through the interaction between ZW10 and the kinetochore protein hZwint-1. Once at kinetochores, ZW10 directly interacts with and therefore recruits dynamitin (hp50), a subunit of the dynactin complex. The dynactin complex in turn interacts with and targets to kinetochores the dynein MT motor complex. (Figure adapted from Musacchio and Hardwick 2002.)

In addition to dynein/dynactin recruitment, the RZZ complex may function in the kinetochore recruitment of Mad1 and Mad2 (Kops et al., 2005a). The loss of mitotic checkpoint function in cells lacking RZZ function may therefore be explained by the loss of Mad1 and Mad2 from kinetochores. However, there is no evidence for a physical interaction between Mad1 or Mad2 and the RZZ complex. In addition, several other known mitotic checkpoint components are also required for Mad1 and Mad2 kinetochore localization. Mad1 and Mad2 kinetochore localization may therefore rely on a fully assembled and functional kinetochore and not specifically the RZZ complex. Further work is required to determine whether the essential mitotic checkpoint function of the RZZ complex is in fact Mad1 and Mad2 kinetochore recruitment or another yet to be identified molecular function.

1.9 Mitotic Checkpoint Silencing

Upon alignment of all chromosomes at the metaphase plate, the mitotic checkpoint needs to be shut down, or silenced, in order to proceed into anaphase. There are several mechanisms that play a role in the silencing of the mitotic checkpoint. In general these silencing mechanisms function by inhibiting the Cdc20-Mad2 complex and by removing mitotic checkpoint proteins off kinetochores.

1.9.1 Dynein/dynactin 'Stripping'

Dynein is a minus end-directed MT motor complex that participates in a wide variety of MT-based motility processes, one of which is the transport of mitotic checkpoint proteins off kinetochores (Figure 1.10). Dynein is composed of heavy, intermediate, light intermediate and light chains (Hirokawa et al., 1998). It is well established that dynein is activated as well as targeted to its cargoes by another multi subunit complex called dynactin. Dynactin physically interacts with dynein intermediate chains and promotes motor processivity (King and Schroer, 2000). During mitosis dynein/dynactin are recruited to kinetochores and function in the transport of kinetochore proteins off kinetochores, a phenomenon known as 'stripping' (Howell et al., 2001; Pfarr et al., 1990; Steuer et al., 1990; Wojcik et al., 2001). Mad1, Mad2, BubR1, Cdc20, CENP-E, Mps1, CENP-F as well as the RZZ complex can all be transported off kinetochores by dynein/dynactin (Howell et al., 2001). The stripping of kinetochore components occurs specifically at kinetochores of attached and aligned chromosomes (Basto et al., 2004). As such, dynein/dynactin mediated transport can explain why levels of these particular kinetochore components decrease dramatically during metaphase. In general the mitotic checkpoint is activated when checkpoint proteins accumulate at kinetochores, whether unattached or tensionless. Conversely, the depletion of kinetochore proteins is predicted to silence the checkpoint. Dynein/dynactin is therefore proposed to promote silencing of the checkpoint by depleting checkpoint proteins off kinetochores that have satisfied the checkpoint requirements such as bi-polar k-MT attachment and chromosome alignment.

Figure 1.10

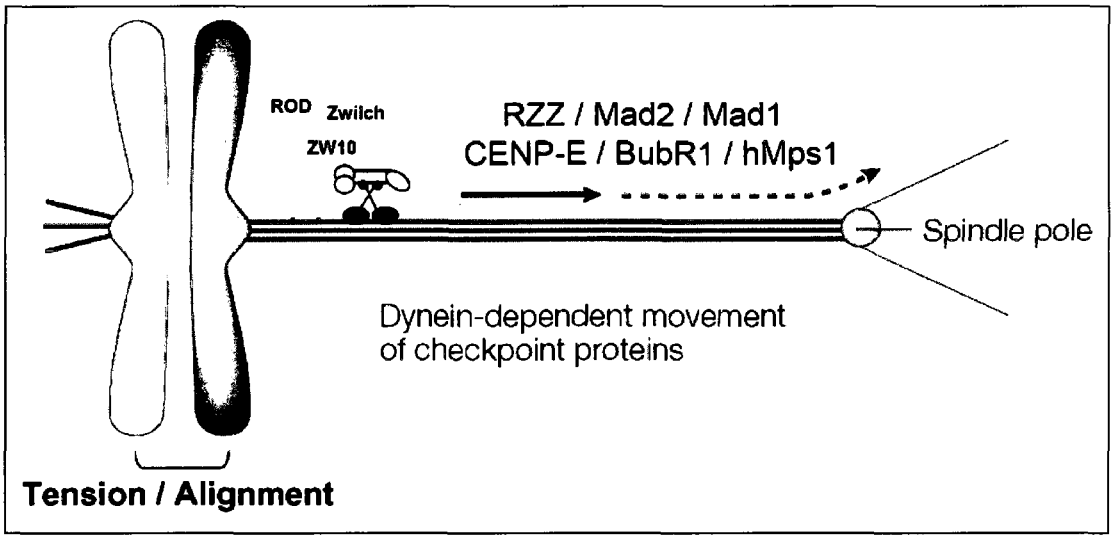

Figure 1.10: **Dynein/dynactin mediated silencing of the mitotic checkpoint.**
Upon the establishment of inter-kinetochore tension, which is indicative of chromosome alignment, the dynein/dynactin motor complex transports mitotic checkpoint proteins off kinetochores and onto spindle poles. Mitotic checkpoint proteins known to be transported by dynein/dynactin include the RZZ complex, Mad1/2, BubR1, CENP-E and Mps1. Removal of these checkpoint components from kinetochores, their site of function, is hypothesized to lead to the silencing of the mitotic checkpoint. (Figure adapted from Musacchio and Hardwick 2002.)

Mechanisms regulating the proper timing of dynein/dynactin transport have yet to be identified but may involve several dynein/dynactin accessory proteins as well as mitotic kinases such as Aurora B (Famulski and Chan, 2007). During mitosis, dynactin is not the only known modulator of dynein motor function. Studies originally performed in *Aspergillus nidulans* identified several proteins which were not part of the dynein or dynactin complexes yet genetically essential for dynein function (Efimov and Morris, 2000; Xiang et al., 1994). Their human homologues include: hLis1, hNudC, hNudE and hNudEL and they have all been shown to play a role in regulating cytoplasmic dynein function (Aumais et al., 2001; Feng et al., 2000; Sasaki et al., 2000; Stehman et al., 2007). Interestingly, hLis1, hNudE and hNudEL also affect the function of kinetochore dynein/dynactin (Liang et al., 2007; Stehman et al., 2007; Vallee et al., 2001). Furthermore, hCENP-F, a large kinetochore protein; hSpindly, a novel anchor for kinetochore dynein; and hCLIP-170, a plus-end MT binding protein are all affect kinetochore dynein/dynactin function (Dujardin et al., 1998; Griffis et al., 2007; Yang et al., 2005; Zhou et al., 2005). At kinetochores, these dynein modulators are involved in a complex network of interactions (Figure 1.11). hLis1, hNudE and dynactin are all predicted to regulate dynein motor activity (Vergnolle and Taylor, 2007). hNudEL and hCENP-F on the other hand are predicted to regulate premature "stripping" of dynein off kinetochores, while hSpindly appears to direct the recruitment of dynein to kinetochores and interacts with p50 (dynamitin) (Chan lab unpublished) (Liang et al., 2007; Yang et al., 2005). Together, this complex network of kinetochore dynein modulators somehow functions to prevent premature (as well as promote timely) checkpoint silencing through dynein/dynactin-mediated transport of mitotic checkpoint proteins off kinetochores.

1.8.2 p31^{comet}

Formation of Mad2-C and its subsequent binding to Cdc20 is essential for mitotic checkpoint arrest. Disrupting the interaction between Mad2-C-Cdc20 is therefore hypothesized to function as a robust and effective mitotic checkpoint silencing mechanism. The hypothesis hinges on the properties of the negative regulator of mitotic checkpoint function called p31^{comet} (Figure 1.12). *In vitro*, p31^{comet} interacts with Mad2-C while it is in complex with either Mad1 or Cdc20 (Habu et al., 2002; Xia et al., 2004). Furthermore, the structure of p31^{comet} resembles that of Mad2-O, thus suggesting that p31^{comet} mimics Mad2-O in order to bind Mad2-C (Yang et al., 2007a). p31^{comet} is in fact able to prevent the dimerization of Mad2-C and Mad2-O and therefore inhibit the conversion of Mad2-O into Mad2-C (Vink et al., 2006). A lack of Mad2-C would result in Cdc20 that was now free to activate the APC/C and therefore induce anaphase onset. During mitotic checkpoint signaling p31^{comet} may be inhibited/modified or sequestered away from kinetochores where Mad2-O is converted into Mad2-C [reviewed in (Musacchio and Salmon, 2007)]. Upon satisfaction of the mitotic checkpoint, p31^{comet} may then be reactivated or reintroduced into the kinetochore region, thus inhibiting conversion of Mad2 into the inhibitory Mad2-C. In support of this, depletion of p31^{comet} from human cells leads to delays in mitotic progression. Although the p31^{comet} mechanism offers an appealing silencing mechanism, p31^{comet} is not conserved in yeast and the molecular pathways regulating it remain unknown.

Figure 1.11

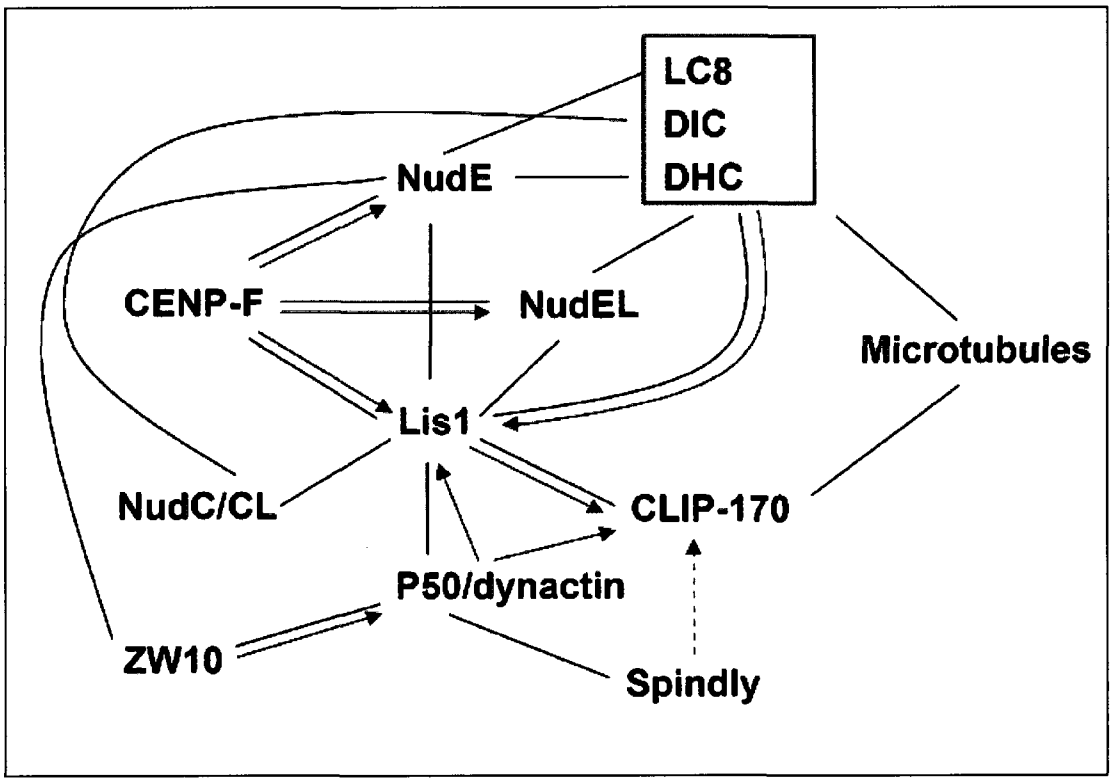

Figure 1.11: **Interaction network of kinetochore dynein modulators.**
Physical interactions are shown with solid black lines. Dependence for kinetochore recruitment is shown with red arrows, where kinetochore localization of the protein at the tip of the arrow is dependent on the protein at the arrows origin. The blue line depicts the direct interaction and the requirement of NudCL for the stability of dynein intermediate chain (DIC). The dynein motor is depicted as a blue box containing light chain 8 (LC8), DIC and dynein heavy chain (DHC).

Figure 1.12

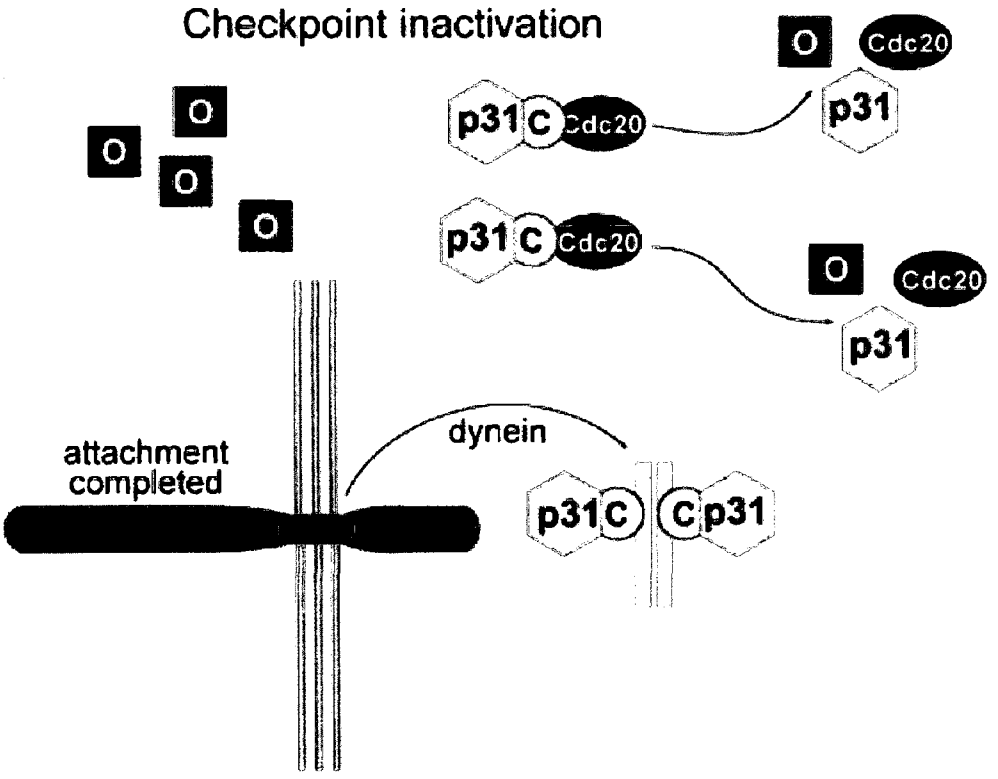

Figure 1.12: **Mitotic checkpoint inactivation through p31^{comet}.**
Upon chromosome alignment the Mad1-Mad2-C complex is removed from kinetochores by dynein/dynactin, and p31^{comet} becomes activated through an unknown mechanism. These events allow p31^{comet} (blue hexagon) to interact with Mad2-C bound to Mad1, preventing the dimerization of Mad2-C with Mad2-O. p31^{comet} thus prevents the conversion of Mad2-O into Mad2-C. Furthermore, p31^{comet} interacts with Mad2-C bound to Cdc20 and induces the dissociation of Mad2-C and Cdc20. p31^{comet} therefore promotes the activation of the APC/C by inhibiting the formation of the Mad2-C-Cdc20 complex. (Figure adapted from De Antoni 2005).

In addition to p31^{comet}-mediated inhibition of Mad2-C formation, mitotic checkpoint inactivation may also involve inducing the dissociation of the already formed Mad2-Cdc20 complexes as well as the MCC. Interestingly non-degrading ubiquitination of Cdc20 leads to the dissociation of Mad2-Cdc20 or BubR1-Cdc20 (Reddy et al., 2007; Stegmeier et al., 2007). Ubiquitination of Cdc20 at anaphase onset may therefore also help silence the checkpoint. In support of this idea a Cdc20 de-ubiquitinating enzyme has been identified, and its function is necessary for proper mitotic checkpoint function (Reddy et al., 2007; Stegmeier et al., 2007). During checkpoint silencing this enzyme may be inactivated or inhibited, therefore driving the ubiquitination of Cdc20 and the subsequent dissociation of Mad2-Cdc20 and BubR1-Cdc20.

It is likely that all of the above mentioned mechanisms function in concert to ensure robust and efficient silencing of the mitotic checkpoint. While dynein/dynactin removes kinetochore complexes involved mitotic checkpoint signaling, p31^{comet} as well as ubiquitination of Cdc20 ensure any remaining signal is inhibited.

1.10 Thesis Focus

The RZZ complex represents an arm of the mitotic checkpoint pathway that is absent from single-celled yeasts, yet is essential for proper chromosome segregation in metozoans. This apparent contradiction poses the interesting argument that the RZZ complex may have evolved to ensure accurate chromosome segregation of the larger and more complex metazoan genomes. Functionally, the RZZ complex is responsible for the kinetochore recruitment of cytoplasmic dynein/dynactin. Although kinetochore dynein/dynactin in required for k-MT attachment and chromosome congression, it remains largely unknown what exact molecular function(s) the RZZ complex plays during mitotic checkpoint signaling. In order examine the molecular function of the RZZ complex during mitosis, I undertook a structure-function study of the hZW10. Having established an extensive mutant library of hZW10, I was able to map the kinetochore and hZwint-1 interaction domains of hZW10. Furthermore, I was able to establish that the interaction between hZW10 and hZwint-1 is essential for checkpoint function because it regulates the turnover and therefore release of kinetochore hZW10. In addition to the structure-function study, I was also able to show that the RZZ complex responds to the loss of inter-kinetochore tension through an Aurora B kinase-dependent mechanism. I found that the RZZ complex accumulates at tension-less kinetochores through a decrease in its kinetochore turnover. Furthermore, inhibition of Aurora B kinase function led to an increase in RZZ turnover and dynein/dynactin-mediated 'stripping' off kinetochores. Finally, through the use of the small molecule norhidroguaiaretic acid (NDGA), I was able to show that dynein/dynactin mediated 'stripping' of kinetochore proteins off kinetochores is not sufficient for mitotic checkpoint silencing, and that spindle pole accumulation of checkpoint proteins leads to continued checkpoint arrest. From these findings I propose a mechanism of mitotic checkpoint signaling as well as silencing that takes into account the dynamic status of kinetochore RZZ complexes and also involves the spindle poles.

Chapter II: *Experimental Procedures*

2.1 Cloning

hZW10 and hZwint-1 cDNAs were amplified from a HeLa cDNA library (Clontech) using specific primers containing BamH1 or XhoI likners, and cloned into the pENTR3C plasmid using BamHI and SalI sites (Invitrogen). hZW10 N- and C-terminal deletion constructs (N1-9, C1-4, C8-10) were amplified from the pENTR3C-hZW10 vector using specific primers (BamHI and XhoI linkers) and cloned into pENTR3C again using BamH1 and SalI sites. All of the ligations were confirmed by restriction endonuclease digestion. hZW10 C-terminal deletions (C5-7, 20-779, 30-779, 35-779, 45-779) were amplified from pENTR3C-hZW10 using attB1/attB2 recombination linkers and cloned into the pDONR221 vector (Invitrogen) through the BP clonase reaction (Gateway technology cloning system, Invitrogen). The recombinants were confirmed by restriction endonuclease digestion. Recombination cloning from the pENTR and pDONR221 vectors into expression vectors was performed using the LR colonase reaction (Gateway technology cloning system, Invitrogen) and confirmed by restriction endonuclease digestion. The expression vectors used were the Gateway destination vectors of: pEGFP, pCG, pJG4-5 and pEG202 (Chan et al., 1998).

GFP-H2B was a kind gift from Dr. G. Wahl. The mCherry-N1-GW vector was generated by converting the mCherry-N1 vector (a gift from Dr. R. Tsien) to a Gateway destination vector. hMad2 was cloned into the mCherry-N1-GW vector from pENTR-TOPO-hMad2 (a gift from Dr. T. Yen) by recombination (Gateway cloning technology, Invitrogen). hBub1 was cloned into pEGFP-GW from pENTR3C-hBub1 using Gateway cloning technology. Aurora B cDNA was amplified from HeLa cDNA (Clontech) using PCR primers with the attB1/attB2 recombination site linkers and recombined into pDONR221 and subsequently into pDEST47 using BP and LR clonases respectively (Gateway cloning technology, Invitrogen). Dynamitin (hp50) cDNA was amplified from HeLa cDNA (Clontech) with BamHI and EcoRI linkers, cloned into pENTR3C using the same sites and subsequently recombined using the LR clonase, into the destination vector pYFP-GW (Gateway cloning technology, Invitrogen). hCyclin-B-GFP was a kind gift from Dr. J. Pines. hBubR1 cDNA (Chan et al. 1998) was amplified with BamHI and XhoI linkers and cloned into pENTR3C using the BamHI and SalI sites. hBubR1 cDNA was then transferred into pEGFP by LR recombination and confirmed with restriction endonuclease digestion (Gateway cloning technology).

2.2 Mutagenesis

hZW10 insertion mutagenesis was done using the GPS-LS linker scanning system (New England Biolabs) and the MGS kit (Finnzymes). pENTR-hZW10 served as the template for mutagenesis. In short, pENTR3C-hZW10 and the Cam^R-transposon were incubated in the presence of the MuA recombinase enzyme. pENTR-hZW10 plasmids with transposon insertions were selected by growth of DH5α *E. coli* on media containing kanamycin and chloramphenicol. Surviving colonies were pooled, and plasmid was purified using a midi-prep plasmid isolation kit (Eppendorf). The transposon was subsequently removed by NotI digestion and gel purification of the linearized pENTR3C-hZW10 plasmid. Following ligation, the transposon-less plasmids were transformed into DH5α and selected on kanamycin. Surviving colonies were screened for insertions using colony PCR with NotI and hZW10 specific primers. Exact insertion location was

determined using BigDye v3.1 capillary sequencing (310 Applied Biosciences capillary sequencer).

hZW10 point mutations were generated using the QuickChange site-directed mutagenesis kit (Stratagene) using pENTR-hZW10 as the template. Mutagenesis was confirmed by sequencing.

2.3 Yeast Two-Hybrid Analysis

Yeast two-hybrid analysis was performed as previously described (Chan et al., 1998). In short, *S. cerevisiae* strain SKY473 was co-transformed with pEG202 and pJG4-5 fusion constructs along with the pSH18-34 reporter plasmid. The transformants were selected on SD media lacking TRP, HIS and URA. Three colonies from each transformation were re-streaked onto SD -TRP, -HIS, -URA supplemented with D-galactose and raffinose (gal/raf) to induce expression. After 2 days of growth, the colonies were again re-streaked onto SD-HIS, -URA, -TRP + gal/raf as well as X-gal. Blue-white selection was documented 2 and 3 days after re-streaking.

The β-galactosidase assay was performed using the yeast β-galactosidase assay kit (Pierce) according to the manufacturer's protocol for quantitative analysis. Yeast growing on SD-HIS, -URA, -TRP, + gal/raf were used for the assay. Each assay was done in triplicate.

For western blotting, yeast growing on the SD-HIS, -TRP, -URA + gal/raf were grown overnight in liquid SD-HIS, -TRP, -URA + gal/raf media. After overnight growth, the OD^{600} of each culture was determined. The culture was then diluted using SD-HIS, -TRP, -URA + gal/raf to an OD^{600} of 0.15 and grown for 6-8 hours, until the OD^{600} reached 0.5-0.7. Yeast were then pelleted, re-suspended in 1X SDS-PAGE loading buffer and frozen at -80^0C for 24 hours. Before loading for SDS-PAGE analysis, the samples were boiled for 7 minutes.

2.4 Cell Culture

HeLa and HEK293 cells were grown in DMEM with 10% FCS at 37°C in 5% CO_2. Cell lines were maintained using common cell culture techniques. For FRAP experiments, HeLa cell medium was supplemented with 1M HEPES buffer (pH 7.4, Gibco) to a final concentration of 7 μM. Vinblastine (Sigma) was used at a final concentration of 0.1 μM unless otherwise stated. S-trityl-L-cystine (STLC) (Sigma) was used at a final concentration of 7 μM. MG132 was used at a final concentration of 12.5 μM (Calbiochem). Taxol (Sigma) was used at a final concentration of 1 μM. ZM447439 (Astra) was used at a final concentration of 2 μM. NDGA (Biomol) was used at a final concentration of 30 μM. Nocodazole (Sigma) was used at a final concentration of 20 nM unless otherwise stated.

2.5 Transient transfection

HeLa cells grown to 60% confluence on # 1.5 glass coverslips placed in 35 mm dishes were transiently transfected with 2-4 μg of the EGFP constructs using 10 μl polyethylenimine (PEI) (1 mg/ml) diluted in 250 μl of opti-MEM (Gibco). The PEI complexes were left on the cells for 24 hours. HEK293 cells were grown to 80% confluence in 35 mm dishes and transfected with 4 μg DNA as outlined above.

2.6 Permanent Cell Line selection

HeLa cells grown to ~80% confluency in 10 cm dishes were co-transfected with 10 μg XmnI linearized EGFP-hZW10 constructs and 10 μg BamHI linearized pCDNA3 vectors using 30 μL PEI (1 mg/ml) (Cedarlane) diluted in 1 mL of Opti-MEM (Gibco) for 48 hours. After 48 hours, geneticin (G418) (Gibco) was added to a final concentration of 500 μg/ml and the cells grown for ~2 weeks. The surviving colonies were collected and sorted for GFP expression using the EPICS Altra HyPer cell sorter (Coulter). The sorted cells were allowed to proliferate for ~1 week and again sorted for GFP expressing cells. Kinetochore localization of the EGFP-hZW10 constructs was confirmed using fluorescence microscopy. YFP-hp50, GFP-H2B and Aurora-B-EGFP permanent cell lines were created as described above; however, the plasmids were not linearized prior to transfection.

2.7 Western Blotting

HEK293 and HeLa cells were harvested for western blotting as previously described (Chan et al., 1998). In short, HeLa cells were lysed with 1% NP40 lysis buffer (50 mM Tris pH 7.5, 150 mM NaCl, 1mM dithiothreitol) with protease and phosphatase inhibitors (10 μg ml^{-1} AEBSF, 10 μg ml^{-1} leupeptin, 5 μg ml^{-1} pepstatin, 5 μg ml^{-1} chymostatin, 10 μg ml^{-1} aprotinin, 10 mM NaF, 1 mM Na_3VO_4, 60 mM β-glycerophosphate and 100 nM microcystin), and insoluble material was pelleted at 12,000*g*. Lysates in 1 × SDS sample buffer were separated by 4–12% gradient SDS–PAGE (BioRad Protein III system); proteins were then transferred onto Immobilon-P membrane (Millipore), blocked using the Odyssey blocking buffer (LiCor) and probed with the appropriate antibodies. Antibodies, diluted in blocking buffer, were each incubated for 1 hour at room temperature and subsequently washed off using PBS-Tween (0.2%). The blots were analyzed using the Odyssey scanner (LiCor) controlled by Odyssey software (LiCor). Images were processed using Adobe Photoshop 7.0 (Adobe Systems Inc).

2.8 GST pull-down

HEK293 cells were co-transfected with GST and EGFP constructs for 24 hours. 10% of the cell lysate was immunoblotted for quantitation of the EGFP constructs using the Odyssey software (Licor). Expression from each cell lysate was normalized to the lowest expressing sample and the corresponding lysate volumes, all brought up to 300 μl with 1% NP40 lysis buffer (1% NP40, 150 mM NaCl, 50 mM Tris-HCl pH 8.0 supplemented with: sodium pyrophosphate, sodium orthovanadate, NaF, β-glycerophosphate, DTT, leupeptin, aprotinin, chymostatin, AEBSF and pepstatin), were incubated with glutathione sepharose beads (Amersham) for 3 hours at 4°C. Ten percent of each normalized lysate was removed prior to addition of the beads as an input control. The beads were subsequently washed 5 times with 1% NP40 lysis buffer, re-suspended in 1X SDS-PAGE loading buffer and immunoblotted along with the input controls.

2.9 siRNA and shRNA

hZW10 siRNA knock-down was achieved using Invitrogen Stealth-siRNA designed after the target sequence previously described (Kops et al., 2005a). HeLa cells were initially transfected with either: 100 nM, 50 nM, 25 nM or 12.5 nM final

concentration siRNA using Oligofectamine (Invitrogen) according to the manufacturer's protocol, and analyzed 72 hours post transfection. The 50 nM siRNA concentration, which had ~90% knockdown, was chosen for all remaining siRNA experiments.

Knock-down of hBubR1 was performed by transiently transfecting 8 μg of pSuper-hBubR1 plasmid (a gift from the Madema Lab, constructed by Dr. Kops) into HeLa cells expressing GFP-H2B using Lipofectamine 2000 according to the manufacturer's protocol. Cells were analyzed 48 hours post transfection.

2.10 Fluorescence microscopy

HeLa cells grown on coverslips and either transiently transfected with EGFP constructs or siRNA or treated with various drug combinations, were processed for fluorescence microscopy as described in (Chan et al., 2000; Liu et al., 2003a). In short, cells were plated on No. 1.5 glass coverslips and used 1-2 d later. For staining, cells were fixed for 7 min in freshly prepared 3.5% paraformaldehyde/PBS, pH 7.0, extracted in KB medium (20 mM Tris-HCl, pH 7.5, 150 mM NaCl, and 0.1% BSA) plus 0.2% Triton X-100 for 5 min at room temperature and rinsed in KB. Primary and secondary antibodies were diluted in KB and added to coverslips for 30-60 min at 37°C in a humidified chamber. After each antibody incubation the coverslips were washed for 5 minutes with KB + Triton-X-100 and then KB. The coverslips were mounted using mowoil (Calbiochem) mounting media. Images were collected using a Zeiss AxioPlan2 microscope equipped with epifluorescence optics at room temperature. Cells were visualized with a 100X Plan-Apochromatic objective (NA1.4) and images were captured with a Photometrics CoolSNAP HQ CCD camera (Roper Scientific Inc., Trenton, NJ) that was controlled with a personal computer running Metamorph software (v7.1, Universal Imaging Corporation, Downingtown, PA). Image processing was performed using Photoshop 7.0 (Adobe Systems Inc., Mountain View CA).

For 3D analysis, Z-stacks were collected every 200 nm with the images displayed as maximum projection of the Z-stack. Kinetochore intensity was measured using Metamorph 6.0 software. Kinetochores were outlined using thresholding and the autotrace function. The outlined regions were used to collect the average intensity from the different channels pertaining to the different antibody staining performed. The signal was normalized to ACA staining for every channel in every cell. Ten cells were analyzed per experiment; the number of kinetochores analyzed is outlined in the figures. The data was statistically analyzed using Microsoft Excel software.

Confocal microscopy was performed using the Zeiss LSM 510 Confocal Laser Scanning Microscope mounted on an Axiovert 100M microscope (LSM 510 version 3.2, Jena, Germany) with a plan Apochromat 63x (NA 1.4) oil immersion lens. Individual immunofluorescence channels were collected sequentially in order to avoid signal bleeding through. Alexa 488 was detected using 488 nm laser excitation and collected with a bandpass filter of 505-550 nm. Alexa 555 was detected using 543 nm laser excitation and emission of 560 nm longpass filter. DAPI stained DNA was imaged with a UV laser (364nm) and a bandpass filter of 385-470 nm. Images were collected at Nyquist sampling rate with pinhole diameter of 1 airy unit. The images were compiled using Imaris (Bitplane) and Photoshop 7.0 (Adobe Systems Inc., Mountain View CA).

Cold stable MTs were generated by replacing the media with ice cold media and subsequently incubating the cells on ice for 10 minutes. The coverslips were subsequently processed for immunofluorescence as outlined above.

Spindle pole intensity was measured using Imaris software from Z-stacks with steps of 0.2 μm collected as outlined above. Spindle pole intensity was measured by outlining the spindle pole, calculating its fluorescence intensity in 3D and then comparing the value to the total fluorescence intensity of the entire cell. In cells with two visible spindle poles, both poles were measured individually and added together before comparing to the total cell intensity. Statistics and graphing were preformed using Excel (Microsoft).

2.11 Live cell FRAP

HeLa cells stably expressing EGFP-hZW10, EGFP-hZW10^{N1} and hAurora-EGFP were plated onto 35mm glass bottom dishes (FluoroDish, World Precision Instruments Inc.). Experiments were performed using the Zeiss NLO 510 multiphoton confocal scanning microscope using a 63X Plan-apochromatic lens equipped with an objective and stage warmer. FRAP was performed as previously described by Howell *et al.*, 2004. Single kinetochores or spindle poles were laser ablated with 10 laser pulses and the subsequent fluorescence recovery was observed for 2-3 minutes at 1-30 sec intervals. Data was collected using Zeiss LSM software (Zeiss), processed using Excel (Microsoft) and graphed using Prism software. The recovered fluorescence intensity signal was calculated based on the area that was laser bleached. The signal was then normalized by subtraction of the background signal obtained from an area outside the cell that had the exact same dimensions as the ablated area. The recovered fluorescence intensity was then adjusted for photobleaching at each time point by measuring the decrease in total fluorescence of the entire cell. Once adjusted for background and photobleaching, the % recovery of the fluorescence signal was calculated and graphed (non-linear regression curve) versus time (Prism software). $T^{1/2}$ values were extrapolated from the graphs and statistical analysis done in Excel (Microsoft). EGFP-hBub1 kinetochore FRAP was analyzed as outlined above; however, the construct was transiently transfected.

2.12 Live cell Imaging

HeLa cells expressing the various fluorescent protein tagged kinetochore proteins were plated onto 35 mm glass bottom dishes (FluoroDish, World Precision Instruments Inc.). Live cell imaging was performed using the Ultraview ERS Rapid confocal imager (PerkinElmer) mounted on a Zeiss Axiovert 200M inverted microscope with an EMCCD Camera (Hamamatsu Corp.). Dishes containing the cells were placed onto the microscope with an environmental control chamber to maintain the temperature at 37°C, and the indicated drugs were added directly to the dishes at the indicated times. The cells were imaged every minute while collecting a stack of images with a Z step size of 1 μm. All images were collected with a 63X plan-apochromatic lens (NA 1.4) using appropriate filter configurations for different fluorescent protein tags (EGFP: excitation at 488 nm and emission filter of 500-550 nm and mCherry: excitation at 561 nm and emission filter of 580-700 nm). In order to reduce phototoxicity, minimum light dosage was used by using relative high gain of the EMCCD camera (~170). Exposure times were 25 ms. Using a scanning stage, Z-stacks (20-30 steps of 1 μm) of ~10 cells were imaged at

different XY positions during each experiment. The data were analyzed using UltraVIEW ERS software (PerkinElmer) and converted into QuickTime (Apple) movie files.

2.13 Electron Microscopy

For electron microscopy (EM), cells were fixed in 3% glutaraldehyde in Millonig's phosphate buffer for 1 h at room temperature. Post-fixation was in 2% OsO4 for 20 minutes. The cells were dehydrated in ethanol, and then infiltrated with Polybed 812 resin (Polysciences). Polymerization was performed at 37^0C for 24 h. Silver-gray sections were cut with an ultramicrotome (Lica) equipped with a diamond knife, and sections were stained with uranyl acetate and lead citrate and examined in an electron microscope (H-7000 Hitachi).

2.14 Antibodies

Table 1-1: *Primary Antibodies*

Antibody target	Species	IF dilution	Western Blot dilution	Source
hZW10	Rabbit	1/1000	1/2000	Chan *et al.* 2000
hZW10	Rat	1/1000	ND	Chan *et al.* 2000
hROD	Rabbit	1/1000	ND	Chan *et al.* 2000
hZwint-1	Rat	1/1000	ND	Starr *et al.* 1998
ACA	Human	1/3000	ND	Dr. Fritzler (U of Calgary)
hBub1	Rat	1/1500	ND	Jablonski *et al.* 1998
hBubR1	Rabbit	1/1000	1/1000	Chan *et al.* 1999
hMad1	Mouse	1/250	ND	Campbell *et al.* 2001
hMad2	Rabbit	1/250	ND	Dr. Salmon (U of North Carolina)
hMps1	Rabbit	1/500	ND	Liu *et al.* 2003
hCENP-E	Rabbit	1/1000	ND	Chan *et al.* 1998
hAurora-B	Rabbit	1/1000	ND	Abcam (ab2254)
hCdc27	Rabbit	1/250	ND	Sudakin *et al.* 2001
hp50	Mouse	1/500	ND	Dr. Valle (Columbia University)
hdIC (74.1)	Mouse	1/250	ND	Abcam (ab23905)
hTubulin	Mouse	1/2000	1/5000	Sigma (B512)
hPericentrin	Rabbit	1/2000	ND	Abcam (ab4448)
hCyclin-B	Mouse	1/500	1/1000	Santa Cruz (sc-245)
hCENP-F	Rabbit	1/750	ND	Chan *et al.* 1998
hCdc20	Rabbit	1/250	ND	Sudakin *et al.* 2001
hMCAK	Rabbit	1/1000	ND	Abcam (ab42676)
hPlk1	Mouse	1/1000	ND	Dr. Lee (NIH)
hHec1	Rabbit	1/1000	ND	Abcam (ab35651)
GFP-IR800	Mouse	ND	1/10,000	Rockland (600-132-215)
GST	Rabbit	ND	1/1000	Chan *et al.* 1998
LexA	Rabbit	ND	1/1000	Abcam (50953)
B42	Rabbit	ND	1/1000	Sigma (B9808)
hSpindly	Rat	1/1000	ND	This study

Table 1-2: *Secondary Antibodies*

Antibody target	Species	IF dilution	Western Blot dilution	Source
Mouse-Alexa488	Goat	1/1000	ND	Molecular Probes (A11029)
Rat-Alexa488	Goat	1/1000	ND	Molecular Probes (A11006)
Rabbit-Alexa488	Goat	1/1000	ND	Molecular Probes (A11034)
Mouse-Alexa555	Goat	1/1000	ND	Molecular Probes (A21424)
Rat-Alexa555	Goat	1/1000	ND	Molecular Probes (A21434)
Rabbit-Alexa555	Goat	1/1000	ND	Molecular Probes (A21428)
Human-Alexa647	Goat	1/1000	ND	Molecular Probes (A21445)
Mouse-Alexa680	Goat	ND	1/10,000	Odyssey (827-08366)
Mouse-IR800	Donkey	ND	1/10,000	Rockland (610-732-129)
Rat-Alexa680	Goat	ND	1/10,000	Molecular Probes (A21096)
Rat-IR800	Donkey	ND	1/10,000	Rockland (612-132-120)
Rabbit-Alexa680	Goat	ND	1/10,000	Molecular Probes (A21109)
Rabbit-IR800	Donkey	ND	1/10,000	Rockland (611-732-127)

2.15 Primers

Table 1-3a: *Primer targets and linker sequences*

Primer	Gene	cDNA target (bp)	Linker	Construct
Ch69	hZW10	1-18	SalI	pENTR3C-hZW10
TJY940	hZW10	2313-2336	SalI	pENTR3C-hZW10
TJY939	hZW10	156-170	BamHI	N1
Ch45	hZW10	225-244	BamHI	N2
Ch228	hZW10	255-281	BamHI	N3
Ch44	hZW10	396-413	BamHI	N4
Ch46	hZW10	645-663	BamHI	N5
Ch47	hZW10	1005-1023	BamHI	N6
Ch48	hZW10	1386-1404	BamHI	N7
Ch49	hZW10	1668-1686	BamHI	N8
Ch50	hZW10	1863-1881	BamHI	N9
Ch57	hZW10	2313-2336	XhoI	N1-N9
Ch160	hZW10	2142-2165	XhoI	C1
Ch159	hZW10	2073-2093	XhoI	C2
Ch227	hZW10	1661-1679	XhoI	C3
Ch226	hZW10	1383-1406	XhoI	C4
Ch445	hZW10	1214-1232	attB2	C5
Ch444	hZW10	1048-1067	attB2	C6
Ch443	hZW10	933-953	attB2	C7
Ch70	hZW10	656-673	XhoI	C8
Ch231	hZW10	397-416	XhoI	C9
Ch230	hZW10	226-245	XhoI	C10
Ch229	hZW10	1-18	BamH1	C1-4, C8-10
Ch447	hZW10	1-18	attB1	C5-7
Ch411	hZW10	2313-2336	attB2	20, 30, 35, 45-779
Ch381	hZW10	60-79	attB1	20-339
Ch383	hZW10	90-109	attB1	30-779
Ch384	hZW10	105-127	attB1	35-779
Ch386	hZW10	135-159	attB1	45-779
Ch483	hZW10	1488-1558		$hZW10^{siR}$ Forward
Ch484	hZW10	1488-1558		$hZW10^{siR}$ Reverse
Ch409	hZW10	13-51		HS11AA Forward
Ch410	hZW10	13-51		HS11AA Reverse
Ch397	hZW10	88-128		GE36AA Forward
Ch398	hZW10	88-128		Ge36AA Reverse
Ch407	hZW10	123-156		S47A Forward
Ch408	hZW10	123-156		S47A Reverse
Ch405	hZW10	128-165		EF48AA Forward
Ch406	hZW10	128-165		EF48AA Reverse

Table 1.3b: *Primer targets and linker sequence*

Primer	Gene	cDNA target (bp)	Linker	Construct
Ch391	hZW10	140-169		S52A Forward
Ch392	hZW10	140-169		S52A Reverse
Ch393	hZW10	150-182		S55A Forward
Ch394	hZW10	150-182		S55A Reverse
Ch395	hZW10	156-190		GLI58AAA Forward
Ch396	hZW10	156-190		GLI58AAA Reverse
Ch399	hZW10	184-225		SE67AA Forward
Ch400	hZW10	184-225		SE67AA Reverse
Ch403	hZW10	189-228		DI69AA Forward
Ch404	hZW10	189-228		DI69AA Reverse
Ch401	hZW10	219-256		SE79AA Forward
Ch402	hZW10	219-256		SE79AA Reverse
Ch312	hZW10	346-390		N123T Forward
Ch313	hZW10	346-390		N123T Reverse
Ch166	hZW10	1782-1820		L600P Forward
Ch167	hZW10	1782-1820		L600P Reverse
Ch314	hZW10	1850-1892		S623G Forward
Ch315	hZW10	1850-1892		S623G Reverse
Ch162	hZW10	1903-1934		W640S Forward
Ch163	hZW10	1903-1934		W640S Reverse
Ch168	hZW10	2050-2083		M690R Forward
Ch169	hZW10	2050-2083		M690R Reverse
Ch164	hZW10	2114-2153		E712V Forward
Ch165	hZW10	2114-2153		E712V Reverse
Ch83	hAurora B	1-20	BamHI	pENTR3C-hAurora-B
Ch84	hAurora B	1053-1072	XhoI	pENTR3C-hAurora-B
Ch71	hp50	1-19	BamHI	pENTR3C-hp50
Ch72	Hp50	1198-1220	EcoR1	pENTR3C-hp50
hBub1 3'	hBub1	1-17	BamHI	pENTR3C-hBub1
hBub1 5'	hBub1	1110-1128	SalI	pENTR3C-hBub1
Ch717	hSpindly	1-19	attB1	pDONR221-hSpindly
Ch718	hSpindly	1801-1819	attB2	pDONR221-hSpindly
Ch374		attB1		attB1 extension Forward
Ch375		attB2		attB2 extension Reverse
Ch114		NotI		NotI mini primer

Table 1.4a: *Complete Primer Sequences*:

Primer	Sequence
Ch69	ATCGTCGACATGGCCTCGTTCGTGAC
TJY940	GTCGACATTTAATTTTAGCAAGGGCAGCTGC
TJY939	GGATCCATGCAGAGCGCGCAG
Ch45	ACTGGATCCAGGATAGAGAGTGAGGTCCG
Ch228	GGATCCCACGTATCAACCGGTGAATTTACAGAC
Ch44	ACTGGATCCACTGGTGCTCAGCGTCTG
Ch46	ACTGGATCCGAGGAGAAGACCCCTATGC
Ch47	ACTGGATCCGAGGACTTGTCTGAGTGCC
Ch48	ACTGGATCCCCTGAAAATACATTGGACC
Ch49	ACTGGATCCCATCAGTTCAGATTGCGTC
Ch50	ACTGGATCCGCAAGTAAAGCAGTCCGGC
Ch57	ACTGTCGACTTATTTAATTTTAGCAAGGGCAGCTGC
Ch160	CTCGAGTTATGGCATCCATTTTGGCACATAGAC
Ch159	CTCGAGTTATGCAAATACTTGGGGTCCTTC
Ch227	CTCGAGTTATCTGAACTGATGCCCGAGG
Ch226	CTCGAGTTATTGGTCAACTGTATTTTCAGGCTC
Ch445	AGAAAGCTGGGTCAGGCTGCCACAATCACATCC
Ch444	AGAAAGCTGGGTCAGCTGCTATTTGTTGGAATCG
Ch443	AGAAAGCTGGGTCAATTTTCCAGGTCAGTGTCAAG
Ch70	ATCCTCGAGCTGATGGGTGGCATAGGG
Ch231	CTCGAGTTATTCCAGACGCTGAGCACCAG
Ch230	CTCGAGTTAGCGGACCTCACTCTCTATCC
Ch229	GGATCCATGGCCTCGTTCGTGAC
Ch447	AAAAAGCAGGCTCCATGGCCTCGTTCGTGAC
Ch411	AGAAAGCTGGGTATTTAATTTTAGCAAGGGCAGCTGC
Ch381	AAAAAGCAGGCTCTCTGGGGACCCGGATCAGC
Ch383	AAAAAGCAGGCTCGCGGGTGGAGGAGATCAAG
Ch384	AAAAAGCAGGCTCCAAGGGTGAGGTGTGCAATATG
Ch386	AAAAAGCAGGCTCGAAGTACAGTGAATTCCTGCCTAG
Ch483	GCAACAACCAGTAGTGACCAGTGCGCCGTTCAACTTTTCTACTC
Ch484	GAGTAGAAAAGTTGAACGGCGCACTGGTCACTACTGGTTGTTGC
Ch409	GTGACAGAAGTTTTGGCAGCCGCCGGGAGGCTGGAAAAG
Ch410	CTTTTCCAGCCTCCCGGCGGCTGCCAAAACTTCTGTCAC
Ch397	CGGGTGGAGGAGATCAAGGCCGCGGTGTGCAATATGATTAG
Ch398	CTAATCATATTGCACACCGCGGCCTTGATCTCCTCCACCCG
Ch407	GATTAGCAAGAAGTACGCTGAATTCCTGCCTAGC
Ch408	GCTAGGCAGGAATTCAGCGTACTTCTTGCTAATC
Ch405	GCAAGAAGTACAGTGCCGCCCTGCCTAGCATGCAGAGC
Ch406	GCTCTGCATGCTAGGCAGGGCGGCACTGTACTTCTTGC
Ch391	GTGAATTCCTGCCTGCCATGCAGAGCGCGC
Ch392	GCGCGCTCTGCATGGCAGGCAGGAATTCAC
Ch393	CCTAGCATGCAGGCCGCGCAGGGCCTGATTAC

Table 1.4b: *Complete Primer Sequences*

Primer	Sequence
Ch394	GTAATCAGGCCCTGCGCGGCCTGCATGCTAGG
Ch395	CATGCAGAGCGCGCAGGCCGCCATTACCCAGGTGG
Ch396	CCACCTGGGTAATGGCGGCCTGCGCGCTCTGCATG
Ch399	CAGGTGGATAAGCTATCTGCCGCCATTGACCTGCTGAAATCC
Ch400	GGATTTCAGCAGGTCAATGGCGGCAGATAGCTTATCCACCTG
Ch403	GGATAAGCTATCTGAAGCCGCTGACCTGCTGAAATCCAGG
Ch404	CCTGGATTTCAGCAGGTCAGCGGCTTCAGATAGCTTATCC
Ch401	GAAATCCAGGATAGAGGCCGCGGTCCGCCGGGATCTTC
Ch402	GAAGATCCCGGCGGACCGCGGCCTCTATCCTGGATTTC
Ch312	CCACTGCTATTGAAGAATATACTTGTGCATTAACAGAGAAGAAG
Ch313	CTTCTTCTCTGTTAATGCACAAGTATATTCTTCAATAGCAGTGG
Ch166	GCACAGAAAGGTGAACCTCTGGAAAGATTATCAAGTGC
Ch167	GCACTTGATAATCTTTCCAGAGGTTCACCTTTCTGTGC
Ch314	GAATTATTCTGCAGCAGGTAAAGCAGTCCGGCAG
Ch315	CTGCCGGACTGCTTTACCTGCTGCAGAATAATTC
Ch162	GACTTGGAATTGTGTCGCAGGATGTCCTGCC
Ch163	GGCAGGACATCCTGCGACACAATTCCAAGTC
Ch168	CCTTATGCAAAACAGTGAGGGATGAAGGACCCC
Ch169	GGGGTCCTTCATCCCTCACTGTTTTGCATAAGG
Ch164	GAACAAGAAATATCAAGAAGTGGTTCCAGTCTATGTGCC
Ch165	GGCACATAGACTGGAACCACTTCTTGATATTTCTTGTTC
Ch83	GGATCCATGGCCCAGAAGGAGAACTCC
Ch84	CTCGAGTCAGGCGACAGATTGAAGGG
Ch71	ATCGGATCCATGGCGGACCCTAAATACGCC
Ch72	ATCGAATTCTCACTTTCCCAGCTTCTTCATCC
hBub1 3'	GGATCCATGGACACCCCGGAAAATGTCC
hBub1 5'	GTCGACTGGCTGGGGACACCAAAGC
Ch717	AAAAAGCAGGCTACATGGAGGCAGATATAATCAC
Ch718	AGAAAGCTGGGTTACTGTTGAGGGCACTGG
Ch374	GGGGACAAGTTTGTACAAAAAAGCAGGCT
Ch375	GGGGACCACTTTGTACAAGAAAGCTGGGT
Ch114	TGCGGCCGCA

2.16 Buffers and Recipes

SD – HIS, -TRP, -URA (1L)
1.35 g Amino Acid Mix (2 g of each: adenine sulfate, alanine, arginine, aspartic acid, aspargine, cystine, glutamic acid, glutamine, glycine, isoleucine, lysine, methionine, phenylalanine, proline, serine, threonine, tyrosine and valine)
6.7 g Yeast Nitrogen Base without amino acids
20 g Dextrose
8 ml 100 mM Leucine
1000 ml ddH20
+/- 15 g Agar

SD – HIS, -TRP, -URA +gal/raff (1L)
1.35 g Amino Acid Mix (2 g of each: adenine sulfate, alanine, arginine, aspartic acid, aspargine, cystine, glutamic acid, glutamine, glycine, isoleucine, lysine, methionine, phenylalanine, proline, serine, threonine, tyrosine and valine)
6.7 g Yeast Nitrogen Base without amino acids
10 g raffinose
20 g D-galactose
8 ml 100 mM Leucine
1000 ml ddH20
+/- 15 g Agar

SD – HIS, -TRP, -URA +gal/raff +X/gal (1L)
1.35 g Amino Acid Mix (2 g of each: adenine sulfate, alanine, arginine, aspartic acid, aspargine, cystine, glutamic acid, glutamine, glycine, isoleucine, lysine, methionine, phenylalanine, proline, serine, threonine, tyrosine and valine)
6.7 g Yeast Nitrogen Base without amino acids
10 g raffinose
20 g D-galactose
8 ml 100 mM Leucine
100 ml 1X PBS
900 ml ddH20
800 µl X-gal (100mg/ml)
15 g Agar

PEI
1 mg PEI (Polysciences, Inc. cat # 23966)
1 ml ddH2O
-adjust pH to 7.0 with HCl
-filter through 0.22 µm membrane
-store at -80°C

Mowiol Mounting Media
Add 2.4 g of Mowiol powder to 6 g of glycerol, stir to mix
Add 6 mL of ddH_2O and leave stirring overnight at room temperature
Add 12 mL of 0.2M phosphate buffer, pH 7.4
Heat to 50°C for 10 minutes with gentle stirring to minimize bubbles
After Mowiol is dissolved, centrifuge at 5000 *g* for 15 minutes
Add 0.1% n-propyl gallate
Aliquot and store at -20°C

3% glutaraldehyde in Millonig's phosphate buffer
1.5 mL 50% Glutaraldehyde
25 mL Solution C
pH 7.4

Solution A: 2.26 g NaH_2P0_4 / 100 mL H_20
Solution B: 2.52 g NaOH / 100 mL H_20
Dextrose, 5.4 % or sucrose 10%
Stock glutaraldehyde 35 or 50% (Fisher Scientific G-151)
$CaCl_2$: 1%

Solution C (PO_4 buffer)
166 mL Solution A
34 mL Solution B
Adjust pH to 7.4
22.2 mL Dextrose
2.2 mL $CaCl_2$

2% OsO_4
0.5 mg OsO_4
50 mL Solution C
pH to 7.4

Chapter III: *Stable hZW10 kinetochore residency, mediated by hZwint-1 interaction, is essential for the mitotic checkpoint.**

* A version of this chapter has been published as Famulski *et al.* 2008 **Journal of Cell Biology** 180: 507-520.

- All of the experiments, figures and the manuscript were prepared by Jakub Famulski

3.1 Abstract

The mitotic checkpoint is an essential surveillance mechanism that ensures high fidelity chromosome segregation during mitosis. Mitotic checkpoint function depends on numerous kinetochore proteins, including ZW10, ROD, and Zwilch (the ROD–ZW10–Zwilch complex). Through an extensive mutagenesis screen of hZW10, we have mapped the kinetochore localization domain of hZW10 as well as the hZwint-1 interaction domain. We find that hZwint-1–noninteracting mutants still localize to kinetochores. In addition, using fluorescence recovery after photobleaching, we have found that hZW10 residency at metaphase kinetochores is brief (half-time of 13 s). However, during prometaphase or at unattached kinetochores, enhanced green fluorescent protein–hZW10 becomes a stable component of the kinetochore. Moreover, we find that stable hZW10 kinetochore residency at prometaphase kinetochores is dependent on its interaction with hZwint-1, and is essential for mitotic checkpoint arrest.

3.2 Introduction

High fidelity chromosome segregation is essential for the maintenance of genomic stability. The mitotic checkpoint is a failsafe mechanism that prevents premature anaphase onset and ensures accurate chromosome segregation. The mitotic checkpoint functions by monitoring proper kinetochore–microtubule (MT) attachments as well as chromosome alignment at the metaphase plate (Rieder et al., 1994; Skibbens et al., 1995). It is composed of several evolutionarily conserved kinetochore proteins including the MADs, the BUBs, and Mps1, as well as ZW10, ROD, and Zwilch [for reviews see (Chan et al., 2005; Karess, 2005)]. These proteins monitor kinetochore-MT attachment and chromosome alignment and participate in the generation and amplification of the "wait anaphase" signal. BubR1, Bub3, Mad2, and Cdc20 are known to function as a mitotic checkpoint complex that directly inhibits the anaphase-promoting complex/cyclosome, an E3 ubiquitin ligase complex that drives ubiquitin-mediated degradation of key mitotic substrates that are required for the maintenance of metaphase arrest (Sudakin et al., 2001). Through the mitotic checkpoint complex, the mitotic checkpoint can initiate and maintain mitotic arrest even in the presence of a single unattached kinetochore (Rieder et al., 1994).

ZW10 and ROD are recently recognized essential components of the mitotic checkpoint (Chan et al., 2000; Karess, 2005; Kops et al., 2005a). Identified in *Drosophila melanogaster*, ZW10 and ROD mutants exhibit identical mitotic phenotypes, including high rates of aneuploidy and chromosome missegregation stemming from the lack of mitotic checkpoint function (Basto et al., 2000; Karess and Glover, 1989; Scaerou et al., 1999; Williams et al., 1992). hZW10 has been shown to be required for hMad1 and hMad2 kinetochore recruitment, which may explain the ZW10 mutant phenotypes (Buffin et al., 2005; Kops et al., 2005a). However, the exact molecular functions of hZW10 or hROD within the mitotic checkpoint remain unknown. ROD and ZW10 are evolutionarily conserved from *Caenorhabditis elegans* to humans yet lack homologues in yeast (Starr et al., 1997). This suggests that ZW10 and ROD may represent an arm of the mitotic checkpoint that evolved to maintain genomic stability of the larger and more complex higher eukaryote genomes. During mitosis, ZW10 and ROD interact with another mitotic checkpoint protein, Zwilch, and form an evolutionarily conserved complex (ROD–ZW10–Zwilch [RZZ]) that localizes to kinetochores from early prometaphase until the onset of anaphase (Williams et al., 1996; Williams and Goldberg, 1994; Williams et al., 2003). The RZZ complex is known to be required for kinetochore recruitment of the MT motor dynein/dynactin (Starr et al., 1998). Dynein/dynactin was found to directly interact with the RZZ complex in a yeast two-hybrid screen, which identified dynamitin, a dynactin subunit, as an interactor of hZW10 (Starr et al., 1998; Yang et al., 2007b). Kinetochore dynein/dynactin is, in turn, required for chromosomal congression, resulting in chromosome alignment at the metaphase plate as well as transport of mitotic checkpoint proteins off kinetochores (Howell et al., 2001; Yang et al., 2007b). Before the onset of anaphase, *D. melanogaster* ROD has been observed to travel from kinetochores along kinetochore-MTs toward the spindle poles but only once chromosomes became bioriented (Basto et al., 2004; Scaerou et al., 1999). This movement of dmROD along kinetochore-MTs is also dependent on kinetochore dynein/dynactin. Dynein/dynactin-

mediated transport of ROD, ZW10, and other mitotic checkpoint proteins off kinetochores in response to biorientation of chromosomes has been hypothesized to contribute to the silencing of the mitotic checkpoint (Howell et al., 2001; Wojcik et al., 2001).

Localization of hROD and hZW10 to kinetochores is correlated with mitotic checkpoint function, as implicated by anti-hZW10 and anti-hROD antibody microinjection experiments (Chan et al., 2000). Understanding how ROD and ZW10 localize to and behave at kinetochores is thus essential for determining the mitotic checkpoint functions of the RZZ complex. hZW10 kinetochore localization has been attributed to the interaction between hZW10 and hZwint-1. hZwint-1 was identified in a yeast two-hybrid screen for hZW10-interacting proteins and is thought to function as a scaffold for hZW10 at kinetochores (Starr et al., 2000). siRNA knockdown of hZwint-1 has been shown to result in the loss of kinetochore hZW10, thus suggesting that hZwint-1 is required for hZW10 recruitment to kinetochores during mitosis (Wang et al., 2004a). However, experiments mapping the hZwint-1 interaction domain of hZW10 have thus far been contradictory. Starr et al. (2000) had originally mapped the hZwint-1 interaction domain to the C terminus of hZW10 yet, in a more recent paper, Wang et al. (2004a) showed that the N terminus of hZW10 is sufficient for hZwint-1 interaction as well as kinetochore localization. To clarify the location of the hZwint-1 interaction, as well as that of the kinetochore localization domains of hZW10, we undertook a very detailed structure function study of hZW10. We have found that the N terminus of hZW10 is indeed sufficient for hZwint-1 interaction; however, it is not sufficient for kinetochore localization. Through our mutagenesis approach we have also discovered that hZW10 kinetochore localization may not solely depend on its interaction with hZwint-1. Instead, we find that the interaction between hZwint-1 and hZW10 increases hZW10 residency at kinetochores lacking proper kinetochore–MT attachments and that this increased residency is essential for proper function of the mitotic checkpoint.

3.3 Results

3.3.1 hZW10 kinetochore localization requires both the C and N terminus

Previous studies have indicated that the kinetochore localization domain of hZW10 mapped to its far N terminus (aa 1–80; Wang et al., 2004a). In addition, this N-terminal domain was shown by the yeast two-hybrid assay to be sufficient for hZwint-1 interaction, thus linking hZwint-1 interaction with hZW10 kinetochore localization. However, Starr et al. (2000), also using the yeast two-hybrid assay, originally showed that the C terminus of hZW10 was required for the hZwint-1 interaction and therefore, presumably, hZW10 kinetochore localization. Thus, it appears that the locations of the hZwint-1 interaction and kinetochore localization domains of hZW10 remain unclear. We therefore set out to map the kinetochore localization domain of hZW10 by creating an extensive series of sequential N- and C-terminal deletion constructs of hZW10 (Fig. 3.1 A). These EGFP-tagged constructs were expressed in HEK293 cells and confirmed by Western blotting (Fig. S3.1, B and D). Analysis of expression levels revealed an approximately twofold over-expression of EGFP-hZW10 (Fig. S3.1 E). However, transient transfection often leads to a broad range of expression levels and, therefore, the overexpression of every construct was not determined. Presence of the EGFP fusions at kinetochores in transfected mitotic HeLa cells was determined using fluorescence microscopy in both prometaphase and metaphase (Fig. 3.1 B). To increase the sensitivity of the kinetochore localization assay, we also treated the transfected cells with vinblastine to eliminate kinetochore–MT attachment and thus enhance hZW10 kinetochore recruitment (Fig. S3.1 F). Our analysis indicated that the first 52 aa of hZW10 (mutant N1) are dispensable for kinetochore localization. Any N-terminal deletions larger than 52 aa, such as 75 aa (mutant N2), resulted in loss of kinetochore localization (Fig. 3.1 B and Fig. S3.1 A). The inability of deletion constructs (N2–9) to localize to kinetochores could reflect the loss of proper folding of the protein. Contrary to published results, we found that the N-terminal 82 aa of hZW10 (mutant C10) was not sufficient for kinetochore localization (Fig. 3.1 B; Wang et al., 2004a). In fact, any deletion from the C terminus resulted in the loss of kinetochore localization (Fig. 3.1 B, Fig. S3.1 C, and Table 2.1), thus indicating that the C terminus of hZW10 is essential for kinetochore localization. However, none of the C-terminal fragments of hZW10 (N5–9) were able to localize to kinetochores. Our deletion-mapping results therefore indicate that the N-terminal boundary for hZW10 kinetochore targeting is near aa 52, whereas the C-terminal boundary extends to the C terminus because no deletions from this end were tolerated.

Figure 3.1: **An extensive mutagenesis screen for the hZW10 kinetochore localization and hZwint-1 interaction domains.**
A) A schematic diagram depicting N- and C-terminal hZW10 deletion constructs. Amino acid sizes are indicated. Yeast two-hybrid interaction with hZwint-1 and kinetochore localization are indicated by a blue plus sign for positive results and a red minus sign for negative results. **B)** HeLa cells transiently transfected with EGFP-hZW10 N- and C-terminal deletion constructs were analyzed for kinetochore localization during mitosis with fluorescence microscopy. Representative images show that only N-terminal deletion N1 retained the ability to localize to the kinetochore. All mutants behaved similarly at both prometaphase and metaphase kinetochores. Bar, 10 μm. **C)** A schematic diagram depicting the locations of the pentapeptide insertion mutants generated in the hZW10 cDNA (aa 1–779) and the $hZW10^{N1}$ cDNA (aa 52–779). Yeast two-hybrid interaction with hZwint-1 and kinetochore localization are indicated by a blue plus sign for positive interaction and a red minus sign for negative interaction. **D)** HeLa cells transiently transfected with the EGFP-hZW10 insertion mutant constructs were analyzed for kinetochore localization during mitosis using fluorescence microscopy. Representative images show that insertion mutations in the C terminus of hZW10 (mutants R, U, and X) abolish kinetochore localization of hZW10. Fluorescence microscopy analysis of remaining constructs is shown in Fig. S3.4A and their kinetochore localization status is summarized in Table 2.2. Chromosomes are stained with DAPI. Bar, 10 μm. **E)** HeLa cells transiently transfected with the EGFP-$hZW10^{N1}$ pentapeptide insertion mutant constructs were analyzed for kinetochore localization during mitosis using fluorescence microscopy. Representative images show that peptide insertions in the C terminus of $hZW10^{N1}$ (mutants $N1^{n}$, N1°, and $N1^{p}$) abolish the ability of hZW10 to localize to the kinetochore. Fluorescence microscopy analysis of remaining constructs is shown in Fig. S3.5 A and their kinetochore localization status is summarized in Table 2.2. Chromosomes are stained with DAPI. Bar, 10 μm.

Figure 3.1

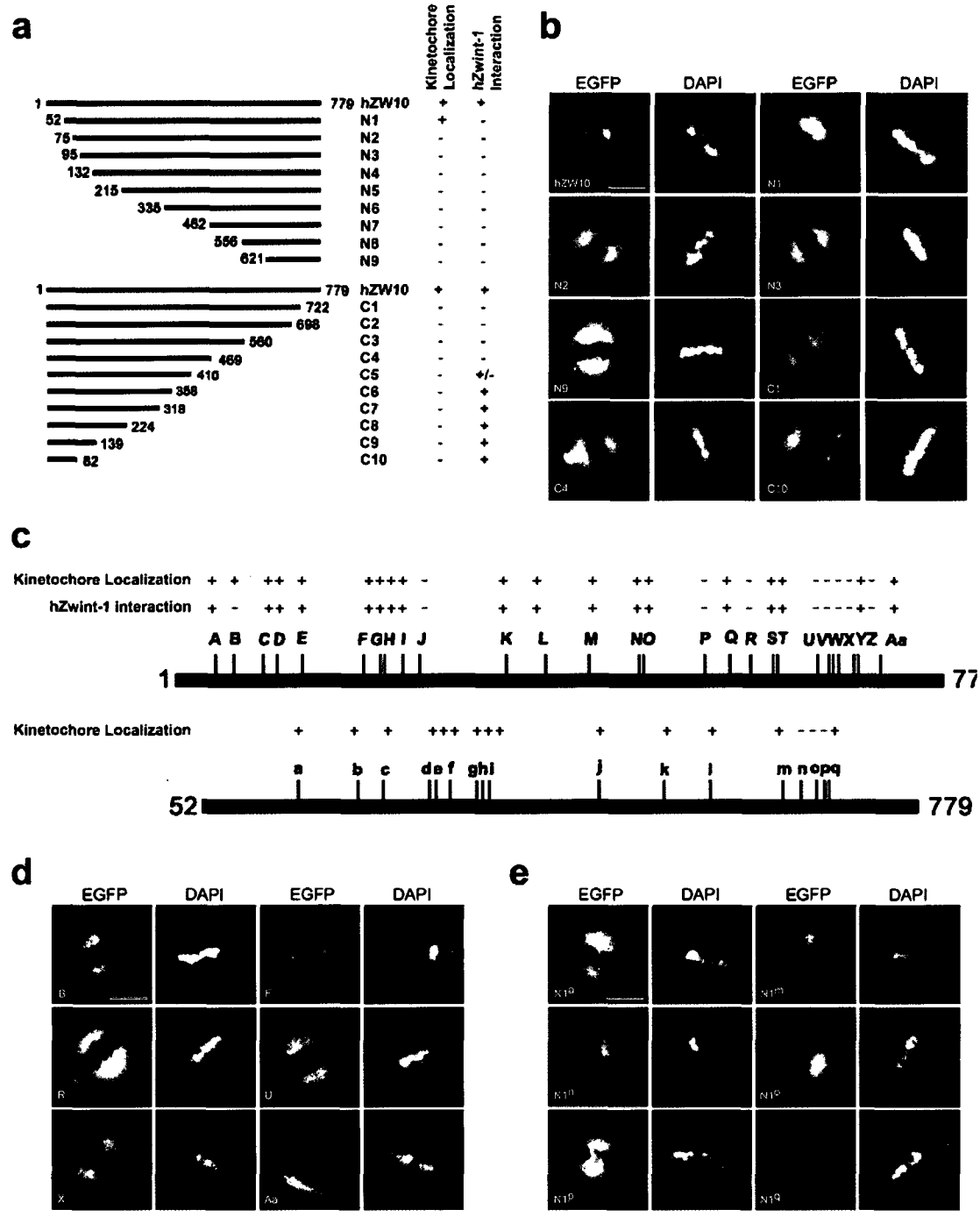
a
Kinetochore Localization
hZwint-1 Interaction
1 779 hZW10 + +
52 N1 + -
75 N2 - -
95 N3 - -
132 N4 - -
215 N5 - -
335 N6 - -
482 N7 - -
556 N8 - -
621 N9 - -
1 779 hZW10 + +
722 C1 - -
698 C2 - -
560 C3 - -
469 C4 - -
410 C5 - +/-
358 C6 - +
318 C7 - +
224 C8 - +
139 C9 - +
82 C10 - +
b
EGFP DAPI EGFP DAPI
hZW10
N1
N2
N3
N9
C1
C4
C10
c
Kinetochore Localization + + ++ + ++++ - + + + ++ - + - ++ ----+- +
hZwint-1 interaction + - ++ + ++++ - + + + ++ - + - ++ ----+- +
A B C D E F G H I J K L M NO P Q R ST UVWXYZ Aa
1 77
Kinetochore Localization + + + +++ +++ + + + + ---+
a b c de f ghi j k l m n o p q
52 779
d
EGFP DAPI EGFP DAPI
B
F
R
U
X
Aa
e
EGFP DAPI EGFP DAPI
N1
N2
N3

3.3.2 The interaction between hZW10 and hZwint-1 is dispensable for kinetochore localization of hZW10

hZW10 kinetochore localization has previously been correlated with hZwint-1 interaction using the yeast two-hybrid assay (Wang et al., 2004a). We therefore analyzed our deletion mutant library for interaction with hZwint-1 using the Lex-A–based yeast two-hybrid assay (Toby and Golemis, 2001). Wild-type hZW10 and hZwint-1 readily interacted in the Lex-A–based yeast two-hybrid assay (Table 2.1). When screening our truncation mutants, we found that all the N-terminal deletion constructs (N1–9) as well as the C-terminal truncations C1–4 lost the ability to interact with hZwint-1. However, constructs C5–10, which all lack at least the C-terminal third of hZW10 (aa 410–779), retained the ability to interact with hZwint-1 (Fig. 3.1 A and Table 2.1). The smallest N-terminal fragment of hZW10, which retained the ability to interact with hZwint-1, was C10, aa 1–82 (Table 2.1). We therefore concluded that the N terminus of hZW10 (aa 1–82) contains the hZwint-1 interaction domain. Interestingly, our results also indicated that the direct interaction between hZW10 and hZwint-1, in the context of the entire protein, requires the C terminus (aa 410–779). Mutants C1–4, although containing the hZwint-1 interaction domain (aa 1–82), did not interact with hZwint-1. These findings may reflect that mutants C1–4 have incorrect folding. To narrow down the N-terminal boundary for the hZwint-1 interaction domain, we also generated several smaller deletions of hZW10 (Fig. S3.2 A). We found that N-terminal deletions of more than 30 aa disrupted the hZW10–hZwint-1 interaction (Fig. S3.2A). These findings narrow down the hZwint-1 interaction domain of hZW10 to aa 30–80. All the constructs with N-terminal deletions ≤ 52 aa retained the ability to localize to kinetochores (Fig. S3.2, B and C). More importantly, mutant C10, which contains the proposed kinetochore localization domain of hZW10 (Wang et al., 2004a), did not localize to kinetochores in our experiments. We therefore conclude that the N terminus of hZW10 is indeed sufficient for hZwint-1 interaction but is not sufficient for kinetochore localization. Our results indicate that the hZW10–hZwint-1 interaction may be dispensable for hZW10 kinetochore recruitment.

To confirm our yeast two-hybrid results, we performed in vitro GST pulldown experiments using GST–hZwint-1 to assay for interaction with EGFP-hZW10 or EGFP-hZW10^{N1}. We observed that GST–hZwint-1 readily pulled down EGFP-hZW10 from HEK293 cell lysates cotransfected with the GST–hZwint-1 and EGFP-hZW10 constructs (Fig. S3.2 D). In contrast, when GST–hZwint-1 was used to pull down EGFP-hZW10^{N1}, we observed a markedly reduced amount of EGFP-hZW10^{N1} associated with GST–hZwint-1 compared with that of EGFP-hZW10. Other hZwint-1–noninteracting mutants behaved similarly to N1 when analyzed by the GST pulldown assay (Fig. S3.2 E). These results suggest that the hZwint-1–noninteracting hZW10 mutants that were identified using the yeast two-hybrid assay also do not interact with hZwint-1 in mammalian tissue culture cells.

3.3.3 The hZW10 kinetochore localization domain resides within the C terminus

To further define the kinetochore localization and hZwint-1 interaction domains of hZW10, we used a random insertion mutagenesis approach. A library of hZW10 insertion mutants were created using transposon-based insertion mutagenesis, where 15 bp were randomly inserted into the hZW10 or N1 cDNA. We selected an array of 27 insertion mutants spanning the hZW10 cDNA and 17 insertion mutants spanning the N1 cDNA for functional analysis (Fig. 3.1 C and Table 2.2). Fluorescence microscopy of

HeLa cells transfected with EGFP fusion insertion mutant constructs identified several kinetochore nonlocalizing mutants, the majority of which were confined to the C terminus of the hZW10 and N1 cDNAs (Table 2.2). Fig. 3.1 D shows representative hZW10 insertion mutants (R, U, and X) that did not localize to kinetochores as well as insertion mutants that retained the ability to localize (B, F, and Aa). Fig. 3.1 E shows representative N1 insertion mutants that were unable to localize to kinetochores ($N1^{n}$, $N1^{o}$, and $N1^{p}$) as well as N1 insertion mutants that did localize ($N1^{a}$, $N1^{m}$, and $N1^{q}$). Analysis of all the remaining insertion mutants is presented in Figs. S3.3 A and S3.4 A and summarized in Table 2.2. Again, the kinetochore nonlocalizing mutants were confirmed for loss of localization in cells lacking kinetochore–MT attachments (Figs. S3.3 B and S3.4 B). The insertion mutagenesis thus confirmed our deletion library results in that the C terminus of hZW10 (aa 536–686) is essential for its kinetochore localization.

The insertion mutants were also assayed for interaction with hZwint-1 using the yeast two-hybrid assay. In concordance with our deletion analysis, we identified an N-terminal hZW10 insertion mutant occurring within the hZwint-1 interaction domain that no longer interacted with hZwint-1 (Table 2.2, mutant B, insertion at aa 61). The lack of interaction with hZwint-1 was again confirmed by GST pulldown (Fig. S3.2 E). This particular insertion mutant still localized to kinetochores when analyzed by fluorescence microscopy (Fig. 3.1 D and S3.3 B). We also found that C-terminal insertion mutants that did not localize to the kinetochore also did not interact with hZwint-1 (Fig. 3.1 C and Table 2.2). These insertion mutations (P, R, U, V, W, X, and Z) occurred between aa 536 and 686. The results from these C-terminal insertion mutants were surprising because the deletion analysis we had preformed identified the N terminus of hZW10 (aa 30–80) as the hZwint-1 interaction domain. We therefore conclude that the C terminus of hZW10 may play an indirect role in the interaction between hZwint-1 and hZW10.

To further validate our insertion mutagenesis results, we generated several single or multiple amino acid substitutions within the hZW10 cDNA, specifically at the C and N termini. These mutations were designed, based on our insertion mutagenesis screen, to specifically disrupt the hZwint-1 interaction and/or kinetochore localization domains of hZW10 (Fig. 3.2 A). In addition, we generated two mutations of hZW10 that have been reported in colon cancer, N123T and S623G (Wang et al., 2004b). Fluorescence microscopy analysis of HeLa cells transiently transfected with the mutant constructs revealed that two of our C-terminal hZW10 point mutants, L600P and W640S, no longer localized to kinetochores (Fig. 3.2 B and Fig. S3.5C). These mutants further confirmed our finding that the kinetochore localization domain of hZW10 resides within the C terminus. In addition, we isolated three N-terminal mutants, GLI58AAA, SE67AA, and DI69AA, that did not interact with hZwint-1 in the yeast two-hybrid assay or the GST pulldown assay yet retained kinetochore localization (Fig. 3.2, Fig. S3.2 E, Fig. S3.5 F, and Table 2.3). These mutants further confirmed that the N terminus of hZW10 contains the hZwint-1 interaction domain and that hZwint-1 interaction is dispensable for hZW10 kinetochore localization. Lastly, we found that the two colon cancer–associated point mutations had no effect on the ability of hZW10 to localize to kinetochores or interact with hZwint-1 (Fig. 3.2).

Figure 3.2: **hZW10 domains specifying hZwint-1 interaction and kinetochore localization are distinct.**
A) A schematic diagram of hZW10 depicting single amino acid changes generated in this study. Conservation of the amino acids chosen for mutagenesis is shown in Figs. S3.3 (A and B) and S3.4 (A and B). Yeast two-hybrid interaction with hZwint-1 and kinetochore localization are indicated by a blue plus sign for positive interaction and a red minus sign for negative interaction. **B)** HeLa cells transiently transfected with the EGFP-hZW10 site-directed mutant constructs were analyzed for kinetochore localization during mitosis using fluorescence microscopy. Representative images show that none of the hZW10 N-terminal mutants interfere with hZW10 localization at kinetochores. Mutations L600P and W640S abolish hZW10 localization at kinetochores. Analysis of all remaining amino acid substitution mutant constructs is shown in Figs. S3 (A and B) and S4 (A and B). All mutants behaved similarly at both prometaphase and metaphase kinetochores. Bar, 10 μm. **C)** A model diagram of hZW10 functional domains mapped by the mutagenesis screen. The N terminus of hZW10 (aa 30–80) contains the direct hZwint-1 interaction domain of hZW10, whereas the C terminus (aa 536–686) contains the kinetochore localization domain.

Figure 3.2

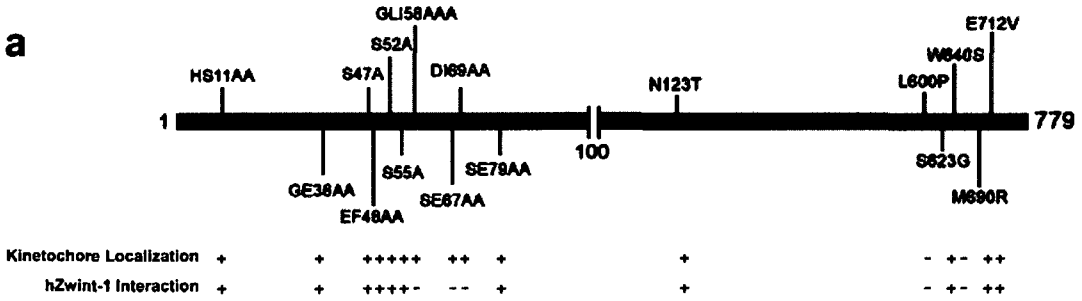
a
GLI58AAA
S52A
E712V
W640S
HS11AA
S47A
DI69AA
N123T
L600P
1
779
100
GE38AA
S55A
SE79AA
S623G
EF48AA
SE67AA
M690R
Kinetochore Localization + + +++++ ++ + + - +- ++
hZwint-1 Interaction + + ++++- -- + + - +- ++

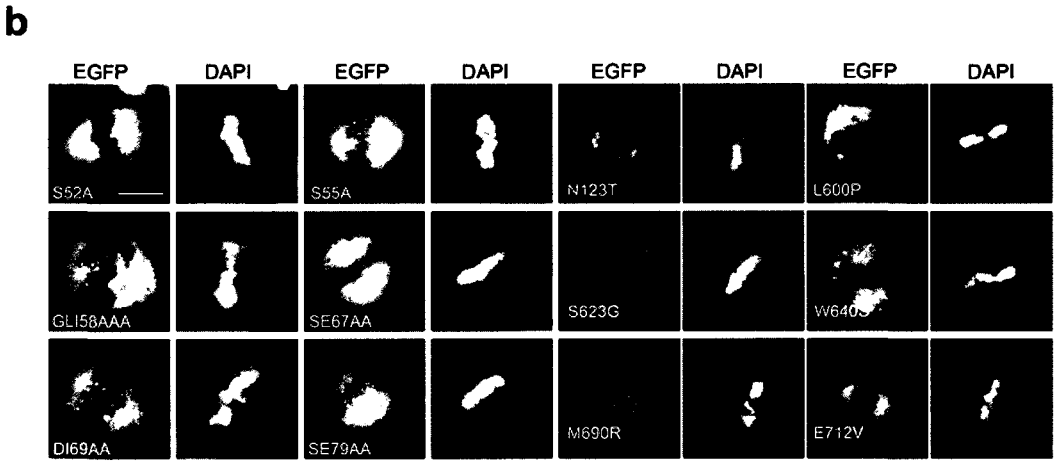
b
EGFP
DAPI
EGFP
DAPI
EGFP
DAPI
EGFP
DAPI
S52A
S55A
N123T
L600P
GLI58AAA
SE67AA
S623G
W640S
DI69AA
SE79AA
M690R
E712V

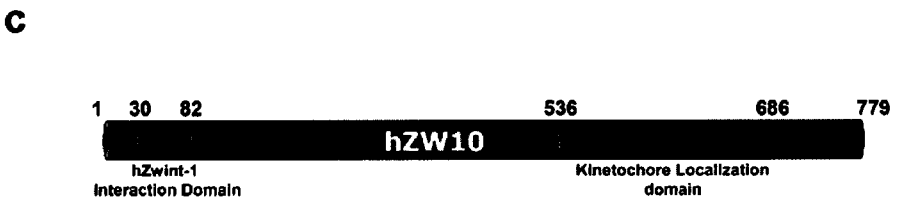
c
1
30
82
536
686
779
hZW10
hZwint-1
Interaction Domain
Kinetochore Localization
domain

Based on our extensive mutagenesis screen of hZW10 for the kinetochore localization and hZwint-1 interaction domain, we conclude that hZW10 contains two separate functional domains (Fig. 3.2 C). hZW10 directly interacts with hZwint-1 through an N-terminal domain (aa 30–80), whereas it localizes to kinetochores through a C-terminal domain (aa 536–686). The C-terminal domain of hZW10 alone, however, is not sufficient for kinetochore localization and the entire protein is likely to be required for proper function. Our conclusions as to the kinetochore localization domain boundaries are made largely based on our insertion and amino acid substitution mutagenesis results. The deletion mutations were not informative and likely did not behave properly in vivo because of problems with folding. As such, we have been unable to isolate a kinetochore localization domain away from the rest of the protein. Although hZwint-1 has been proposed to be required for hZW10 kinetochore localization, we find that disruption of the hZW10–hZwint-1 interaction does not prevent hZW10 kinetochore localization.

3.3.4 hZW10 residency at the kinetochore is influenced by kinetochore–MT attachment as well as the interaction between hZW10 and hZwint-1

Many of the mitotic checkpoint proteins required for generating the wait anaphase signal are known to be dynamic components of the kinetochore. Mad2, the quintessential component of the mitotic checkpoint, is known to be highly dynamic at unattached kinetochores (Shah et al., 2004). FRAP experiments have shown that Mad2 has a $t_{1/2}$, the time required for 50% recovery of fluorescence signal, of 4–5 s (Shah et al., 2004). Mps1, Cdc20, hBubR1, and hBub3 have also been shown to be dynamic components of the kinetochore (Howell et al., 2004). In contrast, structural components of the mitotic checkpoint, such as hHec1 and hNuf2, have been shown to be stable components of kinetochores (Hori et al., 2003). ZW10 and ROD, both essential components of the mitotic checkpoint thought to be involved in checkpoint signaling, may also be dynamic components of kinetochores. Studies using a GFP-tagged dmROD have shown that dmROD is in fact a dynamic component of the kinetochore with a $t_{1/2}$ recovery time of 25–45 s in prometaphase (Basto et al., 2004). However, kinetochore dynamics for dmZW10 or hZW10 remain unexamined.

To analyze hZW10 kinetochore dynamics, we generated a HeLa cell line stably expressing EGFP-hZW10. This cell line was subsequently used for FRAP experiments. We analyzed EGFP-hZW10 turnover at single kinetochores during different stages of mitosis. At the prometaphase kinetochore, we observed very little turnover of EGFP-hZW10 (Fig. 3.3 A). This suggested that EGFP-hZW10 remains stably bound to kinetochores that have not achieved metaphase alignment. At the metaphase kinetochore, we observed rapid turnover of EGFP-hZW10 with a $t_{1/2}$ recovery of 13.8 ± 5.2 s (Fig. 3.3 A). This suggested that hZW10 becomes a dynamic component of the kinetochore once bipolar kinetochore–MT attachment occurs. To verify our prometaphase results, we also analyzed the turnover rate of EGFP-hZW10 in cells treated with 7 μM STLC, a small molecule inhibitor of the kinesin Eg5 that results in monopolar spindles (Skoufias et al., 2006). Similar to prometaphase, we observed no turnover of EGFP-hZW10 in these cells (Fig. S3.4 D). Furthermore, we used 0.1 μM vinblastine to inhibit spindle formation and, therefore, prevent any MT occupancy at kinetochores (Jordan et al., 1992). The

vinblastine treatment also resulted in the stabilization of EGFP-hZW10 at kinetochores with little to no observable turnover (Fig. 3.3 A). The table in Fig. 3.3 C summarizes the $t_{1/2}$ recovery measurements for EGFP-hZW10. Based on the FRAP data, we conclude that hZW10 turnover at the kinetochore occurs only when chromosomes achieve bipolar kinetochore–MT attachments.

We have determined that the N1 hZW10 deletion construct does not interact with hZwint-1 but does localize to kinetochores. We therefore used EGFP-hZW10^{N1} to determine whether the loss of hZwint-1 interaction can alter hZW10 kinetochore dynamics. We generated a HeLa cell line stably expressing the EGFP-hZW10^{N1} and analyzed EGFP-hZW10^{N1} kinetochore turnover by FRAP. Unlike the full-length EGFP-hZW10 fusion construct, we observed EGFP-hZW10^{N1} turnover at prometaphase kinetochores. EGFP-hZW10^{N1} kinetochore turnover at prometaphase had a $t_{1/2}$ recovery of 20 ± 5 s (n = 9; Fig. 3 B). EGFP-hZW10^{N1} also turned over in cells arrested with monopolar spindles (Fig. S3.4 D). EGFP-hZW10^{N1} kinetochore turnover during metaphase had a $t_{1/2}$ recovery of 11.0 ± 5.7 s (n = 8), which is similar to that of full-length EGFP-hZW10 (Fig. 3.3 B). 0.1-μM vinblastine treatments of EGFP-hZW10^{N1}–expressing cells resulted in stabilization of EGFP-N1 at kinetochores, indicating that kinetochore–MT attachments, although not necessarily bipolar, are still required for EGFP-hZW10^{N1} kinetochore turnover (Fig. 3.3 B, bottom). The table in Fig. 3.3 C summarizes the $t_{1/2}$ recovery measurements for EGFP-hZW10^{N1} compared with those of wild-type EGFP-hZW10. The temporal pattern of EGFP-hZW10 kinetochore turnover, which we have determined depends on bipolar kinetochore–MT attachments, is, therefore, also functionally regulated by the interaction of hZW10 with hZwint-1.

Figure 3.3: **hZW10 kinetochore dynamics are regulated by kinetochore–MTs and interaction with hZwint-1.**
A) Time-lapse series showing EGFP-hZW10 recovery after photobleaching at single kinetochores in metaphase (top), prometaphase (middle), or in cells treated with 0.1 μM vinblastine (bottom). The time scale is in minutes:seconds and the kinetochores that were bleached are outlined by white circles and enlarged at the bottom right. Bars: (large) 10 μm; (small) 1 μm. Nonlinear regression curves of percent recovery of the EGFP-hZW10 kinetochore signal from the time of photobleaching are shown at the right. **B)** Time-lapse series showing EGFP-hZW10^{N1} recovery after photobleaching at single kinetochores in metaphase (middle), prometaphase (top), or in cells treated with 0.1 μM vinblastine (bottom). The time scale is in minutes:seconds and the kinetochores that were bleached are outlined by white circles and enlarged in the bottom right. Bars: (large) 10 μm; (small) 1 μm. Nonlinear regression curves of percent recovery of the EGFP-hZW10 kinetochore signal from the time of photobleaching are shown on the right. **C)** Numerical summary of kinetochore $t_{1/2}$ values obtained from FRAP experiments performed on the EGFP-hZW10– and EGFP-hZW10^{N1}–expressing cells.

Figure 3.3

a

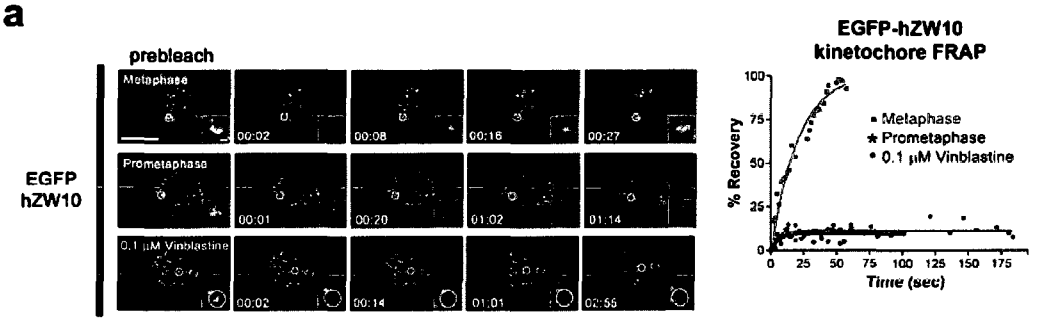

b

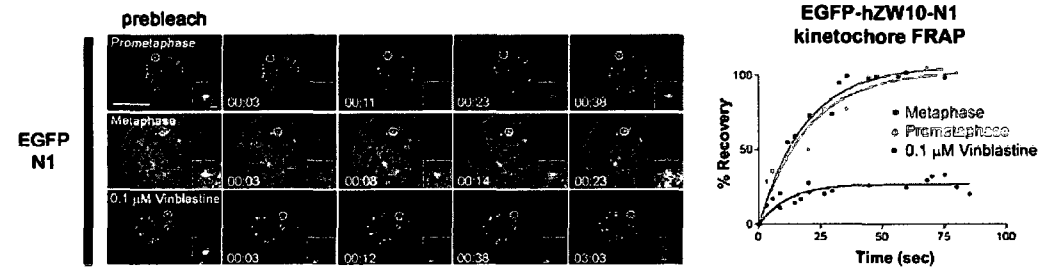

c

EGFP Construct	Prometaphase $t^{1/2}$	Metaphase $t^{1/2}$	0.1 µM VIN $t^{1/2}$
hZW10	No recovery	13.8s ± 5.1s (n=9)	No recovery
N1	20.3s ± 6.1s (n=8)	11.0s ± 5.7s (n=9)	No recovery

3.3.5 hZwint-1 regulation of hZW10 kinetochore dynamics is required for fidelity of the mitotic checkpoint

hZW10 has been shown to be required for mitotic checkpoint fidelity in fly, frog, and human cells (Basto et al., 2000; Chan et al., 2000; Kops et al., 2005a; Scaerou et al., 2001; Williams et al., 1992). We therefore investigated whether the interaction between hZW10 and hZwint-1, which we have shown to regulate hZW10 kinetochore dynamics in prometaphase, is functionally required for mitotic checkpoint fidelity. To assess the fidelity of the mitotic checkpoint in the presence of an hZwint-1–noninteracting hZW10 mutant, endogenous hZW10 was depleted by siRNA while the cells were rescued with either a wild-type EGFP-hZW10 or EGFP-hZW10^{N1} siRNA-resistant construct. Fig. 3.4 A depicts the knockdown of endogenous hZW10 protein by immunoblot, whereas Fig. 3.4 B illustrates immunofluorescence staining for hZW10 siRNA knockdown. In either case, hZW10 is clearly depleted after 72 h of siRNA transfection. To assay mitotic checkpoint function in cells lacking hZW10, cells depleted of hZW10 using siRNA for 72 h were arrested with vinblastine for 16 h and analyzed using fluorescence microscopy. In control cells, the vinblastine-induced mitotic arrest resulted in a mitotic index of ~45% (Fig. 3.4 C). However, in cells knocked down for hZW10 and subsequently arrested with vinblastine, the mitotic index dropped to ~10%, thus indicating escape from mitotic checkpoint arrest (Fig. 3.4 C). To test whether EGFP-hZW10 or EGFP-hZW10^{N1} can rescue the hZW10 siRNA knockdown phenotype, we generated HeLa cell lines stably expressing EGFP-hZW10 or EGFP-hZW10^{N1} siRNA-resistant constructs. We subsequently depleted endogenous hZW10 in the siRNA-resistant cell lines for 72 h, arrested the cells with vinblastine for 16 h, and analyzed using fluorescence microscopy. Fig. 3.5 A shows the depletion of endogenous hZW10 protein and the expression of EGFP-hZW10 siRNA-resistant constructs. In control cells expressing either siRNA-resistant EGFP-hZW10 or EGFP-hZW10^{N1}, the vinblastine-induced mitotic arrest resulted in a mitotic index of ~42 and 43%, respectively. However, when we depleted endogenous hZW10, the EGFP-hZW10^{N1}–expressing cells reached a mitotic index of only ~16%, whereas the mitotic index of the EGFP-hZW10–expressing cells reached ~ 45%, which was similar to the control HeLa cells (Figs. 3.4 and Figs. 3.5). In conclusion, our results indicate that although wild-type EGFP-hZW10 can rescue the depletion of endogenous hZW10, EGFP-hZW10^{N1} is unable to support a sustained mitotic checkpoint arrest in response to vinblastine treatment. We therefore believe that the interaction between hZW10 and hZwint-1, which stabilizes hZW10 at prometaphase kinetochores, is required for mitotic checkpoint fidelity.

Figure 3.4

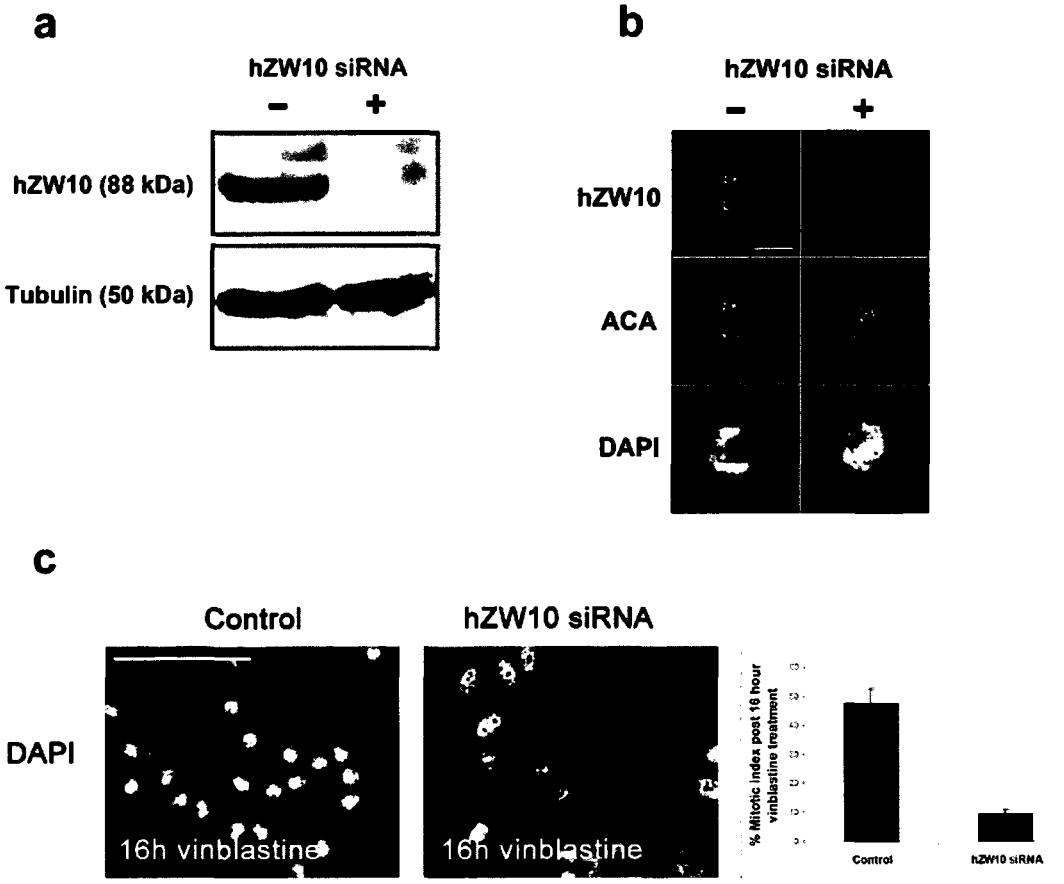

Figure 3.4: **siRNA knockdown of hZW10 results in abrogation of the mitotic checkpoint.**
A) Immunoblot of HeLa lysates from cells transfected with (+) or without (–) 50 nM anti-hZW10 siRNA for 72 h and probed with a rabbit hZW10 polyclonal antibody and a mouse monoclonal (B512) tubulin antibody using the Odyssey IR imaging system. A significant (~90%) reduction in the hZW10 signal was observed. **B)** HeLa cells transfected with (+) or without (–) anti-hZW10 siRNA duplexes for 72 h and stained with rabbit anti-hZW10 polyclonal antibodies, human ACA sera, and DAPI. hZW10 kinetochore signal was not detected in cells transfected with the anti-hZW10 siRNA after 72 h. Bar, 10 μm. **C)** HeLa cells transfected with anti-hZW10 siRNA duplexes for 72 h and arrested with 25 μM vinblastine for 16 h were analyzed for the accumulation of mitotic cells. DNA was stained with DAPI. Representative images indicate an accumulation of mitotic cells after 16 h vinblastine arrest in the control cells but not in the hZW10 siRNA knockdown cells. Bar, 100 μm. A histogram of the percentage of mitotic cells is shown (n = 3 experiments; >300 cells per experiment; error bars show ± SD).

Figure 3.5: **Interaction of hZW10 with hZwint-1 is required for the mitotic checkpoint.**
A) Immunoblot of HeLa cells, HeLa cells stably expressing the EGFP-hZW10 siRNA-resistant construct, or HeLa cells stably expressing the EGFP-hZW10^{N1} siRNA-resistant constructs, all of which were transfected with hZW10 siRNA for 72 h and probed with rabbit polyclonal antibodies against hZW10. Lanes 1 and 2 are control HeLa cells; lane 3 is the molecular mass marker; lanes 4 and 5 are the EGFP-hZW10 stable cell line; and lanes 6 and 7 are the EGFP-hZW10^{N1} stable cell line. Endogenous hZW10 is clearly knocked down, whereas the siRNA-resistant EGFP constructs remain. **B)** Representative images of HeLa cells stably expressing EGFP-hZW10 or EGFP-hZW10^{N1} arrested with 25 μM vinblastine for 16 h or transfected with anti-hZW10 siRNA duplexes for 72 h and arrested with 25 μM vinblastine for 16 h. EGFP-hZW10–siR– or EGFP-N1–siR–expressing cells were analyzed for the accumulation of mitotic cells by the staining of their DNA with DAPI. Bar, 100 μm. A histogram of the percentage of mitotic cells is shown (n = 3; >300 cells per experiment; error bars show ± SD).

Figure 3.5

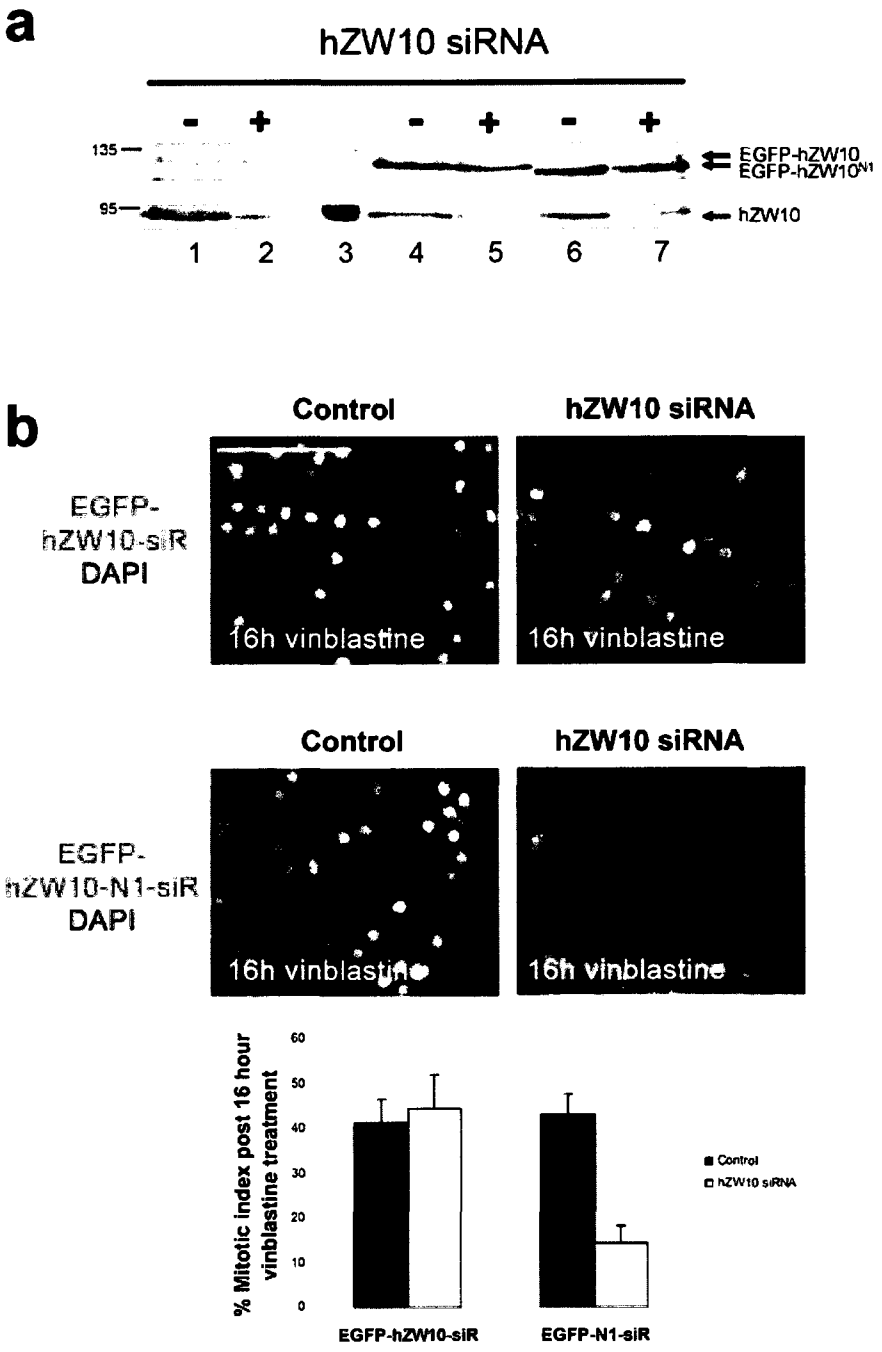
a
hZW10 siRNA
- + - + - +
135
95
EGFP-hZW10
EGFP-hZW10N1
hZW10
1 2 3 4 5 6 7
b
Control
hZW10 siRNA
EGFP-hZW10-siR
DAPI
16h vinblastine
16h vinblastine
Control
hZW10 siRNA
EGFP-hZW10-N1-siR
DAPI
16h vinblastine
16h vinblastine
% Mitotic index post 16 hour vinblastine treatment
60
50
40
30
20
10
0
Control
hZW10 siRNA
EGFP-hZW10-siR
EGFP-N1-siR

3.4 Discussion

In our current study, we have applied a structure function assay to map the kinetochore localization and hZwint-1 interaction domains of hZW10. In addition, we have documented the kinetochore dynamics of hZW10 during prometaphase and metaphase, observing that kinetochore hZW10 becomes dynamic only upon metaphase alignment. We discovered that hZW10 kinetochore dynamics are regulated by kinetochore–MT attachments and the interaction between hZW10 and hZwint-1. We found that although the hZwint-1 interaction is dispensable for hZW10 kinetochore recruitment, it is essential for the stabilization of hZW10 residency at prometaphase kinetochores and mitotic checkpoint function.

Using our extensive mutant library of hZW0, we found that hZW10 contains two functional domains, one within the C terminus (aa 536–686) and the other at the extreme N terminus (aa 30–82). We mapped the kinetochore localization domain of hZW10 to the C terminus and the hZwint-1 interaction domain to the N terminus (Fig. 3.2 C). Both domains are highly conserved in vertebrates (Fig. S3.5, A and D). Interestingly, the C-terminal kinetochore localization domain alone is not sufficient to confer hZW10 kinetochore localization. We therefore hypothesize that hZW10 kinetochore localization may require an interaction between the C and N termini of hZW10. We have attempted to analyze an interaction between the two termini using a yeast two-hybrid approach; however, we have been unsuccessful as of yet. Further biochemical experiments are thus required to thoroughly test our hypothesis. Because our domain mapping results are largely based on yeast two-hybrid assays, we cannot rule out the possibility that these mutants may interact differently at kinetochores in situ. However, based on the sum of all our different mutants, including truncations, insertion, and site-directed mutants, we are confident in the accuracy of the mapped kinetochore localization and hZwint-1 interaction domains of hZW10. The location of hZW10 interaction domains for dynamitin and hROD remains unknown at this time; however, Starr et al. (1998) mapped the dynamitin interaction domain to the C terminus of hZW10 (aa 468–779). Taking into account the mapping by Starr et al. (1998) in combination with our hZW10 C-terminal mutant results, it remains possible that the interaction between hZW10 and dynamitin may also play a role in hZW10 kinetochore localization. Because hZW10 and hROD are interdependent for kinetochore localization (Chan et al., 2000), the interaction between hZW10 and hROD may also be required for hZW10 kinetochore localization as part of the RZZ complex.

Although Wang et al. (2004a) had previously correlated hZW10 kinetochore localization with hZwint-1 interaction, we have found that specific disruption of the hZwint-1 interaction domain, via deletion, insertion, or amino acid substitution, does not preclude hZW10 kinetochore localization. Based on our data, we propose that the hZW10 kinetochore recruitment mechanism may not directly depend on hZwint-1. Using our hZW10 mutant library, we mapped the hZwint-1 interaction domain of hZW10 to its N terminus (aa 30–80). In addition, we have found that the interaction between hZW10 and hZwint-1, in context of the entire protein, also involves the C terminus of hZW10 (aa 410–779). Although previous siRNA-mediated knockdown of hZwint-1 has clearly

shown the loss of hZW10 from kinetochores, our study shows that the loss of direct interaction between hZwint-1 and hZW10 does not affect hZW10 kinetochore localization. hZwint-1 is known to interact with the Ndc80 and Mis12 complexes, which are essential for the assembly of functional kinetochores (Cheeseman et al., 2004; Lin et al., 2006; Obuse et al., 2004). The absence of hZwint-1 may therefore indirectly affect hZW10 kinetochore localization by preventing or altering kinetochore assembly through the disruption of the Ndc80 and/or Mis12 complexes. It has been suggested that the RZZ complex oligomerizes at kinetochores (Scaerou et al., 2001). RZZ complex oligomerization at kinetochores may therefore represent an alternate hZW10 kinetochore recruitment mechanism. Interestingly, we have observed the dimerization of EGFP-hZW10 with GST-hZW10 using in vitro GST pulldown assays (Fig. S3.2 F). We cannot, therefore, rule out the possibility that endogenous hZW10 facilitates the recruitment of hZwint-1–noninteracting hZW10 proteins to kinetochores. We do observe the localization of EGFP-hZW10^{N1} at kinetochores in a subset of cells depleted of endogenous hZW10; however, we cannot determine whether endogenous hZW10 has been completely eliminated from these cells (unpublished data). The initial recruitment of hZW10 to kinetochores during early prometaphase may depend on hZwint-1; however, the dynamic recruitment of kinetochore hZW10 throughout the remainder of mitosis is hZwint-1 independent. Future studies of hZW10, hROD, and hZwilch will need to focus on RZZ complex dimerization in relation to kinetochore localization and its function within the mitotic checkpoint.

In addition to our findings that the hZwint-1 interaction is dispensable for hZW10 kinetochore localization, we have also discovered that hZwint-1 modulates hZW10 kinetochore dynamics. In Fig. 3.6, we outline a model whereby hZW10 kinetochore turnover is regulated by bipolar kinetochore–MT attachments as well as by interaction with hZwint-1. Using FRAP experiments with HeLa cells stably expressing EGFP-hZW10, we have established that hZW10 kinetochore dynamics are regulated by bipolar kinetochore–MT attachments. At prometaphase kinetochores EGFP-hZW10 is stable; however, once bipolar kinetochore–MT attachments are achieved and the chromosomes align at the metaphase plate, EGFP-hZW10 becomes highly dynamic. We therefore believe that the observed hZW10 accumulation at prometaphase or nocodazole-treated kinetochores (Starr et al., 1997) stems from its inability to turn over at kinetochores lacking proper kinetochore–MT attachments (Fig. 3.6 A). In contrast, hZW10 diminishes at metaphase kinetochores because its kinetochore turnover rate becomes rapid upon the establishment of metaphase alignment (Fig. 3.6 B). In our model, we predict that the turnover of kinetochore hZW10 depends on its transport off kinetochores and along kinetochore-MTs mediated by dynein/dynactin. This explains why both the wild-type hZW10 and the hZW10^{N1} mutant do not turn over at kinetochores in vinblastine-treated cells. In the vinblastine-treated cells, no kinetochore-MTs are present and, therefore, dynein/dynactin-mediated transport of hZW10 off kinetochores is not possible.

Interestingly, our results contrast those of Basto et al. (2004), who found GFP-dmROD to be dynamic at prometaphase and colchicine-treated kinetochores in live *D. melanogaster* embryos. We attribute this difference to two factors. First, early-stage embryos undergo very rapid cell divisions, thus requiring a short mitosis. The dynamics

of the RZZ complex may therefore remain unregulated to allow a rapid release of checkpoint proteins from kinetochores, therefore driving quicker anaphase entry. Second, no hZwint-1 homologue has been found in flies. This could suggest that although the fly RZZ complex is dynamic at all kinetochores, human cells regulate the dynamics of the RZZ complex through its interaction with hZwint-1. The regulation of RZZ dynamics in human cells may indicate a need for a more intricate control of chromosome segregation.

hZW10 is the first example of a mitotic checkpoint protein displaying kinetochore turnover that depends on bipolar kinetochore–MT attachments. Moreover, when analyzing the kinetochore turnover of EGFP-hZW10^{N1}, an hZwint-1–noninteracting hZW10 mutant, we observed kinetochore turnover at both prometaphase and metaphase kinetochores. Similar FRAP results were obtained using transient transfection of the DI69AA mutant, a site-directed mutant of hZW10 that also does not interact with hZwint-1 (unpublished data). This indicates that regulation of hZW10 kinetochore turnover between prometaphase and metaphase requires the interaction between hZW10 and hZwint-1. Kinetochore hZwint-1 thus functions to increase the residency time of hZW10 at kinetochores until bipolar MT attachments are achieved (Fig. 3.6 C). Once bipolar kinetochore attachments are achieved, hZW10 is released from hZwint-1 and becomes dynamic at kinetochores, leading to its transport off kinetochores by dynein/dynactin. The release of hZW10 from hZwint-1 in response to bipolar kinetochore–MT attachment may occur through posttranslational modifications of either hZwint-1 or hZW10; however, the mechanism regulating this event remains unknown. In addition, we have observed that the fidelity of the mitotic checkpoint is compromised in the presence of EGFP-hZW10^{N1} and in the absence of endogenous hZW10. This loss of checkpoint fidelity stems from the inability of EGFP-hZW10^{N1} to stably bind prometaphase kinetochores, thus indicating that hZwint-1–mediated stabilization of hZW10 residency at prometaphase kinetochores is essential for mitotic checkpoint function. Our findings support the hypothesis that dynein/dynactin-mediated transport of checkpoint proteins, such as hZW10, off kinetochores functions to silence the mitotic checkpoint and that this mechanism requires tight regulation to maintain checkpoint arrest.

In conclusion, we hypothesize that increased kinetochore residency of hZW10 is required for maintenance of mitotic checkpoint signaling in response to unattached or monopolar attached kinetochore–MTs. Once metaphase alignment is achieved, hZwint-1 no longer stabilizes hZW10 at kinetochores and dynein/dynactin-dependent transport of hZW10 along kinetochore–MTs results in a rapid kinetochore turnover rate of hZW10. We propose that hZW10 kinetochore turnover acts as an indicator for the progression from prometaphase to metaphase, which is also indicative of the establishment of bipolar kinetochore–MT attachments. The fact that rapid turnover of hZW10 is only observed at attached kinetochores, kinetochores that have satisfied the mitotic checkpoint, also supports the hypothesis that dynein/dynactin-mediated transport of hZW10 silences the mitotic checkpoint (Musacchio and Salmon, 2007). Our findings thus indicate that mitotic checkpoint regulation involves a dynamic process at kinetochores rather than a simple on/off status of key mitotic checkpoint proteins at kinetochores. This study also highlights the need to study the kinetics of mitotic checkpoint protein accumulation at kinetochores in vivo.

Figure 3.6: **Model of the mechanisms regulating hZW10 kinetochore dynamics.**

A) hZW10, as part of the RZZ complex, localizes to prometaphase and/or unattached kinetochores where it interacts with hZwint-1. The RZZ complex recruits dynein/dynactin to the kinetochore. The RZZ complex remains stably bound to the kinetochore, via the interaction with hZwint-1, until bipolar kinetochore–MT attachments are achieved. The retention of hZW10 and, therefore, dynein/dynactin at kinetochores prevents premature silencing of the mitotic checkpoint. **B)** At metaphase, when kinetochores have achieved bipolar kinetochore–MT attachments and the chromosomes have aligned at the metaphase plate, hZwint-1 no longer stabilizes hZW10 at kinetochores. Dynein/dynactin is now free to transport the RZZ complex off kinetochores, leading to silencing of the mitotic checkpoint. The RZZ complex continues to cycle on and off the kinetochore with very rapid dynamics to further facilitate removal of remaining checkpoint proteins such as hMad1 and 2. **C)** RZZ complexes containing an hZwint-1–noninteracting mutant of hZW10 localize to kinetochores in prometaphase but do not remain stably bound and turn over at prometaphase kinetochores. These RZZ complexes still depend on the presence of kinetochore–MTs in order for dynein/dynactin-mediated transport off kinetochores but no longer require bipolar kinetochore attachment or the alignment of chromosomes to rapidly turn over at kinetochores. Premature removal of hZW10 from unaligned kinetochores leads to mitotic checkpoint failure.

Figure 3.6

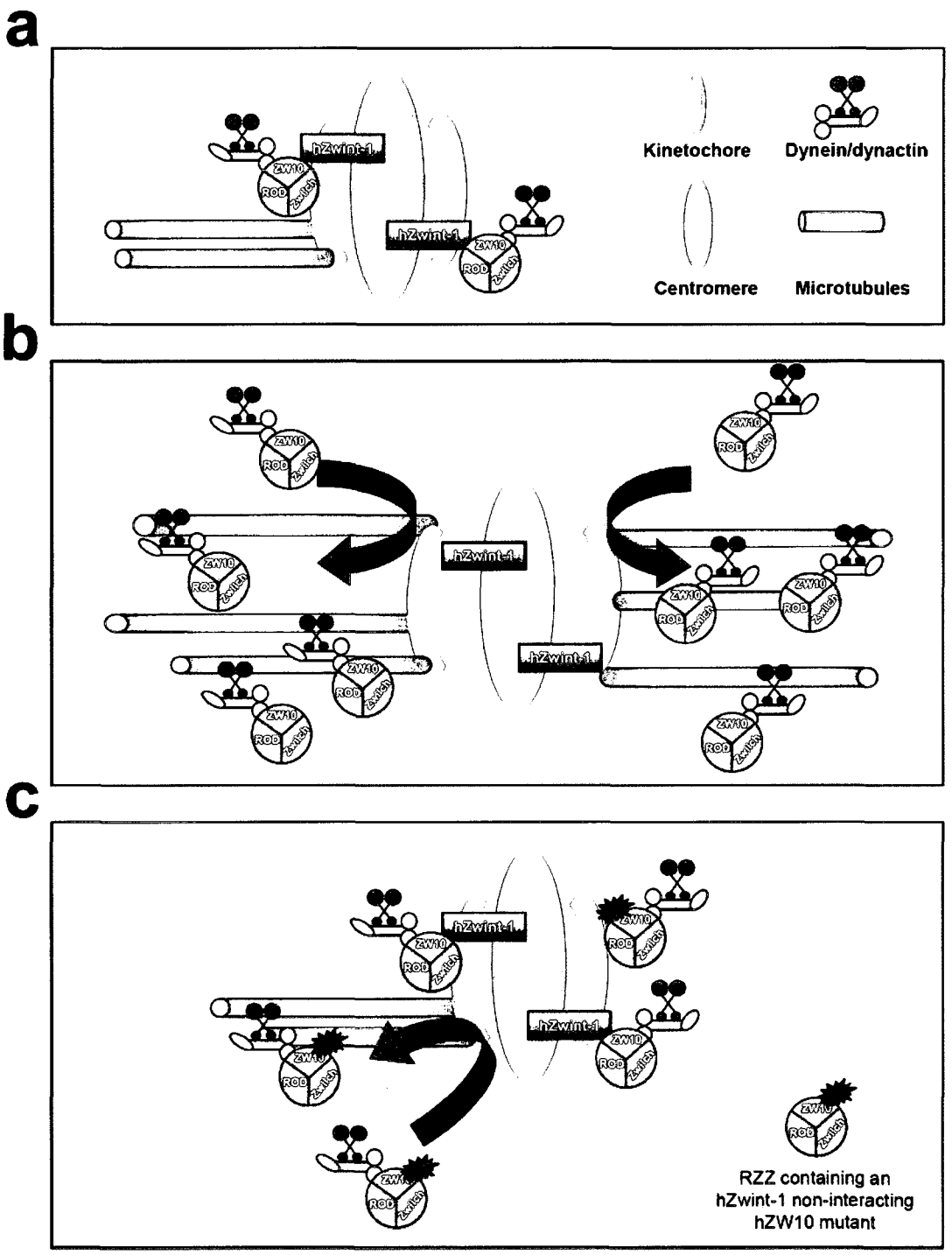
a
hZwint-1
ZW10
ROD
Zwilch
Kinetochore
Dynein/dynactin
Centromere
Microtubules
b
c
RZZ containing an
hZwint-1 non-interacting
hZW10 mutant

3.5 Supplementary Material: *Stable hZW10 kinetochore residency, mediated by hZwint-1 interaction, is essential for the mitotic checkpoint.*

Table 2-1: *hZW10 N- and C-terminal truncation mutants assayed for kinetochore localization and hZwint-1 interaction.*

hZW10 construct	Encoding Amino Acids	Kinetochore localization	hZwint-1 yeast two-hybrid interaction	β-galactosidase assay (+/- one SD)
Full length	1-779	Positive	Positive	187 +/- 20
N1	52-779	Positive	Negative	2.14 +/- 1.9
N2	75-779	Negative	Negative	N/D
N3	85-779	Negative	Negative	N/D
N4	132-779	Negative	Negative	N/D
N5	215-779	Negative	Negative	N/D
N6	335-779	Negative	Negative	N/D
N7	462-779	Negative	Negative	N/D
N8	556-779	Negative	Negative	N/D
N9	621-779	Negative	Negative	N/D
C1	1-772	Negative	Negative	3.4 +/- 0.9
C2	1-698	Negative	Negative	2.6 +/- 0.6
C3	1-560	Negative	Negative	2.5 +/- 0.8
C4	1-496	Negative	Negative	1.0 +/- 0.8
C5	1-410	Negative	Positive	26.6 +/- 3
C6	1-356	Negative	Positive	275 +/- 33
C7	1-318	Negative	Positive	132 +/-62
C8	1-224	Negative	Positive	233 +/- 23
C9	1-139	Negative	Positive	445 +/-128
C10	1-82	Negative	Positive	N/D

Table 2-1: The table depicts the assay of direct interaction between hZwint-1 and hZW10 deletion constructs analyzed with the LexA yeast two-hybrid system using X-gal and the β-galactosidase assay as well as kinetochore localization through fluorescence microscopy analysis of EGFP fusion constructs. Yeast colonies were scored for appearance of blue color, 2 and 3 days after streaking out. Each combination of interactions was re-done in three separate experiments, and confirmed for expression of fusion constructs by western blotting with anti-HA and anti-LexA antibodies (data not shown). The β-galactosidase assay was performed using the Pierce β-galacrosidase assay kit according to manufacturers instructions. N/D - not determined.

Table 2-2: *hZW10 and N1 insertion mutants assayed for kinetochore localization and hZwint-1 interaction.*

hZW10 mutant	Insertion Site (Amino Acid)	Insertion sequence (Amino Acid)*	Kinetochore localization	hZwint-1 yeast two-hybrid interaction[a]	β-galactosidase assay (+/- one SD)[b]
A	43	CGRIS	Positive	Positive	341 +/- 173
B	61	VRPHQ	Positive	Negative	1.3 +/- .3
C	90	CGRTG	Positive	Positive	333 +/- 114
D	106	CGRIL	Positive	Positive	N/D
E	131	CGRKY	Positive	Positive	N/D
F	191	LRPQP	Positive	Positive	N/D
G	208	CGRNL	Positive	Positive	N/D
H	210	VRPHT	Positive	Positive	N/D
I	226	VRPHS	Positive	Positive	N/D
J	248	LRPQL	Negative	Negative	N/D
K	335	VRPHW	Positive	Positive	N/D
L	375	NAAAL	Positive	Positive	N/D
M	421	CGRNN	Positive	Positive	N/D
N	467	DAAAL	Positive	Positive	N/D
O	475	TAAAP	Positive	Positive	N/D
P	536	LRPHQ	Negative	Negative	9.9 +/- 9.6
Q	563	CGRSL	Positive	Positive	N/D
R	583	CGRRR	Negative	Negative	2.4 +/- 0.7
S	607	SAAAA	Positive	Positive	N/D
T	608	MRPHR	Positive	Positive	N/D
U	654	CGRMG	Negative	Negative	3.7 +/- 1.6
V	663	CGRTE	Negative	Negative	2.2 +/- 0.9
W	666	CGRIG	Negative	Negative	1.6 +/- 0.7
X	671	CGRTL	Negative	Negative	2.1 +/- 1.7
Y	682	LRPQL	Positive	Positive	N/D
Z	686	CGRIC	Negative	Negative	1.4 +/- 0.8
Aa	712	CGRKE	Positive	Positive	N/D
a	149	SMRPQ	Positive	N/A	N/A
b	210	TECGR	Positive	N/A	N/A
c	235	CGRIG	Positive	N/A	N/A
d	283	LVFKH	Positive	N/A	N/A
e	289	PCLNT	Positive	N/A	N/A
f	303	QMRPH	Positive	N/A	N/A
g	331	AAALG	Positive	N/A	N/A
h	334	CLNTN	Positive	N/A	N/A
i	390	NAAAL	Positive	N/A	N/A
j	454	LRPHQ	Positive	N/A	N/A
k	520	HVFKH	Positive	N/A	N/A
l	541	CFGIH	Positive	N/A	N/A
m	567	LFKHL	Positive	N/A	N/A
n	640	CLMNW	Negative	N/A	N/A
o	658	AAALN	Negative	N/A	N/A
p	675	TVFKH	Negative	N/A	N/A
q	681	LLRPQ	Positive	N/A	N/A

Table 2-2: The table depicts the assay of direct interactions between hZwint-1 and hZW10 (and hZW10-N1) insertion constructs analyzed with the LexA yeast two-hybrid system using X-gal and the β-galactosidase assay as well as kinetochore localization through fluorescence microscopy analysis of EGFP fusion constructs. a: The exact amino acid insertion sites in hZW10 and hZW10^{N1} 5 amino acid insertion mutants were determined by sequencing. b: The hZwint-1 interaction with hZw10 insertion mutants were assayed as outlined in Table I.

Table 2-3: *hZW10 N-terminal point mutants analyzed for kinetochore localization and hZwint-1 interaction.*

hZW10 point mutation*	Kinetochore localization	hZwint-1 yeast two-hybrid interaction[a]	β-galactosidase assay (+/- one SD)[b]
HS11AA	Positive	Positive	N/D
GE36AA	Positive	Positive	N/D
S47A	Positive	Positive	N/D
EF48AA	Positive	Positive	N/D
S52A	Positive	Positive	N/D
S55A	Positive	Positive	449 +/- 139
GLI58AAA	Positive	Negative	2.7 +/- 0.8
SE67AA	Positive	Negative	1.8 +/- 0.9
DI69AA	Positive	Negative	1.2 +/- 0.4
SE79AA	Positive	Positive	131 +/- 41

Table 2-3: The table depicts the assay of direct interactions between hZwint-1 and hZW10 site directed mutagenesis constructs analyzed with the LexA yeast two-hybrid system using X-gal and the β-galactosidase assay as well as kinetochore localization through fluorescence microscopy analysis of EGFP fusion constructs
a: The point mutations were verified by sequencing. b: The hZwint-1 interaction with hZw10 point mutants were assayed as outlined in Table I

Supplementary Figure 3.1: **Kinetochore localization of hZW10 N- and C-terminal deletion constructs.**
A) HeLa cells transiently transfected with EGFP-hZW10 N-terminal deletion constructs were analyzed for fluorescence at kinetochores during mitosis. Constructs N4, N5, N6, N7 and N8 do not localize to kinetochores. Chromosomes are stained with DAPI. All mutants behaved similarly at both prometaphase and metaphase kinetochores. Scale bar = 10 μm. **B)** Immunoblot of HEK293 lysates from cells transiently transfected with the N-terminal EGFP-hZW10 fusions detected with a mouse monoclonal anti-GFP antibody. **C)** HeLa cells transiently transfected with EGFP-hZW10 C-terminal deletion constructs were analyzed for kinetochore localization during mitosis with fluorescence microscopy. Constructs C2, C3, C5, C6, C7, C8 and C9 do not localize to kinetochores. Chromosomes are stained with DAPI. Scale bar = 10 μm. **D)** Immunoblot of HEK293 lysates from cells transiently transfected with the C-terminal EGFP-hZW10 fusions detected with a mouse monoclonal anti-GFP antibody. **E)** Immunoblot of HeLa lysates from cells transiently transfected with EGFP-hZW10 (lane 2) or EGFP-hZW10^{N1} (lane 3) and probed with anti-hZW10 anitbodies. EGFP-hZW10 and EGFP-hZW10^{N1} products are indicated by an asterix, while endogenous hZW10 is indicated by double asterix. The EGFP constructs are overexpressed ~2 fold compared to endogenous hZW10. **F)** HeLa cells transiently transfected with EGFP-hZW10 C- and N-terminal constructs and arrested with 25 μM vinblastine for 30 minutes were analyzed for kinetochore localization using fluorescence microscopy. Only construct N1 and wildtype hZW10 exhibit kinetochore localization. Scale bar = 10 μm.

Supplementary Figure 3.1

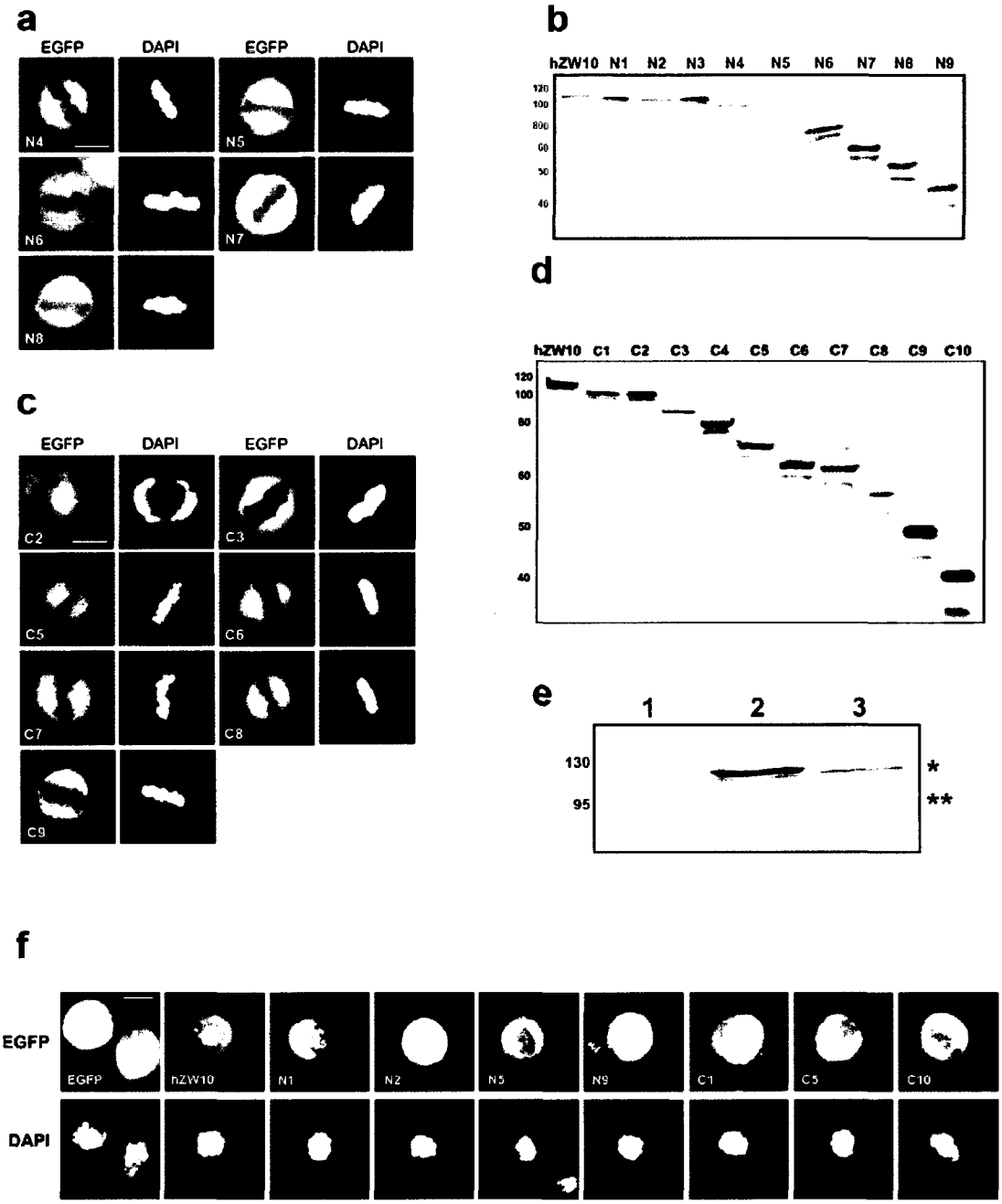

Supplementary Figure 3.2: **The N-terminus of hZW10 is required for interaction with hZwint-1.**
A) A schematic diagram depicting N-terminal hZW10 deletion constructs. Amino acid sizes are indicated. hZW10 kinetochore localization and yeast two-hybrid interaction with hZwint-1 are indicated by a blue plus sign for positive results and a red minus sign for negative results. **B)** Immunoblot of HEK293 lysates from cells transiently transfected with the N-terminal EGFP-hZW10 fusions detected with a mouse monoclonal anti-GFP antibody. **C)** HeLa cells transiently transfected with EGFP-hZW10 N-terminal deletion constructs analyzed for kinetochore localization during mitosis with fluorescence microscopy. All of the N-terminal deletions analyzed localize to kinetochores. Chromosomes are stained with DAPI. All mutants beahved similarly at both prometaphase and metaphase kinetochores. Scale bar = 10 μm. **D)** HEK293 lysates from cells co-transfected with EGFP-hZW10 or EGFP-hZW10^{N1} and GST-hZwint-1 were incubated with GST sepharose beads at 4°C for 3 hours, washed 5X with 1% NP40 lysis buffer, boiled in SDS PAGE loading buffer and analyzed via SDS PAGE gel electrophoresis. 10% of the lysate was loaded as a control, lanes 1-6. EGFP-hZW10 is clearly pulled down by GST-hZwint-1 (lane 9), but not by the GST vector alone (lane7), while EGFP-hZW10-N1, shown by three separate pull-down experiments (lanes10-12), only weakly associates with GST-hZwint-1, and is not pulled down by the GST vector alone (lane 8). **E)** HEK293 lysates from cells co-transfected with hZwint-1-EGFP and GST vector or GST-hZW10 constructs were incubated with GST sepharose beads at 4°C for 3 hours, washed 5X with 1% NP40 lysis buffer, boiled in SDS PAGE loading buffer and analyzed via SDS PAGE gel electrophoresis. 10% of the lysate was loaded as a control, lanes 1-9 (Lane 1: GST-hZW10, 2: GST-C1, 3: GST-C5, 4: GST-C9, 5: GST-N2, 6: GST-N7, 7:GST-hZW10^{DI69AA}, 8: GST-hZW10^{B}, 9: GST vector). GST pulled-down fractions are in lanes 10-18 (lane 10: GST vector, 11: GST-hZW10, 12: GST-C1, 13: GST-C5, 14: GST-C9, 15: GST-N2, 16: GST-N7, 17:GST-hZW10^{DI69AA}, 18: GST-hZW10^{B}). The GST pull-down indicates that only GST-hZW10, GST-C5 and GST-C9 are able to strongly pull-down hZwint-1-EGFP. **F)** HEK293 lysates from cells co-transfected with EGFP-hZW10 and GST-hZW10 were incubated with GST sepharose beads at 4°C for 3 hours, washed 5X with 1% NP40 lysis buffer, boiled in SDS-PAGE loading buffer and analyzed via SDS-PAGE gel electrophoresis. 10% of the lysate was loaded as a control (lanes 1-3). EGFP-hZW10 is clearly pulled down by GST-hZW10 in two reciprocal experiments (lanes 5-6), but not by the GST vector alone (lane 4).

Supplementary Figure 3.2

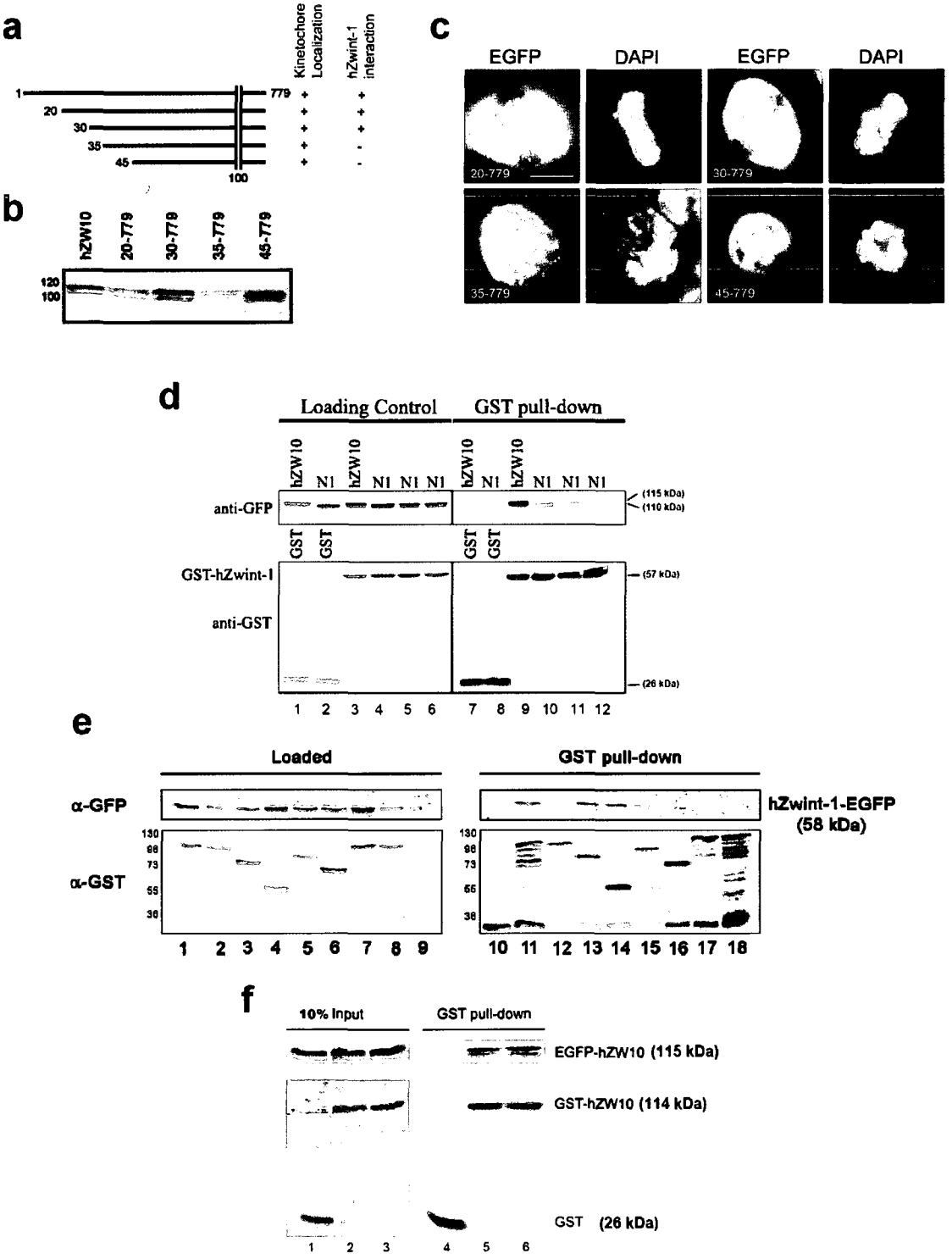

Supplementary Figure 3.3: **Kinetochore localization of hZW10 insertion mutants.**
A) HeLa cells transiently transfected with EGFP-hZW10 5 amino acids insertion constructs were analyzed for kinetochore localization during mitosis with fluorescence microscopy. Insertion mutants J, P, V, W and Z did not localize to kinetochores. Chromosomes are stained with DAPI. All mutants beahved similarly at both prometaphase and metaphase kinetochores. Scale bar = 10 μm. **B)** HeLa cells transiently transfected with EGFP-hZW10 insertion mutant constructs and arrested with 25 μM vinblastine for 30 minutes were analyzed for kinetochore localization using fluorescence microscopy. Only construct B exhibits kinetochore localization. Scale bar = 10 μm. **C)** Immunoblots of HEK293 lysates from cells transiently transfected with EGFP-hZW10 pentapeptide insertion mutant constructs detected with a mouse monoclonal anti-GFP antibody.

Supplementary Figure 3.3

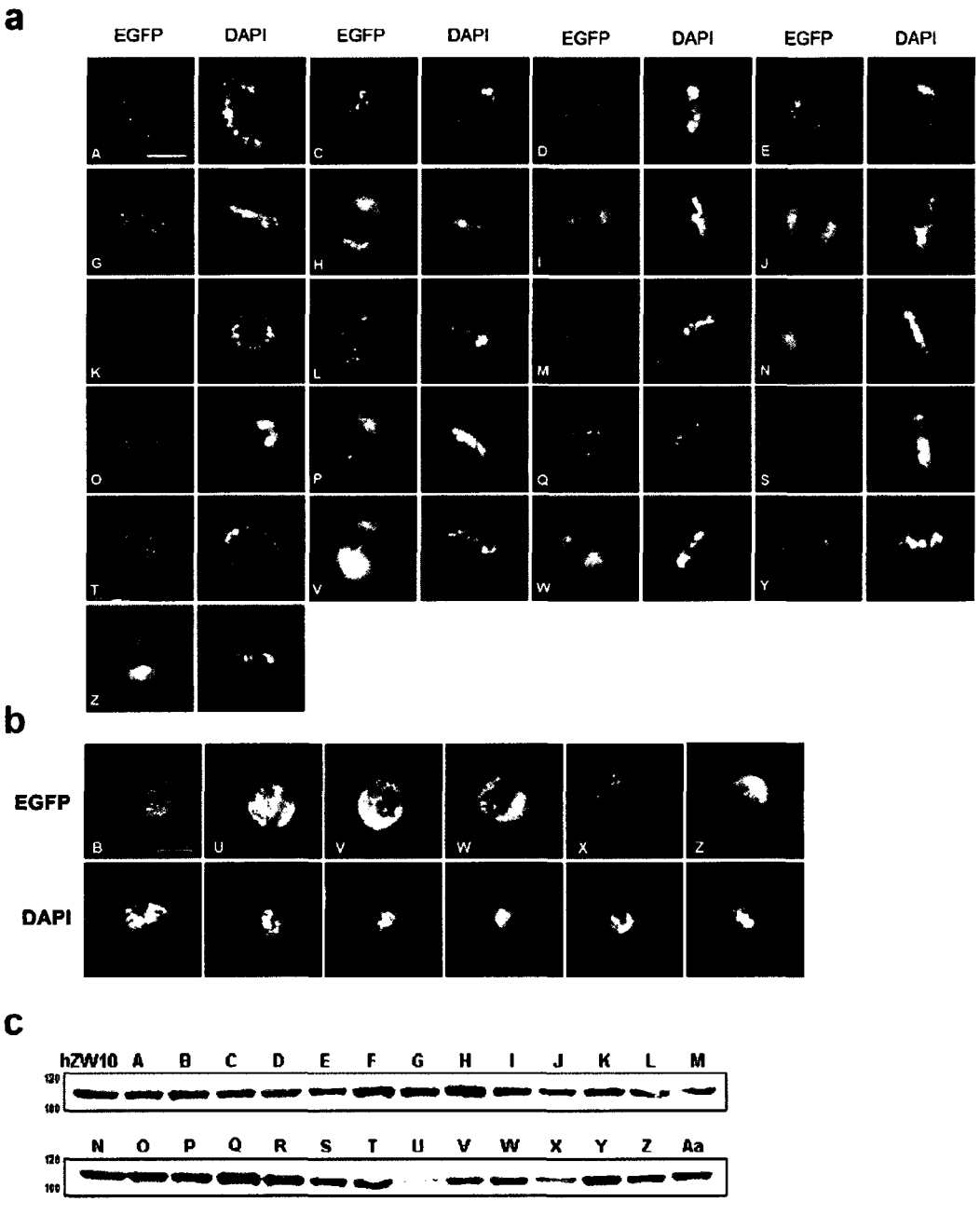

Supplementary Figure 3.4: **Kinetochore localization of hZW10-N1 insertion mutants and EGFP-hZW10-N1 kinetochore dynamics in monopolar cells.** **A)** HeLa cells transiently transfected with EGFP-hZW10^{N1} pentapeptide insertion constructs were analyzed for kinetochore localization during mitosis with fluorescence microscopy. All of the above insertion mutants localize to kinetochores. Chromosomes are stained with DAPI. All mutants beahved similarly at both prometaphase and metaphase kinetochores. Scale bar = 10 μm. **B)** HeLa cells transiently transfected with EGFP-hZW10^{N1} insertion mutant constructs and arrested with 25 μM vinblastine for 30 minutes were analyzed for kinetochore localization using fluorescence microscopy. Constructs N1^{n}, N1^{o} and N1^{p} do not localize to kinetochores. Scale bar = 10 μm. **C)** Immunoblots of HEK293 lysates from cells transiently transfected with the various EGFP-hZW10^{N1} pentapeptide insertion mutant constructs detected with a mouse monoclonal anti-GFP antibody. **D)** Time lapse series showing EGFP-hZW10 (top) and EGFP-hZW10^{N1} (bottom) recovery after photobleaching at single kinetochores in cells arrested with 7 μM STLC. The time scale is in seconds and the kinetochores which were bleached are outlined by white circles and enlarged in the bottom right hand corners. Large scale bar = 10 μm, small scale bar = 1 μm. EGFP-hZW10 is not observed to recover at mono-polar kinetochores thus indicating it binds stably, while EGFP-hZW10^{N1} remains dynamic.

Supplementary Figure 3.4

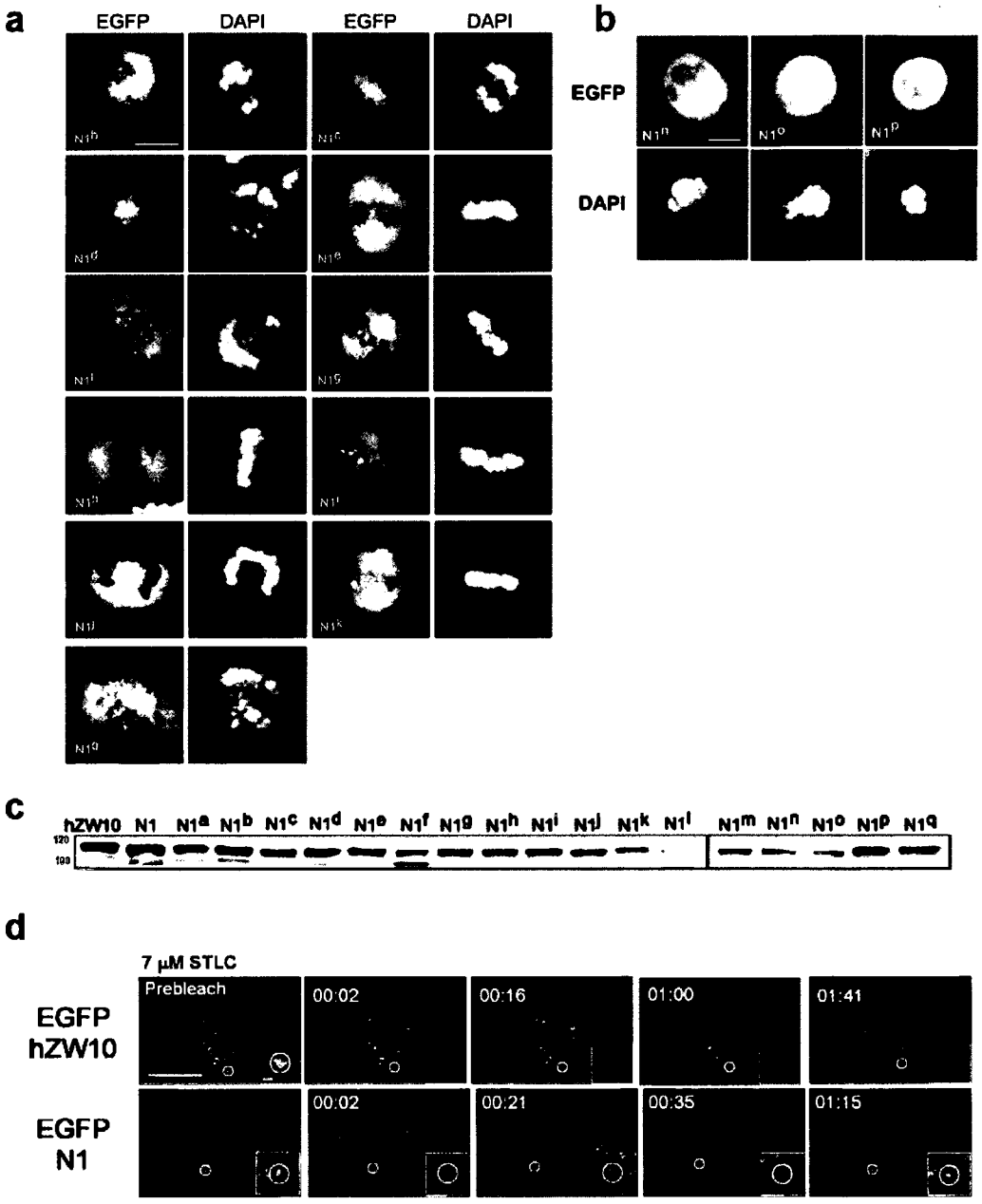

Supplementary Figure 3.5: **Mapping the hZW10 kinetochore localization domain by site-directed mutagenesis.**
A) Clustal-W alignment of the N (top) and C (bottom) -termini of: human (h), mouse (m), chicken (ch), zebrafish (danio), *Xenopus laevis* (xl), *C. elegans* (ce) and *Drosophila* (dm) hZW10 homologues. Sites of site-directed mutagenesis are outlined. Asterisks indicate hZW10 mutations found in colon cancer (Wang et al., 2004b). **B)** Immunoblot of HEK293 lysates from cells transiently transfected with the EGFP-hZW10 single amino acid substitution mutant constructs detected with a mouse monoclonal anti-GFP antibody. **C)** HeLa cells transiently transfected with EGFP-hZW10 site directed mutant constructs and arrested with 25 μM vinblastine for 30 minutes were analyzed for kinetochore localization using fluorescence microscopy. Only construct M690R exhibits kinetochore localization. Scale bar = 10 μm.

Supplementary Figure 3.5

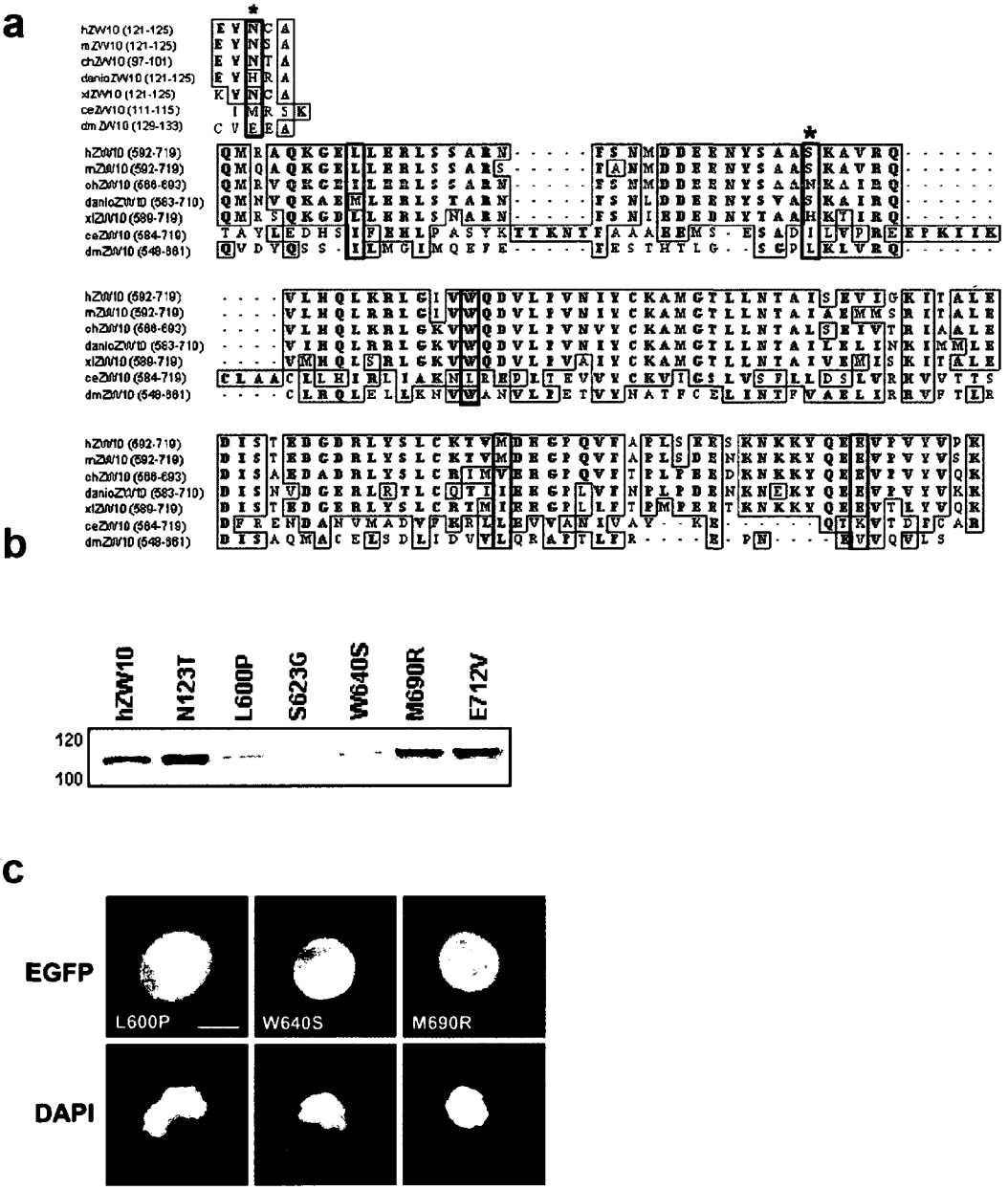

Supplementary Figure 3.5: **Mapping the hZW10 kinetochore localization domain by site-directed mutagenesis.**
D) A Clustal-W alignment of the N-terminus of hZW10 homologues with amino acid substitutions outlined. **E)** Immunoblot of HEK293 lysates from cells transiently transfected with the EGFP-hZW10 N-terminal amino acid substitution mutant constructs detected with a mouse monoclonal anti-GFP antibody. **F)** HeLa cells transiently transfected with EGFP-hZW10 site directed mutant constructs were analyzed for kinetochore localization during mitosis with fluorescence microscopy. All of the alanine mutants retained the ability to localize to kinetochores. Chromosomes are stained with DAPI. All mutants beahved similarly at both prometaphase and metaphase kinetochores. Scale bar = 10 μm.

Supplementary Figure 3.5

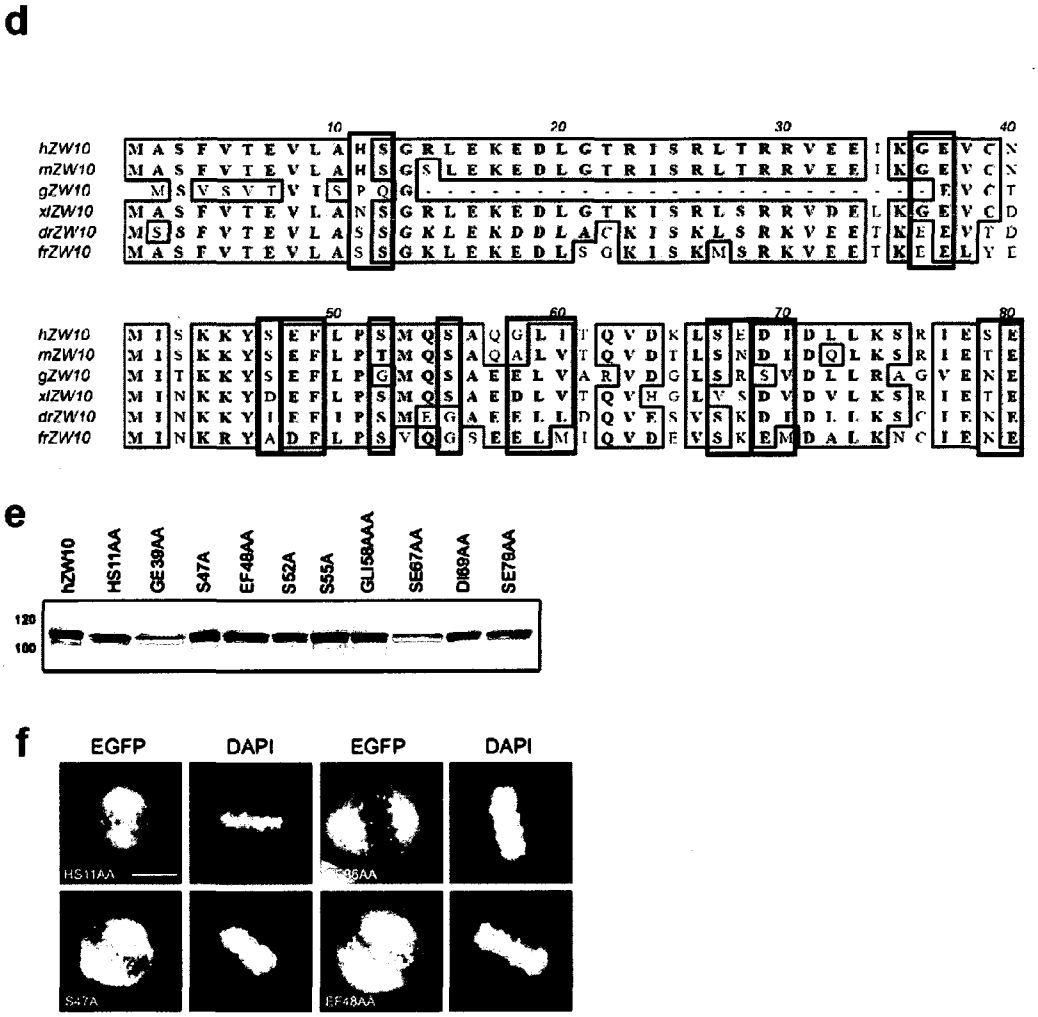

Chapter VI: *Aurora B kinase-dependent recruitment of hZW10 and hROD to tension-less kinetochores.* *

* A version of this chapter has been published as Famulski and Chan. 2007 **Current Biology**, 17:2143-2149.

4.1 Abstract

The mitotic checkpoint ensures proper chromosome segregation by monitoring two critical events during mitosis. One is kinetochore attachment to the mitotic spindle, and the second is the alignment of chromosomes at the metaphase plate, resulting in tension across sister kinetochores [reviewed in (Chan et al., 2005; Musacchio and Salmon, 2007)]. Mitotic-checkpoint proteins are known to accumulate at unaligned chromosomes that have not achieved proper kinetochore-microtubule attachments or established an adequate level of tension across sister kinetochores (Hoffman et al., 2001). Here, we report that hZW10 and hROD, two components of the evolutionarily conserved RZZ complex (Chan et al., 2000; Scaerou et al., 2001), accumulate at kinetochores in response to the loss of tension. By using live-cell imaging and FRAP, we showed that the accumulation of hZW10 at tensionless kinetochores stems from a 4-fold reduction of kinetochore turnover rate. We also found that cells lacking hZW10 escape loss-of-tension-induced mitotic-checkpoint arrest more rapidly than those arrested in response to the lack of kinetochore-microtubule attachments. Furthermore, we show that pharmacological inhibition of Aurora B kinase activity with ZM447439 in the absence of tension, but not in the absence of kinetochore-microtubule attachments, results in the loss of hZW10, hROD, and hBub1 from kinetochores. We therefore conclude that Aurora B kinase activity is required for the accumulation of tension-sensitive mitotic-checkpoint components, such as hZW10 and hROD, in order to maintain mitotic-checkpoint arrest.

4.2 Results and Discussion

4.2.1 Low-Dose Taxol Induces a Mitotic-Checkpoint Response Specific to the Loss of Kinetochore Tension

To study mitotic-checkpoint response to the loss of kinetochore tension, we devised an assay that could monitor the response of mitotic-checkpoint components in both fixed and living cells (Figure S4.1A available online). In short, HeLa cells are first arrested in metaphase with MG132 (a 26S proteosome inhibitor) for 1.5 hr. This ensures that all of the chromosomes have aligned and that full tension is exerted across sister kinetochores. One micromolar of taxol is added for the dampening of microtubule (MT) dynamics, thus reducing kinetochore tension. This concentration of taxol specifically induces the loss of kinetochore tension while retaining kinetochore-microtubule attachments, as outlined in Figure 4.1A and as shown previously (Lampson and Kapoor, 2005). The loss of tension is confirmed by the measurement of the interkinetochore distance with anti-centromere antibody (ACA) staining. The mean interkinetochore distance in MG132-treated cells was 1.9 ± 0.3 μm (n = 100), whereas in the cells treated with MG132 and taxol, the distance was reduced to 0.9 ± 0.1 μm (n = 101), thus indicating the loss of kinetochore tension. Previous work has shown that hBub1 accumulates at tensionless kinetochores (Skoufias et al., 2001). We therefore quantitated the intensity of kinetochore hBub1 in our tension assay. As a control, we also stained the cells for hMad2, a mitotic-checkpoint protein whose kinetochore localization is sensitive to the loss of kinetochore-microtubule attachment but not directly responsive to the loss of tension (Skoufias et al., 2001; Wendell et al., 1993). Our results showed that there was an approximately 2-fold increase in the kinetochore signal of hBub1 when tension was reduced, whereas the hMad2 signal remained unchanged (Figure 4.1B and Figure S4.1B). We confirmed the data by conducting our tension assay analysis in live cells expressing enhanced green fluorescent protein (EGFP)-hBub1 and mCherry-hMad2. Again we observed EGFP-hBub1 but not mCherry-hMad2 respond to the loss of kinetochore tension (Figures 4.1D–1F, Movies S1–S3). Although previous studies have shown that Mad2 remains at a few kinetochores in *Potorous tridactylis* (PTK) cells treated with taxol, we did not detect any hMad2 at tensionless kinetochores in HeLa cells (Waters et al., 1998). Although we cannot exclude the possibility that some hMad2 that is beyond our detection limit remains at kinetochores, we conclude that our assay monitors mitotic-checkpoint protein recruitment to tensionless kinetochores without disturbing kinetochore-MT attachment.

Figure 4.1: **Low-Dose Taxol-Induced Loss of Tension Results in the Accumulation of hBub1 at Tensionless Kinetochores**

A) A representative immunofluorescence image of HeLa cells treated with MG132 or MG132 and taxol, stained with tubulin (green) and ACA (red) antibodies. The insets outline the differences in distance measurements between centromeres in the MG132-treated cells versus cells treated with MG132 and taxol. The scale bar represents 10 μm. **B)** Immunofluorescence images of HeLa cells subjected to the loss-of-tension assay and stained with hBub1, hMad2, and ACA antibodies. Chromosomes were stained with DAPI. hBub1 kinetochore signal is significantly stronger in cells treated with MG132 and taxol, whereas hMad2 signals remain unchanged. The scale bar represents 10 μm.

Figure 4.1

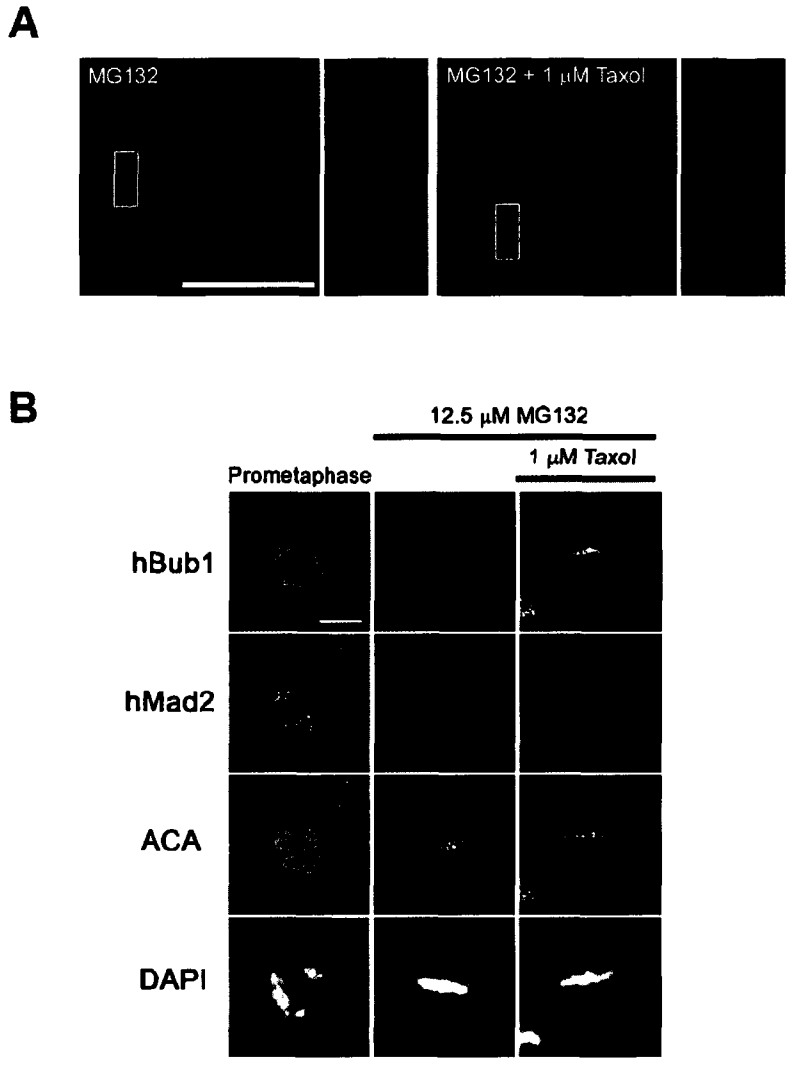

Figure 4.1: **Low-Dose Taxol-Induced Loss of Tension Results in the Accumulation of hBub1 at Tensionless Kinetochores**

A) A representative immunofluorescence image of HeLa cells treated with MG132 or MG132 and taxol, stained with tubulin (green) and ACA (red) antibodies. The insets outline the differences in distance measurements between centromeres in the MG132-treated cells versus cells treated with MG132 and taxol. The scale bar represents 10 μm. **B)** Immunofluorescence images of HeLa cells subjected to the loss-of-tension assay and stained with hBub1, hMad2, and ACA antibodies. Chromosomes were stained with DAPI. hBub1 kinetochore signal is significantly stronger in cells treated with MG132 and taxol, whereas hMad2 signals remain unchanged. The scale bar represents 10 μm.

Figure 4.1

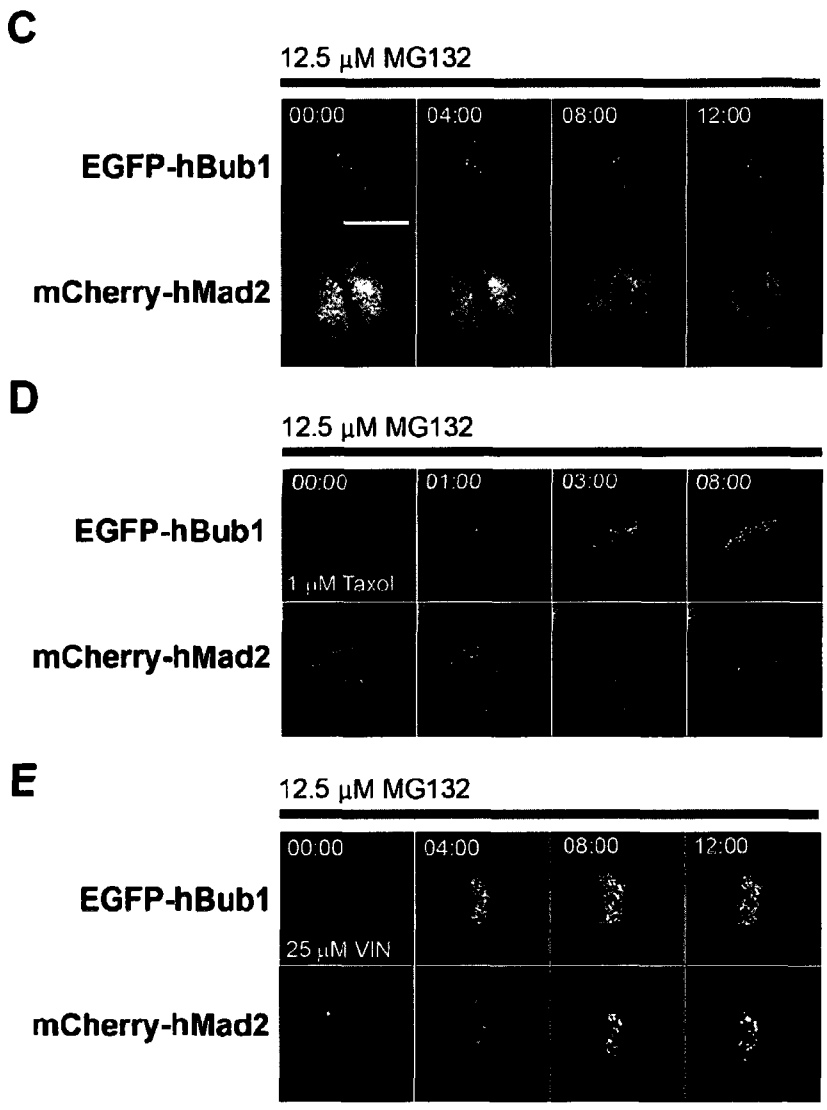

Figure 4.1: **Low-Dose Taxol-Induced Loss of Tension Results in the Accumulation of hBub1 at Tensionless Kinetochores**

C–E) HeLa cells cotransfected with EGFP-hBub1 and mCherry-hMad2 and arrested with MG132 are imaged live with a spinning-disk confocal microscope. Time is indicated in the top right-hand corner as minutes:seconds from the start of imaging. The scale bar represents 10 μm. In the presence of MG132 alone, no significant accumulation of either EGFP-hBub1 or mCherry-hMad2 is observed (C). The addition of taxol only induced EGFP-hBub1 kinetochore accumulation (D). The addition of vinblastine induced both EGFP-hBub1 and mCherry-hMad2 to accumulate at kinetochores (E).

4.2.2 hZW10 and hROD Respond to the Loss of Kinetochore Tension by Accumulating at Tensionless Kinetochores

Having established our loss-of-tension assay, we next analyzed the loss-of-tension response for hZW10 and hROD. Treatment with MG132 alone lead to low levels of kinetochore hZW10 and hROD when compared to prometaphase, whereas levels of hZwint-1, a structural kinetochore protein, remained constant (Figure 4.2A). However, in the presence of taxol, we observed a marked increase of kinetochore associated hZW10 and hROD but not of hZwint-1 or hMad2. Kinetochore intensity measurements indicated an approximately 2-fold increase in hZW10 kinetochore signal and an approximately 1.6-fold increase in hROD signal in response to the loss of kinetochore tension (Figure S4.1C). Tensionless kinetochore accumulation of hZW10 and hROD but not hMad2 suggests that although hZW10 and hROD might be required for the recruitment of hMad2 to kinetochores (Buffin et al., 2005; Kops et al., 2005a), they are not required for the retention of hMad2 at kinetochores that have achieved kinetochore-MT attachments. Although hMad2 is required for maintenance of checkpoint arrest in response to the loss of kinetochore tension (Shannon et al., 2002), our study shows that accumulation of hMad2 at kinetochores is not. This suggests that tension-sensitive kinetochore components, such as the RZZ complex, can signal hMad2-mediated checkpoint arrest without having to recruit hMad2 to kinetochores.

We again confirmed the immunofluorescence data by conducting our tension assay analysis in live cells expressing EGFP-hZW10 and mCherry-hMad2. Similar to EGFP-hBub1, we observed that only EGFP-hZW10 responded to the loss of kinetochore tension, whereas both EGFP-hZW10 and mCherry-hMad2 readily responded to the loss of kinetochore-MT attachments (Figures 4.2B–2D, Movies S4–S6). On the basis of our findings, we propose that hZW10 and hROD are involved in the mitotic-checkpoint response to the loss of tension, a notion that has been previously suggested solely on the basis of observed hZW10 behavior (Basto et al., 2004; Scaerou et al., 2001; Williams et al., 1996). We further investigated the role of hZW10 in the mitotic-checkpoint response to the loss of tension by small interfering RNA (siRNA) depletion. Depletion of hZW10 resulted in an approximately 2-fold faster escape from mitotic arrest in the absence of kinetochore tension (taxol arrest escape: 162.3 ± 61.0 min, n = 12) than in the absence of kinetochore-microtubule attachments and tension (vinblastine arrest escape: 292.0 ± 61.4 min, n = 17) (Figure S4.2 and Movies S7–S11). Mitotic-checkpoint escape was observed as decondensation of chromatin and re-entry into the cell cycle. These results suggest that the accumulation of hZW10 at tensionless kinetochores is essential for the maintenance of mitotic-checkpoint signaling. Because the depletion of other mitotic-checkpoint proteins has not been analyzed in this manner, we cannot rule out the possibility that the depletion of other mitotic-checkpoint proteins might lead to a faster escape from taxol than vinblastine-induced mitotic arrest. In agreement with previous work, we also observed that hZW10 knockdown only slightly affected the generation of kinetochore tension. The mean interkinetochore distance measured only dropped to 1.7 ± 0.4 μm (n = 42) in the siRNA-treated cells (Starr et al., 1998). hZW10 is therefore not essential for the generation of kinetochore tension but is essential for maintenance of checkpoint arrest in its absence.

Figure 4.2

A

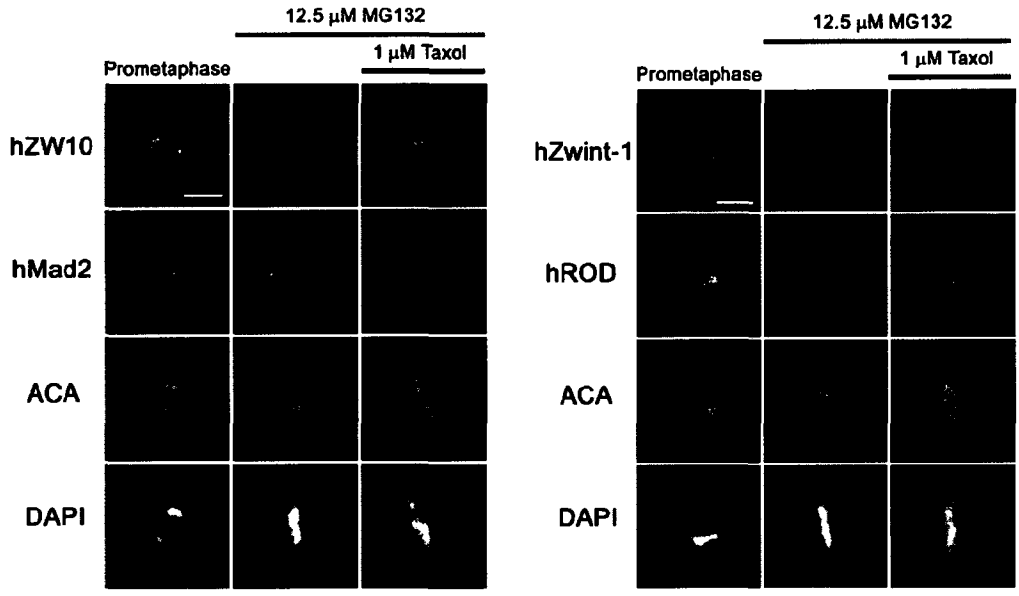

Figure 4.2. **hZW10 and hROD Respond to the Loss of Tension by Accumulating at Tensionless Kinetochores**

A) Immunofluorescence images of HeLa cells subjected to the loss-of-tension assay and stained with hZW10, hMad2, hROD, hZwint-1, and ACA antibodies. Chromosomes were stained with DAPI. hZW10 and hROD are observed to accumulate at tensionless, taxol-treated kinetochores, whereas hZwint-1 and hMad2 kinetochore intensity remains unchanged. The scale bar represents 10 μm.

Figure 4.2. **hZW10 and hROD Respond to the Loss of Tension by Accumulating at Tensionless Kinetochores**

B–D) HeLa cells stably expressing EGFP-hZW10 were transiently transfected with mCherry-hMad2, arrested with MG132 for 1.5 hr, and imaged live with a spinning-disk confocal microscope. Time is indicated in the top right-hand corner as minutes:seconds from the start of imaging. The scale bar represents 10 μm. In the presence of MG132 alone, no significant accumulation of either EGFP-hZW10 or mCherry-hMad2 is observed (B). The addition of taxol only induced EGFP-hZW10 kinetochore accumulation (C). The addition of vinblastine induced both EGFP-hZW10 and mCherry-hMad2 to accumulate at kinetochores (D). **E)** Time-lapse series showing EGFP-hZW10 fluorescence recovery after photobleaching at single kinetochores in metaphase (top panels) and when treated with MG132 and taxol (bottom panels). The time scale indicated is in minutes:seconds. The photobleached kinetochores are outlined with white circles and enlarged in the bottom right-hand corner. EGFP-hZW10 is observed to recover 50% at metaphase kinetochores within approximately 10 s, whereas in the presence of MG132 and taxol, 50% EGFP-hZW10 recovery takes significantly longer, approximately 45 s. The large scale bar represents 10 μm, and the small scale bar represents 1 μm. On the right-hand are nonlinear regression curves representing percent recovery of EGFP-hZW10 kinetochore signals shown as averages from several experiments. Recovery in metaphase is shown in green, and recovery in the presence of MG132 and taxol is shown in red.

Figure 4.2

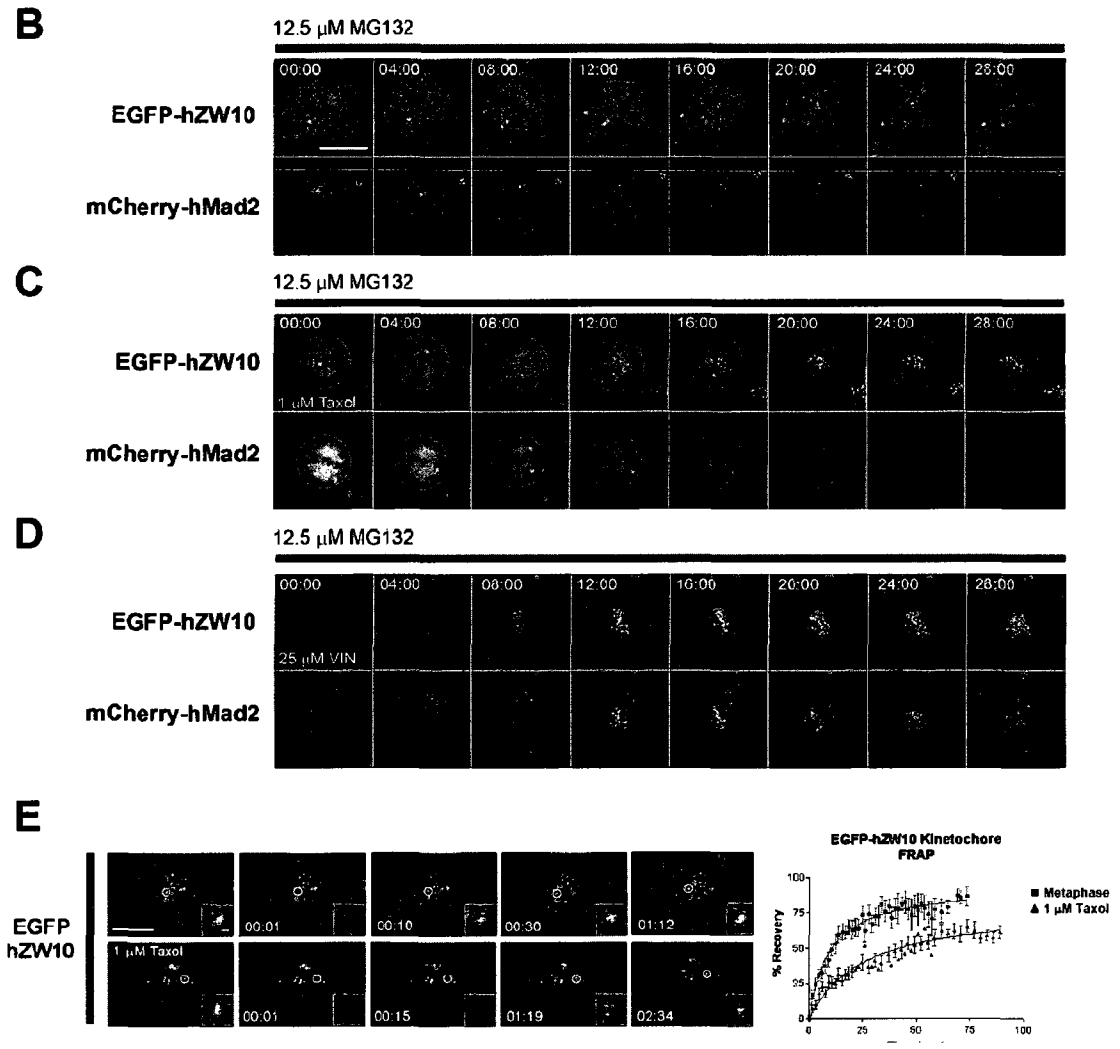
B
12.5 μM MG132
EGFP-hZW10
mCherry-hMad2
00:00
04:00
08:00
12:00
16:00
20:00
24:00
28:00
C
12.5 μM MG132
EGFP-hZW10
1 μM Taxol
mCherry-hMad2
D
12.5 μM MG132
EGFP-hZW10
25 μM VIN
mCherry-hMad2
E
EGFP
hZW10
1 μM Taxol
00:01
00:10
00:30
01:12
00:01
00:15
01:19
02:34
EGFP-hZW10 Kinetochore
FRAP
% Recovery
Metaphase
1 μM Taxol

4.2.3 Dynamitin but Not Dynein Accumulates at Tensionless Kinetochores

hZW10 is known to interact with a subunit of the dynactin complex, dynamitin (hp50), and is responsible for the recruitment of dynein to the kinetochore (Yang et al., 2007b). We therefore analyzed whether hp50 and dynein also accumulated at tensionless kinetochores. Similar to EGFP-hZW10, we found that YFP-hp50 accumulated at tensionless kinetochores, thus indicating that hZW10 remains in complex with dynactin (Figure S4.3A and Movie S12). On the other hand, we found that the dynein intermediate chain does not accumulate at tensionless kinetochores generated by either taxol or low-dose nocodazole (Figure S4.3B). These results indicate that although the localization of dynein to kinetochores might be independent of kinetochore tension, dynactin kinetochore localization clearly increases in response to the loss of tension. The inability of dynein to accumulate at tensionless kinetochores suggests the interaction between dynein and the RZZ complex is inhibited. The accumulation of hZW10 and hROD at tensionless kinetochores might therefore result from the inability of dynein to transport the RZZ complex off kinetochores.

4.2.4 Lack of Kinetochore Tension Reduces the Kinetochore Turnover Rate of hZW10

Having established that hZW10 and hROD localization is sensitive to kinetochore tension, we next analyzed the mechanism responsible for this response. We have recently shown that hZW10 is a stable component of the kinetochore during prometaphase, and a dynamic one during metaphase, depending on bipolar kinetochore-microtubule attachment and chromosome alignment (Ditchfield et al., 2003). However, in our tension assay, we observe an accumulation of hZW10 at tensionless kinetochores even though bipolar kinetochore-MT attachment has been achieved. To test whether the accumulation of hZW10 at tensionless kinetochores results from a reduced rate of turnover, we performed fluorescence recovery after photobleaching (FRAP) analysis on kinetochore EGFP-hZW10 in cells treated with MG132 and taxol. Interestingly, we observed a marked decrease in the rate of EGFP-hZW10 kinetochore turnover, with the time required for 50% fluorescence recovery ($T^{1/2}$) of EGFP-hZW10 increasing to 46.0 ± 22.1 s in the taxol-treated cells (n = 13) from that of 12.2 ± 5.3 s in control metaphase cells (n = 13) (Figure 4.2E). In addition, only 74.9% ± 12.5% of the fluorescence signal was recovered during the 2–3 min of imaging the taxol-treated cells, whereas the normal metaphase recovery was 88.4% ± 9.2%. These findings indicate that although hZW10 still turns over at tensionless kinetochores, the rate of its turnover is reduced nearly 4-fold. Our results are in contrast to that of GFP-tagged dmROD, which is completely transported off kinetochores in the presence of taxol (Basto et al., 2004). We attribute this difference in behavior to the fundamental differences between human somatic cell and fly embryo mitosis. Cell division in fly embryos is syncytial and very rapid. The mechanism of the mitotic checkpoint might therefore be substantially different from that in somatic cells. hZW10 is the first example of a mitotic-checkpoint protein whose accumulation at tensionless kinetochores is regulated by its turnover rate.

When analyzing EGFP-hBub1 kinetochore dynamics, we found that the loss of tension had no effect on EGFP-hBub1 kinetochore turnover rate (MG132 $T^{1/2}$ of 14.0 ± 5.3 s, n = 7 versus MG132 + taxol $T^{1/2}$ of 14.8 ± 5.7 s, n = 16) or its percent recovery (MG132% recovery of 94.9 ± 6.3 versus MG132 + taxol % recovery of 90.3 ± 8.8) (Figure S4.4). This indicates that the mechanism driving the accumulation of hBub1 does not rely on a reduced turnover rate at tensionless kinetochores and therefore differs from that of hZW10. We propose that hBub1 might accumulate at tensionless kinetochores either through oligomerization or through an increase in the number of hBub1 kinetochore binding sites.

4.2.5 hZW10, hROD, and hBub1 Accumulation at Tensionless Kinetochores Requires Aurora B Kinase Activity

Aurora B is believed to be a key component of the mitotic-checkpoint response to the loss of kinetochore tension (Carvalho et al., 2003; Hauf et al., 2003; Lens et al., 2003). Previous studies have shown that inhibition of Aurora B kinase activity or disruption of the chromosome passenger complex results in the escape from mitotic-checkpoint arrest induced by the lack of kinetochore tension but not by the lack of kinetochore-MT attachments (Cimini et al., 2006; Hauf et al., 2003; Lens and Medema, 2003; Lens et al., 2003). Aurora B kinase activity has also been shown to be required for the kinetochore recruitment of hBubR1, hCENP-E, and hMad2 (Hauf et al., 2003; Lens and Medema, 2003). We therefore tested whether there was a connection between Aurora B kinase activity and hZW10 and hROD recruitment to tensionless kinetochores. Aurora B kinetochore localization and dynamics were not affected by the loss of tension, loss of kinetochore MTs, or inhibition of its kinase activity by 2 μM ZM447439, a concentration which has been shown not to affect chromatin condensation (Howell et al., 2004; Lens and Medema, 2003) (Figures S4.5A–S5C, and S4.6A and Movies S13–S15). Although 2 μM ZM447439 had no effect on Aurora B kinetochore localization, it did induce mitotic-checkpoint escape from taxol- but not vinblastine-arrested cells (Figure S4.6A and Movies S16–S18), which is in agreement with previous reports (Hauf et al., 2003; Lens and Medema, 2003). We next repeated our loss-of-tension assay and inhibited Aurora B kinase by adding 2 μM ZM447439 15 min after taxol treatment. Cells treated with ZM447439 failed to accumulate hZW10, hROD, hp50, or hBub1 (Figure 4.3A, Figures S4.3B, S4.3C, and S4.6B, and Movie S19). In fact, hZW10 and hROD appeared to be totally absent from kinetochores, whereas hZwint-1 remained largely unaffected. In order to confirm our results we subjected live cells expressing EGFP-hZW10, or EGFP-hBub1, to our tension and ZM447439 assay. As expected, upon the addition of ZM447439, we observed a rapid loss of EGFP-hZW10 and EGFP-hBub1 from the tensionless kinetochores (Figure 4.3B and Movies S20–S21). In order to investigate whether Aurora B kinase activity is also required for the initial recruitment of EGFP-hZW10 and EGFP-hBub1 to tensionless kinetochores, we added taxol and ZM447439 to the cells at the same time, thus inhibiting Aurora B kinase activity at the time of tension loss. In these cells, we observed no accumulation of either EGFP-hZW10 or EGFP-hBub1 (Figure 4.3C and Movies S22–S23). Lastly, we found that the addition of 2 μM ZM447439 to cells treated with vinblastine reduced but did not totally eliminate kinetochore EGFP-hZW10 and EGFP-hBub1 (Figure 4.3D and Movies S24–S25). We

therefore presume that Aurora B kinase activity is essential for the initial as well as the continuous kinetochore recruitment of hZW10, hROD, hp50, and hBub1 in response to the loss of tension (taxol treated) but not to the loss of kinetochore-MT attachments (vinblastine treated). The retention of hZW10 and hBub1 at kinetochores lacking tension and kinetochore-MT attachments might therefore explain the inability of ZM447439 to induce mitotic-checkpoint escape from vinblastine-treated cells.

4.3 Conclusion

In conclusion, we find that hZW10 and hROD are tension-sensitive components of the mitotic checkpoint and that their accumulation at tensionless kinetochores is regulated by their turnover dynamics in an Aurora B kinase-dependent manner. We propose that Aurora B phosphorylation of the RZZ complex might reduce its kinetochore turnover rate, therefore leading to the accumulation of hp50 and the RZZ complex at tensionless kinetochores (Figure 4.4). Lowering the kinetochore turnover rate of the RZZ complex might involve modification of the interaction between the RZZ complex and dynein. This could prevent dynein-mediated transport of the RZZ complex, and other essential mitotic-checkpoint components, off kinetochores. Mitotic-checkpoint arrest in response to the loss of kinetochore tension would thus be maintained by the prevention of the "shedding" of essential checkpoint proteins from kinetochores, even though bipolar attachment of microtubules has been achieved (Figure 4.4).

Figure 4.3: **Aurora B Kinase Activity Regulates hBub1, hZW10, and hROD Kinetochore Accumulation during Mitotic-Checkpoint Response to the Loss of Tension**

A) Immunofluorescence images of HeLa cells subjected to the loss-of-tension assay with 2 μM ZM447439 treatment 15 min after the addition of taxol. hBub1, hZW10, and hROD are lost from kinetochores even in the presence of taxol. hZwint-1, Mad2, and ACA, on the other hand, retain their kinetochore localization intensities. The scale bar represents 10 μm. **B–D)** HeLa cells stably expressing EGFP-hZW10 or transiently transfected with EGFP-hBub1 were subjected to the loss-of-tension assay and imaged live. Time is indicated in the top right hand corner as minutes:seconds from the start of imaging. The scale bar represents 10 μm. Two micromolars of ZM447439 was added to the media approximately 20 min after taxol addition (B). Both EGFP-hZW10 and EGFP-hBub1 are observed to initially accumulate in response to the loss of tension; however, upon addition of ZM447439, they are both rapidly lost from kinetochores. When Taxol and ZM447439 are added simultaneously, neither EGFP-hZW10 nor EGFP-hBub1 accumulated at the tensionless kinetochores (C). Vinblastine was added to MG132 arrested cells for approximately 12 min, during which EGFP-hZW10 and EGFP-hBub1 accumulated at kinetochores (D). Once 2 μM ZM447439 was added, a significant amount of EGFP-hZW10 and EGFP-hBub1 was lost from kinetochores upon the addition of 2 μM ZM447439; however, a significant pool still remained.

Figure 4.3

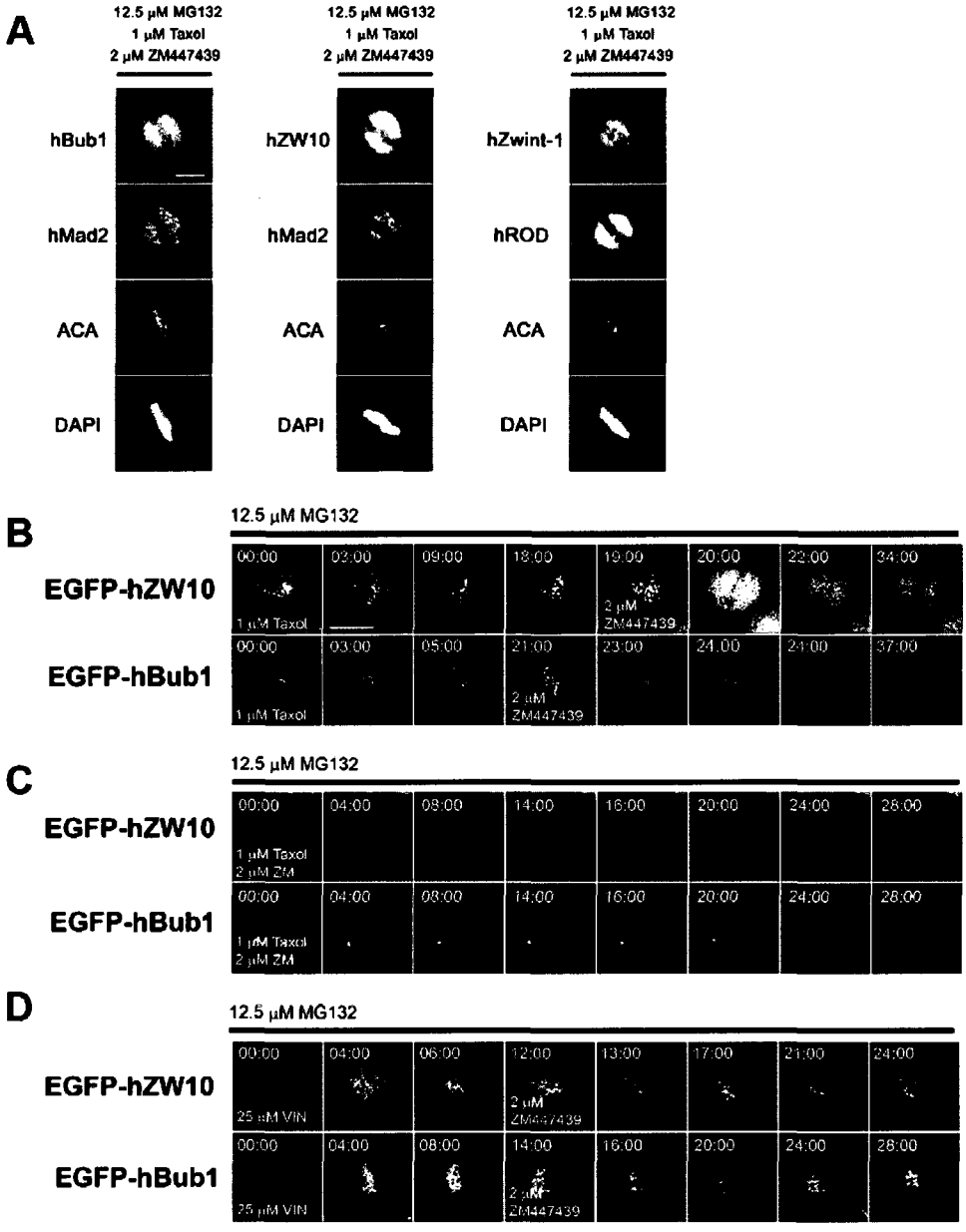
A
12.5 μM MG132
1 μM Taxol
2 μM ZM447439
hBub1
hMad2
ACA
DAPI
hZW10
hZwint-1
hROD
B
12.5 μM MG132
EGFP-hZW10
EGFP-hBub1
1 μM Taxol
2 μM ZM447439
C
EGFP-hZW10
EGFP-hBub1
1 μM Taxol
2 μM ZM
D
EGFP-hZW10
EGFP-hBub1
25 nM VIN

Figure 4.4. **A Model of Aurora B Regulation of the Transport of the RZZ Complex off Kinetochores in Response to the Loss of Kinetochore Tension**

A) The RZZ complex and hp50 accumulate at prometaphase (or vinblastine-treated) kinetochores that lack kinetochore-MT attachments. Dynein is in turn recruited to these kinetochores through the interaction of hp50 and the dynactin complex. The RZZ complex is a stable component of the kinetochore in prometaphase, thus maintaining mitotic-checkpoint signaling. **B)** At kinetochores that have achieved kinetochore-MT attachments but have not established kinetochore tension (curved kinetochore), the kinetochore RZZ complex, in conjunction with hp50, becomes stabilized and thus accumulates at kinetochores. Dynein, however, does not accumulate or stabilize at tensionless kinetochores and continues to cycle, and transport hMad2, off kinetochores by traveling along kinetochore MTs. Dynein/dynactin does not remove the RZZ complex from tensionless kinetochores because at tensionless kinetochores, the Aurora B kinase phosphorylates the RZZ complex. Phosphorylation of the RZZ complex might function to inhibit the interaction between the RZZ complex and dynein. Aurora B phosphorylation thus leads to a reduced turnover rate of the RZZ complex at tensionless kinetochores. The retention of kinetochore RZZ complexes might lead to the retention of other tension-sensitive kinetochore components such as hBubR1 (data not shown), which are also transported by dynein. The retained kinetochore checkpoint components signal hMad2-mediated checkpoint arrest, thus maintaining checkpoint activation. **C)** At kinetochores that are under tension (straight kinetochore), Aurora B is physically removed from phosphorylating the RZZ complex. Dynein/dynactin can now interact with and remove the RZZ complex, and other checkpoint proteins, from kinetochores that have established tension, thus leading to silencing of the checkpoint.

Figure 4.4

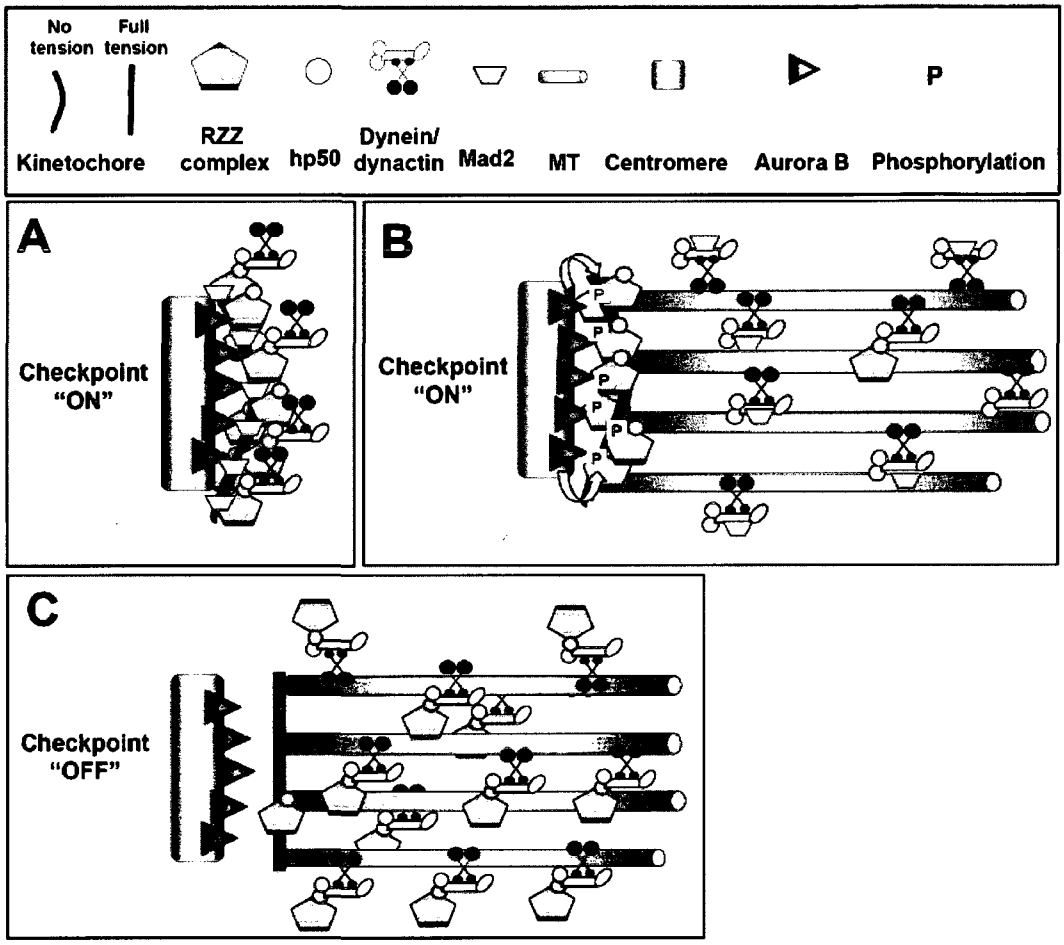
No tension
Full tension
Kinetochore
RZZ complex
hp50
Dynein/ dynactin
Mad2
MT
Centromere
Aurora B
P
Phosphorylation
A
Checkpoint "ON"
B
Checkpoint "ON"
C
Checkpoint "OFF"

4.4 Supplementary Material: *Aurora B kinase-dependent recruitment of hZW10 and hROD to tension-less kinetochores.*

Supplementary Figure 4.1: **Low dose taxol induced loss of tension results in the accumulation of hBub1, hZW10 and hROD at tension-less kinetochores.** **A)** A schematic diagram depicting the loss of tension assay. HeLa cells are seeded for 24 hours and then treated with 12.5 μM MG132 for 1.5 hours. The cells are subsequently either fixed (or analyzed by live cell time-lapse microscopy) or treated with 1 μM taxol for another 30 minutes and then fixed. **B)** A bar graph where individual kinetochore intensity of hMad2 and hBub1 from 10 cells was measured and normalized to that of ACA (n is the number of kinetochores analyzed). Error bars represent +/- standard deviation. **C)** A bar graph where individual kinetochore intensity of hZW10, hROD, hMad2 and hZwint-1 from 10 cells was measured and normalized to that of ACA (n is the number of kinetochores analyzed). Error bars represent +/- standard deviation.

Supplementary Figure 4.1

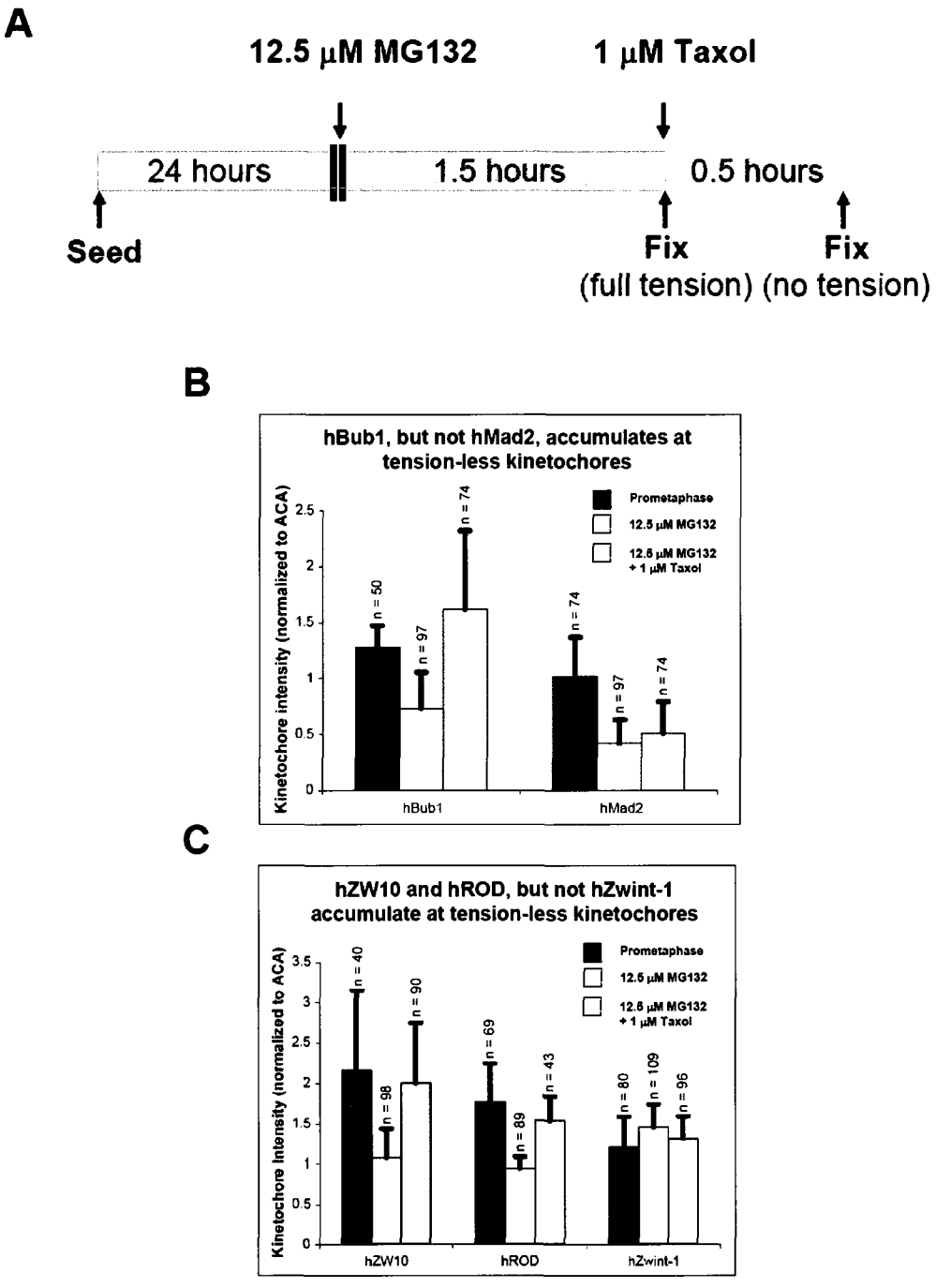

Supplementary Figure 4.2: **MG132 washout assay for mitotic exit and or escape in the presence of vinblastine and/or taxol.**
A) siRNA mediated knockdown of hZW10 shown though immunofluorescence staining of HeLa cells for hZW10 or western blotting of HeLa lysate with anti-hZW10 antibodies. hZW10 is clearly knocked down 72 hours after siRNA transfection. Chromosomes were stained with DAPI and centromeres with ACA antibodies. Sacle bar = 10 μm. **B)** HeLa cells stably expressing GFP-H2B arrested with MG132 for 1 hour were washed with fresh (or drug containing media). Cells (no siRNA transfection) released from MG132 into fresh media entered anaphase 29.4 ± 7.7 minutes (n=12) post MG132 washout (top panel). Cells released from MG132 into either 1 μM taxol (loss of kinetochore tension) (n=12) or 25 μM vinblastine (loss of kinetochore-MT attachment and tension) (n=13) containing media, remained arrested in mitosis (up to 4 hours post MG132 release, the time limit of our imaging assay) (panels 2 and 3). Time is indicated in the top right hand corner as minutes: seconds from the start of imaging. Scale bar = 10 μm. **C)** HeLa cells stably expressing GFP-H2B, and transfected with anti-hZW10 siRNA for 72 hours, arrested with MG132 for 1 hour were washed with fresh (or drug containing) media and imaged live using a spinning disk confocal microscope. Cells released into vinblatine media escaped mitotic arrest, as observed by the de-condensation of chromatin, much later than those released into taxol containing media. Time is indicated as minutes: seconds from the start of filming and/or addition of drug. Scale bar = 10 μm.

Supplementary Figure 4.2

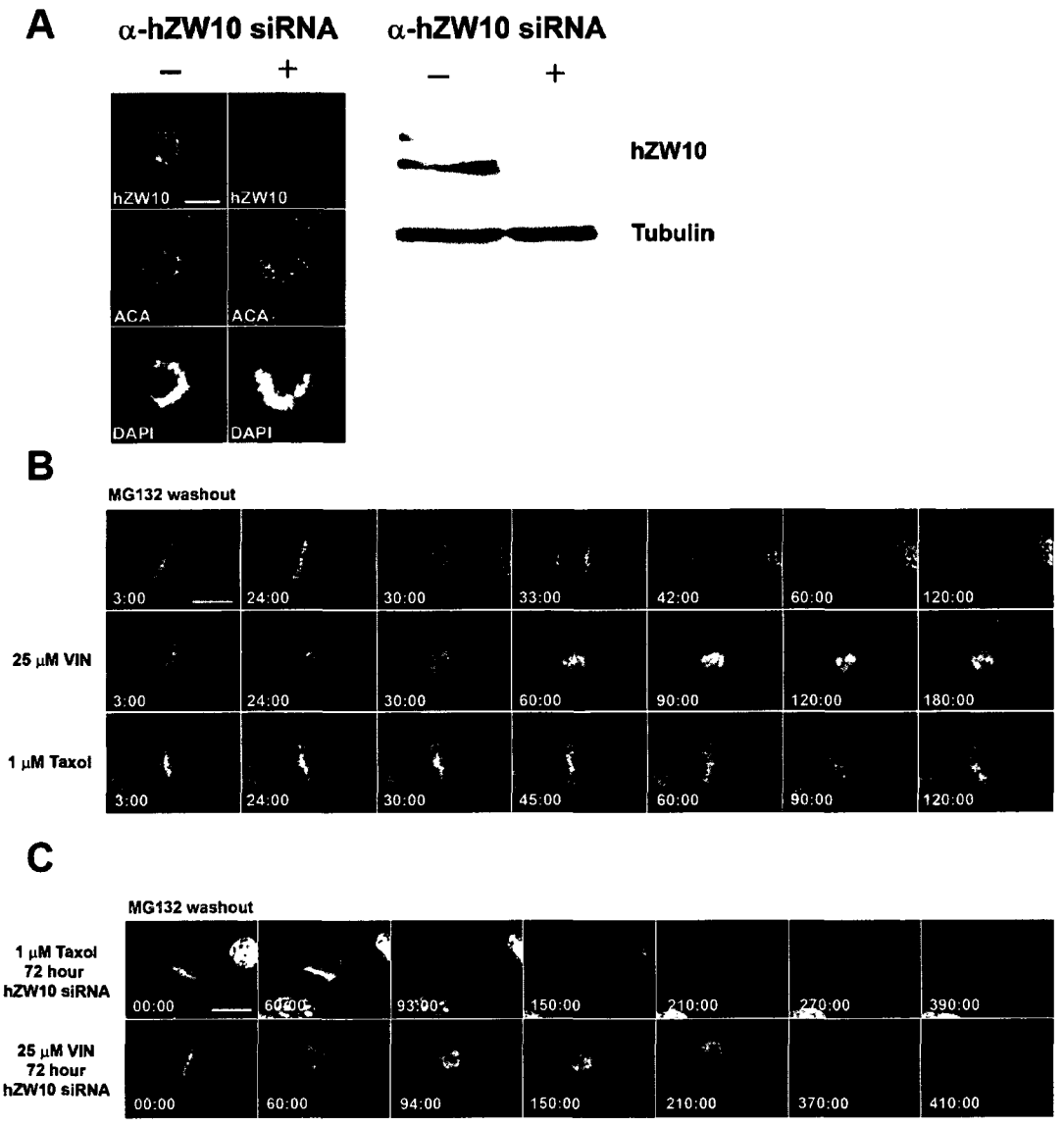

Supplementary Figure 4.3: **hp50 (dynamitin), but not dynein, accumulates at kinetochores in response to the loss of tension.**
A) HeLa cells stably expessing YFP-hp50 were subjected to the loss of tension assay and imaged live using a spinning disk confocal microscope. Time-lapse images show an accumulation of YFP-hp50 at kinetochores after the addition of 1μM taxol. Time is indicated in minutes from the addition of taxol. Scale bar = 10 μm. **B)** Immunofluorescence images of HeLa cells or HeLa cells stably expressing YFP-hp50 subjected to the loss of tension assay and stained with anti-hZW10, and hdIC antibodies (left panel). Chromosomes were stained with DAPI. hZW10 and YFP-hp50 are observed to accumulate at tension-less, taxol-treated, kinetochores, while hdIC kinetochore intensity remains unchanged between MG132 and MG132 + taxol treatments. hdIC does accumulate at kinetochores lacking kinetochore-MT attachments (vinblastine treatment). In addtion to the taxol based tension assay we also preformed a low dose nocodazole, 20 nM, based loss of tension assay (as described in Huang et al. (Huang et al., 2007)). We again stained for hZW10 and hdIC. hZW10 but not hdIC is observed to accumulate at tension-less kinetochores. YFP-hp50 is lost from tension-less kinetochores when treated with 2 μM ZM447439 (right panels). **C)** HeLa cells stably expressing YFP-hp50 were subjected to the loss of tension assay and imaged using a spinning disk confocal microscope. After 20 minutes of 1 μM taxol treatment 2 μM ZM447439 was added to the media and images were collected every 1 minute. YFP-p50 is lost from the tension-less kinetochores within 5 minutes of ZM447439 addition. Time is indicated in minutes post the addition of ZM447439. Scale bar = 10 μm.

Supplementary Figure 4.3

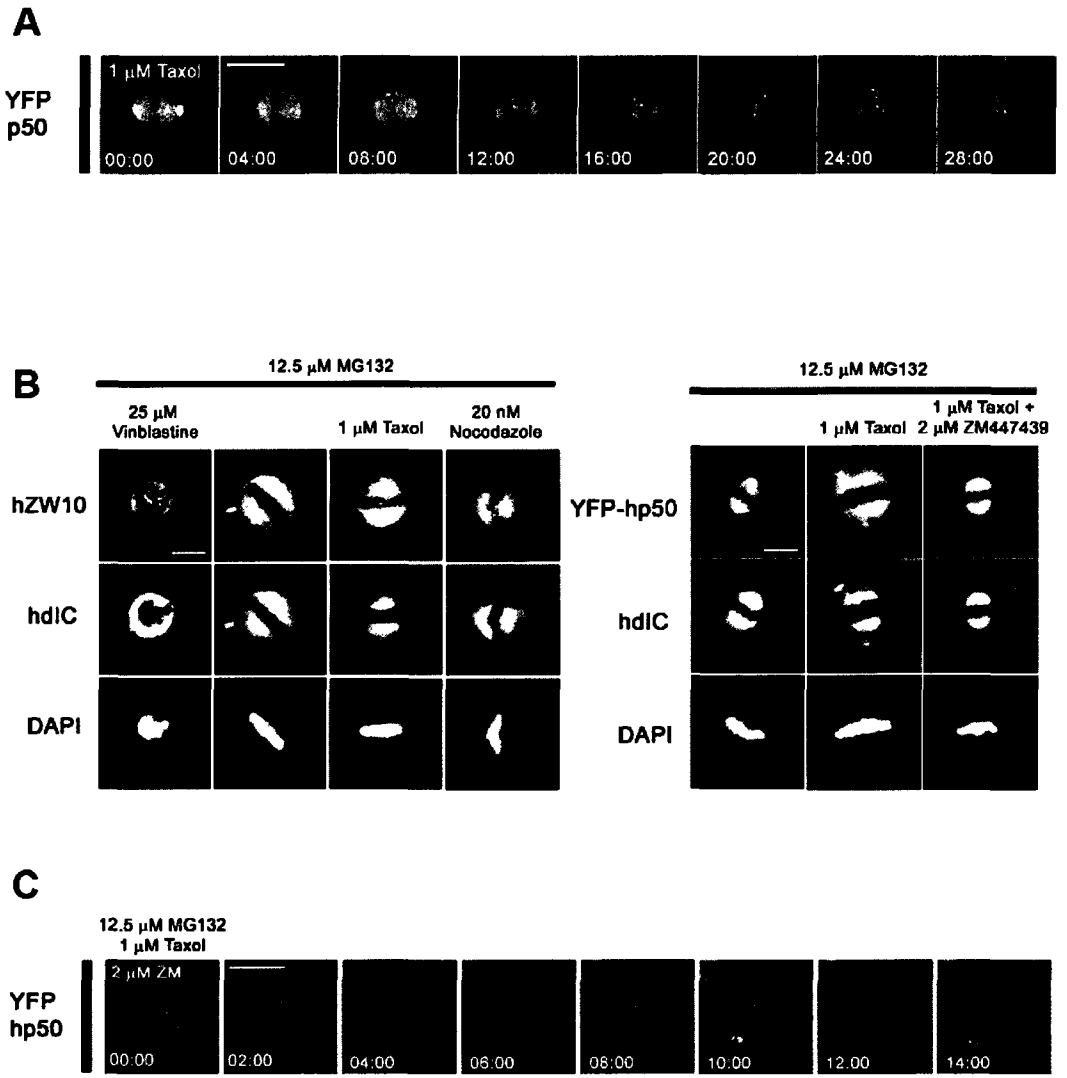

Supplementary Figure 4.4

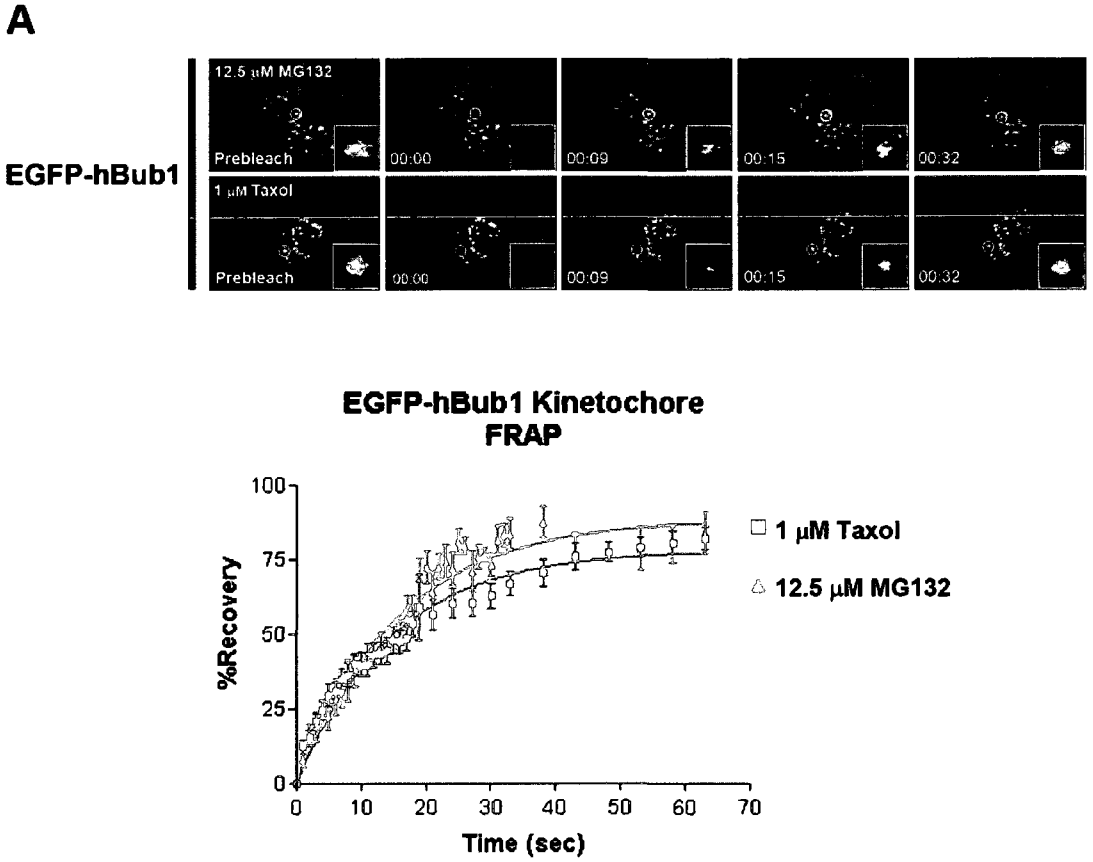

Supplementary Figure 4.4: **EGFP-hBub1 kinetochore turnover is not affected by the loss of kinetochore tension.**
A) Time lapse series showing EGFP-hBub1 fluorescence recovery after photobleaching at single kinetochores in metaphase (top panels) and when treated with MG132 and taxol (bottom panels). The time scale indicated is in minutes:seconds. The photobleached kinetochores are outlined with white circles and enlarged in the bottom right hand corner. Large scale bar = 10 μm, small scale bar = 1 μm. **B)** EGFP-hBub1 is observed to readily turnover at kinetochores in both treatments, with a 50% turnover rate of ~14 seconds. Shown are non-linear regression curves for percent recovery of EGFP-hZW10 and EGFP-hBub1 kinetochore signals shown as averages from several experiments. Recovery in metaphase or MG132 is shown in green, while recovery in the presence of MG132 and taxol is shown in red.

Supplementary Figure 4.5: **Aurora B kinetochore localization and dynamics are unaffected by the loss of tension or 2 μM ZM447439 treatment.**
A) Immunofluorescence images of HeLa cells subjected to the loss of tension assay and stained with anti-Aurora-B antibodies. Aurora-B kinetochore localization appears largely unchanged in response to the loss of tension. Chromosomes are stained with DAPI and the centromeres with ACA antibodies. Scale bar = 10 μm. **B)** HeLa cells stably expressing Aurora B-GFP were subjected to our loss of tension assay (top panel), our assay but with loss of kinetochore-microtubule attachments using vinblastine (middle panel), and our assay but with inhibition of Aurora B kinase activity using 2 μM ZM447439 and imaged live using spinning disk confocal microscopy. Aurora B-GFP kinetochore localization remains largely unchanged in any of the three treatments. The time from addition of taxol, vinblastine or ZM447439 is indicated in minutes. Scale bar = 10 μm. **C)** Time lapse images of HeLa cells stably expressing Aurora B-GFP showing fluorescence recovery of photobleached kinetochores in either MG132 arrested (top panel) or MG132 + 1 μm taxol arrested cells (bottom panel). Kinetochores bleached are outlined with while ovals. Time is indicated in minutes: seconds post bleaching. Below are non linear regression curve analysis of the % fluorescence recovery of kinetochore Aurora B-GFP in either MG132 (green) or the MG132 + 1 μm taxol (red).

Supplementary Figure 4.5

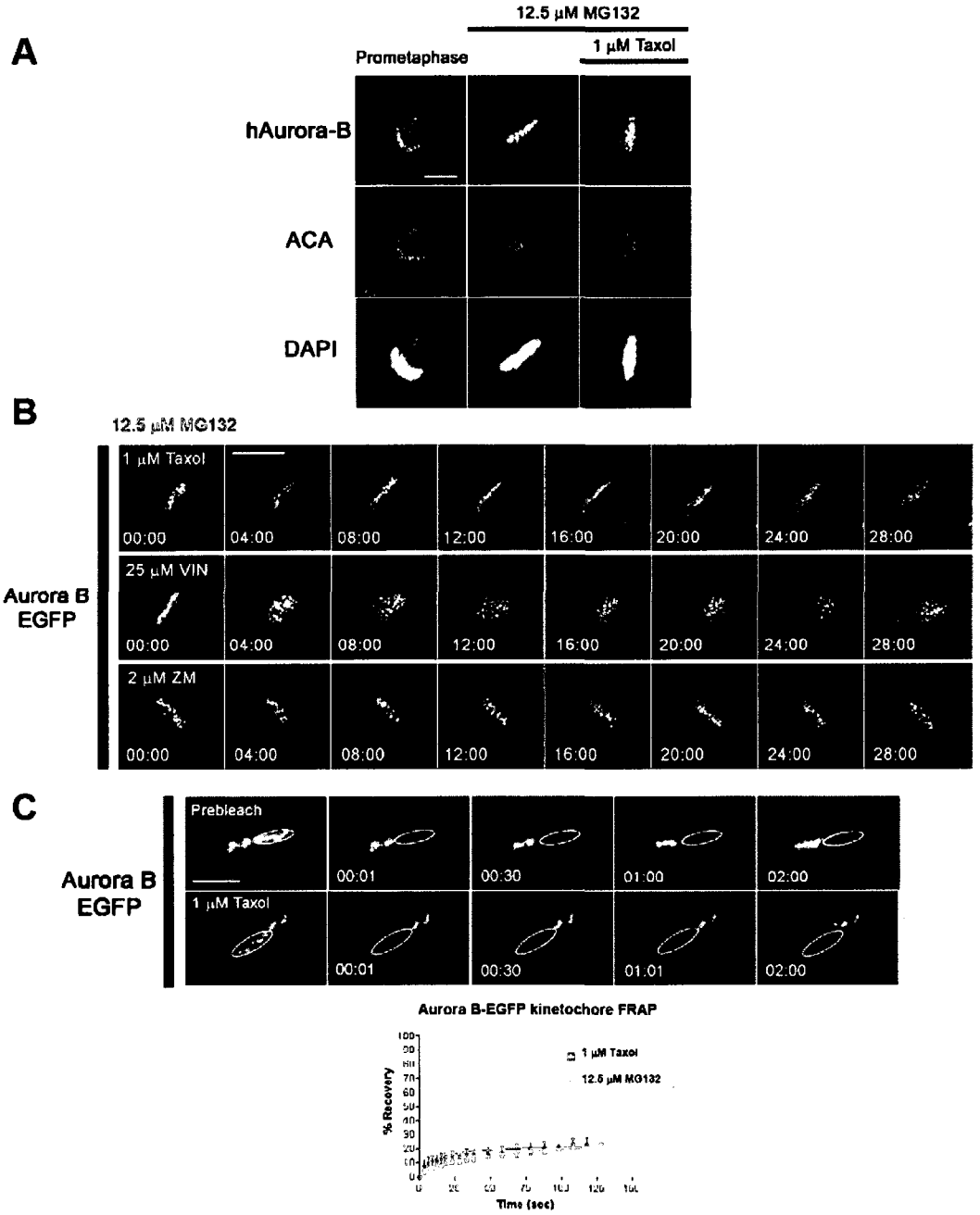

Supplementary Figure 4.6

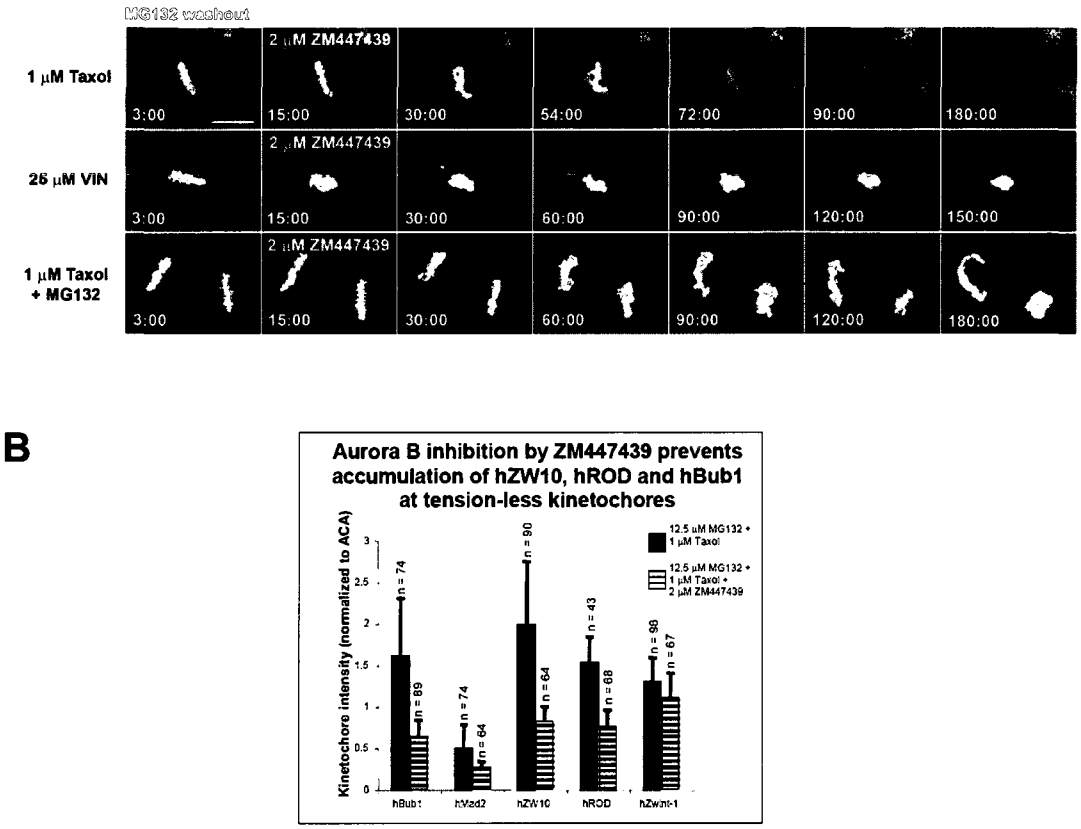

Supplementary Figure 4.6: **Aurora B kinase activity is required for tension-mediated checkpoint arrest and kinetochore accumulation of kinetochore components.**
A) HeLa cells stably expressing GFP-H2B and arrested with MG132 were washed out into either 1 μM taxol or 25 μM vinblastine containing media. After 15 minutes of live cell time-lapse microscopy analysis, 2 μM ZM447439 was added to the media. Cells that were arrested with taxol, top panel, were able to escape mitotic arrest within 63.8 ± 19.4 minutes (n=15) as observed by decondensing chromatin. Treatments with vinblasine or taxol and no MG132 washout resulted in prolonged mitotic arrest even in the presence of ZM447439 indicating that ZM447439 induced checkpoint escape from taxol arrest requires cyclin B and securing degradation, as previously shown [18]. (middle and bottom panels, n=7 and 16 respectively). Time is indicated in minutes:seconds from initiation of imaging. Scale bar = 10 μm. **B)** A bar graph where individual kinetochore intensity of hBub1, hMad2, hZW10, hROD and hZwint-1 from 10 cells was measured and normalized to that of ACA (n is the number of kinetochores analyzed). Error bars represent +/- standard deviation.

Supplementary Movies: Files can be viewed at: http://www.currentbiology.com/cgi/content/full/17/24/2143/DC1/.

Movie 1: **EGFP-hBub1 and mCherry-hMad2 do not respond to MG132 treatment alone.**
HeLa cells transiently transfected with EGFP-hBub1 and mCherry-hMad2 were arrested with 12.5 μM MG132 for 1.5 hours and placed on the spinning disk confocal microscope. The cells were imaged ever 1 minute for 30minutes total. Neither EGFP-hBub1 nor mCherry-hMad2 kinetochore signals are affected by MG132 alone.

Movie 2: **EGFP-hBub1, but not mCherry-hMad2 accumulates at tension less kinetochores.**
HeLa cells transiently transfected with EGFP-hBub1 and mCherry-hMad2 were arrested with 12.5 μM MG132 for 1.5 hours and placed on the spinning disk confocal microscope. Taxol was added to the media with a final concentration of 1 μM. The cells were imaged ever 1 minute for 30minutes total. EGFP-hBub1 is observed to accumulate at tension less kinetochores, while mCherry-hMad2 remains in the cytosol.

Movie 3: **Both, EGFP-hBub1 and mCherry-hMad2 accumulate at kinetochores lacking kinetochore-MT attachments.**
HeLa cells transiently transfected with EGFP-hBub1 and mCherry-hMad2 were arrested with 12.5 μM MG132 for 1.5 hours and placed on the spinning disk confocal microscope. Vinblastine was added to the media with a final concentration of 25 μM. The cells were imaged ever 1 minute for 30minutes total. Both, EGFP-hBub1 and mCherry-hMad2 rapidly accumulate at kinetochores.

Movie 4: **EGFP-hZW10 and mCherry-hMad2 do not respond to MG132 treatment alone.**
HeLa cells stably expressing EGFP-hZW10 and transiently transfected with mCherry-hMad2 were arrested with 12.5 μM MG132 for 1.5 hours and placed on the spinning disk confocal microscope. The cells were imaged ever 1 minute for 30minutes total. Neither EGFP-hZW10 nor mCherry-hMad2 kinetochore signals are affected by MG132 alone.

Movie 5: **EGFP**-hZW10 accumulates at tension less kinetochores.
HeLa cells stably expressing EGFP-hZW10 and transiently transfected with mCherry-hMad2 were arrested with 12.5 μM MG132 for 1.5 hours and placed on the spinning disk confocal microscope. Taxol was added to the media with a final concentration of 1 μM. The cells were imaged ever 1 minute for 30minutes total. Only EGFP-hZW10 is observed to accumulate at tension-less kinetochores.

Movie 6: **EGFP-hZW10 and mCherry-hMad2 accumulate at kinetochores lacking MT attachments.**
HeLa cells stably expressing EGFP-hZW10 and transiently transfected with mCherry-hMad2 were arrested with 12.5 μM MG132 for 1.5 hours and placed on the spinning disk confocal microscope. Vinblastine was added to the media with a final concentration of 25 μM. The cells were imaged ever 1 minute for 30minutes total. A maximal projection of

~25 1 μm Z-stacks is displayed. Both EGFP-hZW10 and mCherry-hMad2 are observed to accumulate kinetochores.

Movie 7: **Exit from mitosis after MG132 washout.**
HeLa cells stably expressing GFP-H2B were arrested with 12.5 μM MG132 for 1.5 hours. The MG132 was then washed out with fresh media and the cells were placed on the spinning disk confocal microscope. The cells were imaged every 3 minutes. Entry into anaphase is observed ~ 30 minutes post MG132 washout.

Movie 8: **Vinblastine arrests cells after MG132 washout.**
HeLa cells stably expressing GFP-H2B were arrested with 12.5 μM MG132 for 1.5 hours. The MG132 was then washed out into media containing 25 μM vinblastine and the cells were placed on the spinning disk confocal microscope. The cells were imaged every 3 minutes. Entry into was anaphase not observed over the time of imaging.

Movie 9: **Taxol arrests cells after MG132 washout.**
HeLa cells stably expressing GFP-H2B were arrested with 12.5 μM MG132 for 1.5 hours. The MG132 was then washed out into media containing 1 μm taxol and the cells were placed on the spinning disk confocal microscope. The cells were imaged every 3 minutes. Entry into anaphase was not observed over the time of imaging.

Movie 10: **Cells knocked down for hZW10 rapidly escape taxol arrest**.
HeLa cells stably expressing GFP-H2B and knocked down for hZW10 using siRNA (72 hour knockdown) were arrested with 12.5 μM MG132 for 1.5 hours. The MG132 was then washed out into media containing 1 μm taxol and the cells were placed on the spinning disk confocal microscope. The cells were imaged every 3 minutes. Escape from mitotic arrest was observed as decondensation of chromatin at ~93 minutes post washout from MG132.

Movie 11: **Cells knocked down for hZW10 escape vinblastine arrest.**
HeLa cells stably expressing GFP-H2B and knocked down for hZW10 using siRNA (72 hour knockdown) were arrested with 12.5 μM MG132 for 1.5 hours. The MG132 was then washed out into media containing 25 μM vinblastine and the cells were placed on the spinning disk confocal microscope. The cells were imaged every 3 minutes. Escape from mitotic arrest was observed as decondensation of chromatin at ~370 minutes post washout from MG132.

Movie 12: **Taxol arrested cells escape mitotic arrest upon treatment with ZM447439.**
HeLa cells stably expressing GFP-H2B were arrested with 12.5 μM MG132 for 1.5 hours. The MG132 was then washed out into media containing 1 μM taxol and the cells were placed on the spinning disk confocal microscope. The cells were imaged every 3 minutes. After 15minutes of imaging ZM447439 was added to a final concentration of 2 μM. The cells were observed to escape mitotic arrest by decondensing their chromatin ~ 72 minutes post MG132 washout.

Movie 13: **Vinblastine arrested cells do not escape mitotic arrest upon treatment with ZM447439.**
HeLa cells stably expressing GFP-H2B were arrested with 12.5 μM MG132 for 1.5 hours. The MG132 was then washed out into media containing 25 μM vinblastine and the cells were placed on the spinning disk confocal microscope. The cells were imaged every 3 minutes. After 15minutes of imaging ZM447439 was added to a final concentration of 2 μM. The cells were not observed to escape mitotic checkpoint arrest for the duration of imaging.
Movie 14: **Taxol arrested cells escape mitotic arrest upon treatment with ZM447439.**
HeLa cells stably expressing GFP-H2B were arrested with 12.5 μM MG132 for 1.5 hours. 1 μM taxol was added to the media and the cells were placed on the spinning disk confocal microscope. The cells were imaged every 3 minutes. The cells were not observed to escape mitotic for the duration of imaging.

Movie 15: **Accumulation of EGFP-hBub1 at tension less kinetochores is disrupted by inhibition of Aurora B kinase activity with ZM447439.**
HeLa cells transiently transfected with EGFP-hBub1 were arrested with 12.5 μM MG132 for 1.5 hours and placed on the spinning disk confocal microscope. Taxol was added to a final concentration of 1 μM and the cells were imaged every 1 minute. After 21 minutes of imaging 2 μM ZM447439 was added. EGFP-hBub1, which has accumulated, is lost from tension-less kinetochores within minutes of adding Z447439.

Movie 16: **Accumulation of EGFP-hZW10 at tension-less kinetochores is disrupted by inhibition of Aurora B kinase activity with ZM447439.**
HeLa cells stably expressing EGFP-hZW10 were arrested with 12.5 μM MG132 for 1.5 hours and placed on the spinning disk confocal microscope. Taxol was added to a final concentration of 1 μM and the cells were imaged every 1 minute. After 19 minutes of imaging 2 μM ZM447439 was added. EGFP-hZW10, which has accumulated, is lost from tension-less kinetochores within minutes of adding ZM447439.

Movie 17: **Accumulation of EGFP-hBub1 at tension less kinetochores is prevented by inhibition of Aurora B kinase activity with ZM447439.**
HeLa cells transiently transfected with EGFP-hBub1 were arrested with 12.5 μM MG132 for 1.5 hours and placed on the spinning disk confocal microscope. Taxol and ZM447439 were added simultaneously to final concentrations of 1 and 2 μM respectively. The cells were imaged every 1 minute. EGFP-hBub1 is not observed to accumulate at tension-less kinetochores.

Movie 18: **Accumulation of EGFP-hZW10 at tension-less kinetochores is prevented by inhibition of Aurora B kinase activity with ZM447439.**
HeLa cells stably expressing EGFP-hZW10 were arrested with 12.5 μM MG132 for 1.5 hours and placed on the spinning disk confocal microscope. Taxol and ZM447439 were added simultaneously to final concentrations of 1 and 2 μM respectively. The cells were imaged every 1 minute. EGFP-hZW10 is not observed to accumulate at tension-less kinetochores.

Movie 19: **EGFP-hBub1 remains at kinetochores lacking MT attachments even in the presence of ZM447439**
HeLa cells transiently transfected with EGFP-hBub1 were arrested with 12.5 μM MG132 for 1.5 hours and placed on the spinning disk confocal microscope. Vinblatine was added to a final concentration of 25 μM and the cells were imaged every 1 minute. After 14 minutes of imaging 2 μM ZM447439 was added. A portion of EGFP-hBub1, which has accumulated at kinetochores, is lost within minutes of adding Z447439, however EGFP-hBub1 does remain on kinetochores throughout the experiment.

Movie 20: **EGFP-hZW10 remains at kinetochores lacking MT attachments even in the presence of ZM447439.**
HeLa cells stably expressing EGFP-hZW10 were arrested with 12.5 μM MG132 for 1.5 hours and placed on the spinning disk confocal microscope. Vinblatine was added to a final concentration of 25 μM and the cells were imaged every 1 minute. After 12 minutes of imaging 2 μM ZM447439 was added. A portion of EGFP-hZW10, which has accumulated at kinetochores, is lost within minutes of adding Z447439, however EGFP-hBub1 does remain on kinetochores throughout the experiment.

Movie 21: **YFP-hp50 accumulates at tension-less kinetochores.**
HeLa cells stably expressing YFP-hp50 were arrested with 12.5 μM MG132 for 1.5 hours and placed on the spinning disk confocal microscope. Taxol was added to a final concentration of 1 μM and the cells were imaged every 1 minute. YFP-hp50 is observed to accumulate at tension less kinetochores.

Movie 22: **YFP-hp50 is lost from tension-less kinetochores upon inhibition of Aurora B kinase activity.**
HeLa cells stably expressing YFP-hp50 were arrested with 12.5 μM MG132 for 1.5 hours. Taxol was added to a final concentration of 1 μM for 15minutes. The cells were placed on the spinning disk confocal microscope, 2 μM ZM447439 was added and the cells were imaged every 1 minute. YFP-hp50 which is observed to accumulate at tension-less kinetochores is lost within minutes of adding 2μM ZM447439.

Movie 23: **Aurora B-EGFP kinetochore localization is not affected by the loss of kinetochore tension.**
HeLa cells stably expressing Aurora B-EGFP were arrested with 12.5 μM MG132 for 1.5 hours and placed on the spinning disk confocal microscope. Taxol was added to a final concentration of 1 μM and the cell were imaged every 1 minute. Aurora B-EGFP kinetochore localization is not affected by the taxol treatment.

Movie 24: **Aurora B-EGFP kinetochore localization is not affected by the loss of kinetochore-MT attachments.**
HeLa cells stably expressing Aurora B-EGFP were arrested with 12.5 μM MG132 for 1.5 hours and placed on the spinning disk confocal microscope. Vinblastine was added to a

final concentration of 25 μM and the cell were imaged every 1 minute. Aurora B-EGFP kinetochore localization is not largely affected by the vinblastine treatment.

Movie 25: **Aurora B-EGFP kinetochore localization is not affected by ZM447439 treatment.**
HeLa cells stably expressing Aurora B-EGFP were arrested with 12.5 μM MG132 for 1.5 hours and placed on the spinning disk confocal microscope. ZM447439 was added to a final concentration of 2 μM and the cell were imaged every 1 minute. Aurora B-EGFP kinetochore localization is not affected by the ZM447439 treatment.

Chapter V: *Nordihydroguaiaretic acid maintains mitotic checkpoint arrest**

Famulski, J.K[1]., J.B., Rattner[3] and Gordon K. Chan[1,2].

1) Department of Oncology, University of Alberta, Edmonton, Alberta, Canada.
2) Experimental Oncology, Cross Cancer Institute, Edmonton, Alberta, Canada
3) Department of Anatomy and Cell Biology, University of Calgary, Calgary, Alberta, Canada

* A version of this chapter has been submitted to Oncogene as Famulski *et al. Nordihydroguaiaretic acid maintains mitotic checkpoint arrest.*

- All of the experiments (except Supplementary figure 5.9B), figures and the manuscript were prepared by Jakub Famulski.

5.1 Abstract

The mitotic checkpoint functions to ensure accurate chromosome segregation by regulating the progression from metaphase to anaphase (Chan *et al.*, 2005; Musacchio and Salmon, 2007). Once the checkpoint has been satisfied, it is inactivated in order to allow the cell to proceed into anaphase and complete the cell cycle. The minus end-directed microtubule motor dynein/dynactin has been implicated in the silencing of the mitotic checkpoint by "stripping" checkpoint proteins off kinetochores (Howell *et al.*, 2001; Wojcik *et al.*, 2001). Here we examine the effects of the small molecule nordihydroguaiaretic acid (NDGA), on the dynein/dynactin-dependent transport of hZW10 from kinetochores to spindle poles, and on the status of the mitotic checkpoint. hZW10 is a known cargo of dynein/dynactin and was therefore used as a readout of its transport activity. We find that hZW10 is a dynamic component of the spindle pole during mitosis, however in the presence of NDGA it becomes stabillized. We also found that hROD, hSpindly, hMad1, hMad2, hBubR1, hCENP-E, hCdc27, Cyclin-B and hMps1 are transported to spindle poles in cells treated with NDGA. Surprisingly, the NDGA treatment did not silence the mitotic checkpoint but instead induced a mitotic checkpoint dependent arrest without affecting kinetochore-MT attachment or tension. We therefore propose, that in addition to dynein/dynactin mediated transport of checkpoint proteins off kinetochores, the dissociation of mitotic checkpoint proteins off spindle poles may be required for silencing of the mitotic checkpoint.

5.2 Introduction

Accurate segregation of chromosomes during mitosis is absolutely required for the maintenance of genomic stability. Failure or improper execution of mitosis is catastrophic for individual cells as well as a potential precursor to malignancy. The mis-segregation of even one chromosome can negatively impact cell survival or conversely lead to mis-regulation of cell growth. Numerous human cancers have been associated with elevated levels of aneuploidy that are thought to result from chromosome mis-segregation [reviewed in (Kops et al., 2005b)]. In order to avoid aneuploidy, mammalian cells have evolved a surveillance mechanism, the mitotic checkpoint, to monitor and ensure accurate chromosome segregation. The mitotic checkpoint ensures accurate chromosome segregation by preventing the progression from metaphase into anaphase [reviewed in (Chan *et al.*, 2005; Musacchio and Salmon, 2007)]. In general, the checkpoint arrests cells in mitosis until all chromosomes have aligned at the metaphase plate. Chromosome alignment depends on the attachment of microtubules (MTs) emanating from spindle poles to chromosomes at kinetochores [reviewed in (Cheeseman and Desai, 2008)]. The checkpoint directly monitors for kinetochore-MT attachments and initiates mitotic arrest in their absence. Molecularly, the mitotic checkpoint directly inhibits the Anaphase Promoting Complex/Cyclosome (APC/C), an E3 ubuiquitin ligase, that is responsible for targeting Cyclin B and securin for degradation through the 26S proteosome (King *et al.*, 1995; Sudakin *et al.*, 1995). This ensures that sister chromatids remain physically connected and that Cdk1 activity remains high. All known essential components of the mitotic checkpoint localize to kinetochores in response to mitotic checkpoint signaling (Musacchio and Salmon, 2007). However, certain kinetochore checkpoint proteins are also known to transiently localize to spindle poles through dynein/dynactin-mediated transport off kinetochores and along kinetochore-MTs (Howell *et al.*, 2001). Moreover, the APC/C as well as cyclin B are known to reside on spindle poles during mitosis (Clute and Pines, 1999; Kraft *et al.*, 2003). These findings raise the question whether spindle pole-associated checkpoint proteins also signal the mitotic checkpoint. Interestingly, it has been recently shown that the END network, consisting of Emi1, NuMa and Dynein/dynactin, functions in spindle pole-specific inhibition of the APC/C and thus maintenance of mitotic checkpoint arrest in very early mitosis (Ban *et al.*, 2007). Furthermore, work on cyclin B has shown that its degradation during the metaphase-anaphase transition occurs specifically at spindle poles and the mitotic spindle (Clute and Pines, 1999). Spindle poles may therefore represent secondary sites of mitotic checkpoint signaling.

It has been recently shown that treatment with the small molecule nordihydroguaiaretic acid (NDGA) results in the accumulation of human *Zeste White 10* (hZW10) at centrosomes and spindle poles (Arasaki *et al.*, 2007). This accumulation has been hypothesized to stem from NDGA enhanced interaction of dynein/dynactin and its cargo. hZW10 is a component of the evolutionarily conserved Roughdeal, ZW10, Zwilch (RZZ) complex that is known to transport along kinetochore-MTs off kinetochores and onto spindle poles via dynein/dynactin (Basto *et al.*, 2004; Chan *et al.*, 2000; Karess, 2005; Wojcik *et al.*, 2001). Furthermore, the RZZ complex is an essential component of the mitotic checkpoint whose kinetochore residency dynamics regulate its function (Famulski and Chan, 2007; Famulski *et al.*, 2008). hZW10 and hROD are known to transiently localize to spindle poles during prometaphase and metaphase (Basto *et al.*,

2000; Chan *et al.*, 2000; Williams and Goldberg, 1994), however, the amount of hZW10 associated with the spindle poles appears significantly increased in the presence of NDGA (Arasaki *et al.*, 2007). Initial studies of NDGA showed that it can enhance the interactions between dynein/dynactin and its cargoe, such as hZW10, although the molecular mechanism of its action remains unknown (Arasaki *et al.*, 2007). At present it is unknown whether hZW10 spindle pole localization plays any functional role within mitotic checkpoint signaling. We therefore sought to investigate the consequence(s) of hZW10 spindle pole accumulation in the presence of NDGA using live cells. Through live cell analysis we have determined that hZW10 becomes totally stable at spindle poles in the presence of NDGA. Furthermore, we were able to catalogue several other kinetochore checkpoint proteins as dynein/dynactin cargoes. Lastly, and surprisingly, we discovered that although NDGA treatment results in the 'stripping' of kinetochore checkpoint proteins off kinetochores, this does not lead to mitotic checkpoint silencing but actually results in mitotic checkpoint arrest. In light of our findings, we propose that mitotic checkpoint silencing requires may require not only kinetochore 'stripping' of checkpoint components, such as the RZZ complex, but also their dissociation from spindle poles.

5.3 Results and Discussion

5.3.1 hZW10 is a dynamic resident of mitotic spindle poles

ZW10 is known to localize to spindle poles during mitosis in human and *Drosophila* cells (Howell *et al.*, 2001; Scaerou *et al.*, 2001; Williams *et al.*, 1992). In order to analyze the localization pattern of hZW10 at spindle poles in live cells, we took advantage of a HeLa cell line stably expressing EGFP-hZW10 (Famulski *et al.*, 2008). Using live cell time lapse microscopy we observed that EGFP-hZW10 began to accumulate at kinetochores during prophase, immediately after nuclear envelope breakdown, but did not localize to the spindle poles until prometaphase (Fig 5.1A). Once all the chromosomes were aligned at the metaphase plate, EGFP-hZW10 vacated both the kinetochores and spindle poles. The behavior of EGFP-hZW10 in live cells was consistent with endogenous hZW10 as monitored through immunofluorescence (Fig S5.1A).

In order to determine the conditions under which hZW10 is able to localize to the spindle poles, HeLa cells were treated with several common inhibitors of mitotic spindle function. These included: vinblastine (Wendell *et al.*, 1993), to remove all kinetochore-MTs; S-trityl-L-cystine (STLC) (Skoufias *et al.*, 2006), an Eg5 kinesin inhibitor to generate monopolar spindles and therefore monopolar k-MT attachments; MG132, to inhibit the proteasome and arrest the cells in late metaphase (Rock *et al.*, 1994); and finally MG132 followed by low dose taxol, which inhibits MT dynamics and therefore abolishes tension between sister kinetochores (Famulski and Chan, 2007). hZW10 only localized to the spindle poles, as confirmed by co-staining with pericentrin, during the MG132 + taxol treatment (Fig S5.1B). In other words, spindle pole localization was restricted to cells with established bi-polar k-MT attachments yet lacking kinetochore tension (MG132 vs MG132 + taxol). Our results therefore indicate that hZW10 spindle pole localization requires k-MT attachments, but the localization is diminished once chromosome alignment and inter-kinetochore tension is achieved. The requirements for

hZW10 spindle pole localization findings are similar to the requirements for dynein/dynactin dependent transport of checkpoint proteins off kinetochores (Mallik *et al.*, 2005; Wojcik *et al.*, 2001). Lastly, we also analyzed the dynamics of EGFP-hZW10 at spindle poles using FRAP (Fig 5.1B). During both prometaphase and metaphase, we found that EGFP-hZW10 is a dynamic component of the spindle pole with 50% fluorescence recovery times ($t^{1/2}$) of 27.7 +/- 11.1 seconds (n=30) and 23.9 +/- 8.7 seconds (n=10) respectively. hZW10 is therefore a dynamic component of the spindle pole during mitosis indicating that it vacates the spindle pole soon after it arrives there.

5.2.2 NDGA induces transport, stabilization and accumulation of hZW10 at spindle poles.

Recently, it has been shown that NDGA can induce the transport of hZW10 to spindle poles and centrosomes by stabilizing the interaction between hZW10 and dynein/dynactin (Arasaki *et al.*, 2007). Although the effect of NDGA on dynein/dynactin transport has not been investigated directly, the observed effect of NDGA on the accumulation of dynein/dynactin and hZW10 at spindle poles during mitosis is clear (Arasaki *et al.*, 2007). We were therefore interested in investigating the mechanism as well as consequence(s) of hZW10 spindle pole accumulation. To do so, we first confirmed the NDGA phenotype by treating HeLa cells with 30 μM NDGA and analyzing hZW10 and pericentrin localization by immunofluorescence staining (Fig 5.2A). After 30 minutes of NDGA treatment, hZW10 was accumulated at spindle poles in all but prophase mitotic cells (Fig 5.2A). Moreover, hZW10 was not observed at kinetochores and appeared to be reduced in the cytoplasm in the presence of NDGA. Fluorescence intensity measurements indicated that in the presence of NDGA, hZW10 spindle pole occupancy increased from ~8.5% of total hZW10 normally found at prometaphase and metaphase spindle poles to ~20% (Fig S5.2A). This constitutes an approximate 2.35 fold increase of hZW10 at spindle poles and was found to be NDGA concentration-dependent (Fig S5.2A).

hZW10 is part of the evolutionarily conserved RZZ complex, which includes hZW10, hRoughdeal (hROD) and hZwilch (Karess, 2005; Scaerou *et al.*, 2001). To date, the function of the complex has been shown to be interdependent on all of its components (Basto *et al.*, 2000; Chan *et al.*, 2000; Williams *et al.*, 2003). We therefore analyzed whether hROD behaved similarly to hZW10 upon treatment with NDGA. Immunofluorescence staining of hROD at spindle poles upon NDGA treatment suggests that the entire RZZ complex accumulates at spindle poles in the presence of NDGA (Fig 5.2B and S5.2B). In addition to the RZZ components, hZW10 is also known to interact with hZwint-1 and dynamitin (hp50) (Starr *et al.*, 2000; Starr *et al.*, 1998). We therefore analyzed whether hZwint-1 and hp50 behave similarly to hZW10 in response to NDGA treatment. Our results show that hp50 but not hZwint-1 accumulates at spindle poles in the presence of NDGA (Fig 5.2B and S5.2C, D). Additionally, we also determined the localization of dynein intermediate chain (dIC) in the presence of NDGA and found that it also accumulated at spindle poles (Fig 5.2B and S5.2E). Since dynein/dynactin mediated transport is the only mechanism known to be responsible for RZZ spindle pole accumulation (Howell *et al.*, 2001), our data suggests that NDGA induces the accumulation of the RZZ complex at the spindle poles through dynein/dynactin mediated transport.

Figure 5.1

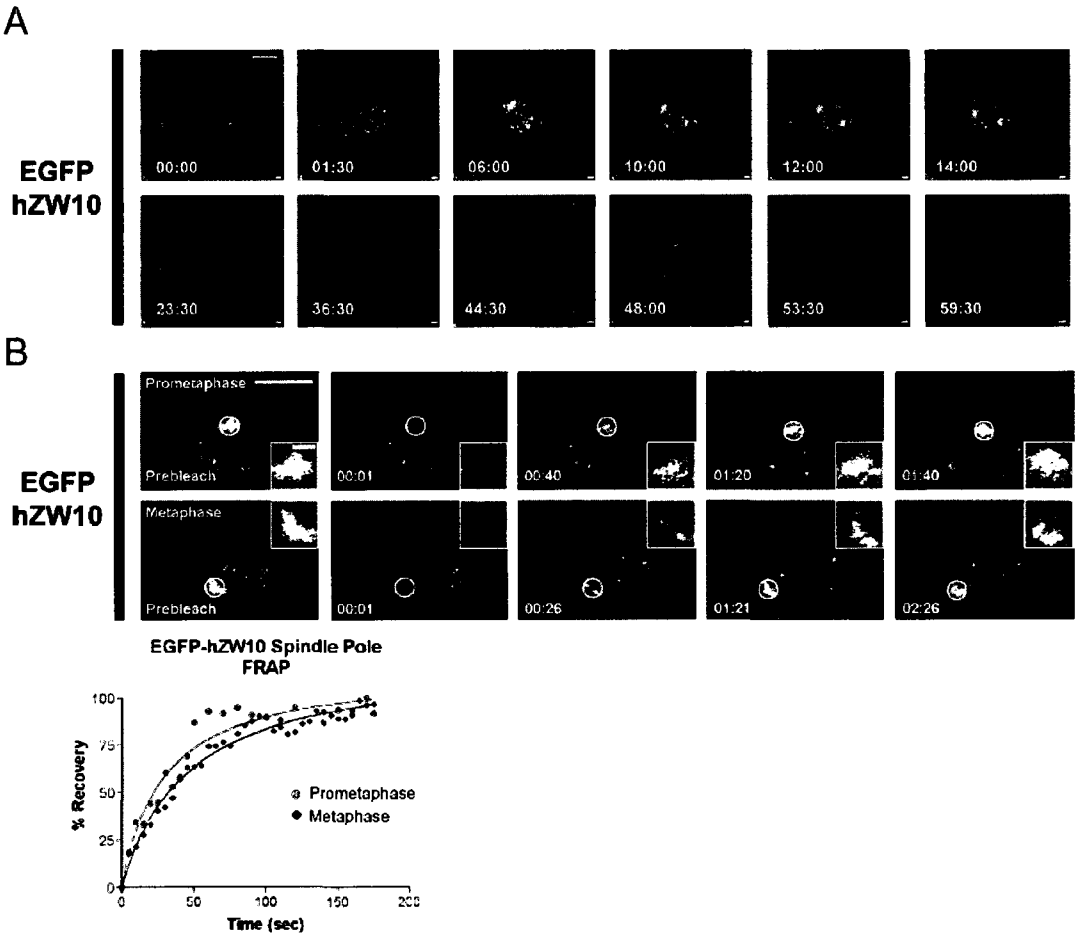

Figure 5.1: **hZW10 is a dynamic component of the spindle pole during mitosis.** **A)** HeLa cells stably expressing EGFP-hZW10 were imaged using a spinning disk confocal microscope. Maximum projections of 20 1 μm Z-stacks collected every 30 seconds are displayed. EGFP-hZW10 is observed to first localize to kinetochore upon nuclear envelope breakdown in prophase and subsequently to the spindle poles starting in prometaphase. Kinetochore and spindle pole associated EGFP-hZW10 remains until all the chromosomes become aligned in metaphase. Upon anaphase onset, EGFP-hZW10 is not detected at kinetochores or spindle poles. Time is shown in minutes:seconds, scale bar = 10 μm. **B)** HeLa cells stably expressing EGFP-hZW10 were analyzed for turnover of EGFP-hZW10 at the spindle poles using FRAP. White circles indicate the spindle pole bleached which is enlarged in the insets. Time-lapse images of the recovery after photobleaching indicate that in both prometaphase (top) and metaphase (bottom), EGFP-hZW10 is dynamic at the spindle poles. Below is a % recovery graph of EGFP-hZW10 at spindle poles showing no difference between the recovery of EGFP-hZW10 at prometaphase (red) or metaphase (blue) spindle poles. Large scale bar = 10 μm, small scale bar = 2 μm.

Having established that NDGA can induce hZW10 accumulation at the spindle poles, we used time-lapse fluorescence microscopy to monitor the accumulation in live cells. Using EGFP-hZW10 expressing HeLa cells, we monitored the dynamics of NDGA-induced EGFP-hZW10 transport to the spindle poles in both prometaphase and metaphase (Fig 5.2C). Our live cell imaging confirmed that NDGA treatment results in the accumulation of EGFP-hZW10 at the spindle poles. The observed accumulation of EGFP-hZW10 began to occur within ~10 minutes of NDGA addition in both prometaphase and metaphase cells. We used FRAP to determine whether the NDGA-dependent over-accumulation of hZW10 at spindle poles resulted from changes in the turn-over of the protein at spindle poles. FRAP analysis revealed that, while EGFP-hZW10 was highly dynamic at spindle poles in untreated cells (Fig 5.1B), NDGA treatment stabilized hZW10 at the spindle pole during both prometaphase and metaphase (Fig 5.2D). We thus conclude that the accumulation of hZW10 at spindle poles in the presence of NDGA occurs because hZW10 is unable to dissociate from the spindle pole. NDGA may be affecting the ability of the RZZ complex to dissociate from the spindle pole, perhaps by directly stabilizing its interaction with dynein/dynactin. Interestingly, our NDGA results are similar to those of ATP depletion studies where mitotic checkpoint proteins are also observed to accumulate at spindle poles (Howell *et al.*, 2001; Yan *et al.*, 2003; Yang *et al.*, 2003). NDGA might therefore alternatively affect ATP-dependent processes involved in the release of checkpoint proteins from spindle poles.

5.2.3 Kinetochore localization and kinetochore-MT attachments are required for hZW10 transport.

Having determined that NDGA can be used to study the hZW10 at spindle poles in living cells, we next set out to analyze what conditions affect hZW10 spindle pole accumulation by treating EGFP-hZW10 expressing cells with various inhibitors of spindle function and NDGA in live cells. EGFP-hZW10 readily accumulated at spindle poles in cells pre-treated with STLC, MG132, MG132 + taxol and ZM447439 (Aurora B kinase inhibitor) but not in those pre-treated with vinblastine (Fig S5.3). The STLC or MG132 pre-treated cells displayed NDGA-induced EGFP-hZW10 spindle pole accumulation with dynamics similar to those observed in normal prometaphase and metaphase. On the other hand, some EGFP-hZW10 still remained at kinetochores in MG132 + taxol pre-treated cells, even after 25 minutes of NDGA treatment (Fig S5.3 middle panel). This suggests that inter-kinetochore tension, and or kinetochore-MT dynamics influence the ability of hZW10 to be released from kinetochores.

We confirmed our live cell experiments by repeating the aforementioned treatments and analyzing the behavior of endogenous hZW10 by immunofluorescence staining (Fig S5.4A). When measuring hZW10 accumulation at the spindle poles, cells pre-treated with STLC or MG132 and then NDGA accumulated up to 19% of total hZW10 at spindle poles, which constitutes an ~2.4 fold increase when compared to normal prometaphase cells (Fig S5.4B). However, cells pre-treated with MG132 + taxol and then NDGA accumulated only ~ 15% of total hZW10 at the spindle poles. This amounts to an ~1.7 fold increase when compared to normal metaphase, and again suggests that inter-kinetochore tension may regulate hZW10 transport off kinetochores. These findings are in agreement with our previous studies showing that hZW10 kinetochore dynamics are regulated by bi-polar k-MT attachments and inter-kinetochore tension (Famulski and Chan, 2007; Famulski *et al.*, 2008).

Figure 5.2

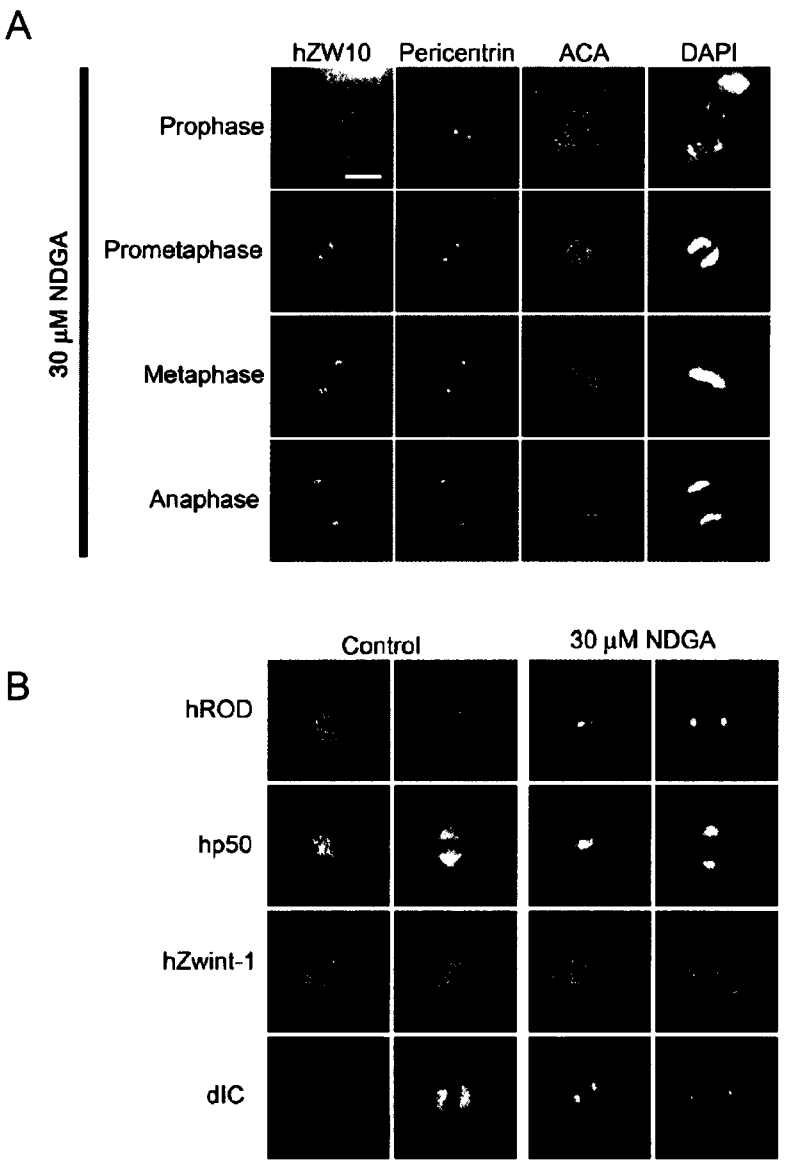

Figure 5.2: **NDGA induces rapid transport and stabilization of the RZZ complex at spindle poles.**
A) HeLa cells treated with 30 μM NDGA for 30 minutes and stained with hZW10, Pericentrin and ACA antibodies. hZW10 co-localizes with pericentrin during prometaphase, metaphase and anaphase. Chromosomes are stained with DAPI. Scale bar = 10 μm. **B)** HeLa cells treated with 30 μM NDGA for 30 minutes and stained with hROD, hp50, hZwint-1 or dIC antibodies. hROD, dIC and hp50 are observed to accumulate at spindle poles. Scale bar = 10 μm.

Figure 5.2

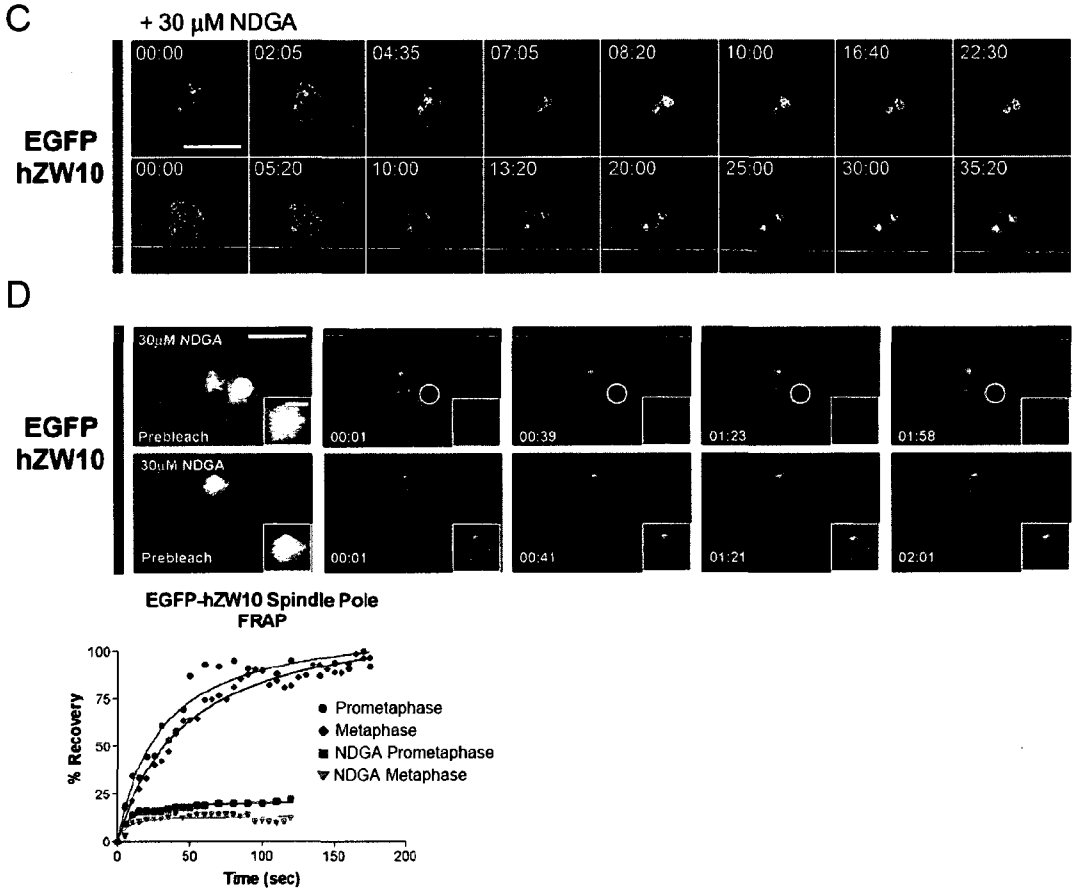

Figure 5.2: **NDGA induces rapid transport and stabilization of the RZZ complex at spindle poles.**

C) HeLa cells stably expressing EGFP-hZW10 were treated with 30 μM NDGA and immediately imaged using the spinning disk confocal microscope. Maximum projections of ~ 20 1 μm Z-stacks are shown. EGFP-hZW10 is transported to the spindle pole within minutes of adding NDGA. Time shown as minutes:seconds, scale bar = 10 μm **D)** HeLa cells stably expressing EGFP-hZW10 were treated with 30 μM NDGA for 30 minutes and analyzed for turnover of EGFP-hZW10 at the spindle poles using FRAP. White circles indicate the spindle pole bleached which is enlarged in the insets. Time-lapse images of the recovery after photobleaching indicate that in the presence of NDGA EGFP-hZW10 is not dynamic at either prometaphase (top) or metaphase (bottom) spindle poles. The percent recovery graph is shown below. Large scale bar = 10 μm, small scale bar = 2 μm.

Based on our live cell and immunofluorescence results, we therefore conclude that hZW10 spindle pole localization requires k-MT attachments and may also be regulated by inter-kinetochore tension.

We confirmed our live cell experiments by repeating the aforementioned treatments and analyzing the behavior of endogenous hZW10 by immunofluorescence staining (Fig S5.4A). When measuring hZW10 accumulation at the spindle poles, cells pre-treated with STLC or MG132 and then NDGA accumulated up to 19% of total hZW10 at spindle poles, which constitutes an ~2.4 fold increase when compared to normal prometaphase cells (Fig S5.4B). However, cells pre-treated with MG132 + taxol and then NDGA accumulated only ~ 15% of total hZW10 at the spindle poles. This amounts to an ~1.7 fold increase when compared to normal metaphase, and again suggests that inter-kinetochore tension may regulate hZW10 transport off kinetochores. These findings are in agreement with our previous studies showing that hZW10 kinetochore dynamics are regulated by bi-polar k-MT attachments and inter-kinetochore tension (Famulski and Chan, 2007; Famulski *et al.*, 2008). Based on our live cell and immunofluorescence results, we therefore conclude that hZW10 spindle pole localization requires k-MT attachments and may also be regulated by inter-kinetochore tension.

In our previous studies we generated and characterized a collection of hZW10 insertion mutants that no longer localize to kinetochores (Famulski *et al.*, 2008). To test whether kinetochore localization is necessary for spindle pole localization we subjected cells transfected with one of our kinetochore non-localization mutants (mutant W: insertion of CGRIG at amino acid 666) to NDGA treatment. Fluorescence microscopy revealed that in the presence of NDGA, EGFP-hZW10^{W} did not accumulate at the spindle poles, while endogenous hROD did (Fig S5.4C). In the presence of NDGA, hZW10 spindle pole localization must therefore require kinetochore localization prior to transport.

5.2.4 Dynein/dynactin transports a select group of mitotic checkpoint proteins from kinetochores to spindle poles.

There are several mitotic checkpoint proteins, that similar to hZW10 and hROD, are thought to be transported from kinetochores and to spindle poles via dynein/dynactin (Howell et al., 2001; Yang et al., 2007b). Reasoning that bona fide dynein/dynactin cargoes would be expected to accumulate at spindle poles upon exposure to NDGA we screened an array of mitotic checkpoint proteins for their response to NDGA. We first examined hBubR1, hBub1, hCENP-E and hMad2, of which, hBubR1, CENP-E and hMad2 have previously been implicated in dynein/dynactin dependent transport (Howell *et al.*, 2001). Upon treatment with NDGA, we observed that hBubR1, hCENP-E and hMad2 accumulated at the spindle poles, while hBub1 did not (Fig 5.3A and S5.6). After 30 minutes of NDGA treatment, hMad2 accumulation at spindle poles mirrored that of hZW10 while hBubR1 accumulated to a much lesser extent. In fact, we believe that in the presence of NDGA hBubR1 spindle pole accumulation is transient (data not shown). The immunofluorescence results were confirmed by time-lapse fluorescence microscopy of HeLa cells transiently transfected with the corresponding YFP and GFP fusion constructs (Fig S5.5). Interestingly, in contrast to endogenous hBubR1, EGFP-hBubR1 was observed to accumulate at spindle poles stably. This likely results from over expression of the construct. When we extended our NDGA assay to test for the transport of other

mitotic checkpoint proteins off kinetochores, we found that hMad1, hMps1, hSpindly, hCdc27 and Cyclin-B were also transported by dynein/dynactin to the spindle poles (Fig S5.7). We also found kinetochore proteins that were insensitive to NDGA induced transport. These included: ACA (anti-centromere antigen: CENP-A, B and C), hCENP-F, hAurora-B, hCdc20, hMCAK, hPlk1 and hHec1 (Fig S5.8). To show that the NDGA induced transport of checkpoint proteins was indeed dynein/dynactin dependent, we depleted cells of hZW10 and thus disrupted the recruitment of dynein/dynactin to the kinetochores (Starr *et al.*, 1998). In NDGA treated cells lacking hZW10, hROD, hMad2, hBubR1 or hCENP-E were not found at spindle poles (Fig 5.3B). Our use of NDGA to characterize dynein/dynactin mitotic cargo is an extension of previous work from Ted Salmon's lab which identified several dynein/dynactin cargoes through the use of ATP depletion (Howell *et al.*, 2001). Our study confirmed that hBubR1, hMad2, and hCENP-E are dynein/dynactin cargo and identified hSpindly, hCdc27, hCyclin-B, the RZZ complex and the hMps1 kinase as additional cargoes. Moreover, we were also able to categorize several kinetochore components which are not dynein/dynactin cargo including hHec1, hBub1, MCAK, hAurora B, hZwint-1, hPlk1, hCENP-F and hCdc20.

5.2.5 The mitotic checkpoint remains active in presence of NDGA despite the absence of checkpoint proteins at kinetochores.

Having observed the effects of NDGA on hZW10 and other mitotic checkpoint protein transport, we next analyzed its effect on mitotic progression as well as checkpoint signaling. We first examined whether NDGA had any effect on k-MT attachments as well as tension. When examining cold stable k-MT attachments we observed no obvious changes in cells treated with NDGA (Fig S5.9A). NDGA treatment also had no effect on k-MT attachments as observed by electron microscopy (Fig S5.9B). Additionally, we found that tension, as measured by inter-kinetochore distance in MG132 treated cells, did not differ significantly upon 30 minute NDGA treatment (MG132: 1.80 +/- 0.21 μm, n = 76 vs MG132 + NDGA: 1.83 +/- 0.34 μm, n = 76).

To assay mitotic checkpoint function, we treated HeLa cells expressing GFP-H2B with NDGA and monitored mitotic progression. Surprisingly, we found that cells treated with NDGA remained arrested in mitosis for extended periods of time (up to 6 hours) (Fig 5.3C), even though key checkpoint proteins, such as hMad2 (Fig 5.3A), were stripped off of kinetochores. Moreover, mitotic cells arrested with NDGA retained high levels of cyclin-B also suggesting that the mitotic checkpoint remained active (Fig S5.10A). Lastly, we observed that hZW10, and Mad2 remained associated with spindle poles throughout the NDGA treatment (Fig S5.10B-C). The NDGA-induced mitotic arrest was also found to be concentration dependent and correlated with the previously observed concentration-dependent induction of hZW10 spindle pole accumulation (Fig S5.2A & S5.10D). In addition, wash out of NDGA after a 30 minute treatment resulted in the dissociation of spindle pole accumulated EGFP-hZW10 within ~ 23 minutes, and 43% of cells exited from mitosis within ~ 45 minutes (Fig S5.10E). In light of all these findings, we hypothesized that NDGA-treated cells may not be able to silence the mitotic checkpoint because checkpoint proteins cannot dissociate off the spindle poles.

To test our hypothesis, we inactivated the mitotic checkpoint by depleting HeLa cells of hBubR1, or hZW10 (Fig S5.11A) by siRNA. GFP-H2B expressing cells depleted of hZW10 or hBubR1 were monitored for their response to NDGA treatment using live

cell time-lapse microscopy. We found that ~50% of cells depleted of hBubR1 or hZW10 escaped NDGA arrest by decondensing their chromatin and exiting mitosis within ~180 minutes (Fig 5.3D and S5.11B). This suggests that although many of the checkpoint proteins are stripped off of kinetochores after NDGA treatment, their release from spindle poles may be also required for proper silencing of the mitotic checkpoint.

To ensure that the observed NDGA induced mitotic checkpoint arrest was not a result of remaining kinetochore associated checkpoint proteins, we compared total kinetochore associated checkpoint proteins in the absence of checkpoint signaling (MG132), to that of NDGA or nocodazole treatment. We found that the levels of hZW10, hBubR1, hBub1 and hMad2 at kinetochores in the presence of NDGA were similar to that in cells treated with MG132 but significantly lower than when the cells were treated with nocodazole (Fig S5.11C). This suggests that NDGA does not result in kinetochore accumulation of mitotic checkpoint proteins to levels found in cells expected to signal the mitotic checkpoint. Furthermore, we observed that mCherry-hMad2 transport did not occur in metaphase cells arrested with MG132 (Fig S5.11D). MG132 arrested metaphase cells normally do not have hMad2 on their kinetochores or spindle poles because the checkpoint has been satisfied. Our results suggest that NDGA does not induce the re-recruitment of checkpoint proteins onto kinetochores or the subsequent transport to the spindle poles.

5.3 Conclusion.

Previous work with the small molecule NDGA showed a significant accumulation of hZW10 at spindle poles. As an extension of that study, we show that the accumulation of hZW10 and perhaps other mitotic checkpoint proteins at spindle poles results in a mitotic checkpoint dependent arrest. Dynein/dynactin-mediated transport off kinetochores has been hypothesized to function as a mitotic checkpoint silencing mechanism. However, we found that while NDGA can induce the "stripping" of kinetochore proteins, this does not lead to silencing of the mitotic checkpoint. In fact, NDGA treatment actually resulted in mitotic checkpoint activation and prolonged mitotic arrest. Our work therefore suggests that mitotic checkpoint silencing may require not only "kinetochore stripping" but also dissociation of checkpoint proteins off spindle poles (Fig 5.4).

Recently it has been shown that the END (Emi1/NuMa/dynein-dynactin) network is responsible for inhibiting spindle pole associated APC/C and therefore stabilizing Cyclin-B in order to maintain mitotic checkpoint activity (Ban *et al.*, 2007). In fact, Cyclin-B degradation during anaphase onset initially occurs on the mitotic spindle (Clute and Pines, 1999), and furthermore, cell fusion experiments have shown that mitotic checkpoint signaling may be restricted to the spindle apparatus (Rieder *et al.*, 1997). We therefore propose that the transient localization of checkpoint proteins at spindle poles may function in mitotic checkpoint signaling by inhibiting spindle pole associated APC/C, therefore stabilizing spindle associated Cyclin-B and thus maintaining mitotic arrest. The dissociation of checkpoint proteins off spindle poles could represent a necessary and final step in silencing of the mitotic checkpoint (Fig 5.4).

Figure 5.3

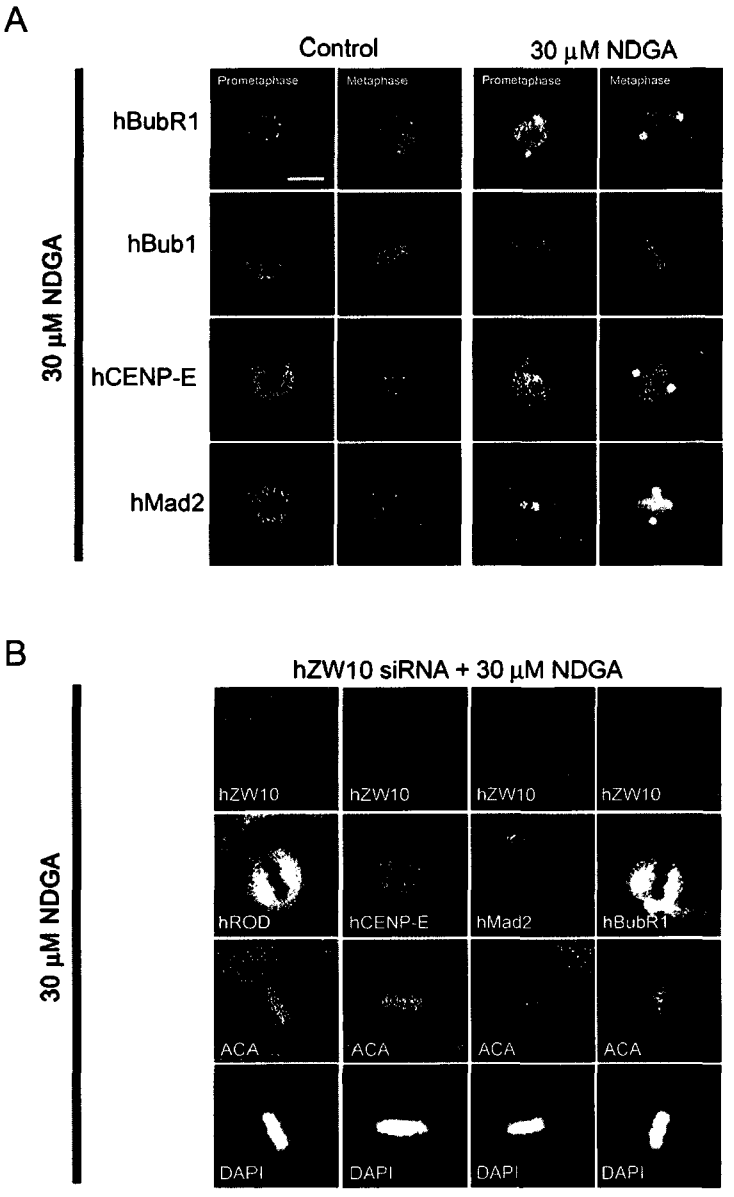

Figure 5.3: **NDGA induces the transport of mitotic checkpoint proteins off kinetochores and activates the mitotic checkpoint.**
A) HeLa cells treated with 30 μM NDGA for 30 minutes and stained with hBubR1, hBub1, hCENP-E or hMad2 antibodies. hBubR1, hCENP-E and hMad2 are observed to accumulate at spindle poles. Scale bar = 10 μm. **B)** HeLa cells transfected with hZW10 siRNA for 72 hours and subsequently treated with 30 μM NDGA for 30 minutes were stained with hZW10, ACA and either, hROD, CENP-E, hBubR1 or hMad2 antibodies. Depletion of hZW10 prevented NDGA induced transport and accumulation of hROD, hCENP-E, hMad2 or hBubR1 onto spindle poles. Scale bar = 10 μm.

Figure 5.3

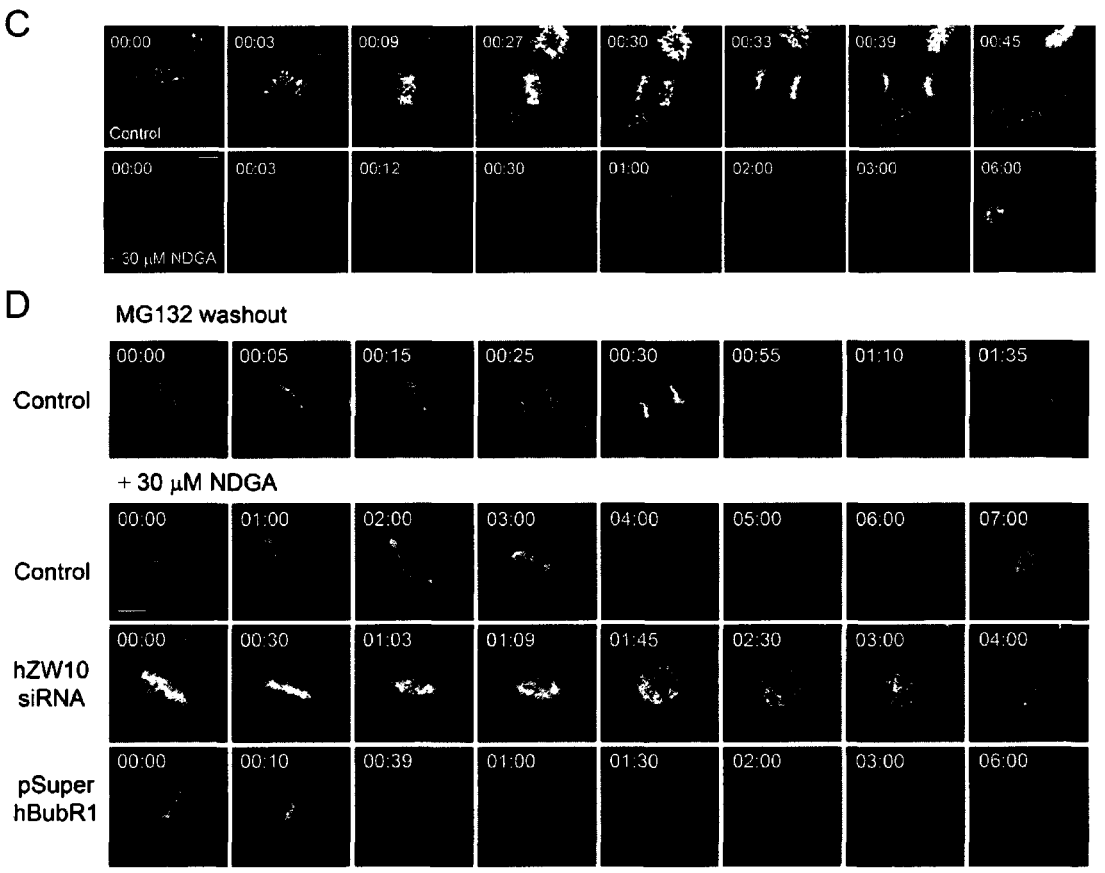

Figure 5.3: **NDGA induces the transport of mitotic checkpoint proteins off kinetochores and activates the mitotic checkpoint.**
C) HeLa cells stably expressing RFP-H1 were analyzed by time lapse microscopy using spinning disk confocal microscopy. Maximum projections of approximately 15 1 μm z-stacks are shown with the time indicated as hours:minutes. The cells do not exit mitosis and remain arrested in a prometaphase like state. Scale bar = 10 μm. **D)** HeLa cells stably expressing GFP-H2B were analyzed by time-lapse microscopy using spinning disk confocal microscopy. The cells were arrested with MG132 for 1 hour, washed with fresh media and imaged every 3 minutes post addition of NDGA. Maximum projections of ~ 20 1 μm Z-stacks are shown. 30 μM NDGA induced a mitotic arrest for up to 6 hours (top) while depletion of hZW10 (middle) using siRNA or hBubR1 (bottom) using shRNA allowed cells to escape NDGA induced mitotic checkpoint arrest as observed by decondensation of chromatin. Time is indicated in hours:minutes. Scale bar = 10 μm

The residual presence of checkpoint components at spindle poles may provide the cell a short delay before the checkpoint is completely silenced. In fact, it is well known that there is a short delay before sister chromatids of aligned chromosomes in metaphase are actually separated in early anaphase (Rieder *et al.*, 1994). Interestingly, chromosomes oscillate at the metaphase plate during this delay (Rieder and Salmon, 1994; Skibbens *et al.*, 1993). These oscillations during the delay may represent the 'testing' of k-MT attachments and the continued checkpoint silencing resulting from spindle pole associated checkpoint components. This delay ensures that if a k-MT attachment should fail, the checkpoint still remains active and thus prevents inaccurate segregation. Alternatively, it has been shown that merotelic k-MT attachments are often solved once the chromosome is already aligned and therefore stripped of its kinetochore checkpoint components (Cimini *et al.*, 2004; Cimini *et al.*, 2003). Again, the spindle pole associated checkpoint proteins may function in maintaining checkpoint arrest until all of the k-MT attachments are corrected and fully functional.

Our study involved the use of the small molecule NDGA to accumulate hZW10 and other checkpoint proteins at spindle poles. This molecule has been previously shown to induce the interaction between dynein and its cargo thus leading to increased dynein/dynactin mediated transport (Arasaki *et al.*, 2007). However, the molecular mechanism of NDGA induced dynein/dynactin transport still remains unknown. In addition to our observed effects, NDGA has also previously been described as a lipoxygenase inhibitor, a potential HER2 and IGF-1 inhibitor as well as a possible MT stabilizing agent. Although NDGA appears to have pleiotropic effects during interphase, our studies show a very direct phenotype during mitosis. As such, the use of NDGA in the narrow window of time that is mitosis is a very powerful method to study dynein/dynactin transport as well as spindle pole accumulation of checkpoint proteins. It will be exciting to determine the molecular function of NDGA in regard to the induction of dynein/dynactin transport and or dynein/dynactin interaction with its cargo.

Figure 5.4

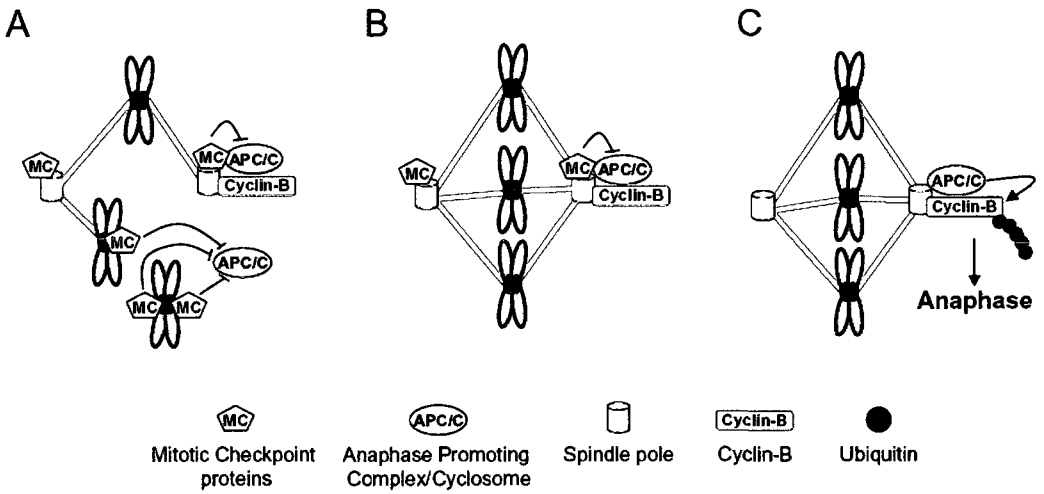

Figure 5.4: **Model of spindle pole generated mitotic checkpoint signaling.**
A) During prometaphase the APC/C (red oval) as well as cyclin-B (yellow oval) localize to the spindle pole. Once kinetochore-MT attachments are achieved, mitotic checkpoint proteins (MC) begin to shuttle onto the spindle pole where they enhance APC/C inhibition. At the same time, mitotic checkpoint proteins at unattached and unaligned chromosomes function to globally inhibit APC/C activity and therefore maintain mitotic checkpoint arrest. **B)** Once chromosomes establish bi-polar kinetochore-MT attachments mitotic checkpoint proteins are depleted off kinetochores and shuttle onto spindle poles where they continue to inhibit APC/C activity ensuring that chromosome alignment is complete and stable. The mitotic checkpoint is therefore still active. **C)** Once all chromosomes are properly aligned at the metaphase plate no more mitotic checkpoint proteins are shuttled off kinetochores and onto the spindle poles. Without the continued presence of spindle pole mitotic checkpoint proteins, the APC/C is now free to ubiquinate (black circle) cyclin-B and thus lead to the onset of anaphase.

5.4 Supplementary Material: *NDGA induced spindle pole accumulation of mitotic checkpoint proteins prevents mitotic checkpoint silencing.*

Supplementary figure 5.1: **hZW10 transiently localizes to spindle poles during mitosis in a kinetochore-MT dependent manner.**
A) HeLa cells exhibiting the different stages of mitosis are stained for hZW10, pericentrin (as a spindle pole marker), and ACA. hZW10 is observed to localize to kinetochores and spindle poles in early prometaphase and early metaphase. hZW10 no longer localizes to the spindle poles during late metaphase and in anaphase. Pericentrin is observed to stain the spindle poles within all of the stages of mitosis. Chromosomes are stained with DAPI. Scale bar = 10 μm. **B)** HeLa cells treated with vinblastine, STLC, MG132 and or MG132+Taxol were stained for hZW10 and pericentrin localization. hZW10 is observed to localize to spindle poles in cells treated with STLC and MG132 + taxol. hZW10 was, however, absent from spindle poles of cells treated with vinblastine or MG132 alone. Pericentrin was observed to stain the spindle poles in all of the treated cells. Chromosomes are stained with DAPI. Scale bar = 10 μm.

Supplementary Figure 5.1

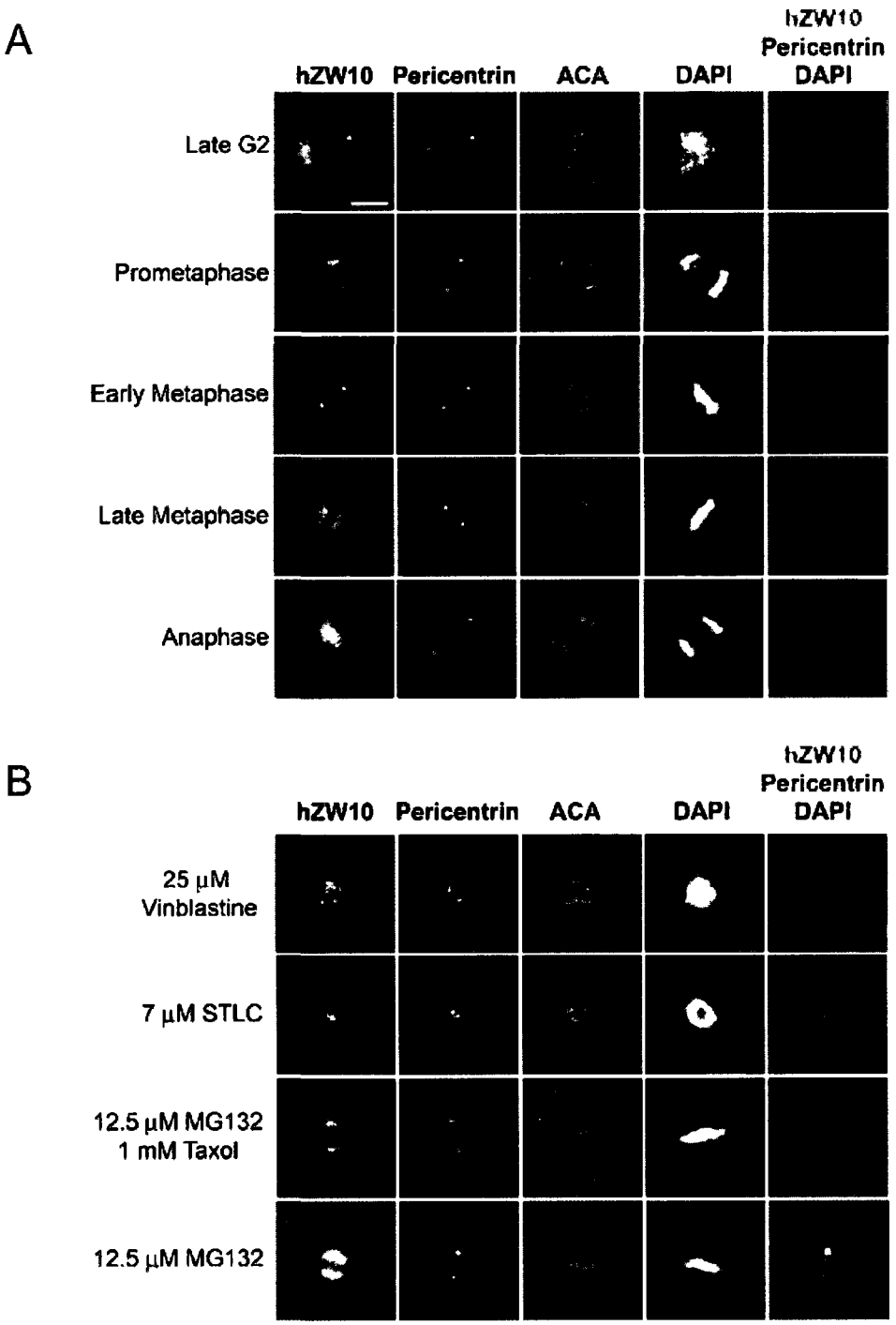

Supplementary figure 5.2: **NDGA induces the accumulation of hROD, hZW10 and hp50 at spindle poles.**
A) Measurement of endogenous hZW10 intensity at spindle poles during mitosis and upon 30 minute treatment with various NDGA concentrations. (Error bars = +/- one SD). **B-E)** HeLa cells treated with 30 μM NDGA for 30 minutes and stained with hZW10, ACA and either: hROD (B), hZwint-1 (C) , hp50 (D) or dIC (E) antibodies. hZW10, hROD, dIC and hp50 are observed to accumulate at spindle poles. Chromosomes are stained with DAPI. Prometaphase cells are shown on the left hand side, while metaphase cells are shown on the right hand side of each set of experiments. Scale bar = 10 μm.

Supplementary Figure 5.2

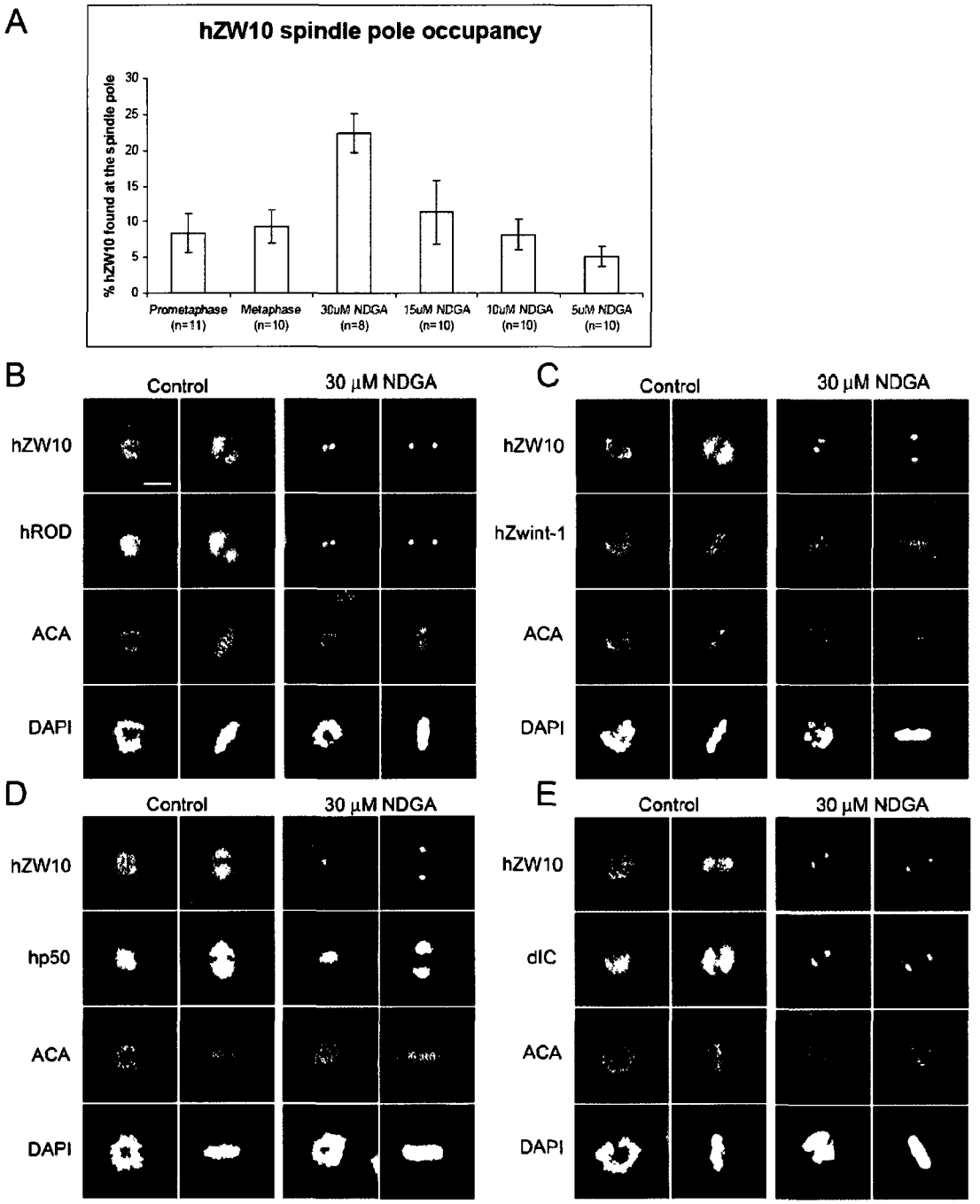

Supplementary Figure 5.3

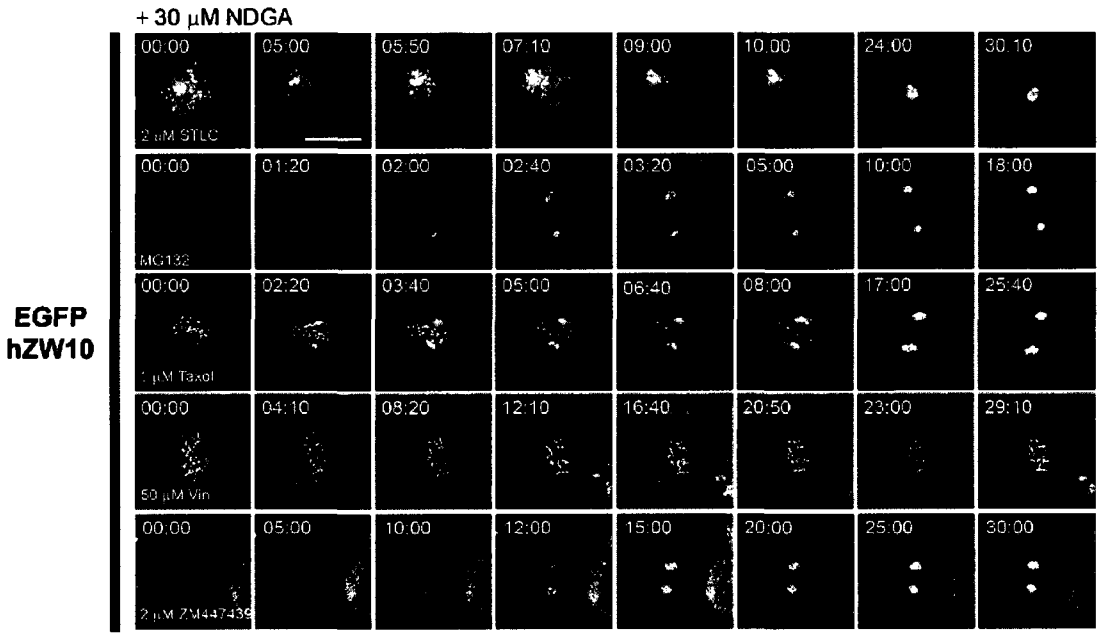

Supplementary figure 5.3: **NDGA induced transport requires kinetochore-MT attachments.**
HeLa cells stably expressing EGFP-hZW10 were pre-treated with either: 2 μM STLC, 12.5 μM MG132, 12.5 μM MG132 and 1 μM taxol, 50 μM vinblastine or 2 μM ZM447439. 30 μM NDGA was added and the cells were immediately imaged using the spinning disk confocal microscope. Z-stacks of 1 μm thickness were collected every minute after NDGA treatment. Maximum projections of ~ 20 Z-stacks are shown. The addition of NDGA induced EGFP-hZW10 transport to the spindle pole in all of the cells except those treated with vinblastine. Scale bar = 10 μm.

Supplementary figure 5.4: **NDGA induced accumulation of hZW10 requires kinetochore-MT attachments.**
A) HeLa cells pre-treated with either vinblastine, MG132, MG132 + taxol, STLC or ZM447439 were treated with 30 μM NDGA for 30 minutes and stained with hZW10 and Pericentrin antibodies. hZW10 is observed to accumulate at spindle poles in all but the vinblastine treated cells. Chromosomes are stained with DAPI. Scale bar = 10 μm. **B)** Measurement of endogenous hZW10 intensity at spindle poles during mitosis and upon treatment with NDGA. (Error bars = +/- one SD). **C)** HeLa cells transiently transfected with EGFP-hZW10-W, treated with 30 μM NDGA and stained with anti-hROD antibodies. No EGFP-hZW10-W accumulates at the spindle pole. Chromosomes are stained with DAPI. Scale bar = 10 μm.

Supplementary Figure 5.4

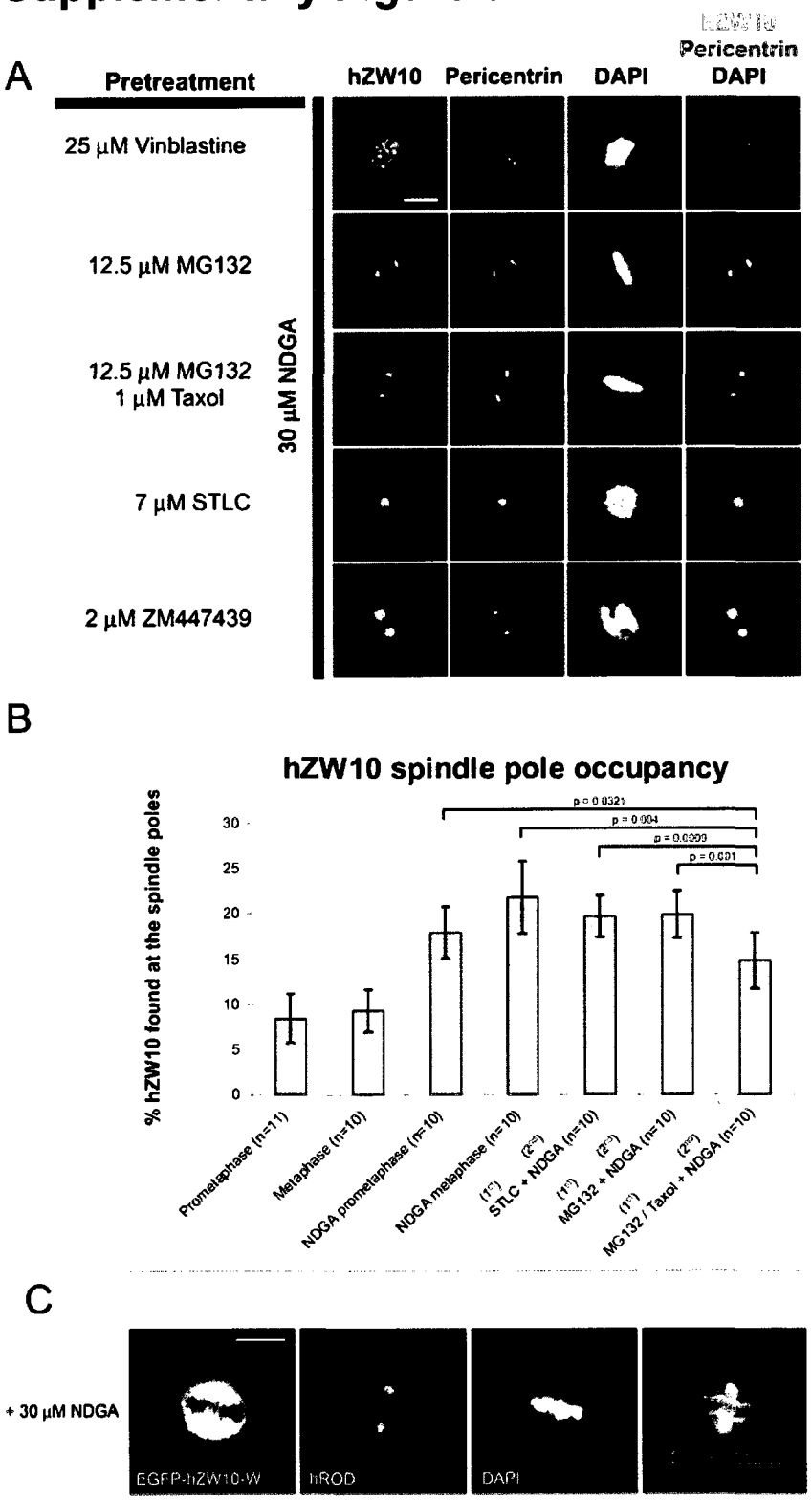

Supplementary Figure 5.5

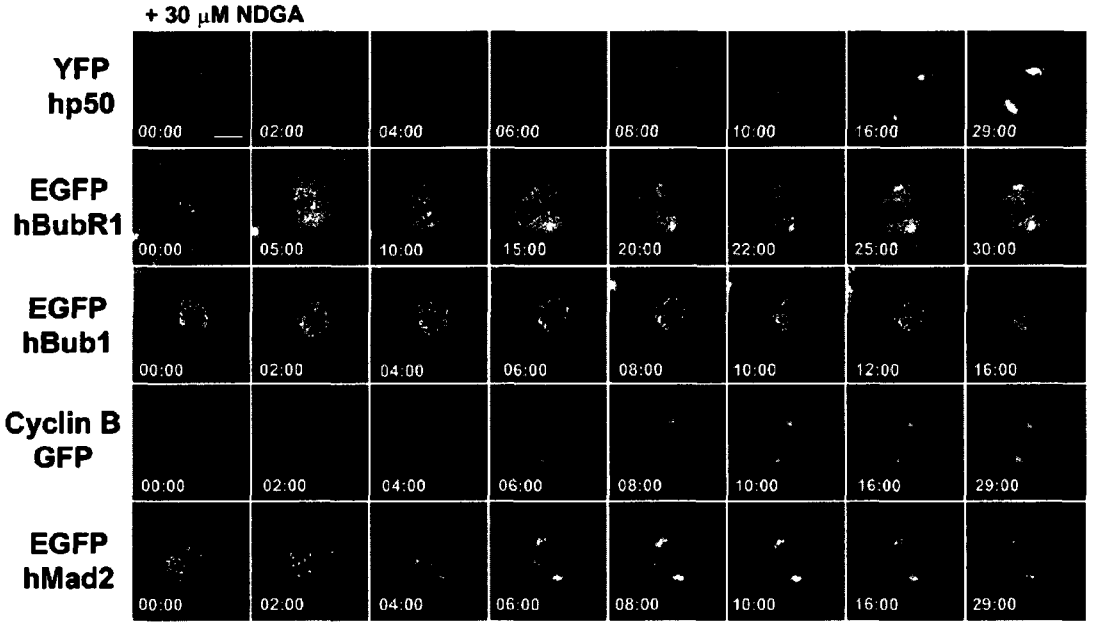

Supplementary figure 5.5: **Live cell analysis of hp50, hBubR1, hBub1, Cyclin B and hMad2 response to NDGA treatment.**
HeLa cells transiently transfected with either: YFP-hp50, EGFP-hBubR1, EGFP-hBub1, GFP-Cyclin-B or EGFP-hMad2 were imaged using a spinning disk confocal microscope. Upon addition of NDGA, the cells were imaged every 1 minute as a Z-stack of ~20 images 1 μm apart. Maximum projections are shown. YFP-hp50, EGFP-hBubR1, Cyclin-B-GFP and EGFP-hMad2 are observed to accumulate at spindle poles upon NDGA treatment. Time is indicated as minutes:seconds. Scale bar = 10 μm.

Supplementary Figure 5.6

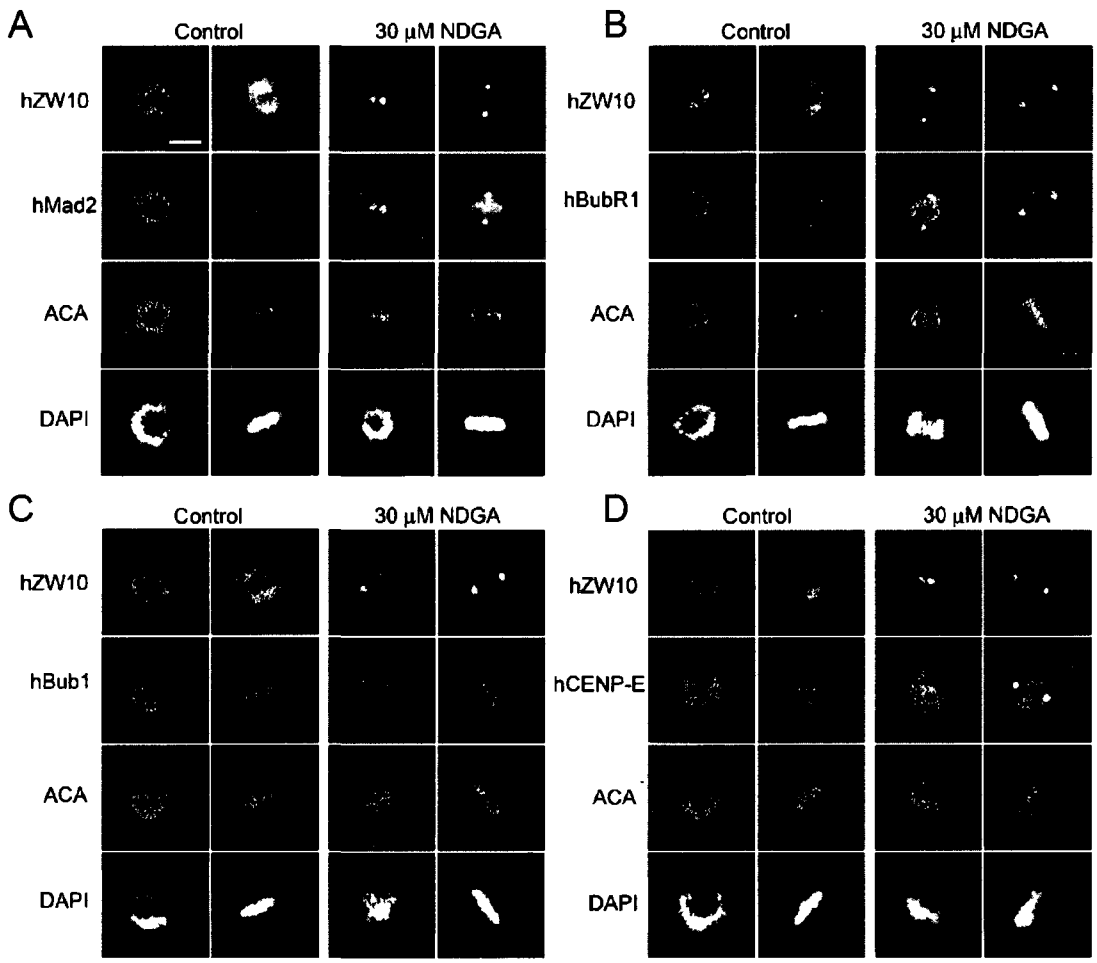

Supplementary figure 5.6: **hMad2, hBubR1 and hCENP-E but not hBub1 are transported to spindle poles in the presence of NDGA.**
A-D) HeLa cells treated with 30 μM NDGA for 30 minutes and stained with hZW10, ACA and either: hMad2 (A), hBubR1 (B) , hBub1 (C) or hCENP-E (D) antibodies. hZW10, hBubR1 and hMad2 are observed to accumulate at spindle poles. Chromosomes are stained with DAPI. Prometaphase cells are shown on the left hand side, while metaphase cells are shown on the right hand side. Scale bar = 10 μm.

Supplementary figure 5.7: **hMps1, hSpindly and hMad1 are transported to spindle poles in the presence of NDGA.**

A-E) HeLa cells treated with 30 μM NDGA for 30 minutes and stained with hZW10, ACA and either: hMps1 (A), hSpindly (B) , hMad1 (C), hCdc27 (D) or hCyclin-B antibodies. hZW10, hMps1, hMad1, hCdc27, hCyclin-B and hSpindly are observed to accumulate at spindle poles. Chromosomes are stained with DAPI. Prometaphase cells are shown on the left hand side, while metaphase cells are shown on the right hand side. Scale bar = 10 μm.

Supplementary Figure 5.7

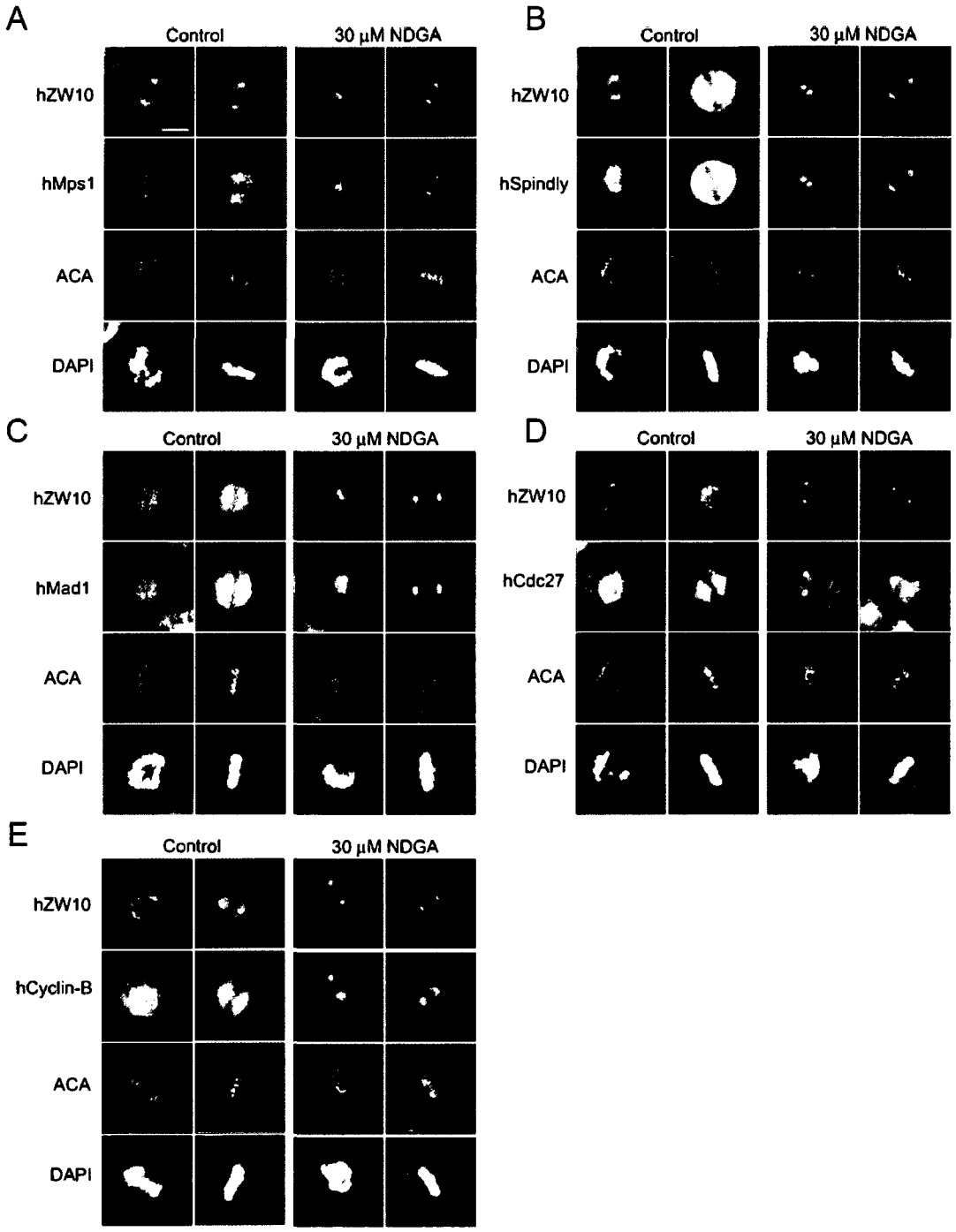

Supplementary figure 5.8: **hAurora B, MCAK, hPlk1, hHec1, hCENP-F and hCdc20 are not transported to spindle poles in the presence of NDGA.**
A-F) HeLa cells treated with 30 μM NDGA for 30 minutes and stained with hZW10, ACA and either: hAurora B (A), MCAK (B) , hPlk1 (C), hHec1 (D), hCENP-F (E) or hCdc20 (F) antibodies. Only hZW10 is observed to accumulate at spindle poles. Chromosomes are stained with DAPI. Prometaphase cells are shown on the left hand side, while metaphase cells are shown on the right hand side. Scale bar = 10 μm.

Supplementary Figure 5.8

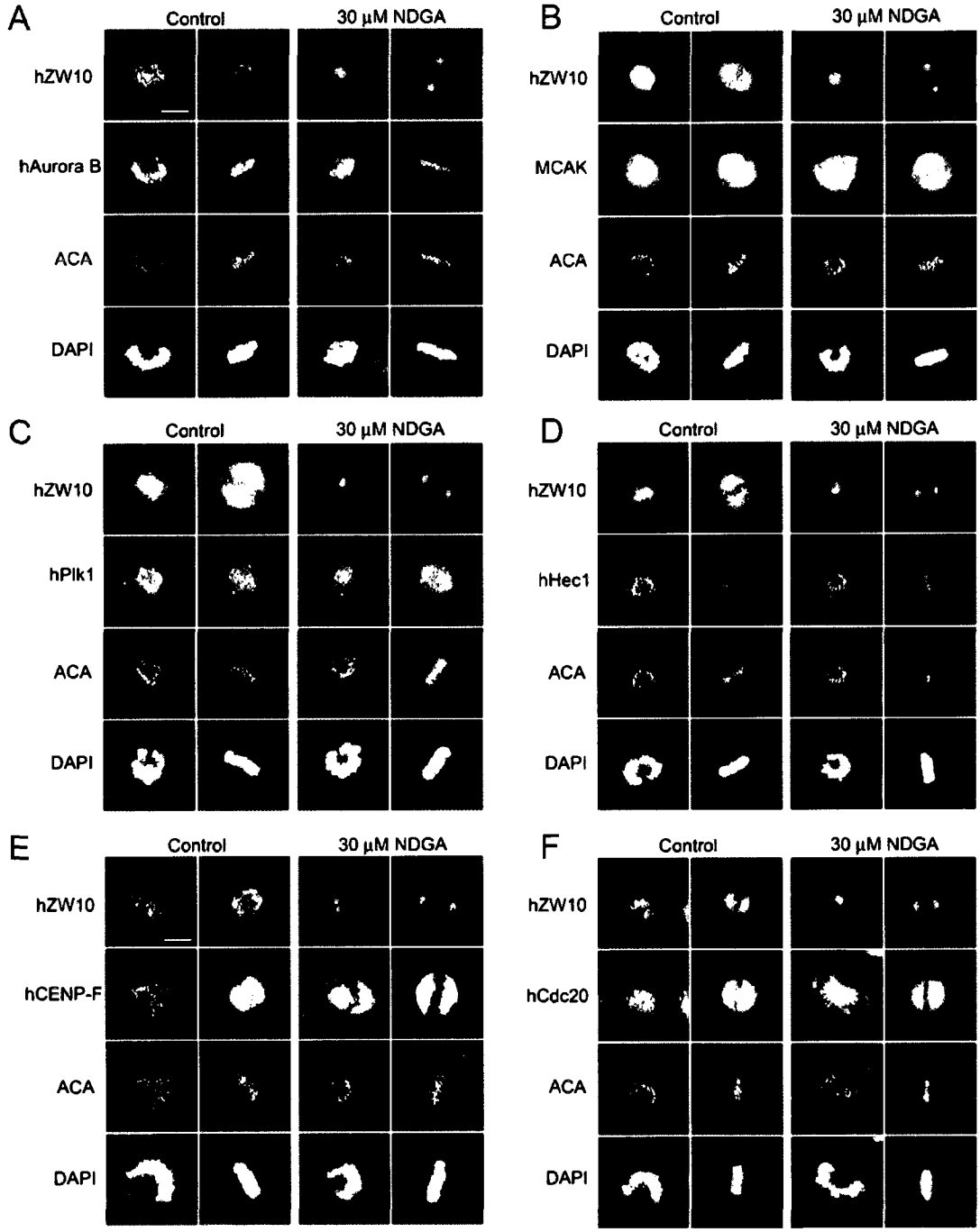

Supplementary figure 5.9: **NDGA treatment does not disrupt kinetochore-MT attachments.**

A) HeLa cells arrested with 12.5 μM MG132 and subsequently treated with NDGA were exposed to ice cold media for 10 minutes and harvested, immunofluorescence and imaged in 3D using confocal microscopy. Tubulin and ACA staining shows that NDGA does not affect k-MT attachments. Insets show enlargements of k-MT attachments. Tubulin is shown in green, ACA in red. Scale bar = 10 μm. ~50 kinetochores per cell, as observed by ACA staining, were analyzed for MT attachments and scored as ratio of attached / total. MG132 n = 3 cells, 164 kinetochores and NDGA n = 10 cells, 490 kinetochores. Error bars = +/- one SD. **B)** HeLa cells treated with NDGA for 0.5 hours (top), 3 hours (middle) or 6 hours (bottom) were fixed and analyzed for kinetochore-MT attachments using electron microscopy. Shown are three different magnifications of chromosomes and their corresponding kinetochore-MTs. In all three NDGA treatments normal kinetochore plates as well as kinetochore-MTs are observed. Yellow arrows indicate kinetochores while the arrow heads indicate kinetochore-MTs.

Supplementary Figure 5.9

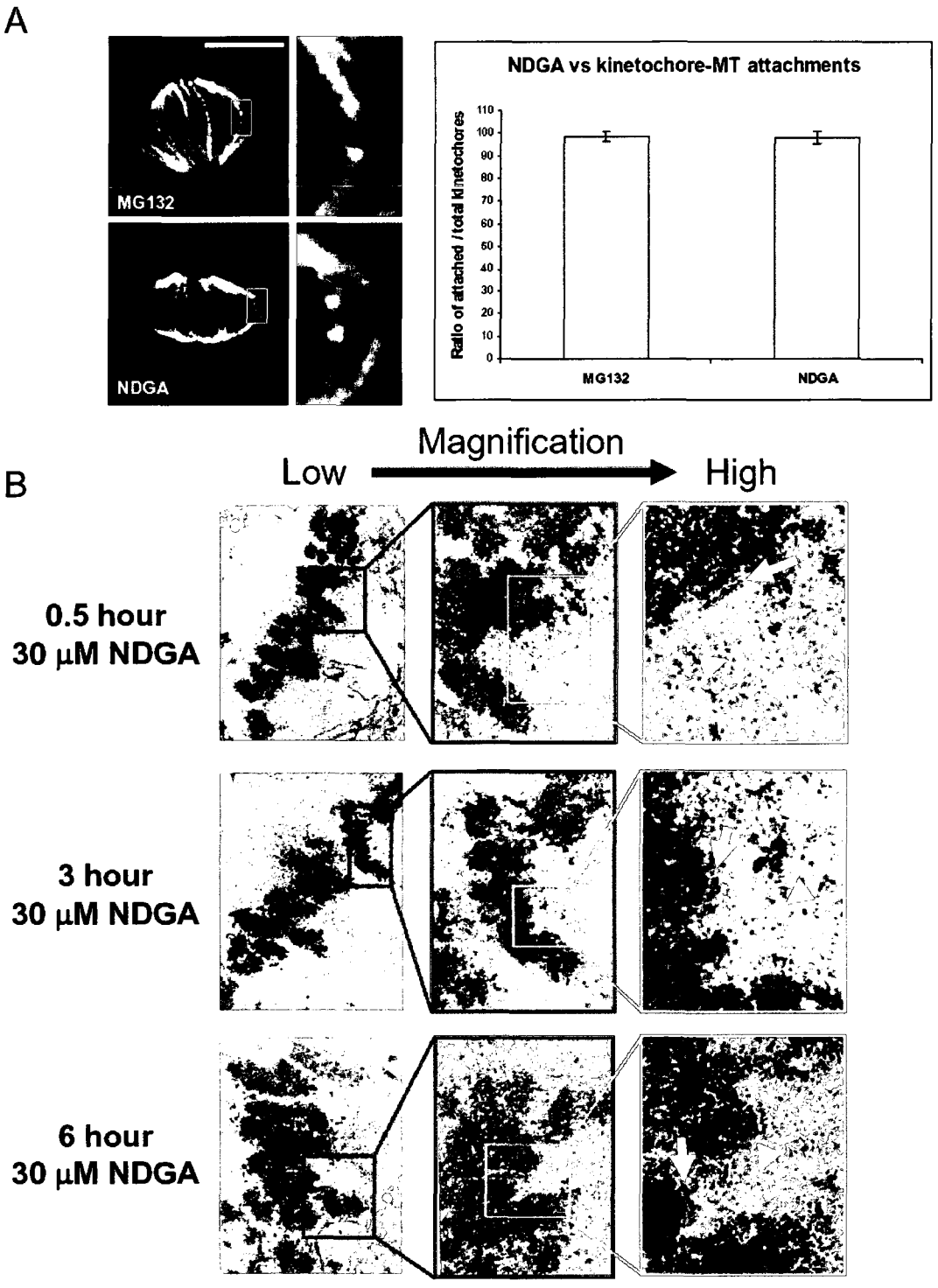

Supplementary figure 5.10: **NDGA induces mitotic checkpoint arrest.**
A) Mitotic HeLa cells were harvested by mitotic shake off and released into either fresh media, media supplemented with 10 μM taxol or 30 μM NDGA. Cell lysates were harvested 0, 2 and 4 hours post shake off and immunoblots were probed with anti-cyclin-B and tubulin antibodies. In the taxol and NDGA treated cells cyclin-B levels remain high thus indicating mitotic checkpoint arrest. **B)** HeLa cells stably expressing EGFP-hZW10 or transiently transfected with EGFP-hBubR1 were treated with 30 μM NDGA and immediately imaged using the spinning disk confocal microscope every 10 minutes as a Z-stack of ~ 20 images 1 μm apart. Maximal projections are shown. EGFP-hZW10 and EGFP-hBubR1 are observed to accumulate and remain on spindle poles for the duration of imaging (up to 6 hours). Time is indicated as hours:minutes. Scale bar = 10 μm. **C)** HeLa cells were treated with 30 μM NDGA for 6 hours, harvested for immunofluorescence and stained with anti-hMad1 and hMad2 antibodies. hMad1 and hMad2 remain associated with spindle poles even after 6 hours of NDGA treatment. Chromosomes are stained with DAPI, scale bar = 10 μm. **D)** HeLa cells stably expressing GFP-H2B were treated with various concentration of NDGA and immediately imaged for mitotic progression. Cells were imaged for 2 hours post addition of NDGA and scored for the ability to exit mitosis by segregating their chromosomes. **E)** HeLa cells stably expressing EGFP-hZW10 were treated with 30 μM NDGA for 30 minutes and washed with fresh media. The cells were immediately imaged for up to 2 hours post NDGA washout. EGFP-hZW10 is observed to dissociate from spindle poles within 23.57 +/- 5 minutes of NDGA washout (n = 7). In 3/7 cells observed, cell division occurred 45 +/- 10 min after NDGA washout (top panels). On the other hand, 4/7 cells remained arrested in mitosis (bottom panel). Time is indicated in minutues:seconds, scale bar = 10 μm.

Supplementary Figure 5.10

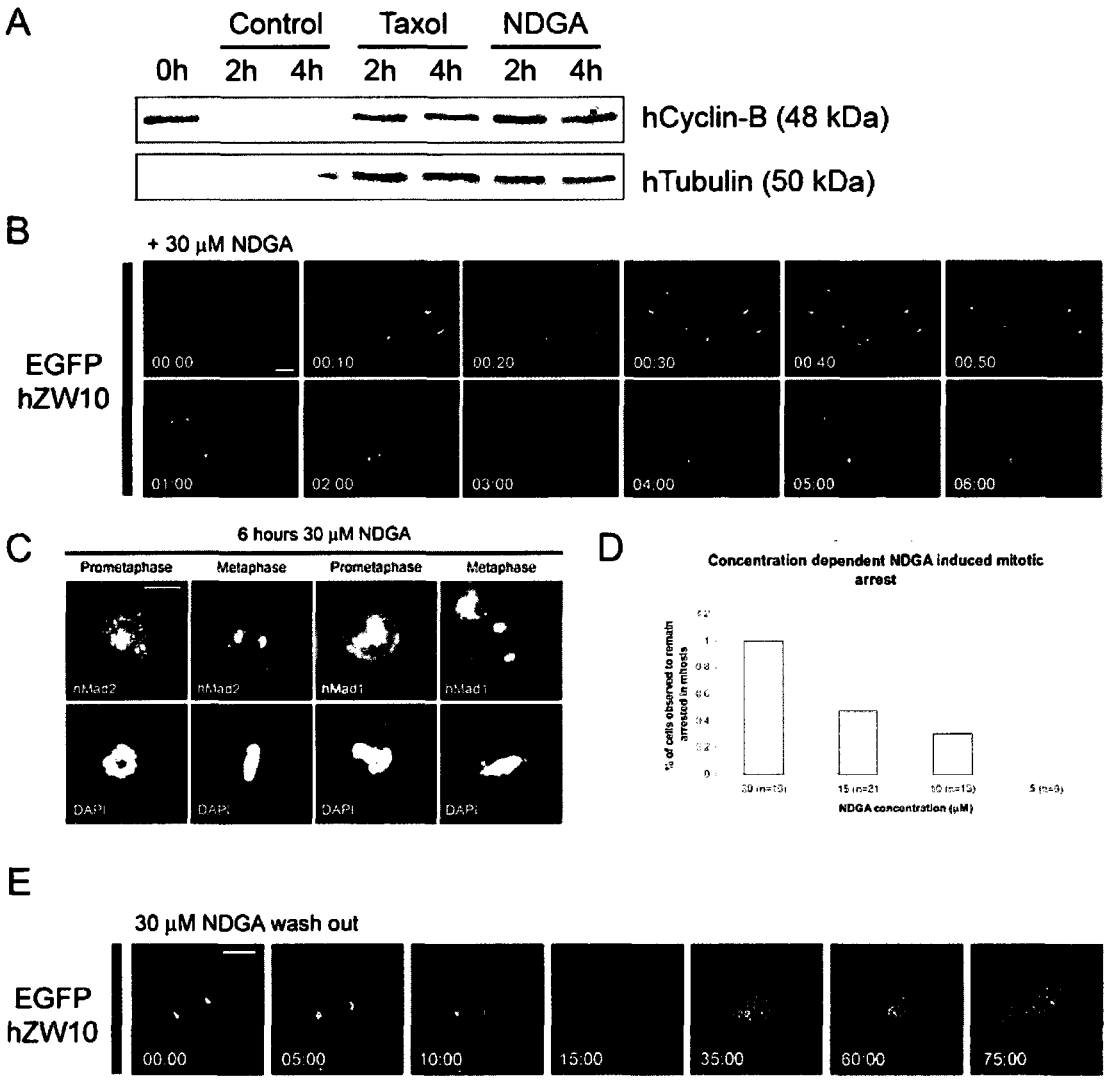

Supplementary figure 5.11: **hZW10 and hBubR1 are required for NDGA induced mitotic checkpoint arrest.**
A) Immunoblots of HeLa cell lysates depleted of hZW10 (top), or hBubR1 (bottom) after 72hours of siRNA (hZW10) or 48 hours of shRNA (hBubR1) and stained with the corresponding antibodies. Tubulin and GFP-H2B are displayed as loading controls. **B)** Percent of live GFP-H2B expressing cells escaping NDGA induced mitotic arrest as observed by decondensation. [+/- one SD] Control n = 51, hZW10 siRNA n=54, hBubR1 shRNA n=32. Timing of hZW10 siRNA escape = 180.8 +/- 70.9 minutes (n = 29). Timing of hBubR1 shRNA escape = 177.6 +/- 68.1 minutes (n = 18). **C)** The ratio of total kinetochore fluorescence intensity / whole cell fluorescence intensity of hZW10, hBub1 or hMad2 was measured in cells treated with MG132, NDGA or Nocodazole. Error bars = +/- one SD. **D)** Prometaphase or MG132 treated (12.5 μM for 1 hour) HeLa cells stably expressing EGFP-hZW10 and transiently transfected with mCherry-hMad2 were treated imaged live upon treatment with 30 μM NDGA. Only EGFP-hZW10 is observed to transport onto spindle poles in the MG132 arrested cells, while both EGFP-hZW10 and mCherry-hMad2 transport onto spindle poles in prometaphase cells. Time is indicated in minutes:seconds.

Supplementary Figure 5.11

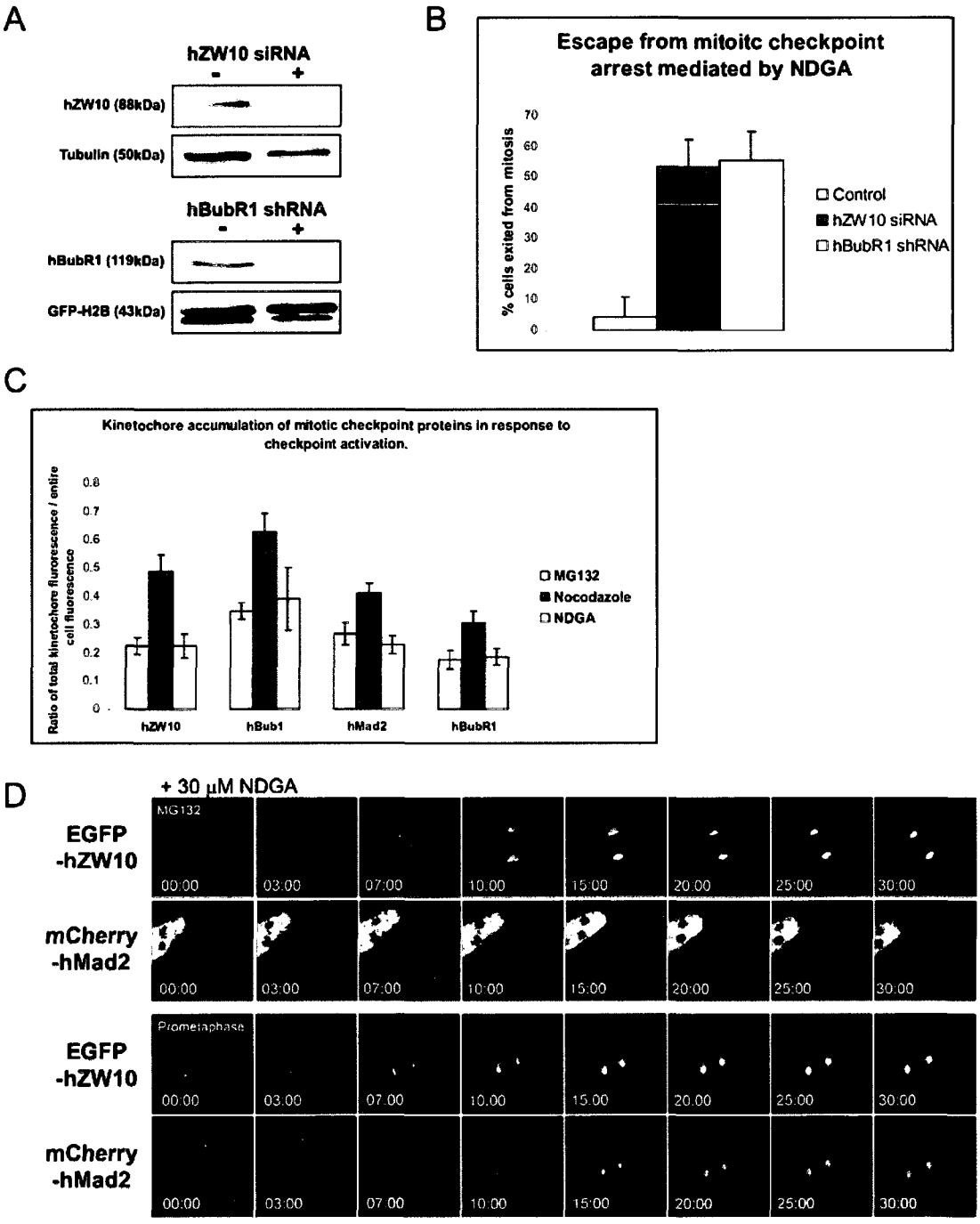

Chapter VI: *Perspectives*

6.1 Synopsis

Zeste White 10 and *Roughdeal* were discovered as essential components of the mitotic checkpoint almost 20 years ago. However, we still know very little as to their molecular function(s) within the mitotic checkpoint. Recently, the loss of RZZ complex function has been correlated with the loss of kinetochore localization of Mad1 and Mad2 (Kops et al., 2005; Basto et al., 2005). However, numerous other kinetochore proteins are also known to be required for Mad1 and Mad2 kinetochore targeting, suggesting that the failure in Mad1/Mad2 kinetochore localization may not be a direct consequence of the absensce of RZZ complex function. Furthermore, no physical interaction between the RZZ complex and Mad1 or Mad2 has been observed. We therefore still do not entirely understand the molecular function(s) of the RZZ complex during mitotic checkpoint signaling and or silencing.

In an attempt to decipher the molecular function(s) of the RZZ complex during mitosis, I have undertaken a structure-function as well as a live cell imaging study of hZW10. The RZZ complex is interdependent on all of its components, and I have therefore interpreted the hZW10 results as representative of the entire complex. I found that there is a direct relationship between the dynamic state of kinetochore- and spindle pole-bound RZZ complexes and the signaling of the mitotic checkpoint. First, I established that at least two separate mechanisms function to regulate kinetochore dynamics of the RZZ complex: the interaction between hZwint-1 and hZW10, and inter-kinetochore tension-sensitive phosphorylation by Aurora B kinase. Second, I have established that stabilization of the RZZ complex at spindle poles results in mitotic checkpoint activation. In the following section I will propose a model that will outline the temporal and biochemical regulation of RZZ complex dynamics at both kinetochores and spindle poles, and I will discuss the implications this regulation for mitotic checkpoint signaling.

6.2 Comprehensive Model

Based on the results reported in Chapters 3-5, I believe that the kinetochore and spindle pole dynamics of the RZZ complex are directly related to the state of mitotic checkpoint signaling. Outlined below are the regulatory pathways that I propose function to ensure proper kinetochore and spindle pole dynamics of the RZZ complex.

6.2.1 Kinetochore Localization of the RZZ Complex

The initial kinetochore recruitment of the RZZ complex likely relies on the interaction between hZwint-1 and hZW10 (Wang et al., 2004; Starr et al., 2000). Once at kinetochores, hZW10 also interacts with hp50 in order for the RZZ complex to recruit dynein/dynactin (Starr et al., 1998). However, more recent studies suggest that hZwint-1 and hp50 may compete for binding to hZW10 (Inoue et al., 2008). A single RZZ complex may therefore be unable to bind hp50 and hZwint-1 at the same time. Interestingly, my biochemical analysis of RZZ complexes indicates that the RZZ complex dimerizes during mitosis. Furthermore, I have shown that the hZW10 alone can dimerize *in vitro* (Famulski et al., 2008). I therefore propose that the RZZ complex is recruited to kinetochores by binding to kinetochore bound hZwint-1, while dynein/dynactin is recruited to kinetochores by interacting with a second RZZ complex that subsequently dimerizes with the hZwint-1 bound RZZ complex (Figure 6.1A).

Figure 6.1

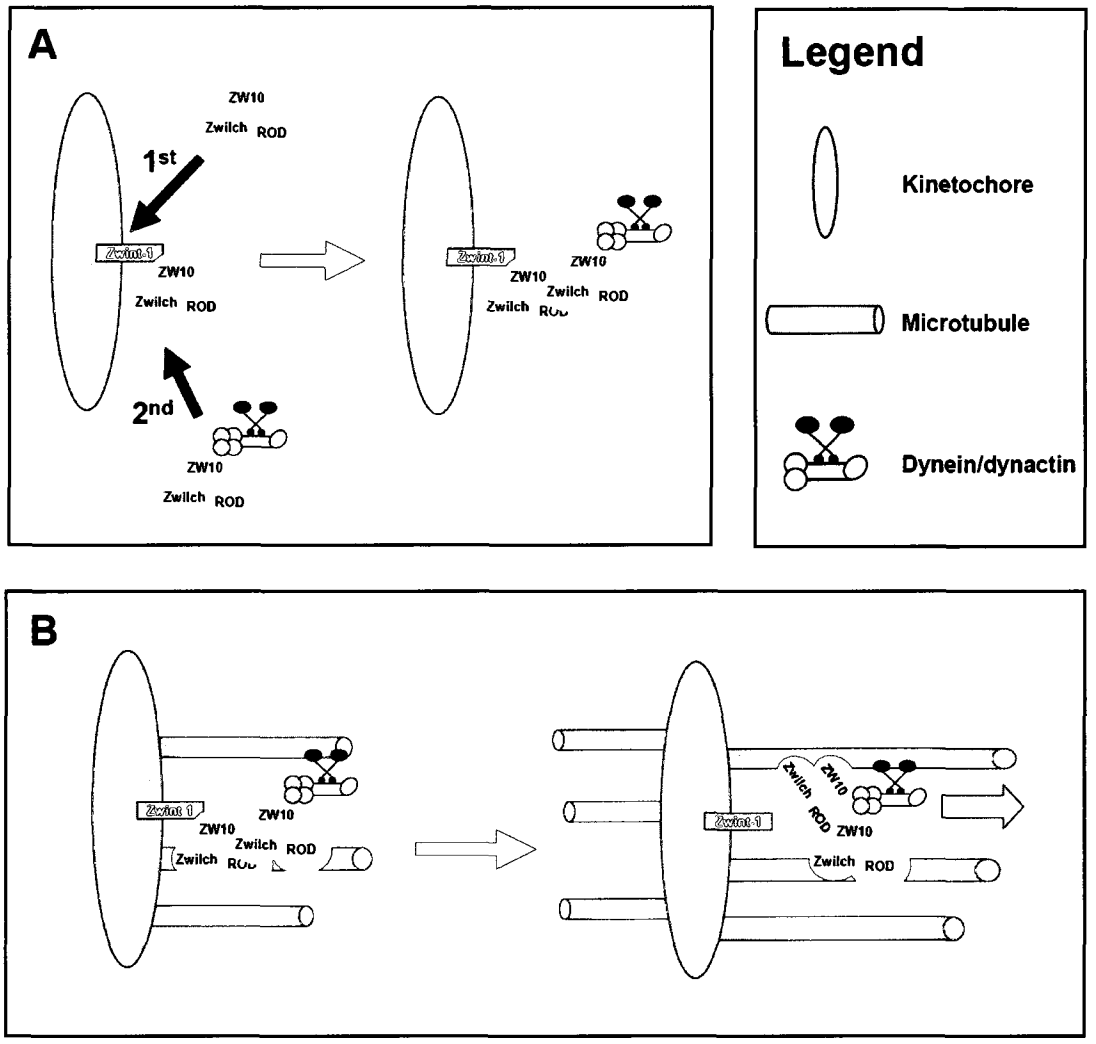

Figure 6.1: Kinetochore recruitment of dynein/dynactin and hZwint-1 mediated stability of kinetochore RZZ.

A) Monomer RZZ complexes first bind to kinetochore bound hZwint-1. Cytoplasmic RZZ complexes bind dynein/dynactin through hZW10 interacting with hp50 (red circle). The RZZ-dynein/dynactin complex is subsequently recruited to kinetochores though the dimerization of the hZwint-1 bound RZZ complex and the dynein/dynactin bound RZZ complex. **B)** In the absence of bi-polar k-MT attachment the interaction between hZwint-1 and hZW10 prevents the dimerized RZZ complexes to both bind to hp50. The RZZ complex is therefore stably bound to kinetochores. Upon establishment of bi-polar k-MT attachments, hZwint-1 no longer inhibits the interaction between hZW10 and hp50 and as such both RZZ complexes are able to interact with hp50 leading to dynein/dynactin mediated transport off kinetochores (blue arrow).

Dimerization of RZZ complexes would explain why I was able to identify hZwint-1 non-interacting mutants of hZW10 that were still able to localize to kinetochores (Chapter 3). Furthermore, oligomerization of the RZZ complex has previously been proposed to explain the very high levels of RZZ complexes that are observed at kinetochores in the presence of MT depolymerizing agents [reviewed in (Karess et al., 2005)]. The mechanism of how, when and where (either in the cytosol or at kinetochores), the RZZ complex dimerizes should be an important focus of future studies.

6.2.2 Kinetochore Stability of the RZZ Complex

Due to its direct interaction with dynein/dynactin, the RZZ complex should be inherently unstable at kinetochores that have established k-MT attachments. The presence of kinetochore MTs provides dynein/dynactin the necessary track on which to transport itself, as well as the RZZ complex, off of kinetochores and onto spindle poles. In fact, the RZZ complex, as observed through EGFP-hZW10 FRAP, is highly dynamic at kinetochores that have achieved bi-polar k-MT attachments, but it is entirely stable at kinetochores devoid of k-MT attachments (Famulski et al., 2008). FRAP of EGFP-hZW10 during prometaphase indicates that the RZZ complex is also totally stable at kinetochores with mono-polar k-MT attachments (Chapter 3). Kinetochore bound RZZ complexes are therefore stabilized by the complete lack of k-MT attachment as well as during the transition from mono-polar to bi-polar k-MT attachment.

My research indicates that the stabilization of RZZ complexes during the transition from mono-polar to bi-polar k-MT attachment depends on the interaction between hZW10 and hZwint-1. FRAP of hZwint-1 non-interacting hZW10 mutants indicates that lack of hZwint-1 interaction de-stabilizes the RZZ complex at kinetochores with mono-polar k-MT attachments, but not at those that lack k-MT attachments entirely. I therefore propose that hZwint-1 physically controls RZZ complex dynamics by negatively regulating the dynein/dynactin-mediated transport of RZZ complexes off kinetochores, up until the time at which bi-polar k-MT attachments are established (Figure 3.6 and 6.1B).

Specifically, I envision that in order for dynein/dynactin to transport the RZZ complex off kinetochores, the hZwint-1 bound RZZ complex needs first to be released from hZwint-1, so that it can subsequently bind to dynein/dynactin that is already bound to the second RZZ complex (Figure 6.1B). Dynactin is known to contain four p50 molecules, which would allow for the interaction of multiple RZZ moieties with a single dynein/dynactin complex (Schroer, 2004). Upon the loss of the hZwint-1 interaction, dynein/dynactin bound to the RZZ complexes is no longer physically tethered to kinetochores and therefore begins to travel off kinetochores, along k-MTs and onto spindle poles. In this model, kinetochore bound hZwint-1 therefore functions as a physical link between RZZ complexes and dynein/dynactin that prevents premature transport of RZZ complexes off kinetochores.

The mechanism responsible for the release of RZZ complexes from hZwint-1 may involve the structural changes that are known to occur at kinetochores and centromeres upon establishment of bi-polar k-MT attachment (Dong et al., 2007; Loncarek et al., 2007). The establishment of bi-polar k-MT attachment may therefore physically alter the structure of kinetochores and in doing so inhibit the interaction between hZW10 and hZwint-1. Alternatively, the establishment of bi-polar k-MT attachment may induce the function of mitotic kinases such as hBub1, hMps1 or hPlk1. These kinases could in turn

phosphorylate hZwint-1 or an RZZ component, and in doing so allow the release of the RZZ complex. To date, the possible post- translational modification of hZwint-1 or RZZ has not been carefully explored and should be an important focus of future studies. Finally, due to the dual function of the KMN network in kinetochore assembly and MT capture, the binding of MTs to kinetochores has been hypothesized to alter protein-protein interactions at kinetochores (Burke and Stukenberg, 2008). Interestingly, hZwint-1 is known to bind the KMN network (Kiyomitsu et al., 2007). Bi-polar k-MT attachment via the KMN network may therefore affect the ability of hZwint-1 to bind hZW10.

6.2.3 Dynein/dynactin-Mediated Kinetochore Turnover of RZZ Complexes

The transport of RZZ complexes off kinetochore that have achieved bi-polar k-MT attachment correlates with the time at which EGFP-hZW10 becomes a dynamic component of kinetochores (Basto et al., 2004; Wojcik et al., 2001; Famulski et al., 2008). Based on these observations, I believe that dynein/dynactin-mediated transport of RZZ complexes off kinetochores drives the dynamic turnover of RZZ complexes at kinetochores. The removal of RZZ complexes off kinetochores by dynein frees up kinetochore binding sites for cytoplasmic RZZ complexes to bind (Figure 6.2). As long as the kinetochore maintains bi-polar k-MT attachment, these newly recruited RZZ complexes are themselves quickly removed off kinetochores by dynein/dynactin-mediated transport. The continued presence of bi-polar k-MT attachment therefore establishes a rapid cycle of kinetochore turnover that leads to the observed depletion of RZZ complexes from kinetochores during metaphase. Although the RZZ complex is observed to vacate kinetochores upon chromosome alignment, I believe the complex actually continues to turnover at these kinetochores, but the rate of turnover is too high to allow visualization of RZZ accumulation. The continued presence of RZZ complexes, even at kinetochores that have satisfied the checkpoint, may function to insure that the checkpoint can be rapidly activated upon the loss of k-MT attachment or chromosome alignment simply by reducing RZZ kinetochore turnover rate.

6.2.3 RZZ Complex-Mediated Mitotic Checkpoint Signaling

My studies on the dynamics of EGFP-hZW10 indicate that it is the stable kinetochore localization of the RZZ complex that is essential for mitotic checkpoint function (Famulski and Chan, 2007; Famulski et al., 2008). I found that the RZZ complex is a dynamic component of the kinetochore only upon bi-polar k-MT attachment and alignment at the metaphase plate. The turnover of the RZZ complex therefore correlates with a condition that in fact satisfies the mitotic checkpoint and has been hypothesized to lead to silencing of the checkpoint. Conversely, I found that the RZZ complex is highly stable at all kinetochores that lack bi-polar k-MT attachments and chromosome alignment (Chapter 3). In other words, the RZZ complex is stably bound to kinetochores that have not satisfied the checkpoint and are in fact known to signal checkpoint-mediated arrest. Interestingly, this pattern of turnover of kinetochore RZZ complexes contrasts completelywith those exhibited by other mitotic checkpoint proteins such as Mad2, Cdc20, Mps1, Bub3 and BubR1 (Shah et al., 2004, Howell et al., 2004). These proteins are dynamic residents of kinetochores regardless of the state of k-MT attachment. Furthermore, it has been hypothesized that the dynamic pools of these checkpoint proteins represent the active components of the mitotic checkpoint amplification cascade or the global inhibitor of the APC/C (Howell et al., 2004).

Figure 6.2

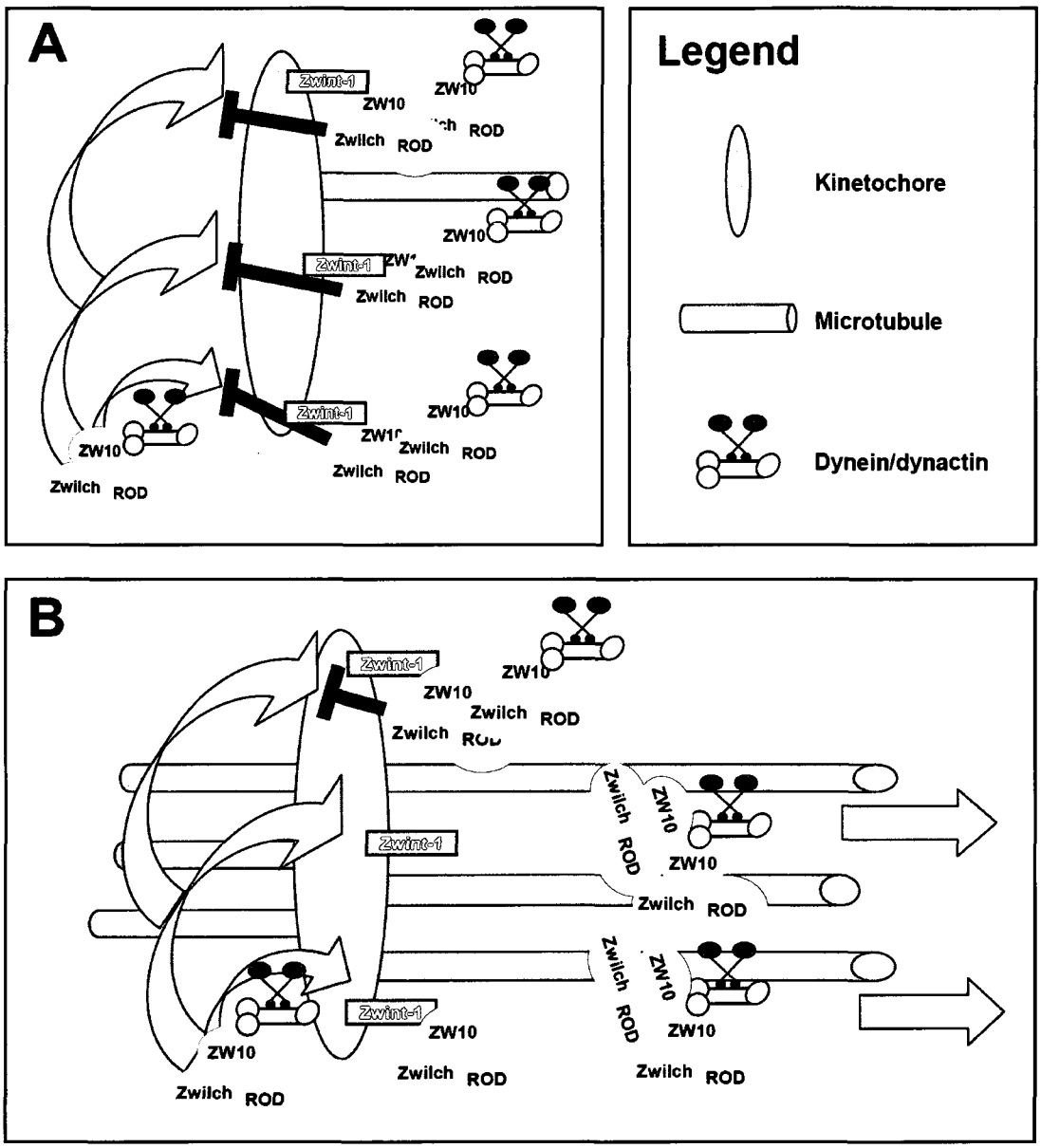

Figure 6.2: Dynein/dynactin mediated RZZ kinetochore turnover.
A) The RZZ complex binds kinetochore associated hZwint-1. There is a limited number of hZwint-1 binding sites at kinetochores. As such, cytoplasmic RZZ complexes cannot turnover (blue arrow) at kinetochores that are already bound by the RZZ. **B)** Once bi-polar k-MT attachments are achieved, dynein/dynactin removes kinetochore RZZ complexes. As RZZ complexes are removed off kinetochores, cytoplasmic RZZ complexes can now bind and therefore establish a continuous turnover of RZZ complexes at kinetochores.

The pattern of hZW10 kinetochore turnover is therefore unprecedented for a mitotic checkpoint protein, and suggests an alternative mechanism for RZZ complex function within the mitotic checkpoint.

In support of the idea that stably bound kinetochore RZZ complexes are essential for mitotic checkpoint function, I observed that hZwint-1 non-interacting hZW10 mutants, which do turnover at mono-polar attached kinetochores, cannot not maintain mitotic checkpoint arrest in the absence of endogenous hZW10 (Figure 3.6) (Famulski et al., 2008). I therefore hypothesize that stably bound RZZ complexes function in mitotic checkpoint signaling by 'activating' or 'sensitizing' the other dynamic residents of kinetochores, such as the MCC or Mad2, that are involved in mediating mitotic checkpoint arrest (Figure 6.3A). Upon the satisfaction of checkpoint requirements, the RZZ complex becomes dynamic via dynein/dynactin-mediated transport, and is therefore no longer able to activate or sensitize the other dynamic kinetochore components (Figure 6.3B). The rate of kinetochore turnover of RZZ complexes is therefore a readout of the state of mitotic checkpoint signaling. Stable RZZ complexes contribute to signaling checkpoint arrest, while highly dynamic RZZ complexes contribute to checkpoint silencing.

6.2.4 Tension Sensitive Regulation of RZZ Complex Kinetochore Dynamics

Inter-kinetochore tension is the mechanical readout of chromosome alignment, and the absence of tension activates the mitotic checkpoint. Since kinetochore dynamics of the RZZ complex correlate with the state of mitotic checkpoint signaling, these dynamics must also be regulated by the absence of inter-kinetochore tension. In contrast to hZwint-1-mediated regulation, the loss of inter-kinetochore tension does not abolish RZZ complex turnover, but instead dampens its rate 4-fold (Famulski and Chan, 2007). RZZ complexes thus accumlate at tension-less kinetochores to levels similar to those observed in prometaphase (Famulski and Chan, 2007). Although hBub1 and hBubR1 also accumulate at kinetochores in the absence of tension (Skoufias et al., 2001) this accumulation does not result from a decrease in kinetochore turnover rate, at least for hBub1 (Famulski and Chan, 2007). Therefore, the regulation of RZZ complex kinetochore turnover at tension-less kinetochores represents a novel mechanism of mitotic checkpoint activation.

The accumulation of RZZ complexes at tension-less kinetochores is essential for mitotic checkpoint function and requires the kinase activity of Aurora B (Figure 6B) (Famulski and Chan, 2007). As discussed above, kinetochore turnover of RZZ complexes is mediated by dynein/dynactin transport of RZZ complexes off kinetochores. I therefore predict that Aurora B phosphorylation, of either the RZZ complex or dynein/dynactin, negatively regulates the ability of dynein/dynactin to transport the RZZ complex off kinetochores (Figure 6.4A). In doing so, Aurora B would control the rate of RZZ complex turnover and therefore mitotic checkpoint activity. No direct evidence for Aurora B-mediated phosphorylation of the RZZ complex or dynein/dynactin has been found to date; however, this possibility has not been ruled out either. Interestingly, phosphorylation of dynein intermediate chain regulates the interaction between dynein and dynactin (Vaughan et al., 2001). Furthermore, work from the Vaughan lab suggests that dynein intermediate chain phosphorylation corresponds to the loss of kinetochore tension (Vaughan, personal communication). Aurora B phosphorylation might therefore

Figure 6.3

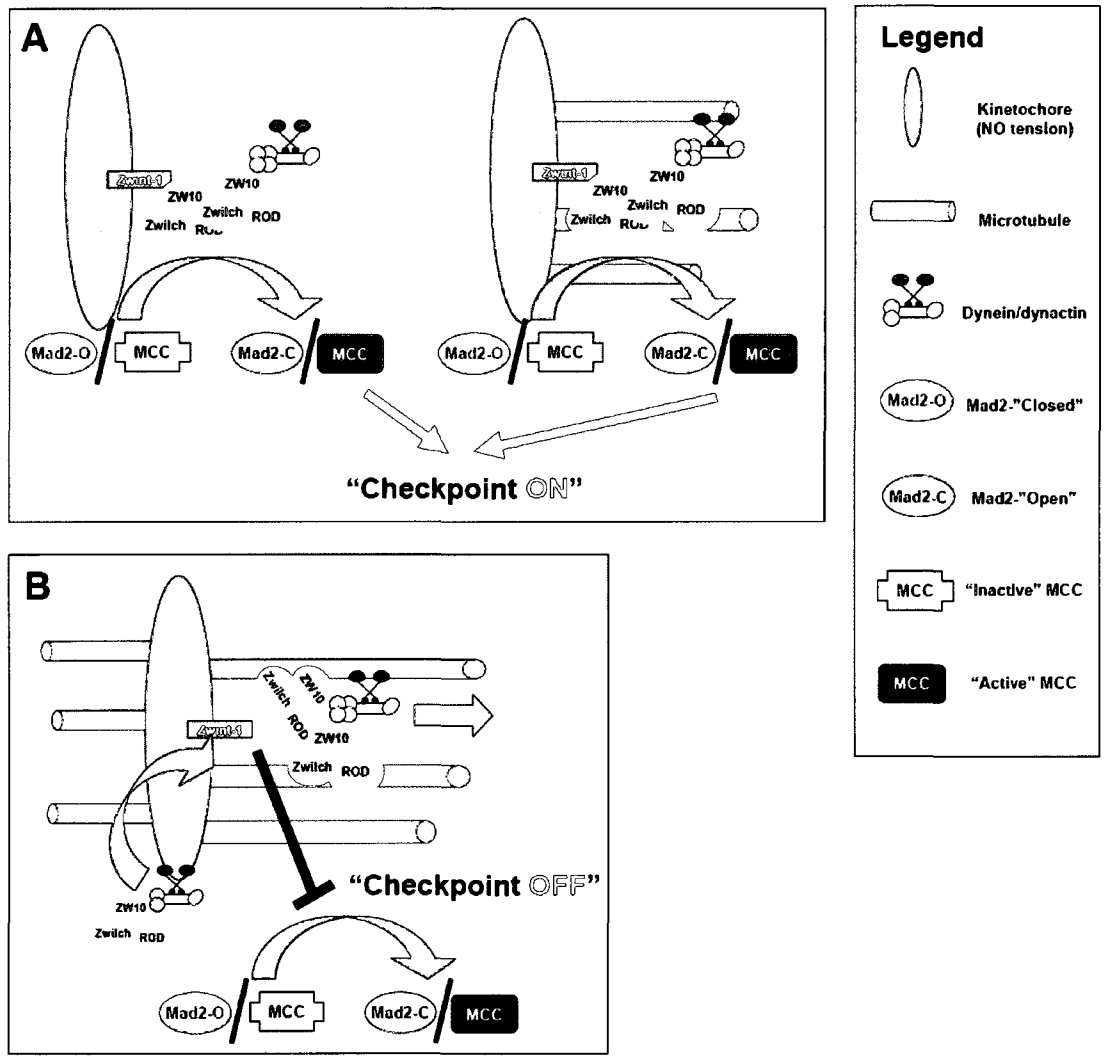

Figure 6.3: Stably bound RZZ complexes activate the mitotic checkpoint.
A) In the absence of bi-polar k-MT attachment, stably bound kinetochore RZZ complexes function as 'activating' scaffolds for the conversion of Mad2-O into Mad2-C or the 'sensitization' of MCC into the active form. **B)** Upon the establishment of bi-polar k-MT attachment, RZZ complexes become dynamic residents of kinetochores and are no longer able to catalyze the activation of Mad2 or the MCC. The checkpoint signal is therefore no longer generated thus leading to checkpoint silencing.

control the transport of RZZ complexes off kinetochores by regulating the interaction between dynein and dynactin (Figure 4.4).

The absence of inter-kinetochore tension is thought to result in the closer proximity of centromere bound Aurora B and its kinetochore bound substrates; for example the RZZ complex (Lens and Medema, 2003). While Aurora B phosphorylates its substrates, the kinetochore bound PP1 phosphatase functions to antagonize it (Emanuele et al., 2008). However, in the absence of tension, the Aurora B kinase activity overwhelms PP1 and thus Aurora B substrates remain phosphorylated. When tension is restored, Aurora B is physically removed from its substrates, thus allowing PP1 to dephosphorylate those substrates. The dephosphorylation of the RZZ complex, or dynein/dynactin, by PP1 may therefore be required to initiate RZZ complex transport off kinetochores and kinetochore turnover (Figure 6.4B).

RZZ complexes that accumulate at tension-less kinetochores are likely to function within the checkpoint differently from the stably bound RZZ complexes found at mono-polar or unattached kinetochores. hMad2 does not localize to kinetochores that have established k-MT attachmentsirrespective of inter-kinetochore tension, even though Mad2 is still essential for checkpoint arrest (Shannon et al., 2002; Waters et al., 1998). RZZ complexes accumulated at tension-less kinetochores are therefore unlikely to function as hMad2, or MCC 'activators' or 'sensitizers'. Instead, it is possible that in the absence of tension RZZ complexes prevent the activation of mitotic inhibitors such as $p31^{comet}$, the ubiquitination of hCdc20, or the dynein/dynactin-mediated 'stripping' of other checkpoint components such as hMps1 or hBubR1.

6.2.5 Spindle Pole-Associated RZZ Complex

Once the RZZ complex is finally released from kinetochores, it is transported along k-MTs and onto spindle poles. I found that RZZ complexes are also dynamic components of spindle poles, probably reflecting the continuous transport of RZZ complexes onto spindle poles from where they likely dissociate back into the cytoplasm. However, RZZ complex dissociation from spindle poles is not instantaneous, so the complex associates at least briefly with the spindle pole. My results with the drug NDGA surprisingly suggest that spindle pole associated RZZ complexes may function similarly to stable RZZ complexes at kinetochores in terms of checkpoint signaling.

I propose that normally during the transition from metaphase to anaphase, there is a brief period during which the majority of kinetochore RZZ complexes are removed, yet spindle pole-associated RZZ complexes still remain (Figure 6.5). During this time, the checkpoint would remain active due to the presence of RZZ at spindle poles. This hypothesis could explain the observed delay in anaphase onset that occurs even after all of the chromosomes have aligned (Inoue et al., 1995) (Figure 6.5). During this same period, chromosomes oscillate at the metaphase plate, perhaps 'testing' mature k-fibers to ensure that they can withstand the stress involved in chromosome congression during anaphase [reviewed in (Gardner and Odde, 2006)]. The spindle pole-mediated mitotic checkpoint silencing delay may therefore provide a fail-safe mechanism in case one of the k-fibers fails the test. Once majority of the RZZ complexes dissociate from the spindle poles, the checkpoint is finally silenced and the cell proceeds into anaphase.

Just as at kinetochores, I further propose that spindle pole turnover of RZZ complexes also continues throughout mitosis, although in the later stages of metaphase the rate is so high that spindle pole localization cannot be observed. In support of this idea, I found

that when NDGA causes the absence of RZZ at the kinetochore but stabilization of RZZ at the spindle pole, the mitotic checkpoint remains active (Figure 5.3).

The spindle pole is known to be the initial site of cyclin-B degradation during the metaphase to anaphase transition (Clute and Pines, 1999), consistent with the residence of the APC/C at these structures (Kraft et al., 2003). The presence of mitotic checkpoint proteins, such as the RZZ complex, at spindle poles may therefore directly inhibit the function of the APC/C. In fact, this type of inhibition occurs early in mitosis and involves the spindle pole associated END network (Ban et al., 2007). The END network directly inhibits cyclin-B degradation specifically at spindle poles and therefore maintains checkpoint arrest.

In conclusion, inhibition of RZZ complex dynamics at either kinetochores or spindle poles leads to activation of the mitotic checkpoint. On the other hand, the establishment of high turnover rates is required for mitotic checkpoint silencing and therefore completion of mitosis. The rate of RZZ complex turnover is therefore a key determinant of mitotic checkpoint signaling status.

6.3 Future Directions

One of the largest underlying problems of the model presented in Figures 6.1-5 is how the hZwint-1-hZW10 interaction is regulated. I believe that in order to answer this question, we must turn to *in vivo* approaches that will allow the examination of these interactions at kinetochores and not in solution. FRET (Fluorescence Resonance Energy Transfer) studies between hZW10, hZwint-1 and hp50 may be a good starting point to uncover how the kinetochore bound RZZ complex interacts with, and is regulated by, hZwint-1 and hp50. FRET readings in living cells could be used to chronicle the timing and abundance of hZW10 and hZwint-1 or hp50 interactions at kinetochores. I would expect to see interaction between hZwint-1 and hZW10 during early mitosis, but then to observe a decrease of that interaction as chromosomes become aligned at the metaphase plate. Conversely, I would expect to see low levels of interaction between hp50 and hZW10 during early mitosis, but an increase in this intereaction as chromosomes begin to align. Furthermore, once these assays are established and quantitated we could begin to test different kinase inhibitors and determine how phosphorylation might regulate these interaction events.

In addition, biochemical studies to better characterize the composition of the RZZ complex and the nature of its dimerization are also necessary to establish a comprehensive understanding of RZZ functions. It may be possible to take advantage of the hZW10 mutant library I created and in order to isolate hZW10 dimerization mutants. Such mutants could then be tested for their effects on RZZ complex localization and turnover at kinetochores, the recruitment of dynein/dynactin, and mitotic checkpoint function.

Another major assumption of my model is that dynein/dynactin-mediated transport off kinetochores drives the kinetochore turnover of RZZ complexes. This hypothesis could be tested by measuring the kinetochore turnover of RZZ complexes in cells depleted of hSpindly, a novel kinetochore component known to be required for dynein/dynactin recruitment (Griffis et al., 2007). In the absence of hSpindly, dynein/dynactin is not recruited to kinetochores despite the presence of RZZ complexes. Depletion of hSpindly would be the opportune circumstance to test whether

dynein/dynactin mediated 'stripping' does in fact induce RZZ complex kinetochore turnover and whether this may have an effect on mitotic checkpoint signaling.

Yet another major unknown in my model is the molecular function of kinetochore stable RZZ complexes during the activation of the mitotic checkpoint. It is known that the RZZ complex is required for kinetochore recruitment of hMad1 and hMad2 (Kops et al., 2005). Although I do not believe the RZZ complex is solely responsible for the recruitment of hMad1 and hMad2 to kinetochores, it is possible that the RZZ complex may play a role in either the kinetochore formation of Mad2-C or the assembly of active MCC. It would be interesting to test this hypothesis by tethering hMad1 to another kinetochore component, such as hBub1, hNdc80 or hMis12, that is known not to depend on the RZZ complex for kinetochore localization. If RZZ complex function in such cells is simultaneously ablated, it will be of considerable interest to determine whether the checkpoint is active, whether Mad2-C is generated, or whether the MCC is assembled when RZZ is absent from the kinetochore but Mad1/Mad2 is present.

My work on the response of RZZ complexes to the loss of kinetochore tension has suggested that Aurora B may phosphorylate the complex in the absence of tension. As such, it would be very interesting to determine both *in vivo* and *in vitro* whether the RZZ complex is in fact an Aurora B substrate. Furthermore, if any of the RZZ complex components are found to be substrates of Aurora B, mutants of these phosophorylation sites would be highly useful reagents in the study both of mitotic checkpoint response to loss of kinetochore tension as well as of Aurora B regulation of RZZ complex dynamic. Once an Aurora B target(s) within either the RZZ complex or dynein/dynactin is identified, it would be interesting to design a FRET-based probe to follow tension-specific phosphorylation by Aurora B, as was recently demonstrated for Aurora B phosphorylation of histone H3 during anaphase (Fuller et al., 2008).

Finally, my work outlining the potential role of spindle poles in mitotic checkpoint signaling and silencing lacks a definitive functional assay. Laser ablation of the spindle poles of cells arrested with NDGA in metaphase, or of cells removed from MG132 arrest, would allow direct testing of the hypothesis that spindle pole-associated checkpoint proteins maintain checkpoint arrest. In addition, it will be interesting to determine whether spindle pole laser ablation could remove the ~10 min delay in anaphase onset that is observed after all chromosomes have aligned (Inoue et al., 1995). It will also be very exciting to uncover the molecular function and target of NDGA. Knowing the target of NDGA will provide a valuable mechanistic clue towards understanding the pathways governing spindle pole-associated checkpoint signaling and silencing. Affinity chromatography of mitotic lysates using NDGA molecules attached to a matrix may be one approach to the identification of the NDGA target.

Figure 6.4

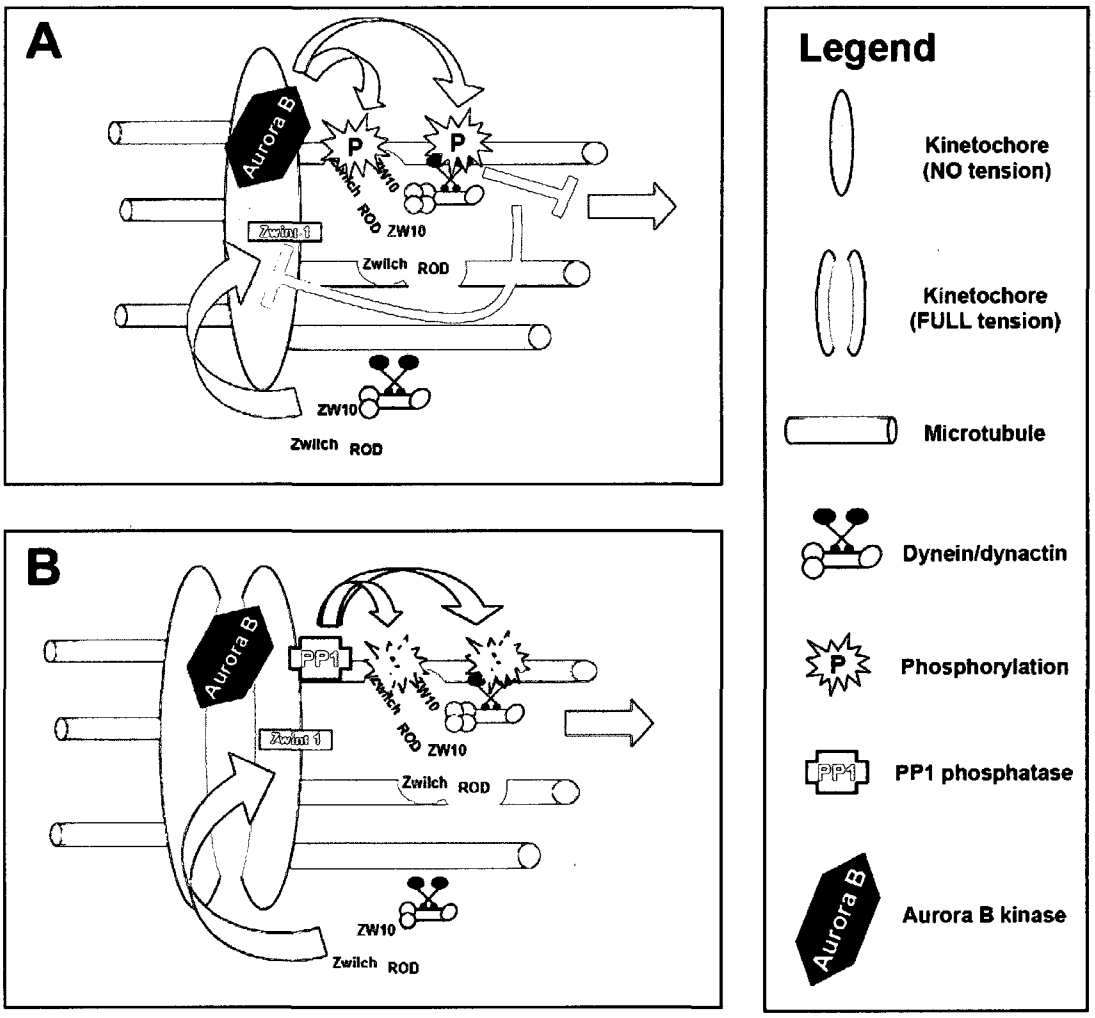

Figure 6.4: Inter-kinetochore tension regulation of RZZ complex dynamics.
A) In the absence of inter-kinetochore tension, Aurora B kinase phosphorylates the RZZ complex or dynein/dynactin. The phosphorylation inhibits dynein/dynactin mediated transport off kinetochores and therefore inhibits RZZ complex turnover. **B)** Once inter-kinetochore tension is established, PP1 phosphatase removes the phosphorylations and dynein/dynactin can transport the RZZ complex off kinetochores. The induced transport allows for dynamic turnover of RZZ complexes at kinetochores.

I therefore propose that in addition to kinetochores, the presence of RZZ complexes at spindle poles also functions to delay mitotic checkpoint silencing specifically upon the initial alignment of chromosomes (Figure 6.5). Furthermore, I believe that this delay corresponds to the time just prior to anaphase onset when chromosomes are observed to oscillate at the metaphase plate [reviewed in (Gardner and Odde, 2006)]. These oscillations may represent the 'testing' of mature k-fibers in order to ensure that they can withstand the stress involved in chromosome congression during anaphase. The spindle pole-mediated mitotic checkpoint silencing delay may therefore function as a fail-safe mechanism in case one of the k-fibers fails the 'testing' and the mitotic checkpoint needs to remain active. Once majority of the spindle pole associated RZZ complexes dissociate, the checkpoint is finally silenced and the cell proceeds into anaphase. Similar to kinetochores, I propose that spindle pole turnover of RZZ complexes also continues throughout mitosis, although in the later stages of metaphase the rate is so high that spindle pole localization is not observed. In support of this idea, I found that in the absence of kinetochore localization but spindle pole stabilization of the RZZ complex, due to the presence of NDGA, the mitotic checkpoint remains active (Figure 5.3).

The mitotic spindle and more precisely the spindle pole is known to be the initial site of cyclin-B degradation during the metaphase to anaphase transition (Clute and Pines, 1999). Additionally, the APC/C is also known to reside at spindle poles (Kraft et al., 2003). The presence of mitotic checkpoint proteins, such as the RZZ complex, at spindle poles may therefore directly inhibit the function of the APC/C. In fact, this type of inhibition occurs early in mitosis and involves the spindle pole associated END network (Ban et al., 2007).

In conclusion, inhibition of RZZ complex dynamics at either kinetochores or spindle poles leads to activation of the mitotic checkpoint. On the other hand, the establishment of high turnover rates is required for mitotic checkpoint silencing and therefore completion of mitosis. The rate of RZZ complex turnover is therefore a key determinant of mitotic checkpoint signaling status.

Figure 6.5

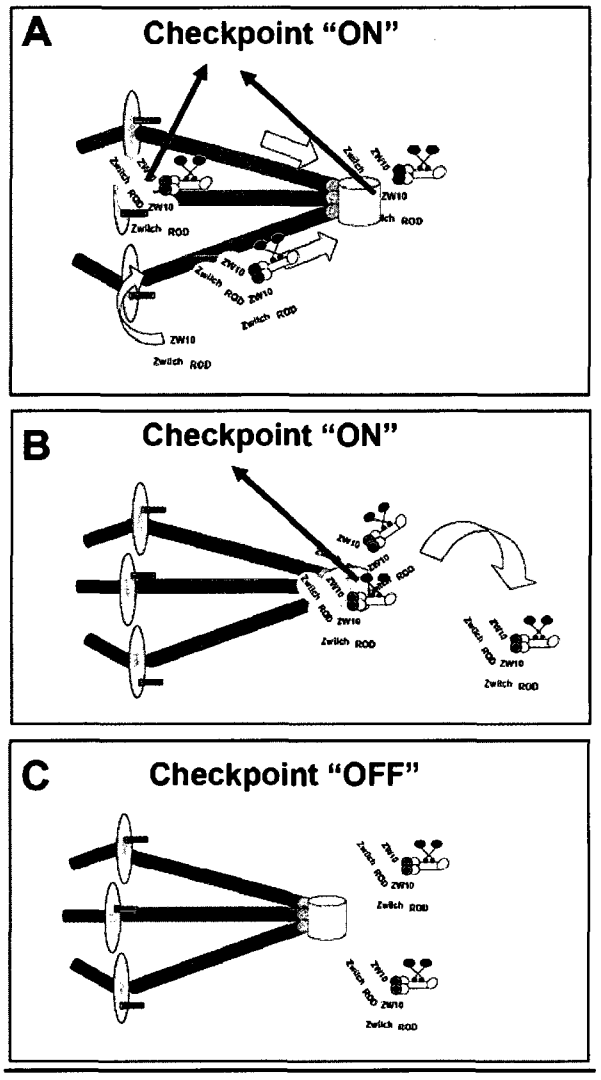

Figure 6.5: RZZ complexes mediate mitotic checkpoint signaling at kinetochores and spindle poles.
A) During the establishment of bi-polar k-MT attachment and chromosome alignment, the RZZ complex can be found at both kinetochores and spindle poles. When stably bound to kinetochores, or spindle poles, the RZZ complex activates the mitotic checkpoint signaling. **B)** Upon the alignment of chromosomes, the RZZ complex is largely depleted from kinetochores. However, there exists a transition period where the last RZZ complexes to have vacated the kinetochore have still not dissociated from spindle poles. The remaining spindle pole RZZ complexes therefore continue to maintain checkpoint signaling. **C)** After the brief delay between chromosome alignment, during which the remaining RZZ complexes dissociate off spindle poles, the checkpoint is no longer activated and anaphase onset can proceed.

Chapter VII: *References*

Abrieu, A., L. Magnaghi-Jaulin, J.A. Kahana, M. Peter, A. Castro, S. Vigneron, T. Lorca, D.W. Cleveland, and J.C. Labbe. 2001. Mps1 is a kinetochore-associated kinase essential for the vertebrate mitotic checkpoint. *Cell.* 106:83-93.

Acquaviva, C., F. Herzog, C. Kraft, and J. Pines. 2004. The anaphase promoting complex/cyclosome is recruited to centromeres by the spindle assembly checkpoint. *Nat Cell Biol.* 6:892-8.

Andersen, S.S., A.J. Ashford, R. Tournebize, O. Gavet, A. Sobel, A.A. Hyman, and E. Karsenti. 1997. Mitotic chromatin regulates phosphorylation of Stathmin/Op18. *Nature.* 389:640-3.

Andrews, P.D., Y. Ovechkina, N. Morrice, M. Wagenbach, K. Duncan, L. Wordeman, and J.R. Swedlow. 2004. Aurora B regulates MCAK at the mitotic centromere. *Dev Cell.* 6:253-68.

Arasaki, K., K. Tani, T. Yoshimori, D.J. Stephens, and M. Tagaya. 2007. Nordihydroguaiaretic acid affects multiple dynein-dynactin functions in interphase and mitotic cells. *Mol Pharmacol.* 71:454-60.

Aumais, J.P., J.R. Tunstead, R.S. McNeil, B.T. Schaar, S.K. McConnell, S.H. Lin, G.D. Clark, and L.Y. Yu-Lee. 2001. NudC associates with Lis1 and the dynein motor at the leading pole of neurons. *J Neurosci.* 21:RC187.

Baker, D.J., K.B. Jeganathan, J.D. Cameron, M. Thompson, S. Juneja, A. Kopecka, R. Kumar, R.B. Jenkins, P.C. de Groen, P. Roche, and J.M. van Deursen. 2004. BubR1 insufficiency causes early onset of aging-associated phenotypes and infertility in mice. *Nat Genet.* 36:744-9.

Ban, K.H., J.Z. Torres, J.J. Miller, A. Mikhailov, M.V. Nachury, J.J. Tung, C.L. Rieder, and P.K. Jackson. 2007. The END network couples spindle pole assembly to inhibition of the anaphase-promoting complex/cyclosome in early mitosis. *Dev Cell.* 13:29-42.

Basto, R., R. Gomes, and R.E. Karess. 2000. Rough deal and Zw10 are required for the metaphase checkpoint in Drosophila. *Nat Cell Biol.* 2:939-43.

Basto, R., J. Lau, T. Vinogradova, A. Gardiol, C.G. Woods, A. Khodjakov, and J.W. Raff. 2006. Flies without centrioles. *Cell.* 125:1375-86.

Basto, R., F. Scaerou, S. Mische, E. Wojcik, C. Lefebvre, R. Gomes, T. Hays, and R. Karess. 2004. In vivo dynamics of the rough deal checkpoint protein during Drosophila mitosis. *Curr Biol.* 14:56-61.

Basu, J., E. Logarinho, S. Herrmann, H. Bousbaa, Z. Li, G.K. Chan, T.J. Yen, C.E. Sunkel, and M.L. Goldberg. 1998. Localization of the Drosophila checkpoint control protein Bub3 to the kinetochore requires Bub1 but not Zw10 or Rod. *Chromosoma.* 107:376-85.

Biggins, S., and A.W. Murray. 2001. The budding yeast protein kinase Ipl1/Aurora allows the absence of tension to activate the spindle checkpoint. *Genes Dev.* 15:3118-29.

Biggins, S., F.F. Severin, N. Bhalla, I. Sassoon, A.A. Hyman, and A.W. Murray. 1999. The conserved protein kinase Ipl1 regulates microtubule binding to kinetochores in budding yeast. *Genes Dev.* 13:532-44.

Black, B.E., and E.A. Bassett. 2008. The histone variant CENP-A and centromere specification. *Curr Opin Cell Biol.* 20:91-100.

Black, B.E., M.A. Brock, S. Bedard, V.L. Woods, Jr., and D.W. Cleveland. 2007a. An epigenetic mark generated by the incorporation of CENP-A into centromeric nucleosomes. *Proc Natl Acad Sci U S A*. 104:5008-13.

Black, B.E., L.E. Jansen, P.S. Maddox, D.R. Foltz, A.B. Desai, J.V. Shah, and D.W. Cleveland. 2007b. Centromere identity maintained by nucleosomes assembled with histone H3 containing the CENP-A targeting domain. *Mol Cell*. 25:309-22.

Bornens, M. 2002. Centrosome composition and microtubule anchoring mechanisms. *Curr Opin Cell Biol*. 14:25-34.

Bradbury, E.M. 1992. Reversible histone modifications and the chromosome cell cycle. *Bioessays*. 14:9-16.

Brinkley, B.R., and E. Stubblefield. 1966. The fine structure of the kinetochore of a mammalian cell in vitro. *Chromosoma*. 19:28-43.

Buffin, E., D. Emre, and R.E. Karess. 2007. Flies without a spindle checkpoint. *Nat Cell Biol*. 9:565-72.

Buffin, E., C. Lefebvre, J. Huang, M.E. Gagou, and R.E. Karess. 2005. Recruitment of Mad2 to the kinetochore requires the Rod/Zw10 complex. *Curr Biol*. 15:856-61.

Burke, D.J., and P.T. Stukenberg. 2008. Linking kinetochore-microtubule binding to the spindle checkpoint. *Dev Cell*. 14:474-9.

Caplow, M., and J. Shanks. 1996. Evidence that a single monolayer tubulin-GTP cap is both necessary and sufficient to stabilize microtubules. *Mol Biol Cell*. 7:663-75.

Carazo-Salas, R.E., O.J. Gruss, I.W. Mattaj, and E. Karsenti. 2001. Ran-GTP coordinates regulation of microtubule nucleation and dynamics during mitotic-spindle assembly. *Nat Cell Biol*. 3:228-34.

Carazo-Salas, R.E., G. Guarguaglini, O.J. Gruss, A. Segref, E. Karsenti, and I.W. Mattaj. 1999. Generation of GTP-bound Ran by RCC1 is required for chromatin-induced mitotic spindle formation. *Nature*. 400:178-81.

Carvalho, A., M. Carmena, C. Sambade, W.C. Earnshaw, and S.P. Wheatley. 2003. Survivin is required for stable checkpoint activation in taxol-treated HeLa cells. *J Cell Sci*. 116:2987-98.

Cassimeris, L., and C. Spittle. 2001. Regulation of microtubule-associated proteins. *Int Rev Cytol*. 210:163-226.

Chan, C.S., and D. Botstein. 1993. Isolation and characterization of chromosome-gain and increase-in-ploidy mutants in yeast. *Genetics*. 135:677-91.

Chan, G.K., S.A. Jablonski, D.A. Starr, M.L. Goldberg, and T.J. Yen. 2000. Human Zw10 and ROD are mitotic checkpoint proteins that bind to kinetochores. *Nat Cell Biol*. 2:944-7.

Chan, G.K., S.A. Jablonski, V. Sudakin, J.C. Hittle, and T.J. Yen. 1999. Human BUBR1 is a mitotic checkpoint kinase that monitors CENP-E functions at kinetochores and binds the cyclosome/APC. *J Cell Biol*. 146:941-54.

Chan, G.K., S.T. Liu, and T.J. Yen. 2005. Kinetochore structure and function. *Trends Cell Biol*. 15:589-98.

Chan, G.K., B.T. Schaar, and T.J. Yen. 1998. Characterization of the kinetochore binding domain of CENP-E reveals interactions with the kinetochore proteins CENP-F and hBUBR1. *J Cell Biol*. 143:49-63.

Chan, G.K., and T.J. Yen. 2003. The mitotic checkpoint: a signaling pathway that allows a single unattached kinetochore to inhibit mitotic exit. *Prog Cell Cycle Res.* 5:431-9.

Chang, D.C., N. Xu, and K.Q. Luo. 2003. Degradation of cyclin B is required for the onset of anaphase in Mammalian cells. *J Biol Chem.* 278:37865-73.

Cheeseman, I.M., J.S. Chappie, E.M. Wilson-Kubalek, and A. Desai. 2006. The conserved KMN network constitutes the core microtubule-binding site of the kinetochore. *Cell.* 127:983-97.

Cheeseman, I.M., and A. Desai. 2008. Molecular architecture of the kinetochore-microtubule interface. *Nat Rev Mol Cell Biol.* 9:33-46.

Cheeseman, I.M., T. Hori, T. Fukagawa, and A. Desai. 2008. KNL1 and the CENP-H/I/K Complex Coordinately Direct Kinetochore Assembly in Vertebrates. *Mol Biol Cell.* 19:587-94.

Cheeseman, I.M., S. Niessen, S. Anderson, F. Hyndman, J.R. Yates, 3rd, K. Oegema, and A. Desai. 2004. A conserved protein network controls assembly of the outer kinetochore and its ability to sustain tension. *Genes Dev.* 18:2255-68.

Chen, R.H. 2002. BubR1 is essential for kinetochore localization of other spindle checkpoint proteins and its phosphorylation requires Mad1. *J Cell Biol.* 158:487-96.

Chen, R.H. 2004. Phosphorylation and activation of Bub1 on unattached chromosomes facilitate the spindle checkpoint. *EMBO J.* 23:3113-21.

Chen, R.H., D.M. Brady, D. Smith, A.W. Murray, and K.G. Hardwick. 1999. The spindle checkpoint of budding yeast depends on a tight complex between the Mad1 and Mad2 proteins. *Mol Biol Cell.* 10:2607-18.

Chen, R.H., A. Shevchenko, M. Mann, and A.W. Murray. 1998. Spindle checkpoint protein Xmad1 recruits Xmad2 to unattached kinetochores. *J Cell Biol.* 143:283-95.

Chen, R.H., J.C. Waters, E.D. Salmon, and A.W. Murray. 1996. Association of spindle assembly checkpoint component XMAD2 with unattached kinetochores. *Science.* 274:242-6.

Chung, E., and R.H. Chen. 2002. Spindle checkpoint requires Mad1-bound and Mad1-free Mad2. *Mol Biol Cell.* 13:1501-11.

Chung, E., and R.H. Chen. 2003. Phosphorylation of Cdc20 is required for its inhibition by the spindle checkpoint. *Nat Cell Biol.* 5:748-53.

Cimini, D. 2007. Detection and correction of merotelic kinetochore orientation by Aurora B and its partners. *Cell Cycle.* 6:1558-64.

Cimini, D., L.A. Cameron, and E.D. Salmon. 2004. Anaphase spindle mechanics prevent mis-segregation of merotelically oriented chromosomes. *Curr Biol.* 14:2149-55.

Cimini, D., B. Moree, J.C. Canman, and E.D. Salmon. 2003. Merotelic kinetochore orientation occurs frequently during early mitosis in mammalian tissue cells and error correction is achieved by two different mechanisms. *J Cell Sci.* 116:4213-25.

Cimini, D., X. Wan, C.B. Hirel, and E.D. Salmon. 2006. Aurora kinase promotes turnover of kinetochore microtubules to reduce chromosome segregation errors. *Curr Biol.* 16:1711-8.

Clute, P., and J. Pines. 1999. Temporal and spatial control of cyclin B1 destruction in metaphase. *Nat Cell Biol.* 1:82-7.

Cohen-Fix, O., J.M. Peters, M.W. Kirschner, and D. Koshland. 1996. Anaphase initiation in Saccharomyces cerevisiae is controlled by the APC-dependent degradation of the anaphase inhibitor Pds1p. *Genes Dev.* 10:3081-93.

Compton, D.A. 1998. Focusing on spindle poles. *J Cell Sci.* 111 (Pt 11):1477-81.

Cooke, C.A., D.P. Bazett-Jones, W.C. Earnshaw, and J.B. Rattner. 1993. Mapping DNA within the mammalian kinetochore. *J Cell Biol.* 120:1083-91.

Cooke, C.A., M.M. Heck, and W.C. Earnshaw. 1987. The inner centromere protein (INCENP) antigens: movement from inner centromere to midbody during mitosis. *J Cell Biol.* 105:2053-67.

Cooke, C.A., B. Schaar, T.J. Yen, and W.C. Earnshaw. 1997. Localization of CENP-E in the fibrous corona and outer plate of mammalian kinetochores from prometaphase through anaphase. *Chromosoma.* 106:446-55.

Davenport, J., L.D. Harris, and R. Goorha. 2006. Spindle checkpoint function requires Mad2-dependent Cdc20 binding to the Mad3 homology domain of BubR1. *Exp Cell Res.* 312:1831-42.

De Antoni, A., C.G. Pearson, D. Cimini, J.C. Canman, V. Sala, L. Nezi, M. Mapelli, L. Sironi, M. Faretta, E.D. Salmon, and A. Musacchio. 2005. The Mad1/Mad2 complex as a template for Mad2 activation in the spindle assembly checkpoint. *Curr Biol.* 15:214-25.

DeLuca, J.G., Y. Dong, P. Hergert, J. Strauss, J.M. Hickey, E.D. Salmon, and B.F. McEwen. 2005. Hec1 and nuf2 are core components of the kinetochore outer plate essential for organizing microtubule attachment sites. *Mol Biol Cell.* 16:519-31.

Desai, A., and T.J. Mitchison. 1997. Microtubule polymerization dynamics. *Annu Rev Cell Dev Biol.* 13:83-117.

Desai, A., S. Rybina, T. Muller-Reichert, A. Shevchenko, A. Hyman, and K. Oegema. 2003. KNL-1 directs assembly of the microtubule-binding interface of the kinetochore in C. elegans. *Genes Dev.* 17:2421-35.

Ditchfield, C., V.L. Johnson, A. Tighe, R. Ellston, C. Haworth, T. Johnson, A. Mortlock, N. Keen, and S.S. Taylor. 2003. Aurora B couples chromosome alignment with anaphase by targeting BubR1, Mad2, and Cenp-E to kinetochores. *J Cell Biol.* 161:267-80.

Dobles, M., V. Liberal, M.L. Scott, R. Benezra, and P.K. Sorger. 2000. Chromosome missegregation and apoptosis in mice lacking the mitotic checkpoint protein Mad2. *Cell.* 101:635-45.

Dujardin, D., U.I. Wacker, A. Moreau, T.A. Schroer, J.E. Rickard, and J.R. De Mey. 1998. Evidence for a role of CLIP-170 in the establishment of metaphase chromosome alignment. *J Cell Biol.* 141:849-62.

Earnshaw, W.C., and B.R. Migeon. 1985. Three related centromere proteins are absent from the inactive centromere of a stable isodicentric chromosome. *Chromosoma.* 92:290-6.

Efimov, V.P., and N.R. Morris. 2000. The LIS1-related NUDF protein of Aspergillus nidulans interacts with the coiled-coil domain of the NUDE/RO11 protein. *J Cell Biol.* 150:681-8.

Elia, A.E., L.C. Cantley, and M.B. Yaffe. 2003. Proteomic screen finds pSer/pThr-binding domain localizing Plk1 to mitotic substrates. *Science*. 299:1228-31.

Emanuele, M.J., W. Lan, M. Jwa, S.A. Miller, C.S. Chan, and P.T. Stukenberg. 2008. Aurora B kinase and protein phosphatase 1 have opposing roles in modulating kinetochore assembly. *J Cell Biol*. 181:241-54.

Ems-McClung, S.C., Y. Zheng, and C.E. Walczak. 2004. Importin alpha/beta and Ran-GTP regulate XCTK2 microtubule binding through a bipartite nuclear localization signal. *Mol Biol Cell*. 15:46-57.

Eytan, E., I. Braunstein, D. Ganoth, A. Teichner, J.C. Hittle, T.J. Yen, and A. Hershko. 2008. Two different mitotic checkpoint inhibitors of the anaphase-promoting complex/cyclosome antagonize the action of the activator Cdc20. *Proc Natl Acad Sci U S A*.

Famulski, J.K., and G.K. Chan. 2007. Aurora B kinase-dependent recruitment of hZW10 and hROD to tensionless kinetochores. *Curr Biol*. 17:2143-9.

Famulski, J.K., L. Vos, X. Sun, and G. Chan. 2008. Stable hZW10 kinetochore residency, mediated by hZwint-1 interaction, is essential for the mitotic checkpoint. *J Cell Biol*. 180:507-20.

Fang, G. 2002. Checkpoint protein BubR1 acts synergistically with Mad2 to inhibit anaphase-promoting complex. *Mol Biol Cell*. 13:755-66.

Fang, G., H. Yu, and M.W. Kirschner. 1998a. The checkpoint protein MAD2 and the mitotic regulator CDC20 form a ternary complex with the anaphase-promoting complex to control anaphase initiation. *Genes Dev*. 12:1871-83.

Fang, G., H. Yu, and M.W. Kirschner. 1998b. Direct binding of CDC20 protein family members activates the anaphase-promoting complex in mitosis and G1. *Mol Cell*. 2:163-71.

Feng, Y., E.C. Olson, P.T. Stukenberg, L.A. Flanagan, M.W. Kirschner, and C.A. Walsh. 2000. LIS1 regulates CNS lamination by interacting with mNudE, a central component of the centrosome. *Neuron*. 28:665-79.

Foltz, D.R., L.E. Jansen, B.E. Black, A.O. Bailey, J.R. Yates, 3rd, and D.W. Cleveland. 2006. The human CENP-A centromeric nucleosome-associated complex. *Nat Cell Biol*. 8:458-69.

Franz, C., R. Walczak, S. Yavuz, R. Santarella, M. Gentzel, P. Askjaer, V. Galy, M. Hetzer, I.W. Mattaj, and W. Antonin. 2007. MEL-28/ELYS is required for the recruitment of nucleoporins to chromatin and postmitotic nuclear pore complex assembly. *EMBO Rep*. 8:165-72.

Fukagawa, T., M. Nogami, M. Yoshikawa, M. Ikeno, T. Okazaki, Y. Takami, T. Nakayama, and M. Oshimura. 2004. Dicer is essential for formation of the heterochromatin structure in vertebrate cells. *Nat Cell Biol*. 6:784-91.

Fuller, B.G., M.A. Lampson, E.A. Foley, S. Rosasco-Nitcher, K.V. Le, P. Tobelmann, D.L. Brautigan, P.T. Stukenberg, and T.M. Kapoor. 2008. Midzone activation of aurora B in anaphase produces an intracellular phosphorylation gradient. *Nature*. 453:1132-6.

Funabiki, H., K. Kumada, and M. Yanagida. 1996a. Fission yeast Cut1 and Cut2 are essential for sister chromatid separation, concentrate along the metaphase spindle and form large complexes. *EMBO J*. 15:6617-28.

Funabiki, H., H. Yamano, K. Kumada, K. Nagao, T. Hunt, and M. Yanagida. 1996b. Cut2 proteolysis required for sister-chromatid seperation in fission yeast. *Nature*. 381:438-41.

Gadea, B.B., and J.V. Ruderman. 2006. Aurora B is required for mitotic chromatin-induced phosphorylation of Op18/Stathmin. *Proc Natl Acad Sci U S A*. 103:4493-8.

Galjart, N. 2005. CLIPs and CLASPs and cellular dynamics. *Nat Rev Mol Cell Biol*. 6:487-98.

Gassmann, R., A. Carvalho, A.J. Henzing, S. Ruchaud, D.F. Hudson, R. Honda, E.A. Nigg, D.L. Gerloff, and W.C. Earnshaw. 2004. Borealin: a novel chromosomal passenger required for stability of the bipolar mitotic spindle. *J Cell Biol*. 166:179-91.

Glotzer, M., A.W. Murray, and M.W. Kirschner. 1991. Cyclin is degraded by the ubiquitin pathway. *Nature*. 349:132-8.

Goshima, G., and M. Yanagida. 2000. Establishing biorientation occurs with precocious separation of the sister kinetochores, but not the arms, in the early spindle of budding yeast. *Cell*. 100:619-33.

Goto, H., Y. Yasui, E.A. Nigg, and M. Inagaki. 2002. Aurora-B phosphorylates Histone H3 at serine28 with regard to the mitotic chromosome condensation. *Genes Cells*. 7:11-7.

Griffis, E.R., N. Stuurman, and R.D. Vale. 2007. Spindly, a novel protein essential for silencing the spindle assembly checkpoint, recruits dynein to the kinetochore. *J Cell Biol*. 177:1005-15.

Gruss, O.J., R.E. Carazo-Salas, C.A. Schatz, G. Guarguaglini, J. Kast, M. Wilm, N. Le Bot, I. Vernos, E. Karsenti, and I.W. Mattaj. 2001. Ran induces spindle assembly by reversing the inhibitory effect of importin alpha on TPX2 activity. *Cell*. 104:83-93.

Gunawardane, R.N., O.C. Martin, K. Cao, L. Zhang, K. Dej, A. Iwamatsu, and Y. Zheng. 2000. Characterization and reconstitution of Drosophila gamma-tubulin ring complex subunits. *J Cell Biol*. 151:1513-24.

Habu, T., S.H. Kim, J. Weinstein, and T. Matsumoto. 2002. Identification of a MAD2-binding protein, CMT2, and its role in mitosis. *EMBO J*. 21:6419-28.

Hardwick, K.G., R.C. Johnston, D.L. Smith, and A.W. Murray. 2000. MAD3 encodes a novel component of the spindle checkpoint which interacts with Bub3p, Cdc20p, and Mad2p. *J Cell Biol*. 148:871-82.

Hardwick, K.G., E. Weiss, F.C. Luca, M. Winey, and A.W. Murray. 1996. Activation of the budding yeast spindle assembly checkpoint without mitotic spindle disruption. *Science*. 273:953-6.

Hartwell, L.H., R.K. Mortimer, J. Culotti, and M. Culotti. 1973. Genetic Control of the Cell Division Cycle in Yeast: V. Genetic Analysis of cdc Mutants. *Genetics*. 74:267-286.

Hauf, S., R.W. Cole, S. LaTerra, C. Zimmer, G. Schnapp, R. Walter, A. Heckel, J. van Meel, C.L. Rieder, and J.M. Peters. 2003. The small molecule Hesperadin reveals a role for Aurora B in correcting kinetochore-microtubule attachment and in maintaining the spindle assembly checkpoint. *J Cell Biol*. 161:281-94.

Hauf, S., I.C. Waizenegger, and J.M. Peters. 2001. Cohesin cleavage by separase required for anaphase and cytokinesis in human cells. *Science*. 293:1320-3.

Hayden, J.H., S.S. Bowser, and C.L. Rieder. 1990. Kinetochores capture astral microtubules during chromosome attachment to the mitotic spindle: direct visualization in live newt lung cells. *J Cell Biol*. 111:1039-45.

He, X., S. Asthana, and P.K. Sorger. 2000. Transient sister chromatid separation and elastic deformation of chromosomes during mitosis in budding yeast. *Cell*. 101:763-75.

Heald, R., R. Tournebize, T. Blank, R. Sandaltzopoulos, P. Becker, A. Hyman, and E. Karsenti. 1996. Self-organization of microtubules into bipolar spindles around artificial chromosomes in Xenopus egg extracts. *Nature*. 382:420-5.

Heit, R., D.A. Underhill, G. Chan, and M.J. Hendzel. 2006. Epigenetic regulation of centromere formation and kinetochore function. *Biochem Cell Biol*. 84:605-18.

Hemmerich, P., S. Weidtkamp-Peters, C. Hoischen, L. Schmiedeberg, I. Erliandri, and S. Diekmann. 2008. Dynamics of inner kinetochore assembly and maintenance in living cells. *J Cell Biol*. 180:1101-14.

Henikoff, S., K. Ahmad, and H.S. Malik. 2001. The centromere paradox: stable inheritance with rapidly evolving DNA. *Science*. 293:1098-102.

Hershko, A. 1991. The ubiquitin pathway for protein degradation. *Trends Biochem Sci*. 16:265-8.

Hinchcliffe, E.H., F.J. Miller, M. Cham, A. Khodjakov, and G. Sluder. 2001. Requirement of a centrosomal activity for cell cycle progression through G1 into S phase. *Science*. 291:1547-50.

Hirokawa, N., Y. Noda, and Y. Okada. 1998. Kinesin and dynein superfamily proteins in organelle transport and cell division. *Curr Opin Cell Biol*. 10:60-73.

Hoffman, D.B., C.G. Pearson, T.J. Yen, B.J. Howell, and E.D. Salmon. 2001. Microtubule-dependent changes in assembly of microtubule motor proteins and mitotic spindle checkpoint proteins at PtK1 kinetochores. *Mol Biol Cell*. 12:1995-2009.

Holloway, S.L., M. Glotzer, R.W. King, and A.W. Murray. 1993. Anaphase is initiated by proteolysis rather than by the inactivation of maturation-promoting factor. *Cell*. 73:1393-402.

Honda, R., R. Korner, and E.A. Nigg. 2003. Exploring the functional interactions between Aurora B, INCENP, and survivin in mitosis. *Mol Biol Cell*. 14:3325-41.

Hori, T., T. Haraguchi, Y. Hiraoka, H. Kimura, and T. Fukagawa. 2003. Dynamic behavior of Nuf2-Hec1 complex that localizes to the centrosome and centromere and is essential for mitotic progression in vertebrate cells. *J Cell Sci*. 116:3347-62.

Howell, B.J., D.B. Hoffman, G. Fang, A.W. Murray, and E.D. Salmon. 2000. Visualization of Mad2 dynamics at kinetochores, along spindle fibers, and at spindle poles in living cells. *J Cell Biol*. 150:1233-50.

Howell, B.J., B.F. McEwen, J.C. Canman, D.B. Hoffman, E.M. Farrar, C.L. Rieder, and E.D. Salmon. 2001. Cytoplasmic dynein/dynactin drives kinetochore protein transport to the spindle poles and has a role in mitotic spindle checkpoint inactivation. *J Cell Biol*. 155:1159-72.

Howell, B.J., B. Moree, E.M. Farrar, S. Stewart, G. Fang, and E.D. Salmon. 2004. Spindle checkpoint protein dynamics at kinetochores in living cells. *Curr Biol.* 14:953-64.

Hoyt, M.A., L. Totis, and B.T. Roberts. 1991. S. cerevisiae genes required for cell cycle arrest in response to loss of microtubule function. *Cell.* 66:507-17.

Hsu, J.Y., Z.W. Sun, X. Li, M. Reuben, K. Tatchell, D.K. Bishop, J.M. Grushcow, C.J. Brame, J.A. Caldwell, D.F. Hunt, R. Lin, M.M. Smith, and C.D. Allis. 2000. Mitotic phosphorylation of histone H3 is governed by Ipl1/aurora kinase and Glc7/PP1 phosphatase in budding yeast and nematodes. *Cell.* 102:279-91.

Huang, H., J. Feng, J. Famulski, J.B. Rattner, S.T. Liu, G.D. Kao, R. Muschel, G.K. Chan, and T.J. Yen. 2007. Tripin/hSgo2 recruits MCAK to the inner centromere to correct defective kinetochore attachments. *J Cell Biol.* 177:413-24.

Hunter, A.W., M. Caplow, D.L. Coy, W.O. Hancock, S. Diez, L. Wordeman, and J. Howard. 2003. The kinesin-related protein MCAK is a microtubule depolymerase that forms an ATP-hydrolyzing complex at microtubule ends. *Mol Cell.* 11:445-57.

Inoue, S., and E.D. Salmon. 1995. Force generation by microtubule assembly/disassembly in mitosis and related movements. *Mol Biol Cell.* 6:1619-40.

Iwanaga, Y., Y.H. Chi, A. Miyazato, S. Sheleg, K. Haller, J.M. Peloponese, Jr., Y. Li, J.M. Ward, R. Benezra, and K.T. Jeang. 2007. Heterozygous deletion of mitotic arrest-deficient protein 1 (MAD1) increases the incidence of tumors in mice. *Cancer Res.* 67:160-6.

Izuta, H., M. Ikeno, N. Suzuki, T. Tomonaga, N. Nozaki, C. Obuse, Y. Kisu, N. Goshima, F. Nomura, N. Nomura, and K. Yoda. 2006. Comprehensive analysis of the ICEN (Interphase Centromere Complex) components enriched in the CENP-A chromatin of human cells. *Genes Cells.* 11:673-84.

Jablonski, S.A., G.K. Chan, C.A. Cooke, W.C. Earnshaw, and T.J. Yen. 1998. The hBUB1 and hBUBR1 kinases sequentially assemble onto kinetochores during prophase with hBUBR1 concentrating at the kinetochore plates in mitosis. *Chromosoma.* 107:386-96.

Jallepalli, P.V., I.C. Waizenegger, F. Bunz, S. Langer, M.R. Speicher, J.M. Peters, K.W. Kinzler, B. Vogelstein, and C. Lengauer. 2001. Securin is required for chromosomal stability in human cells. *Cell.* 105:445-57.

Jansen, L.E., B.E. Black, D.R. Foltz, and D.W. Cleveland. 2007. Propagation of centromeric chromatin requires exit from mitosis. *J Cell Biol.* 176:795-805.

Jelluma, N., A.B. Brenkman, I. McLeod, J.R. Yates, 3rd, D.W. Cleveland, R.H. Medema, and G.J. Kops. 2008a. Chromosomal instability by inefficient Mps1 auto-activation due to a weakened mitotic checkpoint and lagging chromosomes. *PLoS ONE.* 3:e2415.

Jelluma, N., A.B. Brenkman, N.J. van den Broek, C.W. Cruijsen, M.H. van Osch, S.M. Lens, R.H. Medema, and G.J. Kops. 2008b. Mps1 phosphorylates Borealin to control Aurora B activity and chromosome alignment. *Cell.* 132:233-46.

Job, D., O. Valiron, and B. Oakley. 2003. Microtubule nucleation. *Curr Opin Cell Biol.* 15:111-7.

Joglekar, A.P., D. Bouck, K. Finley, X. Liu, Y. Wan, J. Berman, X. He, E.D. Salmon, and K.S. Bloom. 2008. Molecular architecture of the kinetochore-microtubule attachment site is conserved between point and regional centromeres. *J Cell Biol.* 181:587-94.

Jordan, M.A., D. Thrower, and L. Wilson. 1992. Effects of vinblastine, podophyllotoxin and nocodazole on mitotic spindles. Implications for the role of microtubule dynamics in mitosis. *J Cell Sci.* 102 (Pt 3):401-16.

Kalab, P., A. Pralle, E.Y. Isacoff, R. Heald, and K. Weis. 2006. Analysis of a RanGTP-regulated gradient in mitotic somatic cells. *Nature.* 440:697-701.

Kalab, P., K. Weis, and R. Heald. 2002. Visualization of a Ran-GTP gradient in interphase and mitotic Xenopus egg extracts. *Science.* 295:2452-6.

Kalitsis, P., E. Earle, K.J. Fowler, and K.H. Choo. 2000. Bub3 gene disruption in mice reveals essential mitotic spindle checkpoint function during early embryogenesis. *Genes Dev.* 14:2277-82.

Kapoor, T.M., M.A. Lampson, P. Hergert, L. Cameron, D. Cimini, E.D. Salmon, B.F. McEwen, and A. Khodjakov. 2006. Chromosomes can congress to the metaphase plate before biorientation. *Science.* 311:388-91.

Karess, R. 2005. Rod-Zw10-Zwilch: a key player in the spindle checkpoint. *Trends Cell Biol.* 15:386-92.

Karess, R.E., and D.M. Glover. 1989. rough deal: a gene required for proper mitotic segregation in Drosophila. *J Cell Biol.* 109:2951-61.

Keith, K.C., and M. Fitzgerald-Hayes. 2000. CSE4 genetically interacts with the Saccharomyces cerevisiae centromere DNA elements CDE I and CDE II but not CDE III. Implications for the path of the centromere dna around a cse4p variant nucleosome. *Genetics.* 156:973-81.

Khodjakov, A., R.W. Cole, B.R. Oakley, and C.L. Rieder. 2000. Centrosome-independent mitotic spindle formation in vertebrates. *Curr Biol.* 10:59-67.

Khodjakov, A., L. Copenagle, M.B. Gordon, D.A. Compton, and T.M. Kapoor. 2003. Minus-end capture of preformed kinetochore fibers contributes to spindle morphogenesis. *J Cell Biol.* 160:671-83.

King, J.M., and R.B. Nicklas. 2000. Tension on chromosomes increases the number of kinetochore microtubules but only within limits. *J Cell Sci.* 113 Pt 21:3815-23.

King, R.W., J.M. Peters, S. Tugendreich, M. Rolfe, P. Hieter, and M.W. Kirschner. 1995. A 20S complex containing CDC27 and CDC16 catalyzes the mitosis-specific conjugation of ubiquitin to cyclin B. *Cell.* 81:279-88.

King, S.J., and T.A. Schroer. 2000. Dynactin increases the processivity of the cytoplasmic dynein motor. *Nat Cell Biol.* 2:20-4.

Kirschner, M., and T. Mitchison. 1986. Beyond self-assembly: from microtubules to morphogenesis. *Cell.* 45:329-42.

Kitagawa, R., and A.M. Rose. 1999. Components of the spindle-assembly checkpoint are essential in Caenorhabditis elegans. *Nat Cell Biol.* 1:514-21.

Kitajima, T.S., S. Hauf, M. Ohsugi, T. Yamamoto, and Y. Watanabe. 2005. Human Bub1 defines the persistent cohesion site along the mitotic chromosome by affecting Shugoshin localization. *Curr Biol.* 15:353-9.

Kline-Smith, S.L., S. Sandall, and A. Desai. 2005. Kinetochore-spindle microtubule interactions during mitosis. *Curr Opin Cell Biol.* 17:35-46.

Kline, S.L., I.M. Cheeseman, T. Hori, T. Fukagawa, and A. Desai. 2006. The human Mis12 complex is required for kinetochore assembly and proper chromosome segregation. *J Cell Biol.* 173:9-17.

Knowlton, A.L., W. Lan, and P.T. Stukenberg. 2006. Aurora B is enriched at merotelic attachment sites, where it regulates MCAK. *Curr Biol.* 16:1705-10.

Kops, G.J., Y. Kim, B.A. Weaver, Y. Mao, I. McLeod, J.R. Yates, 3rd, M. Tagaya, and D.W. Cleveland. 2005a. ZW10 links mitotic checkpoint signaling to the structural kinetochore. *J Cell Biol.* 169:49-60.

Kops, G.J., B.A. Weaver, and D.W. Cleveland. 2005b. On the road to cancer: aneuploidy and the mitotic checkpoint. *Nat Rev Cancer.* 5:773-85.

Kraft, C., F. Herzog, C. Gieffers, K. Mechtler, A. Hagting, J. Pines, and J.M. Peters. 2003. Mitotic regulation of the human anaphase-promoting complex by phosphorylation. *EMBO J.* 22:6598-609.

Lachner, M., D. O'Carroll, S. Rea, K. Mechtler, and T. Jenuwein. 2001. Methylation of histone H3 lysine 9 creates a binding site for HP1 proteins. *Nature.* 410:116-20.

Lam, A.L., C.D. Boivin, C.F. Bonney, M.K. Rudd, and B.A. Sullivan. 2006. Human centromeric chromatin is a dynamic chromosomal domain that can spread over noncentromeric DNA. *Proc Natl Acad Sci U S A.* 103:4186-91.

Lampson, M.A., and T.M. Kapoor. 2005. The human mitotic checkpoint protein BubR1 regulates chromosome-spindle attachments. *Nat Cell Biol.* 7:93-8.

Lan, W., X. Zhang, S.L. Kline-Smith, S.E. Rosasco, G.A. Barrett-Wilt, J. Shabanowitz, D.F. Hunt, C.E. Walczak, and P.T. Stukenberg. 2004. Aurora B phosphorylates centromeric MCAK and regulates its localization and microtubule depolymerization activity. *Curr Biol.* 14:273-86.

Lauze, E., B. Stoelcker, F.C. Luca, E. Weiss, A.R. Schutz, and M. Winey. 1995. Yeast spindle pole body duplication gene MPS1 encodes an essential dual specificity protein kinase. *EMBO J.* 14:1655-63.

Lee, M.J., F. Gergely, K. Jeffers, S.Y. Peak-Chew, and J.W. Raff. 2001. Msps/XMAP215 interacts with the centrosomal protein D-TACC to regulate microtubule behaviour. *Nat Cell Biol.* 3:643-9.

Lens, S.M., and R.H. Medema. 2003. The survivin/Aurora B complex: its role in coordinating tension and attachment. *Cell Cycle.* 2:507-10.

Lens, S.M., J.A. Rodriguez, G. Vader, S.W. Span, G. Giaccone, and R.H. Medema. 2006. Uncoupling the central spindle-associated function of the chromosomal passenger complex from its role at centromeres. *Mol Biol Cell.* 17:1897-909.

Lens, S.M., R.M. Wolthuis, R. Klompmaker, J. Kauw, R. Agami, T. Brummelkamp, G. Kops, and R.H. Medema. 2003. Survivin is required for a sustained spindle checkpoint arrest in response to lack of tension. *EMBO J.* 22:2934-47.

Li, R., and A.W. Murray. 1991. Feedback control of mitosis in budding yeast. *Cell.* 66:519-31.

Li, Y., and R. Benezra. 1996. Identification of a human mitotic checkpoint gene: hsMAD2. *Science.* 274:246-8.

Liang, Y., W. Yu, Y. Li, L. Yu, Q. Zhang, F. Wang, Z. Yang, J. Du, Q. Huang, X. Yao, and X. Zhu. 2007. Nudel modulates kinetochore association and function of cytoplasmic dynein in M phase. *Mol Biol Cell.* 18:2656-66.

Lin, Y.T., Y. Chen, G. Wu, and W.H. Lee. 2006. Hec1 sequentially recruits Zwint-1 and ZW10 to kinetochores for faithful chromosome segregation and spindle checkpoint control. *Oncogene*. 25:6901-14.

Liu, S.T., G.K. Chan, J.C. Hittle, G. Fujii, E. Lees, and T.J. Yen. 2003a. Human MPS1 kinase is required for mitotic arrest induced by the loss of CENP-E from kinetochores. *Mol Biol Cell*. 14:1638-51.

Liu, S.T., J.C. Hittle, S.A. Jablonski, M.S. Campbell, K. Yoda, and T.J. Yen. 2003b. Human CENP-I specifies localization of CENP-F, MAD1 and MAD2 to kinetochores and is essential for mitosis. *Nat Cell Biol*. 5:341-5.

Liu, S.T., J.B. Rattner, S.A. Jablonski, and T.J. Yen. 2006. Mapping the assembly pathways that specify formation of the trilaminar kinetochore plates in human cells. *J Cell Biol*. 175:41-53.

Lowery, D.M., D.H. Mohammad, A.E. Elia, and M.B. Yaffe. 2004. The Polo-box domain: a molecular integrator of mitotic kinase cascades and Polo-like kinase function. *Cell Cycle*. 3:128-31.

Luo, X., Z. Tang, J. Rizo, and H. Yu. 2002. The Mad2 spindle checkpoint protein undergoes similar major conformational changes upon binding to either Mad1 or Cdc20. *Mol Cell*. 9:59-71.

Luo, X., Z. Tang, G. Xia, K. Wassmann, T. Matsumoto, J. Rizo, and H. Yu. 2004. The Mad2 spindle checkpoint protein has two distinct natively folded states. *Nat Struct Mol Biol*. 11:338-45.

Maiato, H., J. DeLuca, E.D. Salmon, and W.C. Earnshaw. 2004a. The dynamic kinetochore-microtubule interface. *J Cell Sci*. 117:5461-77.

Maiato, H., C.L. Rieder, and A. Khodjakov. 2004b. Kinetochore-driven formation of kinetochore fibers contributes to spindle assembly during animal mitosis. *J Cell Biol*. 167:831-40.

Mallik, R., D. Petrov, S.A. Lex, S.J. King, and S.P. Gross. 2005. Building complexity: an in vitro study of cytoplasmic dynein with in vivo implications. *Curr Biol*. 15:2075-85.

Mao, Y., A. Abrieu, and D.W. Cleveland. 2003. Activating and silencing the mitotic checkpoint through CENP-E-dependent activation/inactivation of BubR1. *Cell*. 114:87-98.

Mao, Y., A. Desai, and D.W. Cleveland. 2005. Microtubule capture by CENP-E silences BubR1-dependent mitotic checkpoint signaling. *J Cell Biol*. 170:873-80.

Mapelli, M., F.V. Filipp, G. Rancati, L. Massimiliano, L. Nezi, G. Stier, R.S. Hagan, S. Confalonieri, S. Piatti, M. Sattler, and A. Musacchio. 2006. Determinants of conformational dimerization of Mad2 and its inhibition by p31comet. *EMBO J*. 25:1273-84.

Maure, J.F., E. Kitamura, and T.U. Tanaka. 2007. Mps1 kinase promotes sister-kinetochore bi-orientation by a tension-dependent mechanism. *Curr Biol*. 17:2175-82.

McCleland, M.L., R.D. Gardner, M.J. Kallio, J.R. Daum, G.J. Gorbsky, D.J. Burke, and P.T. Stukenberg. 2003. The highly conserved Ndc80 complex is required for kinetochore assembly, chromosome congression, and spindle checkpoint activity. *Genes Dev*. 17:101-14.

McEwen, B.F., J.T. Arena, J. Frank, and C.L. Rieder. 1993. Structure of the colcemid-treated PtK1 kinetochore outer plate as determined by high voltage electron microscopic tomography. *J Cell Biol.* 120:301-12.

McEwen, B.F., G.K. Chan, B. Zubrowski, M.S. Savoian, M.T. Sauer, and T.J. Yen. 2001. CENP-E is essential for reliable bioriented spindle attachment, but chromosome alignment can be achieved via redundant mechanisms in mammalian cells. *Mol Biol Cell.* 12:2776-89.

McEwen, B.F., A.B. Heagle, G.O. Cassels, K.F. Buttle, and C.L. Rieder. 1997. Kinetochore fiber maturation in PtK1 cells and its implications for the mechanisms of chromosome congression and anaphase onset. *J Cell Biol.* 137:1567-80.

McIntosh, J.R. 1991. Structural and mechanical control of mitotic progression. *Cold Spring Harb Symp Quant Biol.* 56:613-9.

Meraldi, P., V.M. Draviam, and P.K. Sorger. 2004. Timing and checkpoints in the regulation of mitotic progression. *Dev Cell.* 7:45-60.

Morgan, D.O. 1997. Cyclin-dependent kinases: engines, clocks, and microprocessors. *Annu Rev Cell Dev Biol.* 13:261-91.

Morrow, C.J., A. Tighe, V.L. Johnson, M.I. Scott, C. Ditchfield, and S.S. Taylor. 2005. Bub1 and aurora B cooperate to maintain BubR1-mediated inhibition of APC/CCdc20. *J Cell Sci.* 118:3639-52.

Murnion, M.E., R.R. Adams, D.M. Callister, C.D. Allis, W.C. Earnshaw, and J.R. Swedlow. 2001. Chromatin-associated protein phosphatase 1 regulates aurora-B and histone H3 phosphorylation. *J Biol Chem.* 276:26656-65.

Murray, A.W., and M.W. Kirschner. 1989. Cyclin synthesis drives the early embryonic cell cycle. *Nature.* 339:275-80.

Murray, A.W., M.J. Solomon, and M.W. Kirschner. 1989. The role of cyclin synthesis and degradation in the control of maturation promoting factor activity. *Nature.* 339:280-6.

Musacchio, A., and E.D. Salmon. 2007. The spindle-assembly checkpoint in space and time. *Nat Rev Mol Cell Biol.* 8:379-93.

Nachury, M.V., T.J. Maresca, W.C. Salmon, C.M. Waterman-Storer, R. Heald, and K. Weis. 2001. Importin beta is a mitotic target of the small GTPase Ran in spindle assembly. *Cell.* 104:95-106.

Nakano, M., S. Cardinale, V.N. Noskov, R. Gassmann, P. Vagnarelli, S. Kandels-Lewis, V. Larionov, W.C. Earnshaw, and H. Masumoto. 2008. Inactivation of a human kinetochore by specific targeting of chromatin modifiers. *Dev Cell.* 14:507-22.

Nasmyth, K. 2002. Segregating sister genomes: the molecular biology of chromosome separation. *Science.* 297:559-65.

Nezi, L., G. Rancati, A. De Antoni, S. Pasqualato, S. Piatti, and A. Musacchio. 2006. Accumulation of Mad2-Cdc20 complex during spindle checkpoint activation requires binding of open and closed conformers of Mad2 in Saccharomyces cerevisiae. *J Cell Biol.* 174:39-51.

Nicklas, R.B. 1997. How cells get the right chromosomes. *Science.* 275:632-7.

Nicklas, R.B., S.C. Ward, and G.J. Gorbsky. 1995. Kinetochore chemistry is sensitive to tension and may link mitotic forces to a cell cycle checkpoint. *J Cell Biol.* 130:929-39.

Nousiainen, M., H.H. Sillje, G. Sauer, E.A. Nigg, and R. Korner. 2006. Phosphoproteome analysis of the human mitotic spindle. *Proc Natl Acad Sci U S A.* 103:5391-6.

O'Connell, C.B., and A.L. Khodjakov. 2007. Cooperative mechanisms of mitotic spindle formation. *J Cell Sci.* 120:1717-22.

Obuse, C., O. Iwasaki, T. Kiyomitsu, G. Goshima, Y. Toyoda, and M. Yanagida. 2004. A conserved Mis12 centromere complex is linked to heterochromatic HP1 and outer kinetochore protein Zwint-1. *Nat Cell Biol.* 6:1135-41.

Ohi, R., T. Sapra, J. Howard, and T.J. Mitchison. 2004. Differentiation of cytoplasmic and meiotic spindle assembly MCAK functions by Aurora B-dependent phosphorylation. *Mol Biol Cell.* 15:2895-906.

Okada, M., I.M. Cheeseman, T. Hori, K. Okawa, I.X. McLeod, J.R. Yates, 3rd, A. Desai, and T. Fukagawa. 2006. The CENP-H-I complex is required for the efficient incorporation of newly synthesized CENP-A into centromeres. *Nat Cell Biol.* 8:446-57.

Peters, A.H., D. O'Carroll, H. Scherthan, K. Mechtler, S. Sauer, C. Schofer, K. Weipoltshammer, M. Pagani, M. Lachner, A. Kohlmaier, S. Opravil, M. Doyle, M. Sibilia, and T. Jenuwein. 2001. Loss of the Suv39h histone methyltransferases impairs mammalian heterochromatin and genome stability. *Cell.* 107:323-37.

Peters, J.M. 2006. The anaphase promoting complex/cyclosome: a machine designed to destroy. *Nat Rev Mol Cell Biol.* 7:644-56.

Petronczki, M., P. Lenart, and J.M. Peters. 2008. Polo on the Rise-from Mitotic Entry to Cytokinesis with Plk1. *Dev Cell.* 14:646-59.

Pfarr, C.M., M. Coue, P.M. Grissom, T.S. Hays, M.E. Porter, and J.R. McIntosh. 1990. Cytoplasmic dynein is localized to kinetochores during mitosis. *Nature.* 345:263-5.

Pfleger, C.M., and M.W. Kirschner. 2000. The KEN box: an APC recognition signal distinct from the D box targeted by Cdh1. *Genes Dev.* 14:655-65.

Pinsky, B.A., and S. Biggins. 2005. The spindle checkpoint: tension versus attachment. *Trends Cell Biol.* 15:486-93.

Prinz, S., E.S. Hwang, R. Visintin, and A. Amon. 1998. The regulation of Cdc20 proteolysis reveals a role for APC components Cdc23 and Cdc27 during S phase and early mitosis. *Curr Biol.* 8:750-60.

Reddy, S.K., M. Rape, W.A. Margansky, and M.W. Kirschner. 2007. Ubiquitination by the anaphase-promoting complex drives spindle checkpoint inactivation. *Nature.* 446:921-5.

Reis, A., M. Levasseur, H.Y. Chang, D.J. Elliott, and K.T. Jones. 2006. The CRY box: a second APCcdh1-dependent degron in mammalian cdc20. *EMBO Rep.* 7:1040-5.

Rieder, C.L., and S.P. Alexander. 1990. Kinetochores are transported poleward along a single astral microtubule during chromosome attachment to the spindle in newt lung cells. *J Cell Biol.* 110:81-95.

Rieder, C.L., R.W. Cole, A. Khodjakov, and G. Sluder. 1995. The checkpoint delaying anaphase in response to chromosome monoorientation is mediated by an inhibitory signal produced by unattached kinetochores. *J Cell Biol.* 130:941-8.

Rieder, C.L., A. Khodjakov, L.V. Paliulis, T.M. Fortier, R.W. Cole, and G. Sluder. 1997. Mitosis in vertebrate somatic cells with two spindles: implications for the

metaphase/anaphase transition checkpoint and cleavage. *Proc Natl Acad Sci U S A*. 94:5107-12.

Rieder, C.L., and E.D. Salmon. 1994. Motile kinetochores and polar ejection forces dictate chromosome position on the vertebrate mitotic spindle. *J Cell Biol.* 124:223-33.

Rieder, C.L., A. Schultz, R. Cole, and G. Sluder. 1994. Anaphase onset in vertebrate somatic cells is controlled by a checkpoint that monitors sister kinetochore attachment to the spindle. *J Cell Biol.* 127:1301-10.

Ris, H., and P.L. Witt. 1981. Structure of the mammalian kinetochore. *Chromosoma.* 82:153-70.

Rock, K.L., C. Gramm, L. Rothstein, K. Clark, R. Stein, L. Dick, D. Hwang, and A.L. Goldberg. 1994. Inhibitors of the proteasome block the degradation of most cell proteins and the generation of peptides presented on MHC class I molecules. *Cell.* 78:761-71.

Rosasco-Nitcher, S.E., W. Lan, S. Khorasanizadeh, and P.T. Stukenberg. 2008. Centromeric Aurora-B activation requires TD-60, microtubules, and substrate priming phosphorylation. *Science.* 319:469-72.

Ruchaud, S., M. Carmena, and W.C. Earnshaw. 2007. Chromosomal passengers: conducting cell division. *Nat Rev Mol Cell Biol.* 8:798-812.

Salmon, E.D., D. Cimini, L.A. Cameron, and J.G. DeLuca. 2005. Merotelic kinetochores in mammalian tissue cells. *Philos Trans R Soc Lond B Biol Sci.* 360:553-68.

Sandall, S., F. Severin, I.X. McLeod, J.R. Yates, 3rd, K. Oegema, A. Hyman, and A. Desai. 2006. A Bir1-Sli15 complex connects centromeres to microtubules and is required to sense kinetochore tension. *Cell.* 127:1179-91.

Sasaki, S., A. Shionoya, M. Ishida, M.J. Gambello, J. Yingling, A. Wynshaw-Boris, and S. Hirotsune. 2000. A LIS1/NUDEL/cytoplasmic dynein heavy chain complex in the developing and adult nervous system. *Neuron.* 28:681-96.

Scaerou, F., I. Aguilera, R. Saunders, N. Kane, L. Blottiere, and R. Karess. 1999. The rough deal protein is a new kinetochore component required for accurate chromosome segregation in Drosophila. *J Cell Sci.* 112 (Pt 21):3757-68.

Scaerou, F., D.A. Starr, F. Piano, O. Papoulas, R.E. Karess, and M.L. Goldberg. 2001. The ZW10 and Rough Deal checkpoint proteins function together in a large, evolutionarily conserved complex targeted to the kinetochore. *J Cell Sci.* 114:3103-14.

Scholey, J.M., I. Brust-Mascher, and A. Mogilner. 2003. Cell division. *Nature.* 422:746-52.

Schuyler, S.C., and D. Pellman. 2001. Microtubule "plus-end-tracking proteins": The end is just the beginning. *Cell.* 105:421-4.

Schwab, M., A.S. Lutum, and W. Seufert. 1997. Yeast Hct1 is a regulator of Clb2 cyclin proteolysis. *Cell.* 90:683-93.

Shah, J.V., E. Botvinick, Z. Bonday, F. Furnari, M. Berns, and D.W. Cleveland. 2004. Dynamics of centromere and kinetochore proteins; implications for checkpoint signaling and silencing. *Curr Biol.* 14:942-52.

Shannon, K.B., J.C. Canman, and E.D. Salmon. 2002. Mad2 and BubR1 function in a single checkpoint pathway that responds to a loss of tension. *Mol Biol Cell.* 13:3706-19.

Sharp, D.J., G.C. Rogers, and J.M. Scholey. 2000. Microtubule motors in mitosis. *Nature*. 407:41-7.

Skibbens, R.V., C.L. Rieder, and E.D. Salmon. 1995. Kinetochore motility after severing between sister centromeres using laser microsurgery: evidence that kinetochore directional instability and position is regulated by tension. *J Cell Sci.* 108 (Pt 7):2537-48.

Skibbens, R.V., V.P. Skeen, and E.D. Salmon. 1993. Directional instability of kinetochore motility during chromosome congression and segregation in mitotic newt lung cells: a push-pull mechanism. *J Cell Biol.* 122:859-75.

Skoufias, D.A., P.R. Andreassen, F.B. Lacroix, L. Wilson, and R.L. Margolis. 2001. Mammalian mad2 and bub1/bubR1 recognize distinct spindle-attachment and kinetochore-tension checkpoints. *Proc Natl Acad Sci U S A.* 98:4492-7.

Skoufias, D.A., S. DeBonis, Y. Saoudi, L. Lebeau, I. Crevel, R. Cross, R.H. Wade, D. Hackney, and F. Kozielski. 2006. S-trityl-L-cysteine is a reversible, tight binding inhibitor of the human kinesin Eg5 that specifically blocks mitotic progression. *J Biol Chem.* 281:17559-69.

Sluder, G. 1979. Role of spindle microtubules in the control of cell cycle timing. *J Cell Biol.* 80:674-91.

Sluder, G., and D.A. Begg. 1983. Control mechanisms of the cell cycle: role of the spatial arrangement of spindle components in the timing of mitotic events. *J Cell Biol.* 97:877-86.

Spencer, F., and P. Hieter. 1992. Centromere DNA mutations induce a mitotic delay in Saccharomyces cerevisiae. *Proc Natl Acad Sci U S A.* 89:8908-12.

Starr, D.A., R. Saffery, Z. Li, A.E. Simpson, K.H. Choo, T.J. Yen, and M.L. Goldberg. 2000. HZwint-1, a novel human kinetochore component that interacts with HZW10. *J Cell Sci.* 113 (Pt 11):1939-50.

Starr, D.A., B.C. Williams, T.S. Hays, and M.L. Goldberg. 1998. ZW10 helps recruit dynactin and dynein to the kinetochore. *J Cell Biol.* 142:763-74.

Starr, D.A., B.C. Williams, Z. Li, B. Etemad-Moghadam, R.K. Dawe, and M.L. Goldberg. 1997. Conservation of the centromere/kinetochore protein ZW10. *J Cell Biol.* 138:1289-301.

Stegmeier, F., M. Rape, V.M. Draviam, G. Nalepa, M.E. Sowa, X.L. Ang, E.R. McDonald, 3rd, M.Z. Li, G.J. Hannon, P.K. Sorger, M.W. Kirschner, J.W. Harper, and S.J. Elledge. 2007. Anaphase initiation is regulated by antagonistic ubiquitination and deubiquitination activities. *Nature*. 446:876-81.

Stehman, S.A., Y. Chen, R.J. McKenney, and R.B. Vallee. 2007. NudE and NudEL are required for mitotic progression and are involved in dynein recruitment to kinetochores. *J Cell Biol.* 178:583-94.

Stern, B.M., and A.W. Murray. 2001. Lack of tension at kinetochores activates the spindle checkpoint in budding yeast. *Curr Biol.* 11:1462-7.

Steuer, E.R., L. Wordeman, T.A. Schroer, and M.P. Sheetz. 1990. Localization of cytoplasmic dynein to mitotic spindles and kinetochores. *Nature*. 345:266-8.

Sudakin, V., G.K. Chan, and T.J. Yen. 2001. Checkpoint inhibition of the APC/C in HeLa cells is mediated by a complex of BUBR1, BUB3, CDC20, and MAD2. *J Cell Biol.* 154:925-36.

Sudakin, V., D. Ganoth, A. Dahan, H. Heller, J. Hershko, F.C. Luca, J.V. Ruderman, and A. Hershko. 1995. The cyclosome, a large complex containing cyclin-selective ubiquitin ligase activity, targets cyclins for destruction at the end of mitosis. *Mol Biol Cell.* 6:185-97.

Sullivan, B.A., and G.H. Karpen. 2004. Centromeric chromatin exhibits a histone modification pattern that is distinct from both euchromatin and heterochromatin. *Nat Struct Mol Biol.* 11:1076-83.

Sullivan, K.F. 2001. A solid foundation: functional specialization of centromeric chromatin. *Curr Opin Genet Dev.* 11:182-8.

Sumara, I., E. Vorlaufer, C. Gieffers, B.H. Peters, and J.M. Peters. 2000. Characterization of vertebrate cohesin complexes and their regulation in prophase. *J Cell Biol.* 151:749-62.

Sunkel, C.E., and D.M. Glover. 1988. polo, a mitotic mutant of Drosophila displaying abnormal spindle poles. *J Cell Sci.* 89 (Pt 1):25-38.

Tanaka, T., J. Fuchs, J. Loidl, and K. Nasmyth. 2000. Cohesin ensures bipolar attachment of microtubules to sister centromeres and resists their precocious separation. *Nat Cell Biol.* 2:492-9.

Tang, Z., R. Bharadwaj, B. Li, and H. Yu. 2001. Mad2-Independent inhibition of APCCdc20 by the mitotic checkpoint protein BubR1. *Dev Cell.* 1:227-37.

Tang, Z., H. Shu, D. Oncel, S. Chen, and H. Yu. 2004a. Phosphorylation of Cdc20 by Bub1 provides a catalytic mechanism for APC/C inhibition by the spindle checkpoint. *Mol Cell.* 16:387-97.

Tang, Z., Y. Sun, S.E. Harley, H. Zou, and H. Yu. 2004b. Human Bub1 protects centromeric sister-chromatid cohesion through Shugoshin during mitosis. *Proc Natl Acad Sci U S A.* 101:18012-7.

Taylor, S.S., E. Ha, and F. McKeon. 1998. The human homologue of Bub3 is required for kinetochore localization of Bub1 and a Mad3/Bub1-related protein kinase. *J Cell Biol.* 142:1-11.

Taylor, S.S., D. Hussein, Y. Wang, S. Elderkin, and C.J. Morrow. 2001. Kinetochore localisation and phosphorylation of the mitotic checkpoint components Bub1 and BubR1 are differentially regulated by spindle events in human cells. *J Cell Sci.* 114:4385-95.

Taylor, S.S., and F. McKeon. 1997. Kinetochore localization of murine Bub1 is required for normal mitotic timing and checkpoint response to spindle damage. *Cell.* 89:727-35.

Terada, Y., M. Tatsuka, F. Suzuki, Y. Yasuda, S. Fujita, and M. Otsu. 1998. AIM-1: a mammalian midbody-associated protein required for cytokinesis. *EMBO J.* 17:667-76.

Tighe, A., O. Staples, and S. Taylor. 2008. Mps1 kinase activity restrains anaphase during an unperturbed mitosis and targets Mad2 to kinetochores. *J Cell Biol.* 181:893-901.

Toby, G.G., and E.A. Golemis. 2001. Using the yeast interaction trap and other two-hybrid-based approaches to study protein-protein interactions. *Methods.* 24:201-17.

Topper, L.M., M.S. Campbell, S. Tugendreich, J.R. Daum, D.J. Burke, P. Hieter, and G.J. Gorbsky. 2002. The dephosphorylated form of the anaphase-promoting complex

protein Cdc27/Apc3 concentrates on kinetochores and chromosome arms in mitosis. *Cell Cycle*. 1:282-92.

Townsley, F.M., A. Aristarkhov, S. Beck, A. Hershko, and J.V. Ruderman. 1997. Dominant-negative cyclin-selective ubiquitin carrier protein E2-C/UbcH10 blocks cells in metaphase. *Proc Natl Acad Sci U S A*. 94:2362-7.

Tyler-Smith, C., and G. Floridia. 2000. Many paths to the top of the mountain: diverse evolutionary solutions to centromere structure. *Cell*. 102:5-8.

Uhlmann, F., D. Wernic, M.A. Poupart, E.V. Koonin, and K. Nasmyth. 2000. Cleavage of cohesin by the CD clan protease separin triggers anaphase in yeast. *Cell*. 103:375-86.

Vader, G., C.W. Cruijsen, T. van Harn, M.J. Vromans, R.H. Medema, and S.M. Lens. 2007. The chromosomal passenger complex controls spindle checkpoint function independent from its role in correcting microtubule kinetochore interactions. *Mol Biol Cell*. 18:4553-64.

Vader, G., R.H. Medema, and S.M. Lens. 2006. The chromosomal passenger complex: guiding Aurora-B through mitosis. *J Cell Biol*. 173:833-7.

Vallee, R.B., C. Tai, and N.E. Faulkner. 2001. LIS1: cellular function of a disease-causing gene. *Trends Cell Biol*. 11:155-60.

van Vugt, M.A., and R.H. Medema. 2005. Getting in and out of mitosis with Polo-like kinase-1. *Oncogene*. 24:2844-59.

Vaughan, P.S., J.D. Leszyk, and K.T. Vaughan. 2001. Cytoplasmic dynein intermediate chain phosphorylation regulates binding to dynactin. *J Biol Chem*. 276:26171-9.

Vergnolle, M.A., and S.S. Taylor. 2007. Cenp-F links kinetochores to Ndel1/Nde1/Lis1/dynein microtubule motor complexes. *Curr Biol*. 17:1173-9.

Vink, M., M. Simonetta, P. Transidico, K. Ferrari, M. Mapelli, A. De Antoni, L. Massimiliano, A. Ciliberto, M. Faretta, E.D. Salmon, and A. Musacchio. 2006. In vitro FRAP identifies the minimal requirements for Mad2 kinetochore dynamics. *Curr Biol*. 16:755-66.

Visintin, R., S. Prinz, and A. Amon. 1997. CDC20 and CDH1: a family of substrate-specific activators of APC-dependent proteolysis. *Science*. 278:460-3.

Vos, L.J., J.K. Famulski, and G.K. Chan. 2006. How to build a centromere: from centromeric and pericentromeric chromatin to kinetochore assembly. *Biochem Cell Biol*. 84:619-39.

Voullaire, L., R. Saffery, J. Davies, E. Earle, P. Kalitsis, H. Slater, D.V. Irvine, and K.H. Choo. 1999. Trisomy 20p resulting from inverted duplication and neocentromere formation. *Am J Med Genet*. 85:403-8.

Wadsworth, P., and A. Khodjakov. 2004. E pluribus unum: towards a universal mechanism for spindle assembly. *Trends Cell Biol*. 14:413-9.

Waizenegger, I.C., S. Hauf, A. Meinke, and J.M. Peters. 2000. Two distinct pathways remove mammalian cohesin from chromosome arms in prophase and from centromeres in anaphase. *Cell*. 103:399-410.

Walczak, C.E. 2003. The Kin I kinesins are microtubule end-stimulated ATPases. *Mol Cell*. 11:286-8.

Wang, H., X. Hu, X. Ding, Z. Dou, Z. Yang, A.W. Shaw, M. Teng, D.W. Cleveland, M.L. Goldberg, L. Niu, and X. Yao. 2004a. Human Zwint-1 specifies localization

of Zeste White 10 to kinetochores and is essential for mitotic checkpoint signaling. *J Biol Chem.* 279:54590-8.

Wang, Z., J.M. Cummins, D. Shen, D.P. Cahill, P.V. Jallepalli, T.L. Wang, D.W. Parsons, G. Traverso, M. Awad, N. Silliman, J. Ptak, S. Szabo, J.K. Willson, S.D. Markowitz, M.L. Goldberg, R. Karess, K.W. Kinzler, B. Vogelstein, V.E. Velculescu, and C. Lengauer. 2004b. Three classes of genes mutated in colorectal cancers with chromosomal instability. *Cancer Res.* 64:2998-3001.

Waters, J.C., R.H. Chen, A.W. Murray, and E.D. Salmon. 1998. Localization of Mad2 to kinetochores depends on microtubule attachment, not tension. *J Cell Biol.* 141:1181-91.

Waters, J.C., R.V. Skibbens, and E.D. Salmon. 1996. Oscillating mitotic newt lung cell kinetochores are, on average, under tension and rarely push. *J Cell Sci.* 109 (Pt 12):2823-31.

Wei, R.R., J. Al-Bassam, and S.C. Harrison. 2007. The Ndc80/HEC1 complex is a contact point for kinetochore-microtubule attachment. *Nat Struct Mol Biol.* 14:54-9.

Wendell, K.L., L. Wilson, and M.A. Jordan. 1993. Mitotic block in HeLa cells by vinblastine: ultrastructural changes in kinetochore-microtubule attachment and in centrosomes. *J Cell Sci.* 104 (Pt 2):261-74.

Wiese, C., A. Wilde, M.S. Moore, S.A. Adam, A. Merdes, and Y. Zheng. 2001. Role of importin-beta in coupling Ran to downstream targets in microtubule assembly. *Science.* 291:653-6.

Wigge, P.A., and J.V. Kilmartin. 2001. The Ndc80p complex from Saccharomyces cerevisiae contains conserved centromere components and has a function in chromosome segregation. *J Cell Biol.* 152:349-60.

Wilde, A., S.B. Lizarraga, L. Zhang, C. Wiese, N.R. Gliksman, C.E. Walczak, and Y. Zheng. 2001. Ran stimulates spindle assembly by altering microtubule dynamics and the balance of motor activities. *Nat Cell Biol.* 3:221-7.

Williams, B.C., M. Gatti, and M.L. Goldberg. 1996. Bipolar spindle attachments affect redistributions of ZW10, a Drosophila centromere/kinetochore component required for accurate chromosome segregation. *J Cell Biol.* 134:1127-40.

Williams, B.C., and M.L. Goldberg. 1994. Determinants of Drosophila zw10 protein localization and function. *J Cell Sci.* 107 (Pt 4):785-98.

Williams, B.C., T.L. Karr, J.M. Montgomery, and M.L. Goldberg. 1992. The Drosophila l(1)zw10 gene product, required for accurate mitotic chromosome segregation, is redistributed at anaphase onset. *J Cell Biol.* 118:759-73.

Williams, B.C., Z. Li, S. Liu, E.V. Williams, G. Leung, T.J. Yen, and M.L. Goldberg. 2003. Zwilch, a new component of the ZW10/ROD complex required for kinetochore functions. *Mol Biol Cell.* 14:1379-91.

Winey, M., L. Goetsch, P. Baum, and B. Byers. 1991. MPS1 and MPS2: novel yeast genes defining distinct steps of spindle pole body duplication. *J Cell Biol.* 114:745-54.

Winey, M., and B.J. Huneycutt. 2002. Centrosomes and checkpoints: the MPS1 family of kinases. *Oncogene.* 21:6161-9.

Wojcik, E., R. Basto, M. Serr, F. Scaerou, R. Karess, and T. Hays. 2001. Kinetochore dynein: its dynamics and role in the transport of the Rough deal checkpoint protein. *Nat Cell Biol.* 3:1001-7.

Wollman, R., E.N. Cytrynbaum, J.T. Jones, T. Meyer, J.M. Scholey, and A. Mogilner. 2005. Efficient chromosome capture requires a bias in the 'search-and-capture' process during mitotic-spindle assembly. *Curr Biol.* 15:828-32.

Wong, O.K., and G. Fang. 2007. Cdk1 phosphorylation of BubR1 controls spindle checkpoint arrest and Plk1-mediated formation of the 3F3/2 epitope. *J Cell Biol.* 179:611-7.

Wu, H., Z. Lan, W. Li, S. Wu, J. Weinstein, K.M. Sakamoto, and W. Dai. 2000. p55CDC/hCDC20 is associated with BUBR1 and may be a downstream target of the spindle checkpoint kinase. *Oncogene.* 19:4557-62.

Xia, G., X. Luo, T. Habu, J. Rizo, T. Matsumoto, and H. Yu. 2004. Conformation-specific binding of p31(comet) antagonizes the function of Mad2 in the spindle checkpoint. *EMBO J.* 23:3133-43.

Xiang, X., S.M. Beckwith, and N.R. Morris. 1994. Cytoplasmic dynein is involved in nuclear migration in Aspergillus nidulans. *Proc Natl Acad Sci U S A.* 91:2100-4.

Yan, X., F. Li, Y. Liang, Y. Shen, X. Zhao, Q. Huang, and X. Zhu. 2003. Human Nudel and NudE as regulators of cytoplasmic dynein in poleward protein transport along the mitotic spindle. *Mol Cell Biol.* 23:1239-50.

Yang, M., B. Li, D.R. Tomchick, M. Machius, J. Rizo, H. Yu, and X. Luo. 2007a. p31comet blocks Mad2 activation through structural mimicry. *Cell.* 131:744-55.

Yang, Z., J. Guo, Q. Chen, C. Ding, J. Du, and X. Zhu. 2005. Silencing mitosin induces misaligned chromosomes, premature chromosome decondensation before anaphase onset, and mitotic cell death. *Mol Cell Biol.* 25:4062-74.

Yang, Z., U.S. Tulu, P. Wadsworth, and C.L. Rieder. 2007b. Kinetochore dynein is required for chromosome motion and congression independent of the spindle checkpoint. *Curr Biol.* 17:973-80.

Yang, Z.Y., J. Guo, N. Li, M. Qian, S.N. Wang, and X.L. Zhu. 2003. Mitosin/CENP-F is a conserved kinetochore protein subjected to cytoplasmic dynein-mediated poleward transport. *Cell Res.* 13:275-83.

Yao, X., A. Abrieu, Y. Zheng, K.F. Sullivan, and D.W. Cleveland. 2000. CENP-E forms a link between attachment of spindle microtubules to kinetochores and the mitotic checkpoint. *Nat Cell Biol.* 2:484-91.

Yu, H. 2007. Cdc20: a WD40 activator for a cell cycle degradation machine. *Mol Cell.* 27:3-16.

Zachariae, W., M. Schwab, K. Nasmyth, and W. Seufert. 1998. Control of cyclin ubiquitination by CDK-regulated binding of Hct1 to the anaphase promoting complex. *Science.* 282:1721-4.

Zhang, X., W. Lan, S.C. Ems-McClung, P.T. Stukenberg, and C.E. Walczak. 2007. Aurora B phosphorylates multiple sites on mitotic centromere-associated kinesin to spatially and temporally regulate its function. *Mol Biol Cell.* 18:3264-76.

Zhou, J., J. Yao, and H.C. Joshi. 2002. Attachment and tension in the spindle assembly checkpoint. *J Cell Sci.* 115:3547-55.

Zhou, X., R. Wang, L. Fan, Y. Li, L. Ma, Z. Yang, W. Yu, N. Jing, and X. Zhu. 2005. Mitosin/CENP-F as a negative regulator of activating transcription factor-4. *J Biol Chem*. 280:13973-7.

Zinkowski, R.P., J. Meyne, and B.R. Brinkley. 1991. The centromere-kinetochore complex: a repeat subunit model. *J Cell Biol*. 113:1091-110.